

9 June 2006 | \$10

Science



Origins of
Civilization

 AAAS

MX3005P™ System

Most Flexible

MX3000P® System

Most Affordable



Performance runs in the family.
Choose the personal QPCR system that's right for you.

Stratagene now offers two affordable, fully-featured quantitative PCR (QPCR) systems. The new five-color Mx3005P™ QPCR System includes expanded features to support a wider range of real-time QPCR applications, such as simultaneous five-target detection and alternative QPCR probe chemistries. The Mx3000P® QPCR System is still the most affordably priced four-color 96-well system available.

- A four- or five-color instrument, with user-selected filters
- Advanced optical system design for true multiplexing capability, and wider application support
- MxPro™ QPCR Software with enhanced data analysis and export functionality

Need More Information? Give Us A Call:

Stratagene US and Canada

Order: 800-424-5444 x3

Technical Service: 800-894-1304 x2

Stratagene Europe

Order: 00800-7000-7000

Technical Service: 00800-7400-7400

Stratagene Japan K.K.

Order: 3-5821-8077

Technical Service: 3-5821-8076

www.stratagene.com

Mx3000P® is a registered trademark of Stratagene in the United States.
Mx3005P™ and MxPro™ are trademarks of Stratagene in the United States.



Simplify Gene Silencing Experiments with *Silencer*[®] Pre-designed siRNA



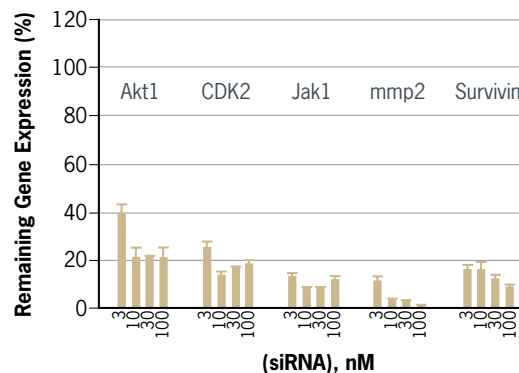
Fast. Easy. Guaranteed.

- Ready to use siRNAs provided in as little as 4 days
- Searchable database makes it simple to find siRNAs for human, mouse, and rat genes
- Efficient gene knockdown guaranteed
- Now save 18% when you purchase 3 siRNAs per gene

Tired of wasting time with poorly designed siRNAs? *Silencer*[®] Pre-designed siRNAs—highly effective, ready-to-use siRNAs available for all human, mouse and rat genes—provide guaranteed gene silencing. Each one has been designed using a carefully optimized algorithm and then manufactured to exacting quality standards to provide potent and specific gene silencing.

Verify Gene Silencing Results and Save 18%

Journal article reviewers generally require that you verify gene silencing results with a second siRNA. *Silencer* Pre-designed siRNAs make it easy to comply. Ambion guarantees that at least two *Silencer* Pre-designed siRNAs will knockdown target mRNA levels by $\geq 70\%$ when three are purchased for the same gene.



Potency of *Silencer*[®] siRNAs at Low Concentrations. The algorithm Ambion uses to design *Silencer* Pre-designed siRNAs results in efficient gene silencing. Most *Silencer* siRNAs are effective at 3-10 nM.

Learn how you can get fast, easy and guaranteed siRNAs at
www.ambion.com/info/siRNA

Ambion RNAi Resources

On the Web: RNA Interference Resource

Protocols, data, references, and more
www.ambion.com/RNAi

Via Mail: RNA Interference Research Guide

New tools and techniques for performing RNAi
Request a free copy at www.ambion.com/contact/litreq

Via e-mail: Silencer E-Newsletter

Experimental tips, new tools for RNAi, and exclusive special offers
Sign up at www.ambion.com/contact/litreq

Via phone: RNAi Specialists

Assistance with experimental setup, design, and troubleshooting
See www.ambion.com/contact
for our full list of toll free phone numbers

GE Healthcare



Post impressionism by illustra Experts in the art of nucleic acid amplification

Introducing illustra from GE Healthcare. Our name is new. But you'll find some of our products like GenomiPhi, TempliPhi and Ready-To-Go Kits reassuringly familiar. That's because we have over 20 years' experience in nucleic acids.

And over the coming months, we'll be bringing some exciting new additions to our collection.

So when it's an amplification or purification product you need, there's only one name to remember: illustra.

Purify. Amplify. Simplify. **Life Sciences Re-imagined.**

The amplification and purification collection:

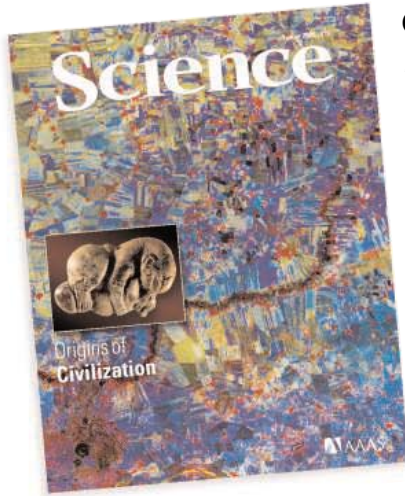
TempliPhi
GenomiPhi
PuReTaq Ready-To-Go PCR Beads
Hot Start Master Mix
QuickPrep
MicroSpin
Sephadex DNA Grade
MicroSpin S-300 HR Columns
GFX
AutoSeq
NAP Columns
RNAspin



imagination at work

illustra

www.gehealthcare.com/illustra



COVER

Merged satellite images from the 1960s and 1990s (30 km east-west by 40 km north-south) of the landscape of northeastern Syria, before intensive agriculture and other recent development altered ancient sites. The red spot near the center marks Tell Brak, the site of a massive ancient city that may have been home to one of the first urban civilizations. A nearby site yielded a stamp seal, dated to about 3500 B.C.E., in the shape of a lioness killing a calf or a gazelle. See page 1458.

Main image: Eric Rupley/University of Michigan; **inset:** Hamoukar Expedition/Oriental Institute/University of Chicago

DEPARTMENTS

- 1435 *Science Online*
- 1437 *This Week in Science*
- 1442 *Editors' Choice*
- 1444 *Contact Science*
- 1447 *NetWatch*
- 1449 *Random Samples*
- 1469 *Newsmakers*
- 1541 *New Products*
- 1542 *Science Careers*

EDITORIAL

- 1441 *Mission Creep in the IRB World*
by C. K. Gunsalus et al.

NEWS OF THE WEEK

- Florida Law Bans Academics From Doing Research in Cuba 1450
- Wild Birds Only Partly to Blame in Spreading H5N1 1451
- Ceramic Sponges That Sop Up Sulfur Could Boost Energy Technologies 1453
- >> *Report p. 1508*

SCIENCESCOPE

- Diversity Remains Elusive for Flagship NSF Program 1454
- Twenty Years After Chernobyl, Legal Fallout Lingers 1455
- Looking Way Back for the World's Climate Future 1456
- >> *Review p. 1485*
- Measuring the Hidden Cost of a Pay Raise 1456
- Ancient 'Reef' Stirs Debate Over Early Signs of Life in Australian Rocks 1457

NEWS FOCUS

- North Versus South, Mesopotamian Style 1458
 - Syria's Open Door: Will It Last?
 - At Home on a No-Frills Tell
 - A Rising Star in the Trenches
- Scandals Shake Chinese Science 1464
 - Crime Scene Investigation: How to Handle Misconduct
- DNA's Molecular Gymnastics 1467

1458



LETTERS

- Don't Sell Social Science Short D. S. Ojima et al. 1470
- Photosynthetic Oxygen Production W. Junge and J. Clausen. Response J. E. Penner-Hahn and C. F. Yocum; H. Dau and M. Haumann
- Making Choices Without Deliberating H. L. Bekker
- Response A. Dijksterhuis et al.

CORRECTIONS AND CLARIFICATIONS

1472

BOOKS ET AL.

- Unknown Quantity** A Real and Imaginary History of Algebra
J. Derbyshire, reviewed by V. Katz 1473

Browsings

1474

POLICY FORUM

- HIV Testing in China 1475
Z. Wu, X. Sun, S. G. Sullivan, R. Detels

PERSPECTIVES

- Evolutionary Response to Rapid Climate Change W. E. Bradshaw and C. M. Holzapfel 1477
- Toward Robots That Can Sense Texture by Touch R. Crowder >> *Report p. 1501* 1478
- Getting a Better Picture of the Ocean's Nitrogen Budget Z. S. Kolber >> *Report p. 1517* 1479
- Multiferroics as Quantum Electromagnets Y. Tokura 1481
- Microtubules Make Tracks for Cellulose C. Lloyd >> *Research Article p. 1491* 1482
- Can a Fraction of a Quantum Be Better Than a Whole One? C. M. Pegrum >> *Report p. 1495* 1483

Assistance!



SCIENCE @ WORK

At Sigma, we're pulling with you

For a change think inside the box and choose the assay kit that truly facilitates your cell biology research. You have better ways to spend your time than developing and validating cell biology assays. With more than 100 kits available, let our assay kits do the work for you.

Inside each kit is everything you need to make assaying simpler than ever before. Plus, we have technical experts on hand worldwide to further assist in getting the very best from your research.

Our assay kits are just one of the many cell biology solutions that we offer to more than a million scientists every day. From the widest selection of products to the best technical support, we're the research partner of choice around the world.

So when you need assistance in finding an easier way to assay, count on Sigma.

sigma.com/assaykits



SCIENCE EXPRESS

www.scienceexpress.org

ECOLOGY

The Importance of Demographic Niches to Tree Diversity

R. Condit et al.

Data from a vast long-term survey of tropical forests contradict the prevailing view that tree species richness results from variability in rates of recruitment and mortality.

10.1126/science.1124712

MICROBIOLOGY

Selective Silencing of Foreign DNA with Low GC Content by the H-NS Protein in *Salmonella*

W. W. Navarre et al.

Bacteria can recognize and silence invading foreign DNA by virtue of its lower overall GC content.

10.1126/science.1128794

ASTROPHYSICS

Massive-Star Supernovae as Major Dust Factories

B. E. K. Sugerman et al.

A 2003 supernova produced 10 times the dust seen after other such stellar explosions, implying that supernovae were dust factories in the early universe.

10.1126/science.1128131

CELL BIOLOGY

Polo-Like Kinase Cdc5 Controls the Local Activation of Rho1 to Promote Cytokinesis

S. Yoshida et al.

In yeast, regulatory enzymes work together to activate actin in the contractile ring, causing it to constrict and separate daughter cells during cell division.

10.1126/science.1126747

REVIEW

OCEANS

The Pliocene Paradox (Mechanisms for a Permanent El Niño)

A. V. Fedorov et al.

>> *News story p. 1456*

1485

BREVIA

PLANETARY SCIENCE

The Breakup of a Main-Belt Asteroid 450 Thousand Years Ago

D. Nesvorný, D. Vokrouhlický, W. F. Bottke

The close orbits of six objects around the asteroid Datura suggest that it partially broke up in response to a collision just 450,000 years ago.

1490

RESEARCH ARTICLE

PLANT SCIENCE

Visualization of Cellulose Synthase Demonstrates Functional Association with Microtubules

A. R. Paredez, C. R. Somerville, D. W. Ehrhardt

Cellulose synthase makes and deposits cellulose along plant cell walls as it is carried along microtubules.

>> *Perspective p. 1482*

1491

REPORTS

APPLIED PHYSICS

Flip-Flopping Fractional Flux Quanta

T. Ortlev et al.

The *d*-wave symmetry of high-temperature superconductors can be manipulated to form a logic gate in an electronic circuit.

>> *Perspective p. 1483*

1495

PHYSICS

Coherent State Evolution in a Superconducting Qubit from Partial-Collapse Measurement

N. Katz et al.

Partial measurement of the quantum state of a superconducting qubit can be used to probe and control it while avoiding the collapse often caused by a complete measurement.

1498

APPLIED PHYSICS

High-Resolution Thin-Film Device to Sense Texture by Touch

V. Maheshwari and R. F. Saraf

A sensor composed of alternating gold and cadmium sulfide nanoparticle layers is as sensitive as the human finger and could be useful in robotic surgery or other applications.

>> *Perspective p. 1478*

1501

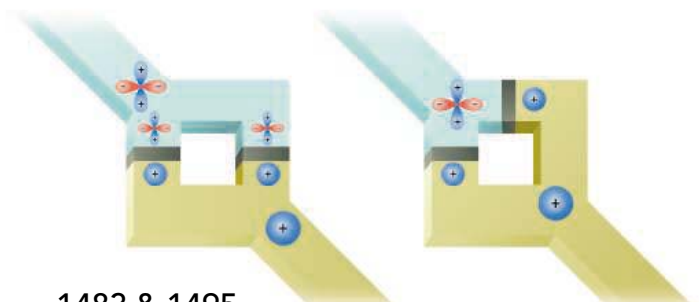
MATERIALS SCIENCE

Converting Ceria Polyhedral Nanoparticles into Single-Crystal Nanospheres

X. Feng et al.

Combining titanium with ceria in a flame produces spherical rather than jagged nanoparticles that efficiently cut and smoothly polish silicon wafers for chips.

1504



1483 & 1495

CONTENTS continued >>



HUMAN FRONTIER SCIENCE PROGRAM

12 Quai Saint-Jean, 67080 Strasbourg Cedex, FRANCE
Phone: +33 (0)3 88 21 51 27/34 Fax: +33 (0)3 88 32 88 97
E-mail: fellow@hfsp.org Web site: <http://www.hfsp.org>

POSTDOCTORAL OPPORTUNITIES FOR INTERDISCIPLINARY RESEARCH IN THE LIFE SCIENCES

The Human Frontier Science Program (HFSP) supports basic research in the life sciences with emphasis on **novel, innovative, and interdisciplinary** approaches that involve scientific exchange across national and disciplinary boundaries. Recent developments in emerging fields at the interface of biological and physical sciences open up new approaches to understand the mechanisms of living organisms. This indicates a clear need for participation of scientists from outside the life sciences to reveal the structures and networks that characterize the living state. Therefore the HFSP supports postdoctoral investigators who explore new areas within the life sciences or who use their expertise in chemistry, physics, mathematics, computer science, or engineering to bear on a biological question. Initially the program provides **fellowships for training of postdoctoral researchers** in another country (~150K USD over 3 years). HFSP fellows returning to their home country may then apply for a Career Development Award (300K USD over 3 years) to start their independent research program.

Nationals from one of the HFSP supporting countries can apply to work in any other country, while other nationals can apply for training only in a supporting country. Current supporting members are: *Australia, Canada, the European Union, France, Germany, Italy, Japan, the Republic of Korea, New Zealand, Switzerland, the United Kingdom, and the United States of America.*

Important fellowship deadlines for award year 2007:
Compulsory pre-registration for password: **24 August 2006**
Submission of applications: **31 August 2006**

Long-Term Fellowships

Long-Term Fellowships are intended for applicants with a Ph.D. degree in the life sciences who are expected to **broaden their horizon and to move into a new research area that is different from their doctoral studies or previous postdoctoral training.** Applicants that propose a significant departure from their previous research are viewed favorably.

Cross-Disciplinary Fellowships

Cross-Disciplinary Fellowships are intended for applicants with a Ph.D. degree in physics, chemistry, mathematics, engineering, or computer sciences who wish to **gain research experience in the life sciences in proposing a significant change in discipline.** Those with some experience in the life sciences are expected to move into a new research area.

Fellows receive support for up to 3 years of training in an outstanding laboratory of their choice in another country. The final year can be used to return to the home country. As a rule, fellows who choose to return to their home country can defer their final year for up to two years for extended research training while being funded through other sources. HFSP fellows who return to their home country are **invited to apply for a Career Development Award** to establish themselves as independent young investigators.

The online submission system will become available in summer 2006 on the HFSP web site.

Short-Term Fellowships

Short-Term Fellowships are intended for researchers early in their careers and provide up to 3 months of support to **learn techniques in a new area of research or establish new collaborations in another country.** Applications are accepted throughout the year.

Application guidelines with more details are available on the HFSP web site (www.hfsp.org).

REPORTS CONTINUED...

CHEMISTRY

Regenerative Adsorption and Removal of H₂S from Hot Fuel Gas Streams by Rare Earth Oxides 1508

M. Flytzani-Stephanopoulos, M. Sakhodin, Z. Wang
Hydrogen sulfide, an inhibitor of solid-oxide fuel cells, can be removed by cerium and lanthanum oxides and then regenerated with any sulfur-free gas.

>> *News story p. 1453*

CLIMATE CHANGE

Near-Synchronous Interhemispheric Termination of the Last Glacial Maximum in Mid-Latitudes 1510

J. M. Schaefer et al.
Dates on moraines from mid-latitudes around the world imply that after the last Ice Age glaciers retreated simultaneously in response to warming by increased CO₂ levels.

CLIMATE CHANGE

Changes in North Atlantic Radiocarbon Reservoir Ages During the Allerød and Younger Dryas 1514

S. Bondevik, J. Mangerud, H. H. Birks, S. Gulliksen, P. Reimer
Different radiocarbon ages of the atmosphere and North Atlantic trace shifts in ocean circulation and upwelling during climate fluctuations 15,000 to 10,000 years ago.

ECOLOGY

Transatlantic Abundance of the N₂-Fixing Colonial Cyanobacterium *Trichodesmium* 1517

C. S. Davis and D. J. McGillicuddy Jr.
The higher than expected abundance of a cyanobacterium in the Sargasso Sea suggests that its contribution to the oceanic nitrogen cycle is larger than has been assumed.

>> *Perspective p. 1479*

PLANT SCIENCE

TOPLESS Regulates Apical Embryonic Fate in *Arabidopsis* 1520

J. A. Long, C. Ohno, Z. R. Smith, E. M. Meyerowitz
A gene product specifies which cells make up the plant shoot by coordinating repression of transcription, probably of root-associated genes.

MICROBIOLOGY

Tim50 Maintains the Permeability Barrier of the Mitochondrial Inner Membrane 1523

M. Meinecke et al.
An opportunistic bacterial pathogen found in patients with cystic fibrosis contains a previously undescribed secretory apparatus that may be necessary for its virulence.

CELL BIOLOGY

A Virulence Locus of *Pseudomonas aeruginosa* Encodes a Protein Secretion Apparatus 1526

J. D. Mougous et al.
A regulatory protein blocks the large channels in the mitochondrial inner membrane, maintaining the mitochondrion's essential proton gradient.

MEDICINE

Preserved CD4⁺ Central Memory T Cells and Survival in Vaccinated SIV-Challenged Monkeys 1530

N. L. Letvin et al.
Monkeys infected with a cousin of the HIV virus and showing a robust immediate immune response have better immune memory for the virus later and survive longer.

NEUROSCIENCE

Long-Term Potentiation of Neuron-Glia Synapses Mediated by Ca²⁺-Permeable AMPA Receptors 1533

W.-P. Ge et al.
Synapses between hippocampal neurons and nearby glial cells can become stronger after stimulation, just as excitatory neuron-neuron synapses can show long-term potentiation.

NEUROSCIENCE

Language Control in the Bilingual Brain 1537

J. Crinion et al.
As bilingual people speak one language and then the other, their basal ganglia switch the specific processing circuits accordingly.



1520



ADVANCING SCIENCE. SERVING SOCIETY

SCIENCE (ISSN 0036-8075) is published weekly on Friday, except the last week in December, by the American Association for the Advancement of Science, 1200 New York Avenue, NW, Washington, DC 20005. Periodicals Mail postage (publication No. 484460) paid at Washington, DC, and additional mailing offices. Copyright © 2006 by the American Association for the Advancement of Science. The title SCIENCE is a registered trademark of the AAAS. Domestic individual membership and subscription (51 issues): \$139 (\$74 allocated to subscription). Domestic institutional subscription (51 issues): \$650; Foreign postage extra: Mexico, Caribbean (surface mail) \$55; other countries (air assist delivery) \$85. First class, airmail, student, and emeritus rates on request. Canadian rates with GST available upon request, GST #1254 88122. Publications Mail Agreement Number 1069624. Printed in the U.S.A.

Change of address: Allow 4 weeks, giving old and new addresses and 8-digit account number. Postmaster: Send change of address to AAAS, P.O. Box 96178, Washington, DC 20090-6178. Single-copy sales: \$10.00 current issue, \$15.00 back issue prepaid includes surface postage; bulk rates on request. Authorization to photocopy material for internal or personal use under circumstances not falling within the fair use provisions of the Copyright Act is granted by AAAS to libraries and other users registered with the Copyright Clearance Center (CCC) Transactional Reporting Service, provided that \$18.00 per article is paid directly to CCC, 222 Rosewood Drive, Danvers, MA 01923. The identification code for Science is 0036-8075. Science is indexed in the Reader's Guide to Periodical Literature and in several specialized indexes.

CONTENTS continued >>>



www.roche-applied-science.com



Genome Sequencer 20 System

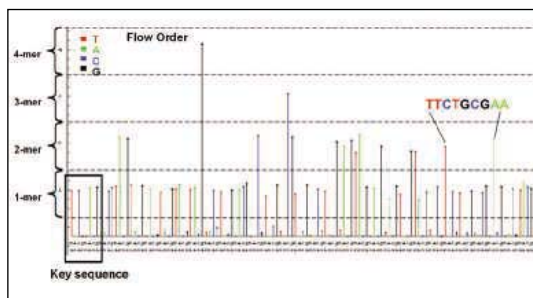
First to the Finish

Sequence genomes like never before

- Compare microbial genomes in weeks, not years
- *De novo* sequence a bacterial genome in fewer than 5 days
- Sequence more than 100 BACs per month
- Sequence >200,000 miRNAs, SAGE tags, or ditags (e.g., CAGE) in 5.5 hours

Coming soon:

Ultra-deep sequencing of amplicons – identify rare SNP patterns or cancer-associated mutations from complex samples



Flowgram of a GS 20 read

Harness the horsepower of the newest revolution in sequencing today — visit www.roche-applied-science.com/sis/sequencing/genome or contact your local sales representative.

454 LIFE SCIENCES



Diagnostics



miRNA in fly and plant immune responses.

SCIENCE'S STKE

www.stke.org SIGNAL TRANSDUCTION KNOWLEDGE ENVIRONMENT

PERSPECTIVE: Innate Immune Defense Through RNA Interference

J. H. Fritz, S. Girardin, D. J. Philpott

From *Drosophila* to *Arabidopsis*, RNAi provides protection from microbial infection.

ST ON THE WEB: Flymove

This site offers multimedia resources for learning about developmental biology using the model organism *Drosophila*; in Educator Sites.

ST ON THE WEB: LOCATE—Subcellular Localization Database

Find out where in the cell a protein resides using this searchable and browseable database of mouse proteins; in Protein Databases.

WRN activity stops in cancer cells.



SCIENCE'S SAGE KE

www.sageke.org

SCIENCE OF AGING KNOWLEDGE ENVIRONMENT

NEWS FOCUS: The Age of Cancer

M. Leslie

Cancer cells quiet gene behind premature aging disorder.

GENETICALLY ALTERED MICE: Werner Mice

Several strains designed to model a premature aging syndrome are described.

SCIENCE NOW

www.sciencenow.org DAILY NEWS COVERAGE

See Spot Recover

Dogs cured of an immune disease could point to better gene therapy.

Wriggle for Your Lives!

When snakes attack, frog embryos pop from their eggs and skedaddle.

An Asteroid, Cobbled Together

After a long, problematic journey, a spacecraft is finally revealing secrets of a porous asteroid.

No longer a gusher for chemists.

SCIENCE CAREERS

www.sciencereers.org

CAREER RESOURCES FOR SCIENTISTS

UK: A Melting Pot for Postdocs

A. Forde

Postdoc training that brings together an interdisciplinary group of researchers has interesting career consequences.

US: Marketing Molecules

J. Kling

Biology and nanotechnology start-ups get headlines, but chemistry also offers plenty of entrepreneurial opportunities.

US: 'P' Is for Petroleum

GrantDoctor

The narrowed scope of the American Chemical Society's Petroleum Research Fund means fewer funding opportunities for chemists.

GRANTSNET: International Grants and Fellowship Index

A. Kotok

Get the latest listing of funding opportunities from Europe, Asia, and the Americas.



SCIENCE PODCAST



Listen to the 9 June edition of the *Science* Podcast to hear about a new touch sensor for robotics, how ideas on the earliest cities are changing, the workings of the bilingual brain, and other stories.

www.sciencemag.org/about/podcast.dtl

Separate individual or institutional subscriptions to these products may be required for full-text access.








yield of dreams.

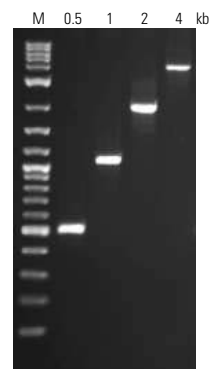
Taq DNA Polymerase from New England Biolabs

HIGH YIELD, ROBUST AND RELIABLE PCR REACTIONS IN CONVENIENT FORMATS

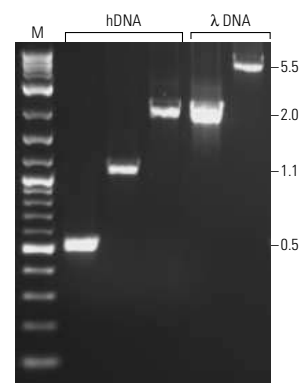
Looking for the right solution for your high yield PCR? Choose recombinant *Taq* DNA Polymerase from New England Biolabs. As the leader in enzyme technology, New England Biolabs provides the highest quality recombinant *Taq* at exceptional value. Our expanded selection of *Taq* based products includes kits, master mixes, and a choice of reaction buffers. Choose *Taq* DNA polymerase from NEB for guaranteed Performance, Convenience and Results.

- **Taq with Standard Buffer**  **M0273S/L**
Compatible with existing assay systems and high throughput applications, is always detergent free and available with or without MgCl₂
- **Taq with ThermoPol Buffer**  **M0267S/L**
Promotes high yields under demanding conditions, available with or without MgSO₄ and detergent
- **Taq 2X Master Mix**  **M0270S/L**
Just add template and primers
- **NEW Quick-Load™ Taq 2X Master Mix**  **M0271S/L**
Load PCR products directly onto agarose gels
- **Taq PCR Kits**  **E5000S/E5100S**
Contains reagents for 200 PCR reactions, available with or without controls

 = Recombinant



Selective and specific PCR amplification from Human Genomic DNA: Specific amplicons of 0.5, 1, 2, and 4 kb from human genomic DNA were amplified by *Taq* DNA Polymerase with Standard Buffer for 30 cycles. Marker (M) shown is 2-Log DNA Ladder (NEB #N3200).



Versatility of the Taq 2X Master Mix: 30 ng human genomic DNA (hDNA) or 0.1 ng lambda DNA (λ DNA) was amplified in the presence of 200 nM primers in a 25 μl volume. Marker (M) shown is 2-Log DNA Ladder (NEB #N3200).

For more information and international distribution network, please visit www.neb.com

- **New England Biolabs Inc.** 240 County Road, Ipswich, MA 01938 USA 1-800-NEB-LABS Tel. (978) 927-5054 Fax (978) 921-1350 info@neb.com
- **Canada** Tel. (800) 387-1095 info@ca.neb.com
- **Germany** Tel. 0800/246 5227 info@de.neb.com
- **UK** Tel. (0800) 318486 info@uk.neb.com
- **China** Tel. 010-82378266 beijing@neb-china.com



In Southern Time

Ice core records have shown that during the last deglaciation, temperatures in Antarctica began to rise around 18,000 years ago, about 3000 years before similar signals are seen for Greenland. How did temperatures change at the intervening latitudes? **Schaefer *et al.*** (p. 1510) addressed this puzzle by determining the dates at which a variety of mid-latitude glaciers from both hemispheres began to retreat, using ^{10}Be dating of terminal moraines, and comparing their data with an even larger database of existing measurements. These glaciers all began to retreat at about the same time, mostly between 19,000 and 17,000 years ago, which is consistent with rising temperatures in Antarctica and the global increase of atmospheric CO_2 concentrations. These data support the idea that the last glacial termination was forced by greenhouse gases, and suggest that warming in the high northern latitudes was delayed by the occurrence of hypercold winters.

Coming Attractions from the Pliocene?

During the Pliocene, solar insolation and CO_2 levels were similar to present conditions, but the poles were warm enough that there were no ice sheets in the Northern Hemisphere, and sea level was 25 meters higher than at present. **Fedorov *et al.*** (p. 1485; see the news story by **Kerr**) review observations of and theories about climate in the early Pliocene (from 5 to 3 million years ago) and discuss how these might be reconciled.

Superconductor Logic

It has been proposed that the d -wave symmetry of high-temperature superconductors could provide the possibility of a π -phase element, an important tool for logical operations in which the memory is stored as polarity of the magnetic flux. **Ortlepp *et al.*** (p. 1495, published online 20 April; see the Perspective by **Pegrum**) report the design and test of a flip-flop gate based on fractional flux quanta in a high-temperature superconductor circuit.

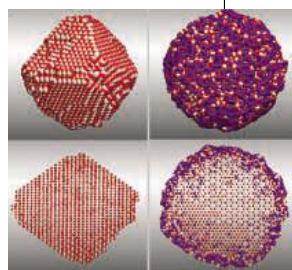
Spying on Solid-State Qubits

Quantum computation requires the manipulation of superpositions of quantum mechanical states and making measurements of the final state of the system. Dephasing and decoherence processes influence how the system (or the wave function describing the system) evolves and requires the use of error correction. However, error correction itself requires measurements that

usually would collapse the somewhat fragile quantum states. **Katz *et al.*** (p. 1498) make partial quantum measurements on a solid-state qubit in which the wave function neither completely evolves nor completely collapses. Such a partial measurement can then be used to provide feedback on the evolution and control of the qubit.

Abrasives in the Round

A primary use for cerium oxide (ceria) nanoparticles is as an abrasive for the planarization and polishing of semiconductor wafers. However, the particles tend to have faceted shapes that scratch the wafers and lead to the formation of defects on the polished surface. **Feng *et al.*** (p. 1504) find that the addition of titanium to the flame-processing method produces rounded particles with no sharp facets. The particles develop an outer shell of titanium oxide that reduces the surface energy and favors a more spherical shape. These rounded particles increase the silica removal rate and produce fewer defects in the wafers.



Touch and Glow

Artificial tactile sensors with sensitivity comparable to human fingers would be especially useful for robotic surgery applications. In general, however, scaling up such devices beyond millimeter dimensions has been a major hurdle. **Maheshwari and Saraf** (p. 1501; see the Perspective by

Crowder) fabricated a thin-film sensor that is large enough to image a penny and that, like a finger, achieves a height resolution of less than 5 micrometers at 10 kilopascals of applied pressure. The fabrication process relies on simple self-assembly of alternating gold and semiconducting (CdS) nanoparticle layers, separated by dielectric layers. At biases greater than 8 volts, applied stress enhances electron tunneling between the layers and induces electroluminescence that is linearly proportional to the pressure, which is then detected with a charge-coupled device camera

Scrubbing Sulfur

The potential usefulness of high-temperature solid oxide fuel cells that can run on hydrocarbon fuels is limited by the sensitivity of their nickel-based anodes to sulfur impurities. One way to combat sulfur poisoning is to convert the fuel to reformat (CO and H_2) and then remove hydrogen sulfide (H_2S) with a sorbent, but sorbents have proven difficult to regenerate in high-temperature operation. **Flytzani-Stephanopoulos *et al.*** (p. 1508; see the news story by **Service**) demonstrate reversible adsorption of H_2S on cerium and lanthanum oxide surfaces at temperatures as high as 800°C . The sorbent would be cycled between scrubbing incoming reformat of H_2S and using the spent fuel to desorb the sulfur and regenerate a fresh surface. The flow rates can be high enough to reduce contact times to the millisecond range while still reducing H_2S to levels below 1 part per million.

Continued on page 1439



Advancing RNAi Technology.

Dharmacon...the world's most trusted siRNA resource

- The largest and most referenced siRNA supplier
- Target any unique human, mouse or rat gene
- Highest level of guaranteed silencing available
- Innovative technologies to enhance specificity
- Breakthrough siRNA transfection reagents
- Expert technical support

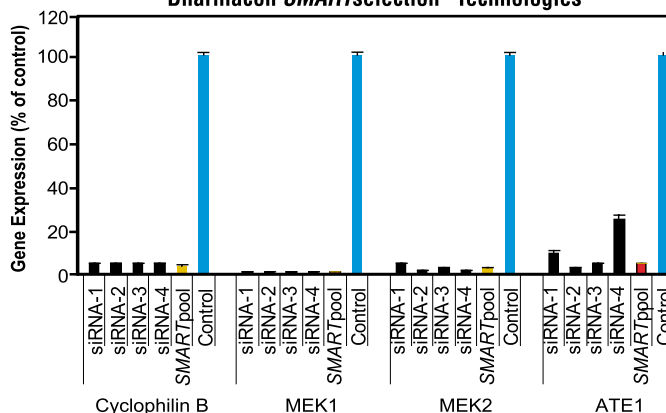
Leading RNAi researchers count on Dharmacon's state-of-the-art *SMARTselection*[™] and *SMARTpool*[®] technologies for potent and specific gene silencing. Four individual siRNAs and a *SMARTpool* siRNA reagent are available for over 66,000 unique human, mouse, and rat genes - each with the industry's best performance guarantee and backed by our expert technical support. Simply use our on-line *siGENOME*[™] search tool to identify the siRNA reagents for your target gene.

No wonder Dharmacon is the most frequently referenced siRNA supplier in peer-reviewed journals!



Want to know more about RNAi?
Visit our website to request your FREE copy of the RNAi Technical Reference & Application Guide today.

Potent Gene Silencing with Dharmacon *SMARTselection*[™] Technologies



DHARMACON
RNA TECHNOLOGIES

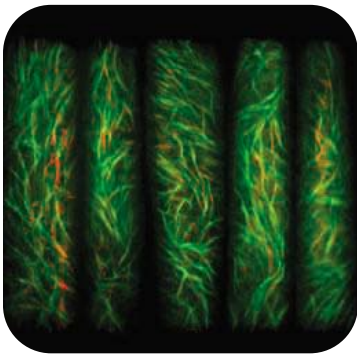
Continued from page 1437

Which Way Is Up?

Plants need to determine which end is “up” long before they emerge as seedlings from the ground. For *Arabidopsis*, the first indications of an apical-basal axis are seen in the initial embryonic cell division that separates a smaller apical cell from a larger basal cell. These cells generally go on to form shoots or roots. **Long et al.** (p. 1520) have now cloned the *topless* gene, mutations in which can alter the fate of the apical pole. The TOPLESS protein bears features that resemble transcriptional co-repressors. Mutations in a histone deacetylase affect Topless function, and thus chromatin remodeling likely plays a key role. These findings suggest that auxin-mediated axis formation precedes transcription-mediated axis stabilization.

Special Secretion Makes for Virulence

Virulence factors are important in converting harmless bacteria into effective pathogens. **Mougous et al.** (p. 1526) provide evidence for an unusual form of bacterial protein secretion in *Pseudomonas aeruginosa* that is important in the control of virulence in the late stages of chronic infection in cystic fibrosis patients. The major protein exported by the secretion apparatus is Hcp1. The authors present the crystal structure of Hcp1, which forms a hexameric ring with a large internal diameter, and suggest that it acts as a conduit for the passage of exported proteins.



Directing Plant Cell Growth

Plant cells are surrounded by a cell wall made up of cellulose fibrils, and these fibrils are synthesized by a large multisubunit complex that is embedded in the plasma membrane. **Paredes et al.** (p. 1491, published online 20 April; see the Perspective by **Lloyd**) visualized the activity of this enzyme, cellulose synthase, in living plant cells using fluorescent tags. Movies show the cellulose synthases moving along trajectories defined by microtubules. The organization of the microtubules directs the organization of the growing cellulose fibrils which, in turn, may govern the shape of the growing cell.

Surviving SIV

Any future HIV (human immunodeficiency virus) vaccine will rely on inducing either antibodies that neutralize the virus, or cell-mediated immunity by cytotoxic T lymphocytes (CTLs). The former initiative is being frustrated by the ability of the virus to mutate and escape antibody binding. Although a related problem of viral escape is faced by CTLs, it does appear that a robust cell-mediated immune response can lower the levels of replicating virus after acute infection, and this set-point is known to affect the course of subsequent infection and progression to AIDS. Using infection of monkeys with the pathogenic SIV, the simian cousin of HIV, **Letvin et al.** (p. 1530) offer direct experimental evidence that generation of a robust cellular response by vaccination corresponds with increased survival. This finding also correlated with the persistence of high numbers of so-called central memory T cells and suggests that finding ways of preserving these important lymphocytes may help in improving cell-mediated HIV vaccines.

Language Control Tower

New words can arise when they are introduced into one language from another. Until these words become widely familiar, they are likely to cause monolingual individuals to stumble when hearing or reading them. Bilinguals, of course, encounter no such problems. How these individuals switch smoothly between languages has been mysterious; in neuroimaging studies, the two languages activate precisely the same brain areas. **Crinion et al.** (p. 1537) have used a semantic priming task as a finer probe of behavioral and neural adaptation in populations of German-English and Japanese-English bilinguals. They identify the left caudate, which is part of the basal ganglia, as an area that monitors which language is being used and switches the processing machinery into the appropriate mode.

CREDIT: PAREDEZ ET AL.

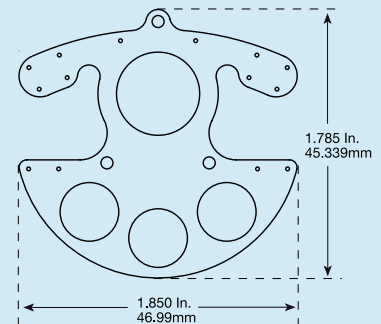
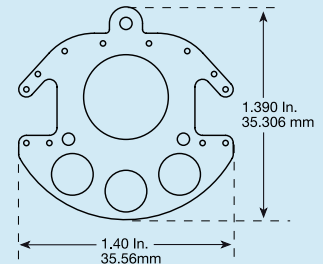
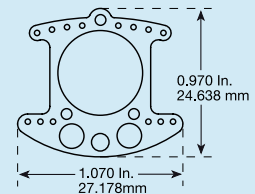
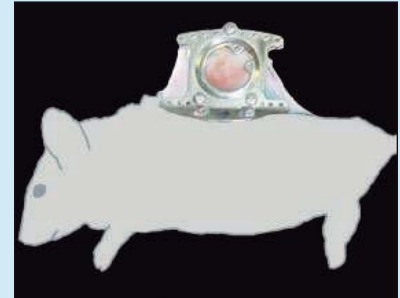
CLEARLY OBSERVE & RECORD

Now, with the **TITANIUM DORSAL SKINFOLD CHAMBER** you can see anti-tumor effects and early vascular events.

Allows you to nondestructively record and visualize microvascular functions.

Uses standard 12mm microscope glass slips.

Titanium Construction.



APJ TRADING CO., INC.

(805) 368-6701

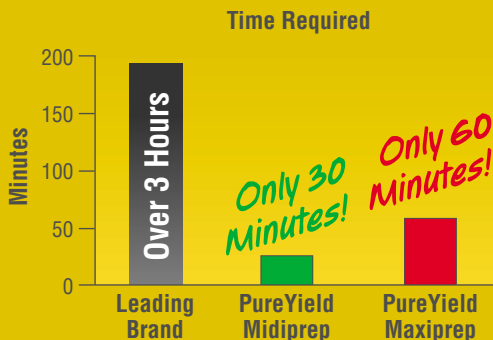
FAX 805/639/0142

E-Mail: apjpaul@aol.com

www.apjtrading.com



and maxiprep
Break the midiprep^v speed limit.



New **PureYield™** plasmid preps deliver transfection-quality DNA in record time. Recover up to 1mg of plasmid DNA in less than 60 minutes (maxiprep) or up to 200µg in only 30 minutes (midiprep). No post-elution alcohol precipitation required. Race through your next plasmid prep.

Request a **FREE SAMPLE*** at: www.promega.com/pureyield

*Samples to qualified customers where available, while supplies last.

Mission Creep in the IRB World

The authors are all at the University of Illinois Urbana-Champaign and participated in the Center for Advanced Study Steering Committee to Study Human Research Protections.

C. K. Gunsalus, Edward M. Bruner, Nicholas C. Burbules, Leon Dash, Matthew Finkin, Joseph P. Goldberg, William T. Greenough, Gregory A. Miller, and Michael G. Pratt.

THE SYSTEM IN THE UNITED STATES FOR PROTECTING HUMAN PARTICIPANTS IN RESEARCH engages the earnest efforts of thousands of scientists, community volunteers, and administrators. Through untold hours of service on Institutional Review Boards (IRBs), they watch over the safety of human research subjects. Unfortunately, much of that effort is increasingly misdirected as the system succumbs to “mission creep” that could compromise its central goals. Our IRB system is endangered by excessive paperwork and expanding obligations to oversee work that poses little risk to subjects. The result is that we have simultaneous overregulation and underprotection.

IRBs were established after the 1979 Belmont Report from the Department of Health, Education, and Welfare, with the goal of protecting human subjects involved in potentially risky medical and behavioral research. But IRBs’ burdens have grown to include studies involving interviews, journalism, secondary use of public-use data, and similar activities that others conduct regularly without oversight. Most of these activities involve minimal risks—surely less than those faced during a standard physical or psychological examination, the metric for everyday risk in the federal regulations. And IRBs are pressured to review an expanding range of issues from research design and conflicts of interest to patient privacy. These are beyond the scope of research protection and are best left to others.

The IRB system is being overwhelmed by a focus on procedures and documentation at the expense of thoughtful consideration of the difficult ethical questions surrounding the welfare of human subjects, especially as complex clinical trials burgeon. Their work is afflicted by unclear definitions of terms such as “risk,” “harm,” and “research.” Because ethical behavior is difficult to measure, many IRBs rely on stylized documentation over substantive review, out of concern that one case in a thousand could slip through and generate bad publicity or penalties, or potentially shut down research. The result is that many protocols receive exaggerated review, and the paper piles up. Society loses as potentially productive research is discouraged or self-censored.

Ironically, this obsession with paperwork and mechanical monitoring may undermine protection of human subjects. IRB members spend too much time editing documents, marking typos, and asking for more details.

One researcher, 10 years into a longitudinal study, was asked by an IRB to remove the term “anemia” from consent forms because participants might not understand it. Such actions, about which we hear frequently, carry a serious risk: They reduce trust in the guidance of IRBs and may alienate some researchers enough to turn them into scofflaws.

Oversight of the IRB process by federal agencies reinforces these tendencies. “Poor or missing ‘Standard Operating Procedures’” and “poor minute-keeping” account for about half of all U.S. Food and Drug Administration citations, and quorum failures for another 13%, according to one review. In seeking compliance, universities have multiplied the number of IRBs, depleting the supply of willing and competent faculty. All this has generated a trend in which researchers increasingly think of IRBs as the “ethics police.” In fact, all researchers must take primary responsibility for professional, ethical conduct. Our systems should reinforce that, not work against or substitute for it; the IRB should be a resource, not the source, for ethical wisdom. All compliance systems require the buy-in and collaboration of the regulated, and it will be a sad day if scholars come to see human protection in research as the source of frustrating delays and expensive paperwork.

What can be done? Our University of Illinois white paper,* based on 2 years of study after an interdisciplinary conference of researchers and IRB leaders, addresses the problems of mission creep and offers possible solutions. Our recommendations include the exemption from IRB oversight of some activities that have ethical standards of their own, distinct from the biomedical tradition. We also support gathering information in a national clearinghouse that supports IRBs and researchers alike. This would provide examples of good and poor practices rooted in disciplinary standards, and help IRBs make priority determinations about what constitutes risk and harm in different human research settings.

The IRB system is in trouble, and that means trouble for the safety and efficacy of research on human subjects. We should refocus our efforts on the core issues and stop expanding the mission into less productive territory.

— C. K. Gunsalus, Edward M. Bruner, Nicholas C. Burbules, Leon Dash, Matthew Finkin, Joseph P. Goldberg, William T. Greenough, Gregory A. Miller, Michael G. Pratt



10.1126/science.1121479

* www.law.uiuc.edu/conferences/whitepaper/

ECOLOGY

From Acorns to Lyme Disease

Lyme disease, caused by the spirochaete bacterium *Borrelia burgdorferi*, has acquired notoriety in the United States and wilder parts of Europe. It is transmitted by blood-sucking ticks, usually among deer and small mammals. But Ixodes ticks are not fussy and will feed on any vertebrate, including humans. As human activities encroach into wooded and heathland environments, we run the risk of tick infestation and possible Lyme disease transmission. For 13 years, Ostfeld *et al.* looked at the environmental parameters that might predict how severe the upcoming Lyme season might be. Classically, deer abundance and weather were thought to influence numbers of ticks and hence predict the risk of human infection, but it turns out that small mammal abundance over the previous year is a much better indicator. Mice and chipmunks, whose numbers are determined by food supply in the prior year, are important hosts for the tiny juvenile stages of the ticks, which, because they are unnoticeable, tend not to be removed from the skin and can be extremely abundant in summer. Consequently, the acorn supply for mice and chipmunks 2 years previously makes an excellent measure of Lyme disease risk. — CA

PLoS Biol. 4, e145 (2006).



Acorns (right) and mouse (left).

EVOLUTION

Counting Sheep

The environment can be a powerful force in evolution, as the great mass extinctions across geological time testify. Yet classical models of the genetics of populations often assume the simplifying condition of a constant environment, begging the question of what happens to the heritability and selection of specific traits in times of change. Details of the phenotype of Soay sheep—first introduced to the Scottish archipelago of St. Kilda in the Bronze Age and to the main island of Hirta in 1932—have been collected since 1985 and provide a case study of microevolution through changeable times.

Wilson *et al.* analyzed the birth weight of Soay sheep across a 20-year period during which the sheep experienced both low and high mortality rates associated with changing environmental circumstances. Birth weight is a heritable trait that is under potentially strong selective pressure, with

larger lambs having a better chance of survival. Under harsh conditions, the researchers find that their models are consistent with a strong selection for increased birth weight among lambs, which is also associated with a low genetic variation. Favorable conditions result in a reduced selection on birth weight. Thus, for this trait in Soay sheep, the environment acts as a constraint on the microevolutionary potential of the population. — GR

PLoS Biol. 4, e216 (2006).

ANTHROPOLOGY

From Fertile Soil to Fertile Society?

The rise of agriculture at the beginning of the Holocene era is thought to have contributed to large increases in ancient populations. One measure of population growth that can be evaluated with reasonable certainty based on archaeological evidence is the number of juveniles in grave sites. Growing populations have proportionally more children, whereas the converse is true of populations in decline.

Bocquet-Appel and Naji studied the skeleton records in 62 ancient North American cemeteries, and observed that local societal transitions from foraging to agriculture were followed by a significant increase in the juvenile (aged 5 to 19) human remains. This trend parallels a similar but earlier transition in Europe. Thus, regardless of

when agriculture developed globally, it appears to have occasioned a local increase in birth rate (and consequently population) during the ensuing several hundred years. The global data hint that many foraging populations may have stagnated in the years approaching the various transitions, or even declined slightly on account of taxed resources or emerging diseases — BH

Curr. Anthro. 47, 341 (2006).

ECOLOGY

Bleach Prospects for Reef Recovery

Coral bleaching, whereby corals lose their photosynthetic algal symbionts, is now widespread throughout tropical reefs. Loss of algae from corals severely reduces nutrient flow through these ecosystems, with worrying impacts on the diversity and biomass of other reef-dwelling organisms, especially fish. Evidence is fast accumulating that warming events trigger these events. Less is known, however, about the ability of reef communities to recover from bleaching. Graham *et al.* assessed the changes that took place after the bleaching of 75 to 90% of coral in the Seychelles in 1998, the result of a strong El Niño event that year. A total of 50,000 m² were surveyed. The structure of the reef habitats changed markedly after the death of branching and soft corals. By 2005, the structural complexity of the reefs was reduced, and the habitats were dominated by rubble, encrusting corals, and algal fields. There were concomitant reductions in fish diversity, including some local extinctions. The



Soay sheep.

CREDITS (TOP TO BOTTOM): KELLY OGGENFUS/INSTITUTE OF ECOSYSTEM STUDIES, ALASTAIR WILSON/UNIV. OF EDINBURGH

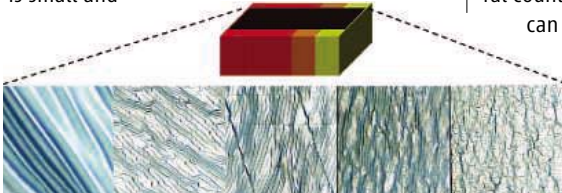
recovery of the reefs has been slower than typically observed in more-continental reefs, probably because of the isolation of the Seychelles, which would reduce the rate of dispersal of larvae from elsewhere. If bleaching events are regular, the prospects for recovery are not good. — AMS

Proc Natl. Acad. Sci. U.S.A. **103**, 8425 (2006).

MATERIALS SCIENCE

Buckle Up for Softy

Tensile or compressive tests to measure the elastic modulus of a material are often limited by the size and shape of test specimens. Local indentation probing is useful for hard metals or ceramics, but less so for soft materials. The elastic modulus is a stiffness indicator but also reflects such properties as adhesion and swelling. Researchers are seeking alternative methods to measure complex samples such as a contact lens, which is small and



Hydrogel buckling patterns (cross-linker concentration increases from left to right).

soft and may need to be studied under hydrated conditions.

Wilder *et al.* address this problem by inverting a technique used to characterize thin films. They measure the modulus of a compressed polymer by coating the surface with a stiffer material of known modulus. The periodicity of the buckling response depends primarily on the modulus ratio between the stiff film and softer substrate, and thus the unknown modulus can be determined from optical measurements of

the buckled film. Modulus values from measurements of a model poly(dimethylsiloxane) system coated with a polystyrene film agreed well with those obtained from compression tests. The technique can also quantify spatial variations in modulus through a single experiment, as demonstrated on a hydrogel sample that was prepared with a spatial concentration gradient of cross-linking agent. — MSL

Macromolecules **39**, 10.1021/ma060266b (2006).

CHEMISTRY

Anion Induction

In traditional asymmetric catalysis, a chiral catalyst binds directly to the reagent and thereby facilitates the reaction path to one product isomer while hindering the path to its enantiomer, or mirror image. Mayer and List show that asymmetric induction can also arise from pairing of an achiral cationic catalyst with a chiral counterion. Chiral amine derivatives

can promote transfer hydrogenation of α,β -unsaturated aldehydes. The authors have now probed the same reaction class using protonated morpholine, an achiral amine, in combination with binaphthol-based chiral phosphate anions. This catalyst system is particularly effective for aromatic substrates, yielding product distributions that favor one enantiomer by 98:1 or higher ratios. Sterically unhindered aliphatic substrates, such as citral and farnesal, are also reduced in high enantiomeric excess. Because the reaction proceeds in aprotic solvent and requires a secondary, rather than tertiary, amine salt catalyst, the authors propose that induction occurs via an ion pair between the phosphate and an iminium intermediate, formed by amine displacement of the aldehyde oxygen. — JSY

Angew. Chem. Int. Ed. **45**, 10.1002/anie.200600512 (2006).

10.1002/anie.200600512 (2006).

Q: How can I organize and protect my back issues of *Science*?

A: Custom-made library file cases!



Designed to hold 12 issues, these handsome storage boxes are covered in a rich burgundy leather-like material. Each slipcase includes an attractive label with the *Science* logo.

Great gift idea!

One \$15
Three \$40
Six \$80

..... **Order Form**

TNC Enterprises Dept.SC
P.O. Box 2475
Warminster, PA 18974

Please send me _____slipcasses.

Add \$3.50 per slipcase for postage and handling. PA residents add 6% sales tax. Cannot ship outside U.S.

Name (Please print) _____

Address (No P.O. Box numbers please) _____

City, State, Zip _____

Bill my: Master Card VISA AmEx

Name _____

Card No. _____

Exp. Date _____

Signature _____

Order online:
www.tncenterprises.net/sc

Unconditionally Guaranteed



www.stke.org

<< Keeping LAT Out

T cell anergy prevents self-reactive T cells that escape elimination in the thymus from responding. T cell anergy is associated with decreased interleukin 2 (IL-2) production and decreased proliferation in response to antigen-specific stimulation. Hundt *et al.* show that although phosphorylation of the tyrosine kinase ZAP-70 is not

impaired, phosphorylation of the ZAP-70 substrate, linker of activated T cells (LAT), is decreased. LAT serves as a scaffold recruiting various downstream effectors to the immunological synapse. Thus, lack of LAT phosphorylation prevents activation of phospholipase Cg1 (PLCg-1) and phosphatidylinositol 3-kinase (PI3K). There was no decrease in LAT abundance in the anergic cells, but LAT was selectively excluded from the immunological synapse because of reduced palmitoylation of LAT, which may explain the altered signaling properties in anergic T cells. — NG

Immunity **24**, 513 (2006).

1200 New York Avenue, NW
Washington, DC 20005

Editorial: 202-326-6550, FAX 202-289-7562
News: 202-326-6500, FAX 202-371-9227

Bateman House, 82-88 Hills Road
Cambridge, UK CB2 1LQ

+44 (0) 1223 326500, FAX +44 (0) 1223 326501

SUBSCRIPTION SERVICES For change of address, missing issues, new orders and renewals, and payment questions: 866-434-AAAS (2227) or 202-326-6417, FAX 202-642-1065. Mailing addresses: AAAS, P.O. Box 96178, Washington, DC 20090-6178 or AAAS Member Services, 1200 New York Avenue, NW, Washington, DC 20005

INSTITUTIONAL SITE LICENSES please call 202-326-6755 for any questions or information

REPRINTS: Author Inquiries 800-635-7181

Commercial Inquiries 803-359-4578
Corrections 202-326-6501

PERMISSIONS 202-326-7074, FAX 202-682-0816

MEMBER BENEFITS Bookstore: AAAS/BarnesandNoble.com bookstore www.aaas.org/bn; Car purchase discount: Subaru VIP Program 202-326-6417; Credit Card: MBNA 800-847-7378; Car Rentals: Hertz 800-654-2200 CDP#343457, Dollar 800-800-4000 #AA1115; AAAS Travels: Betchart Expeditions 800-252-4910; Life Insurance: Seabury & Smith 800-424-9883; Other Benefits: AAAS Member Services 202-326-6417 or www.aaasmember.org.

science_editors@aaas.org (for general editorial queries)

science_letters@aaas.org (for queries about letters)

science_reviews@aaas.org (for returning manuscript reviews)

science_bookrevs@aaas.org (for book review queries)

Published by the American Association for the Advancement of Science (AAAS), *Science* serves its readers as a forum for the presentation and discussion of important issues related to the advancement of science, including the presentation of minority or conflicting points of view, rather than by publishing only material on which a consensus has been reached. Accordingly, all articles published in *Science*—including editorials, news and comment, and book reviews—are signed and reflect the individual views of the authors and not official points of view adopted by the AAAS or the institutions with which the authors are affiliated.

AAAS was founded in 1848 and incorporated in 1874. Its mission is to advance science and innovation throughout the world for the benefit of all people. The goals of the association are to: foster communication among scientists, engineers and the public; enhance international cooperation in science and its applications; promote the responsible conduct and use of science and technology; foster education in science and technology for everyone; enhance the science and technology workforce and infrastructure; increase public understanding and appreciation of science and technology; and strengthen support for the science and technology enterprise.

INFORMATION FOR CONTRIBUTORS

See pages 102 and 103 of the 6 January 2006 issue or access www.sciencemag.org/feature/contribinfo/home.shtml

EDITOR-IN-CHIEF **Donald Kennedy**

EXECUTIVE EDITOR **Monica M. Bradford**

DEPUTY EDITORS NEWS EDITOR

R. Brooks Hanson, Katrina L. Kelner Colin Norman

EDITORIAL SUPERVISOR SENIOR EDITORS Barbara Jasny, Phillip D. Szurmi; **SENIOR EDITOR/PERSPECTIVES** Lisa D. Chong; **SENIOR EDITORS** Gilbert J. Chin, Pamela J. Hines, Paula A. Kiberstis (Boston), Marc S. Lavine (Toronto), Beverly A. Purnell, L. Bryan Ray, Guy Riddihough (Manila), H. Jesse Smith, Valda Vinson, David Voss; **ASSOCIATE EDITORS** Jake S. Yeston, Laura M. Zahn; **ONLINE EDITOR** Stewart Willis; **ASSOCIATE ONLINE EDITOR** Tara S. Marathe; **BOOK REVIEW EDITOR** Sherman J. Suter; **ASSOCIATE LETTERS EDITOR** Etta Kavanagh; **INFORMATION SPECIALIST** Janet Kegg; **EDITORIAL MANAGER** Cara Tate; **SENIOR COPY EDITORS** Jeffrey E. Cook, Cynthia Howe, Harry Jach, Barbara P. Ordway, Jennifer Sills, Trista Wagoner; **COPY EDITOR** Peter Mooreside; **EDITORIAL COORDINATORS** Carolyn Kyle, Beverly Shields; **PUBLICATION ASSISTANTS** Ramatoulaye Dou, Chris Filiatreau, Joi S. Granger, Jeffrey Hearn, Lisa Johnson, Scott Miller, Jerry Richardson, Brian White, Anita Wynn; **EDITORIAL ASSISTANTS** Lauren Kmeck, Patricia M. Moore, Brendan Nardozi, Michael Rodewald; **EXECUTIVE ASSISTANT** Sylvia S. Kihara

NEWS SENIOR CORRESPONDENT Jean Marx; **DEPUTY NEWS EDITORS** Robert Coontz, Jeffrey Mervis, Leslie Roberts, John Travis; **CONTRIBUTING EDITORS** Elizabeth Culotta, Polly Shulman; **NEWS WRITERS** Yudhijit Bhattacharjee, Adrian Cho, Jennifer Couzin, David Grimm, Constance Holden, Jocelyn Kaiser, Richard A. Kerr, Eli Kintisch, Andrew Lawler (New England), Greg Miller, Elizabeth Pennisi, Robert F. Service (Pacific NW), Erik Stokstad; **Katherine Unger** (intern); **CONTRIBUTING CORRESPONDENTS** Barry A. Cipra, Jon Cohen (San Diego, CA), Daniel Ferber, Ann Gibbons, Robert Iron, Mitch Leslie (NetWatch), Charles C. Mann, Evelyn Strauss, Gary Taubes, Ingrid Wickelgren; **COPY EDITORS** Linda B. Felaco, Rachel Curran, Sean Richardson; **ADMINISTRATIVE SUPPORT** Scherraine Mack, Fannie Groom BUREAUS: Berkeley, CA: 510-652-0302, FAX 510-652-1867, New England: 207-549-7755, San Diego, CA: 760-942-3252, FAX 760-942-4979, Pacific Northwest: 503-963-1940

PRODUCTION DIRECTOR James Landry; **SENIOR MANAGER** Wendy K. Shank; **ASSISTANT MANAGER** Rebecca Doshi; **SENIOR SPECIALISTS** Jay Covert, Chris Redwood; **SPECIALIST** Steve Forrester **PREFLIGHT DIRECTOR** David M. Tompkins; **MANAGER** Marcus Spiegler; **SPECIALIST** Jessie Mudjitaba

ART DIRECTOR Joshua Moglia; **ASSOCIATE ART DIRECTOR** Kelly Buckheit; **ILLUSTRATORS** Chris Bickel, Katharine Sutfitt; **SENIOR ART ASSOCIATES** Holly Bishop, Laura Creveling, Preston Huey; **ASSOCIATE** Nayomi Kevitiyagala; **PHOTO EDITOR** Leslie Blizard

SCIENCE INTERNATIONAL

EUROPE (science-int.com) **EDITORIAL:** **INTERNATIONAL MANAGING EDITOR** Andrew M. Sugden; **SENIOR EDITOR/PERSPECTIVES** Julia Fahrenkamp-Uppenbrink; **SENIOR EDITORS** Caroline Ash (Geneva: +41 (0) 222 346 3106), Stella M. Hurlley, Ian S. Osborne, Stephen J. Simpson, Peter Stern; **ASSOCIATE EDITOR** Joanne Baker **EDITORIAL SUPPORT** Alice Whaley; **DEBORAH DENNISON ADMINISTRATIVE SUPPORT** Janet Clements, Phil Marlow, Jill White; **NEWS:** **INTERNATIONAL NEWS EDITOR** Eliot Marshall **DEPUTY NEWS EDITOR** Daniel Clery; **CORRESPONDENT** Gretchen Vogel (Berlin: +49 (0) 30 2809 3902, FAX +49 (0) 30 2809 8365); **CONTRIBUTING CORRESPONDENTS** Michael Balter (Paris), Martin Enserink (Amsterdam and Paris), John Bohannon (Berlin); **INTERN** Laura Blackburn

ASIA Japan Office: Asca Corporation, Eiko Ishioka, Fusako Tamura, 1-8-13, Hirano-cho, Chuo-ku, Osaka-shi, Osaka, 541-0046 Japan; +81 (0) 6 6202 6272, FAX +81 (0) 6 6202 6271; asca@os.gulf.or.jp; **ASIA NEWS EDITOR** Richard Stone +66 2 662 5818 (rstone@aaas.org) **JAPAN NEWS BUREAU** Dennis Normile (contributing correspondent, +81 (0) 3 3391 0630, FAX 81 (0) 3 5936 3531; dnormile@gol.com); **CHINA REPRESENTATIVE** Hao Xin, +86 (0) 10 6307 4439 or 6307 3676, FAX +86 (0) 10 6307 4358; haoxin@earthlink.net; **SOUTH ASIA** Pallava Bagla (contributing correspondent +91 (0) 11 2271 2896; pbagla@vsnl.com) **AFRICA** Robert Koenig (contributing correspondent, rob.koenig@gmail.com)

EXECUTIVE PUBLISHER **Alan I. Leshner**

PUBLISHER **Beth Rosner**

FULFILLMENT & MEMBERSHIP SERVICES (membership@aaas.org) **DIRECTOR** Marlene Zenzel; **MANAGER** Waylon Butler; **SYSTEMS SPECIALIST** Andrew Vargo; **CUSTOMER SERVICE SUPERVISOR** Pat Butler; **SPECIALISTS** Laurie Baker, Tamara Alfson, Karena Smith, Vicki Linton; **CIRCULATION ASSOCIATE** Christopher Refice; **DATA ENTRY SUPERVISOR** Cynthia Johnson

BUSINESS OPERATIONS AND ADMINISTRATION DIRECTOR Deborah Rivera-Wienhold; **BUSINESS MANAGER** Randy Yi; **SENIOR BUSINESS ANALYST** Lisa Donovan; **BUSINESS ANALYST** Jessica Tierney; **FINANCIAL ANALYST** Michael LoBue, Farida Yeasmin; **RIGHTS AND PERMISSIONS: ADMINISTRATOR** Emilie David; **ASSOCIATE** Elizabeth Sandler; **MARKETING: DIRECTOR** John Meyers; **MARKETING MANAGERS** Darryl Walter, Allison Pritchard; **MARKETING ASSOCIATES** Julianne Weigel, Mary Ellen Crowley, Catherine Featherston, Alison Chandler, Lauren Lamoureux; **INTERNATIONAL MARKETING MANAGER** Wendy Sturley; **MARKETING/MEMBER SERVICES EXECUTIVE:** Linda Rusk; **JAPAN SALES** Jason Hannafor; **SITE LICENSE SALES: DIRECTOR** Tom Ryan; **SALES AND CUSTOMER SERVICE** Mehan Dossani, Kiki Forsythe, Catherine Holland, Wendy Wise; **ELECTRONIC MEDIA: MANAGER** Lizbeth Harman; **PRODUCTION ASSOCIATES** Sheila Mackall, Amanda K. Skelton, Lisa Stanford, Nichelle Johnston; **APPLICATIONS DEVELOPER** Carl Saffell

ADVERTISING DIRECTOR WORLDWIDE AD SALES Bill Moran

PRODUCT (science_advertising@aaas.org); **MIDWEST** Rick Bongiovanni: 330-405-7080, FAX 330-405-7081 • **WEST COAST/W. CANADA** Teola Young: 650-964-2266 **EAST COAST/ E. CANADA** Christopher Breslin: 443-512-0330, FAX 443-512-1607 • **UK/EUROPE/ASIA** Tracey Peers (Associate Director): +44 (0) 1782 752530, FAX +44 (0) 1782 752531 **JAPAN** Mashu Yoshikawa: +81 (0) 33235 5961, FAX +81 (0) 33235 5852 **TRAFFIC MANAGER** Carol Maddox; **SALES COORDINATOR** Deandra Simms

CLASSIFIED (advertise@sciencereaders.org); **U.S.: SALES DIRECTOR** Gabrielle Boguslawski: 718-491-1637, FAX 202-289-6742; **INSIDE SALES MANAGER** Daryl Anderson: 202-326-6543; **WEST COAST/MIDWEST** Kristine von Zedlitz: 415-956-2531; **EAST COAST** Jill Downing: 631-580-2445; **CANADA, MEETINGS AND ANNOUNCEMENTS** Kathleen Clark: 510-271-8349; **LINE AD SALES** Emmet Tesfaye: 202-326-6740; **SALES COORDINATORS** Erica Bryant, Rohan Edmondson Christopher Normile, Joyce Scott, Shirley Young; **INTERNATIONAL SALES MANAGER** Tracy Holmes: +44 (0) 1223 326525, FAX +44 (0) 1223 326532; **SALES** Christina Harrison, Svetlana Barnes; **SALES ASSISTANT** Helen Moroney; **JAPAN:** Jason Hannafor: +81 (0) 52 789 1860, FAX +81 (0) 52 789 1861; **PRODUCTION: MANAGER** Jennifer Rankin; **ASSISTANT MANAGER** Deborah Tompkins; **ASSOCIATES** Christine Hall; Amy Hardcastle; **PUBLICATIONS ASSISTANTS** Robert Buck; Mary Lagnaoui

AAAS BOARD OF DIRECTORS **RETIRING PRESIDENT, CHAIR** Gilbert S. Omenn; **PRESIDENT** John P. Holdren; **PRESIDENT-ELECT** David Baltimore; **TREASURER** David E. Shaw; **CHIEF EXECUTIVE OFFICER** Alan I. Leshner; **BOARD** Rosina M. Bierbaum; John E. Dowling; Lynn W. Enquist; Susan M. Fitzpatrick; Alice Gast; Thomas Pollard; Peter J. Stang; Kathryn D. Sullivan



ADVANCING SCIENCE. SERVING SOCIETY

SENIOR EDITORIAL BOARD

John I. Brauman, *Chair, Stanford Univ.*
Richard Leslie, *Harvard Univ.*
Robert May, *Univ. of Oxford*
Marcia McNutt, *Monterey Bay Aquarium Research Inst.*
Linda Partridge, *Univ. College London*
Vera C. Rubin, *Carnegie Institution of Washington*
Christopher R. Somerville, *Carnegie Institution*
George M. Whitesides, *Harvard University*

BOARD OF REVIEWING EDITORS

Joanna Aizenberg, *Bell Labs/Lucent*
R. McNeill Alexander, *Leeds Univ.*
David Altshuler, *Broad Institute*
Arturo Alvarez-Buylla, *Univ. of California, San Francisco*
Richard Amadio, *Univ. of Wisconsin, Madison*
Meinrat O. Andreae, *Max Planck Inst., Mainz*
Kristi S. Anseth, *Univ. of Colorado*
Cornelia I. Bargmann, *Rockefeller Univ.*
Brenda Bass, *Univ. of Utah*
Ray H. Baughman, *Univ. of Texas, Dallas*
Stephen J. Benkovic, *Pennsylvania St. Univ.*
Michael J. Bevan, *Univ. of Washington*
Ton Bisseling, *Wageningen Univ.*
Pina Bissell, *Lawrence Berkeley National Lab*
Peer Bork, *EMBL*
Dennis Bray, *Univ. of Cambridge*
Stephen Buratowski, *Harvard Medical School*
Jillian M. Burriak, *Univ. of Alberta*
Joseph A. Burns, *Cornell Univ.*
William P. Butz, *Population Reference Bureau*
Doreen Cantrell, *Univ. of Dundee*
Peter Carmeliet, *Univ. of Leuven, VIB*
Gerhard Ceder, *MIT*
Mildred Cho, *Stanford Univ.*
David Clapham, *Children's Hospital, Boston*
David Clary, *Oxford University*
J. M. Claverie, *CNRS, Marseille*

Jonathan D. Cohen, *Princeton Univ.*
F. Fleming Crim, *Univ. of Wisconsin*
William Cumberland, *UCLA*
George O. Daley, *Children's Hospital, Boston*
Caroline Dean, *John Innes Centre*
Judy DeLoache, *Univ. of Virginia*
Edward DeLong, *MIT*
Robert Desimone, *MIT*
Dennis Discher, *Univ. of Pennsylvania*
Julian Downward, *Cancer Research UK*
Denis Duboule, *Univ. of Geneva*
Christopher Dye, *WHO*
Richard Ellis, *Cal Tech*
Gerhard Ertl, *Fritz-Haber-Institut, Berlin*
Douglas H. Erwin, *Smithsonian Institution*
Paul Everitt, *Univ. of Cambridge*
Barry G. Falkowski, *Rutgers Univ.*
Ernst Fehr, *Univ. of Zurich*
Tom Fenchel, *Univ. of Copenhagen*
Alain Fischer, *INSEEM*
Jeffrey S. Flier, *Harvard Medical School*
Chris D. Frith, *Univ. College London*
R. Gadagkar, *Indian Inst. of Science*
John Gearhart, *Johns Hopkins Univ.*
Jennifer M. Graves, *Australian National Univ.*
Christian Haass, *Ludwig Maximilians Univ.*
Dennis L. Hartmann, *Univ. of Washington*
Chris Hawkesworth, *Univ. of Bristol*
Martin Heimann, *Max Planck Inst., Jena*
James A. Hendler, *Univ. of Maryland*
Ary A. Hoffmann, *La Trobe Univ.*
Evelyn L. Hu, *Univ. of California, SB*
Olli Ikkala, *Helsinki Univ. of Technology*
Meyer B. Jackson, *Univ. of Wisconsin Med. School*
Stephen Jackson, *Univ. of Cambridge*
Daniel Kahne, *Harvard Univ.*
Bernhard Keimer, *Max Planck Inst., Stuttgart*
Elizabeth A. Kellog, *Univ. of Missouri, St. Louis*
Alan B. Krueger, *Princeton Univ.*
Lee Kump, *Penn State*
Virginia Lee, *Univ. of Pennsylvania*

Anthony J. Leggett, *Univ. of Illinois, Urbana-Champaign*
Michael Lenoir, *NIAID, NIH*
Norman L. Letwin, *Beth Israel Deaconess Medical Center*
Olle Lindvall, *Univ. Hospital, Lund*
Richard Losick, *Harvard Univ.*
Ke Lu, *Chinese Acad. of Sciences*
Andrew P. MacKenzie, *Univ. of St. Andrews*
Raul Madariaga, *Ecole Normale Supérieure, Paris*
Rick Matzeis, *Univ. of Edinburgh*
Michael Malim, *King's College, London*
Eve Marder, *Brandeis Univ.*
George M. Martin, *Univ. of Washington*
William McGinnis, *Univ. of California, San Diego*
Virginia Miller, *Washington Univ.*
H. Yasushi Miyashita, *Univ. of Tokyo*
Edward Moser, *Norwegian Univ. of Science and Technology*
Andrew Murray, *Harvard Univ.*
Naoto Nagosa, *Univ. of Tokyo*
James Northrup, *Stanford Univ. School of Med.*
Roeland Nolte, *Univ. of Maastricht*
Erica Nowotny, *European Research Advisory Board*
Helen N. Olson, *Univ. of Texas, SW*
Erin O'Shea, *Univ. of California, SF*
Elinor Ostrom, *Indiana Univ.*
Jonathan T. Overpeck, *Univ. of Arizona*
John Pendry, *Imperial College*
Phillippe Poulin, *CNRS*
Mary Power, *Univ. of California, Berkeley*
David J. Read, *Univ. of Sheffield*
Les Real, *Emory Univ.*
Colin Renfrew, *Univ. of Cambridge*
Trevor Robbins, *Univ. of Cambridge*
Nancy Ross, *Virginia Tech*
Edward M. Rubin, *Lawrence Berkeley National Lab*
Gary Ruvkun, *Mass. General Hospital*
J. Roy Sambles, *Univ. of Exeter*
David S. Schimel, *National Center for Atmospheric Research*
Christoph Schulz, *Albert-Ludwigs-Universität*
Paul Schulze-Lefert, *Max Planck Inst., Cologne*
Terrence J. Sejnowski, *The Salk Institute*
David Sibley, *Washington Univ.*

George Somero, *Stanford Univ.*
Christopher R. Somerville, *Carnegie Institution*
John Steitz, *Yale Univ.*
Edward I. Stiefel, *Princeton Univ.*
Thomas Stocker, *Univ. of Bern*
Jerome Strauss, *Univ. of Pennsylvania Med. Center*
Motoyuki Takahashi, *Univ. of Tokyo*
Tamara Tarr, *Brown Univ.*
Glenn Telling, *Univ. of Kentucky*
Marc Tessier-Lavigne, *Genentech*
Craig B. Thompson, *Univ. of Pennsylvania*
Michiel van der Klis, *Astronomical Inst. of Amsterdam*
Bert van der Kooy, *Univ. of Toronto*
Derek Vogelstein, *Johns Hopkins*
Christopher A. Walsh, *Harvard Medical School*
Christopher T. Walsh, *Harvard Medical School*
Graham Warren, *Yale Univ. School of Med.*
Colin Watts, *Univ. of Dundee*
Julia R. Weertman, *Northwestern Univ.*
Daniel M. Wegner, *Harvard University*
Ellen D. Williams, *Univ. of Maryland*
R. Sanders Williams, *Duke University*
Ian A. Wilson, *The Scripps Res. Inst.*
Jerry Workman, *Stowers Inst. for Medical Research*
John R. Yates III, *The Scripps Res. Inst.*
Martin Zatz, *NIMH, NIH*
Walter Ziegler-Schaberger, *Max Planck Inst., Munich*
Huda Zoghbi, *Baylor College of Medicine*
Maria Zuber, *MIT*

BOOK REVIEW BOARD

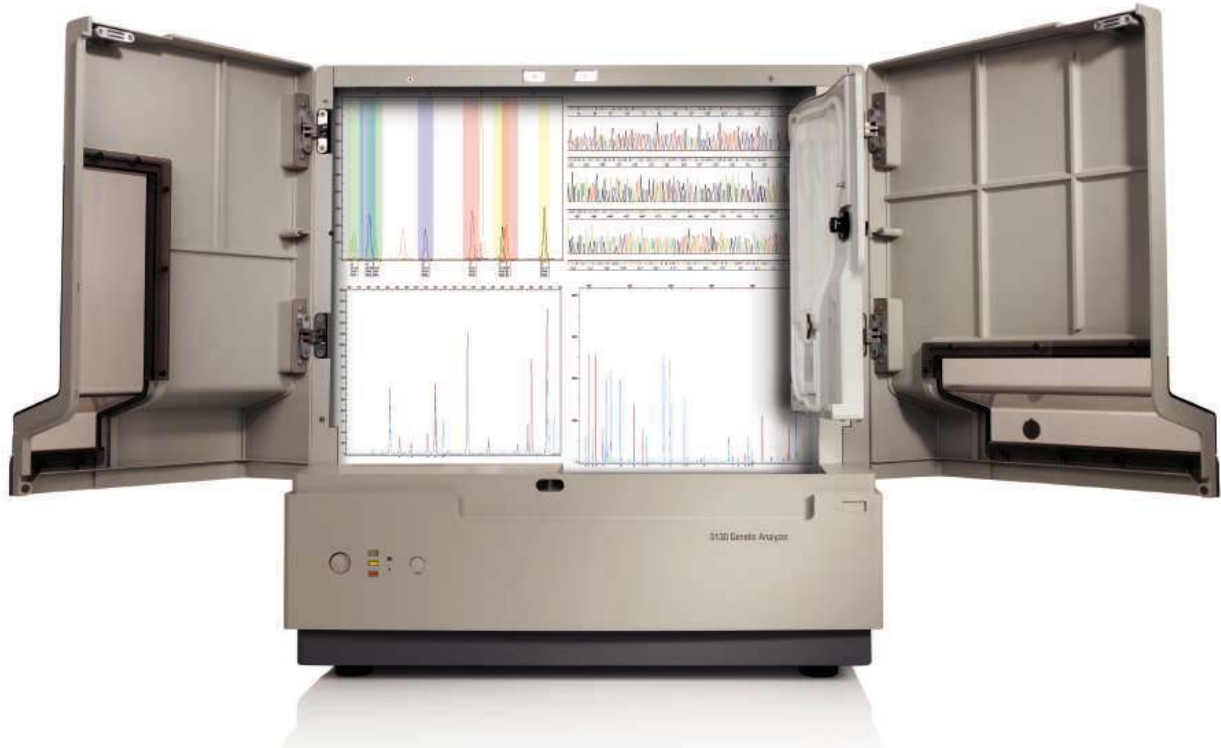
John Aldrich, *Duke Univ.*
David Bloom, *Harvard Univ.*
Linda Schiebinger, *Stanford Univ.*
Richard Swedner, *Univ. of Chicago*
Ed Wasserman, *DuPont*
Lewis Wolpert, *Univ. College, London*

Now Available!

SNPlex™ Genotyping System on
the 3130x/ Genetic Analyzer.

Accept No Limitations.

The improved SNPlex Genotyping System now performs cost effective and customizable genotyping projects on the 3130x/ Genetic Analyzer.



The Genetic Analyzer that does more than just sequencing:

SNPlex Genotyping System* • *De novo* sequencing • Resequencing • Comparative sequencing
Mutation/heterozygote detection • SAGE • SNP validation and screening • Genotyping • Microsatellite analysis
AFLP • Conformation analysis • TRFLP • MLST • Relative fluorescent quantitation

Applied Biosystems 3130 and 3130x/ Genetic Analyzers

The 4-capillary 3130 and 16-capillary 3130x/ Genetic Analyzers provide reference-standard data quality and sophisticated, hands-free automation capabilities across a wider range of sequencing, resequencing and fragment analysis applications. The 3130 Series systems leverage the same technology, reagents, and software interface that make our larger production-scale systems so successful, bringing superior performance within the reach of almost any lab. Learn more at: <http://info.appliedbiosystems.com/3130series>.

AB Applied
Biosystems



*Not supported on the 3130 Genetic Analyzer.

For Research Use Only. Not for use in diagnostic procedures. ABI PRISM, Applied Biosystems and BigDye are registered trademarks and AB (Design), POP-7 and SNPlex are trademarks of Applied Biosystems or its subsidiaries in the US and/or certain other countries. The Applied Biosystems 3130/3130x/ Genetic Analyzers include patented technology licensed from Hitachi Ltd. as part of a strategic partnership between Applied Biosystems and Hitachi Ltd., as well as patented technology of Applied Biosystems. © 2006 Applied Biosystems. All rights reserved.



Every
great idea

goes
through



an
evolution.



Introducing New Poly Bottles for Mallinckrodt® Solvents.



For over 130 years, Mallinckrodt Baker has delivered breakthrough solutions for chemists and researchers. Our latest is a high density polyethylene (HDPE) poly bottle for our Mallinckrodt brand ACS and histological grade solvents.

Our new poly bottles are designed to enhance laboratory safety while helping to reduce shipping and disposal costs compared to traditional glass containers. And with specifications that meet or exceed ACS and

histology standards, our new reagent grade solvents in poly bottles are your best choice for quality and value.

So the next time your application calls for reagent grade solvents, remember Mallinckrodt Laboratory Chemicals.

For a copy of the latest Mallinckrodt Laboratory Chemicals catalog, visit www.mallbaker.com/sci

tyco / Specialty Products

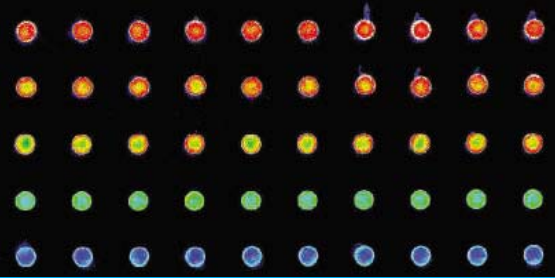
Mallinckrodt® is a trademark of Mallinckrodt Inc.
©2006 Mallinckrodt Baker, Inc. All rights reserved.

iPod is a registered trademark of Apple Computer, Inc., which does not sponsor, authorize or endorse this advertisement.

M™ Mallinckrodt®
CHEMICALS

Mallinckrodt Baker





TOOLS

TELLTALE SPOTS

ProMAT is a free program for analyzing protein microarrays (above). Relatives of DNA chips, the microarrays can help researchers identify proteins lurking in a drop of blood or a particular cell type and measure their concentrations. The software, which works for ELISA microarrays, can also help users gauge the reliability of their data. To download it, visitors need to register by e-mail with the program's creators at the Pacific Northwest National Laboratory in Richland, Washington. >> www.pnl.gov/statistics/ProMAT/index.htm

WEB LOGS

Speaking of Systems

To discourage tree-cutting and save topsoil, China has begun taxing disposable chopsticks, triggering higher prices and a search for alternative sources by Japanese importers. This unexpected side effect of a conservation measure caught the eye of geoscientist and environmental engineer Daniel Collins of the Massachusetts Institute of Technology. His new blog Down to Earth brings a pragmatic attitude to discussions of ecosystem engineering, land use, natural hazards, and related subjects. Other topics that Collins has considered include safety concerns about a new dump for Hurricane Katrina refuse. >>

getdowntoearth.blogspot.com

COMMUNITY SITE

Life From Scratch

So-called synthetic biologists have already reconstructed the polio and 1918 pandemic flu viruses and someday might be able to design and build bacteria that pump out drugs or hunt down cancer cells. The effort to craft new biological components and systems or refine existing ones intrigues scientists, but it also raises questions about whether artificial bugs could harm human health or the environment. Tended by researchers at the Massachusetts Institute of Technology (MIT) and other universities, this meeting place for synthetic biologists features a news roundup and listing of recent research and policy papers, including ones that led up to a meeting last month that pondered self-regulation of the field (*Science*, 26 May, p. 1116). The tools section offers a long list of software, Web sites, and other resources for working with DNA, RNA, and proteins. For instance, you can link to MIT's Registry of Standard Biological Parts, a catalog of cellular building blocks such as DNA sequences that stop the production of messenger RNA. >>

syntheticbiology.org

IMAGES

Tooth Marks >>

Munching tough leaves produces scratches on the teeth of a mantled howler monkey (top).

By contrast, deep pits and gouges (below) reveal a tufted capuchin monkey's penchant for crunching nuts and seeds. Dental

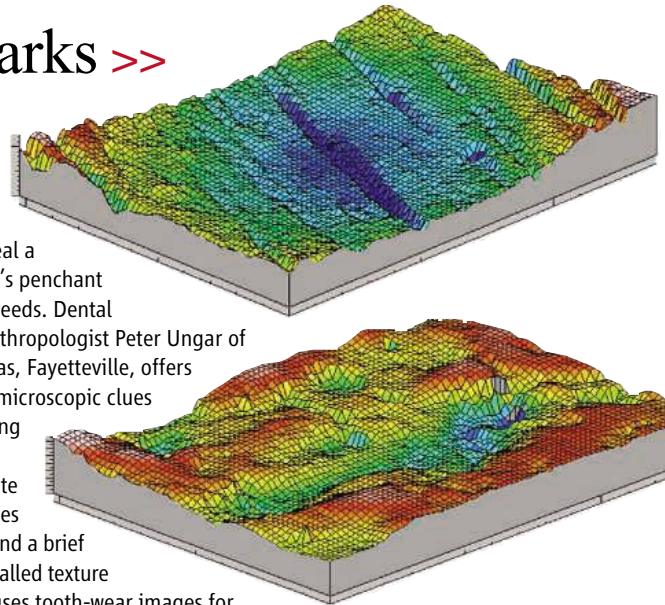
Microwear from paleoanthropologist Peter Ungar of the University of Arkansas, Fayetteville, offers

an introduction to such microscopic clues to primate diets, including the dining habits of our ancient ancestors. The site

features background pages on studying tooth wear and a brief tutorial on one method called texture

analysis. A database houses tooth-wear images for two monkey species and two types of early humans. Ungar

hopes researchers will contribute results for many more vertebrates, from dinosaurs to humans. >> www.uark.edu/microwear



IMAGES

Ozone Tracker

In a few months, spring in Antarctica will mean not only that sunlight returns and the penguins get amorous. It will also herald the reappearance of the Antarctic ozone hole, a thinning of Earth's shield against ultraviolet radiation caused by humanmade chemicals.

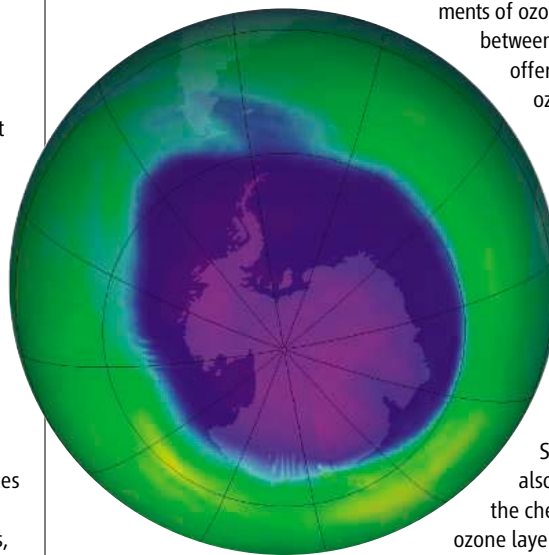
NASA's Ozone Hole Watch posts daily satellite measurements of ozone levels over the South Pole

between July and December. The site also offers statistical summaries and maps of ozone readings dating back to 1979.

Despite the phase-out of ozone-destroying

chlorofluorocarbons, the hole remains large. In 2005, for example, its average size during the peak period of September through October was 24 million square kilometers—below 1998's record of 26 million square kilometers but still the third largest on record (left,

September 2005). Visitors can also watch animations that follow the chemical reactions that gnaw at the ozone layer. >> ozonewatch.gsfc.nasa.gov



Send site suggestions to >> netwatch@aaas.org

Archive: www.sciencemag.org/netwatch

Call for Nominations for the AAAS International Scientific Cooperation Award

The AAAS International Scientific Cooperation Award, presented at the AAAS Annual Meeting, February 2007 in San Francisco, is given to an individual or small group in the scientific and engineering community that has contributed substantially to the understanding or development of science or engineering across national boundaries. The award is open to all regardless of nationality or citizenship. Nominees must be living at the time of their nomination. The recipient receives US \$5000 award, a commemorative plaque, complimentary registration, and reimbursement for reasonable travel and hotel expenses. Please see our website for additional details:

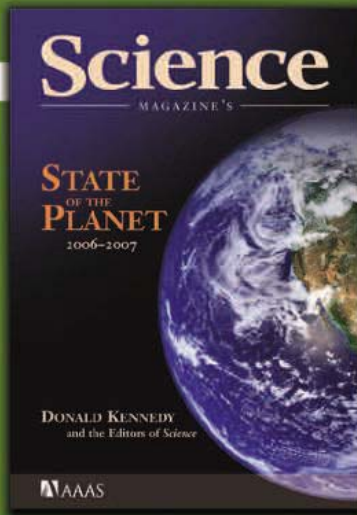
<http://www.aaas.org/aboutaaas/awards/int/index.shtml>

Nominations should be typed and include the following:

- ▶ nominator's name, address, phone number
- ▶ nominee's name, title, institutional affiliation, address, phone number; two letters of support; curriculum vitae (3 page maximum); a summary statement (250 words) and a longer detailed statement of the actions for which the candidate is nominated; any documentation (books, articles, or other materials) illuminating the significance of the nominee's achievement may also be submitted

All materials become the property of AAAS. Completed nominations should be submitted to: Linda Stroud, International Scientific Cooperation Award Liaison, AAAS Office of International Initiatives, 1200 New York Avenue, NW, Washington, DC 20005, USA, Fax: (202) 289-4958.

All materials must be received by 1 August 2006.



Science
MAGAZINE'S
STATE OF THE PLANET
2006-2007
DONALD KENNEDY
and the Editors of Science
AAAS

Science Magazine's
State of the Planet
2006-2007

Donald Kennedy, Editor-in-Chief,
and the Editors of Science
The American Association for
the Advancement of Science

The most authoritative voice in American science,
Science magazine, brings you current knowledge on
the most pressing environmental challenges, from
population growth to climate change to biodiversity loss.

COMPREHENSIVE • CLEAR • ACCESSIBLE

ISLANDPRESS Science
AAAS

islandpress.org



Big News

AAAS Science Journalism Awards Call for Entries

The AAAS Science Journalism Awards honor distinguished reporting on science by professional journalists. The awards are an internationally recognized measure of excellence in science reporting for a general audience. They go to individuals (rather than institutions, publishers or employers) for coverage of the sciences, engineering and mathematics.

U.S. CATEGORIES

Awards will be presented for U.S. submissions in the following categories:

- ▶ Large Newspaper
- ▶ Magazine
- ▶ Television
- ▶ Small Newspaper
- ▶ Online
- ▶ Radio

INTERNATIONAL CATEGORY

Open to journalists worldwide, across all news media.

- ▶ Children's Science News

Deadline: August 1, 2006
www.aaas.org/SJAwards



SPONSORED BY
Johnson & Johnson
PHARMACEUTICAL RESEARCH
& DEVELOPMENT, L.L.C.



ADVANCING SCIENCE. SERVING SOCIETY



Brain injuries can destroy the ability to recognize faces, and some people are born without the skill. This condition, known as face blindness or prosopagnosia, was thought to be exceedingly rare, but now a survey of 1600 people has revealed that up to 2% of the population may be afflicted.

Cognitive neuroscientist Bradley Duchaine of University College London and colleagues used the Internet to recruit participants and conduct a facial recognition survey. The subjects first viewed a face for 3 seconds. They were then presented with three face photos—the original one and two others—and asked to indicate the one they recognized. More difficult tests followed, in which participants were shown larger numbers of faces and asked whether they recognized people in different poses in altered lighting.

The team, whose research is as yet unpublished, found that dozens of the subjects had serious enough problems with facial recognition that their daily lives would likely be affected. "It's a neglected condition," says Duchaine. Cognitive neuroscientist Martha Farah of the University of Pennsylvania calls prosopagnosics "the ivory-billed woodpecker of neurological patients: They were rare, and some researchers even doubted that they existed." Duchaine's team has found some cases in which prosopagnosia seems to run in the family, but the neurological and genetic bases for the condition remain to be unraveled.

TEETH OF CIVILIZATION

Without the agricultural surpluses made possible by the shift some 10,000 years ago from hunting and gathering to farming, the rise of towns and cities would not have been possible. But a survey of skeletal data from farming sites around the world shows that civilization took a toll on health—especially dental health.

Anthropologist Clark Larsen of Ohio State University in Columbus reviewed several dozen studies covering hundreds of skeletons from both hunter-gatherer and ancient farming societies. In the June issue of *Quaternary International*, he reports that farmers' teeth show dramatically increased incidences of cavities compared to hunter-gatherers, probably as a result of eating more carbohydrate-loaded plants and less meat. What's more, a reduction in the size of the face and jaw, from eating softer foods such as cooked porridge, led to crowding of the teeth in the farmers. The shift away from meat eating also led to iron-deficiency anemia, as shown by a pathological increase in bone porosity in the skulls. Higher population densities also took their toll, Clark reports, allowing infectious diseases such as syphilis, tuberculosis, and leprosy—all of which leave telltale marks on the skeleton—to spread much more readily.

Brian Hayden, an archaeologist at Simon Fraser University in Burnaby, Canada, speculates that the shift to farming also led to psychological stresses from increased population density: "Health took a back seat right from the beginning."

Robots for Town & Country

The Defense Advanced Research Projects Agency (DARPA) plans to add a "new level of complexity" to next year's Grand Challenge, a contest that pits robot vehicles bristling with radar, cameras, and Global Positioning System antennae against one another over a lengthy course.

The first two Grand Challenges were desert runs. This time, the autonomous machines will negotiate an urban environment. Their assignment: to safely complete a 93-kilometer simulated military supply mission in under 6 hours, merging with traffic, avoiding obstacles, negotiating busy intersections, obeying traffic signals, executing U-turns, and finding alternate routes when necessary. For traffic, the vehicles will have to contend with one another as well as "teleoperated" ones, says Jan Walker of DARPA.



Only four vehicles completed last year's Grand Challenge, which was won by "Stanley," a souped-up Volkswagen Touareg (above) designed by a team at Stanford University. This year, team leader Sebastian Thrun says they're starting with a VW Passat.

The race, to be run on 3 November 2007, carries a \$2 million prize for the winner. Final deadline for entry is 5 October 2006.

I'm Your Guide

Japan and Korea are in a neck-and-neck competition to produce the world's most human-looking android. Below is Korea's latest entry, developed by the Korean Institute for Industrial Technology and unveiled last month. Unlike Japan's Actroid, introduced in 2003, EveR-1, as "she" is known, can look you in the eye because a camera that recognizes movement is located in the head. She can hold short conversations in Korean and English with her 400-word vocabulary, moving her lips correspondingly. She has 15 facial expressions and will show displeasure if you poke her. Her lower half has yet to be worked out, but scientists say EveR-1 can serve educational functions such as museum guide and reading to children.



SCHOLARLY COMMUNICATION

Florida Law Bans Academics From Doing Research in Cuba

Beginning next month, Florida researchers won't be able to travel to Cuba to carry out any studies. Although the United States allows such interactions, the state has banned faculty members at Florida's public universities from having any contact with the island nation under a law enacted last week. "This law shuts down the entire Cuban research agenda," says Damián Fernández, director of the Cuban Research Institute at Florida International University (FIU) in Miami.

Cuba is one of six countries that the U.S. State Department has designated as a "sponsor of terrorism," although U.S. scholars can travel to Cuba for research if they first obtain a government license. The Florida measure, which passed the state legislature unanimously, essentially closes that loophole by disallowing state-funded institutions from using public or private funds to facilitate travel to such countries. (The list includes North Korea, Iraq, Iran, Libya, and Sudan.)

"Florida's taxpayers don't want to see their resources being used to support or subsidize terrorist regimes at a time when America is fighting a war on terror," says David Rivera, a Republican Cuban-American state legislator who introduced the bill. Florida researchers won't miss out on anything by not going to Cuba, he adds: "I don't think there's anything there that cannot be studied in the Dominican Republic or other Caribbean islands."

Rivera introduced a similar measure 2 years ago that failed. But political observers say the indictment in January of an FIU education professor and his wife, on charges of spying on the Cuban exile community for Cuba, made a big difference this time around. "The case showed that we need to protect the reputation and educational integrity of our universities, and that's what this law does," says Rivera.

Academics say the law will hurt efforts to



Don't go there. A newly enacted Florida law, sponsored by David Rivera (*inset*), will force the state's academics to abandon research projects such as this University of Florida–led study of Cuban agriculture.

learn about Cuba's agriculture, ecology, and marine environment—all topics that could have a significant effect on Florida's economy. Agricultural economist William Messina and his colleagues at the University of Florida, Gainesville, for example, have been researching citrus farming in Cuba, the world's third-largest producer of grapefruit. "Their grapefruit yield has gone up in the past few years as a result of new policies that promote collaborations between Cuban farmers and foreign agricultural and food-processing companies," says Messina. Those collaborations, he says, have meant tougher competition for Florida grapefruit growers trying to sell to Western Europe. Researchers in the state have been carrying out similar studies of Cuba's shellfish, sugar, and tomato industries.

Environmental researchers are also chagrined by the new law. FIU geographer Jennifer Gebelein, for example, is currently in

Cuba looking at the impact on Cuba's coral reefs of land-cover changes around the island. The work is important from a conservation standpoint "because Cuba's coral reefs are a center of marine and biological diversity in the Caribbean," says Lauretta Burke, a geographer and senior associate at the World Resources Institute in Washington, D.C. Gebelein is scrambling to finish her fieldwork before the law goes into effect on 1 July.

Marine scientist Frank Muller-Karger of the University of South Florida, St. Petersburg, says that Cuba's plans for offshore oil exploration make scientific exchanges between Florida and the island more important than ever before. "Any major pollution event off the coast of Cuba may reach Florida, and many important fisheries in the Keys may be connected to Cuba," he says.

Not all academics are opposed to the ban, however. Jorge Rey, a Cuban exile and an ecologist at the University of Florida, Vero Beach, says doing research in Cuba is a "scientifically risky proposition" because the Cuban government strictly controls what sites researchers can access. "There's also the danger of U.S. scholars being used by the Cuban government for propaganda," he says, echoing one of Rivera's arguments in support of the legislation.

FIU's Fernández doesn't buy that line of reasoning. He says the new law will actually weaken U.S. national security instead of strengthening it. "The notion that you cannot study your alleged enemy goes against any strategic thought," he says. "It would be laughable if it weren't so serious."

Fernández and others are backing a plan by the American Civil Liberties Union (ACLU) of Florida to challenge the law in court. ACLU officials declined to describe the basis for the suit, but Executive Director Howard Simon says the Florida law is troubling on many fronts. Not only does it inject politics into academic research, he says, "it may also interfere with the policies of the federal government" by affecting U.S. relations with another country.

—YUDHIJIT BHATTACHARJEE





AVIAN INFLUENZA

Wild Birds Only Partly to Blame in Spreading H5N1

Experts studying the H5N1 avian influenza epidemic have long been at odds over whether wild birds play a major role in spreading the deadly disease. Last week, after poring over the latest surveillance data, a group meeting in Rome reached a consensus: Wild birds play a role in the virus's huge geographic jumps, they said in a statement at the end of the meeting, but the main means of transmission is the commercial poultry trade. With that question at least partially settled, one research group introduced a new puzzle by raising doubts about whether the right sampling techniques are being used in wild bird surveillance programs.

Meanwhile, as human H5N1 cases continue to surface in Indonesia, World Health Organization (WHO) scientists have concluded that although there may have been cases of human-to-human transmission in a family cluster, there is still no evidence that the behavior of the virus is changing.

Much of the attention at the International Scientific Conference on Avian Influenza and Wild Birds, jointly sponsored by the Rome-based United Nations Food and Agriculture Organization (FAO) and the World Organization for Animal Health in Paris, focused on the results of the European Union's wild bird surveillance program. According to FAO, among nearly 100,000 dead and live wild birds tested for the H5N1 virus over the past 10 months, 741 proved positive, all of them dead. The H5N1-infected birds came from 13 European countries, with Germany the hardest hit.

Although the European surveillance program did not find any live birds carrying the virus—considered proof positive that they are involved in its spread—other recent studies have, says Jan Slingenbergh, an FAO veterinarian. “It’s now commonly accepted that wild birds do play a role [in spreading the virus] over long distances,” he says. On the other hand, William Karesh, a veterinarian at the Wildlife Conservation Society in New York City and longtime skeptic of a dominant role for wild birds, says he’s pleased that “the FAO acknowledges the major mode [for spread] is the poultry trade and the globalization of the wild bird trade.” He adds, “We’re getting away from the either-or thinking and recognizing that there are many methods of spreading the virus.”

But the conference could not resolve a host of questions, including which species, if

any, form a natural reservoir for the virus. A group from Erasmus University in Rotterdam, Netherlands, presented yet-to-be-published results suggesting that healthy birds can carry the virus and go undetected, as has been suggested by recent studies. They experimentally infected six species of wild ducks with the H5N1 virus and saw a spectrum of responses ranging from quick death to no clinical signs of illness. Perhaps even more significant, they found that the virus is shed far more heavily in an infected bird’s pharynx than through its feces. Thijs Kuiken, a veterinary pathologist involved in the study, says this raises questions about the conclusiveness of current sampling techniques that rely on cloacal swabs or the collection of bird droppings. For future

important; so many clues could be clarified,” says Slingenbergh.

Separately, WHO is continuing to follow the largest cluster of human H5N1 cases uncovered so far, involving an initial apparent case in a 37-year-old Indonesian woman living in rural Sumatra who was buried before tissue samples were collected and seven subsequent lab-confirmed cases. Six of the seven, all members of an extended family, died. The pattern of infections suggests that this could be an unusual instance of human-to-human transmission. Gina Samaan, a WHO epidemiologist in Jakarta, says, “It is a possibility, but we cannot rule out environmental contamination.” As in previous clusters, says Samaan, the infection passed among blood rel-

Dead in the water. Wild swans were some of the first victims of H5N1 in Europe.



surveillance programs, “our strong recommendation is that people take swabs from the throat as well,” he says.

Karesh says it may be premature “to say that respiratory secretion is more important than fecal excretion as a general rule.” He agrees, however, that both throat and cloacal swabs would be ideal although not always feasible.

To determine just how far wild birds may be carrying the virus and where they pick it up, FAO is hoping to raise \$6.8 million for a new surveillance program that would begin before the fall migration. The plan is to capture wild birds, test them for H5N1, and fit them with radio transmitters. The birds would then be tracked by satellites and tested again at the end of their migrations. “It’s critically

atives and not among in-laws or husband and wife; this may indicate a genetic predisposition to contracting H5N1.

Practically, however, Samaan says that although the cluster is unusual for its size, it resembles others in that all those who contracted the virus were in close contact with infected patients. So far, there is no indication that the virus has spread beyond the family and into the community, and lab studies indicate “that it remains a purely avian virus,” she says. What would set off alarm bells about a pandemic, she says, would be seeing three or four generations of illness spaced out over a month or more and spreading beyond an immediate family.

—DENNIS NORMILE



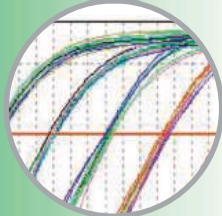
- Mastercycler ep® *realplex* real-time PCR System



- epMotion® 5070 automated pipetting system



- Highly precise pipetting tools



- Comprehensive software for optimized data analysis



Automated real-time PCR that pays for itself

Precision pipetting · Reproducible results · Affordable automation

Eppendorf Automation and real-time Systems (ARTS™) combine the most accurate and reproducible pipetting with the fastest and most sensitive real-time cycling.

That means you get highly consistent and reproducible results within and across experiments. You can even perform reactions in lower volumes—and with fewer replicates, so you will also save significantly on reagents!

Visit: www.epMotion.info or www.realplex.com

Mastercycler ep *realplex*:

- Real-time PCR in less than 30 minutes
- User-friendly software
- Highly sensitive optical system

epMotion 5070 automated pipetting system

- Easy operation via control panel or PC
- Preinstalled, validated applications/consumables
- High-precision pipetting from 1 µl to 1.000 µl

eppendorf
In touch with life

www.eppendorf.com · Email: info@eppendorf.com · Application support: 516-515-2258

In the U.S.: Eppendorf North America, Inc. 800-645-3050 · In Canada: Eppendorf Canada Ltd. 800-263-8715

Your local distributor: www.eppendorf.com/worldwide · Application support: Phone +49 180 366 67 89

Practice of the patented polymerase chain reaction (PCR) process requires a license. The Eppendorf [or appropriate trademark] Thermal Cycler is an Authorized Thermal Cycler and may be used with PCR licenses available from Applied Biosystems. Its use with Authorized Reagents also provides a limited PCR license in accordance with the label rights accompanying such reagents. This is a Licensed Real-Time Thermal Cycler under Applera's United States Patent No. 6,814,934 and corresponding claims in non-U.S. counterparts thereof, for use in research and for all other applied fields except human in vitro diagnostics. No right is conveyed expressly, by implication or by estoppel under any other patent claim.

CHEMISTRY

Ceramic Sponges That Sop Up Sulfur Could Boost Energy Technologies

Fuel cells and coal-burning plants may seem worlds apart technologically, but they share a common enemy: sulfur. Even a trace of it in the hydrogen gas that feeds fuel cells will poison the catalysts that convert hydrogen into electricity. Next-generation coal plants that will convert coal into a hydrogen-rich gas must also remove sulfur before the gas can be transformed into liquid fuels or used in fuel cells. Current technologies for capturing sulfur have made some progress, but often at a high cost. Now, new work with compounds called rare earth oxides could shift sulfur removal—and energy-generating technologies potentially stymied by sulfur—into high gear.

On page 1508, chemical engineer Maria Flytzani-Stephanopoulos and colleagues at Tufts University in Medford, Massachusetts, report turning a type of ceramic powder into a chemical sponge that quickly sops up sulfur and then can be “wrung out” and reused over and over. “It looks potentially important,” says Michael Krumpelt, a chemical technology scientist at Argonne National Laboratory in Illinois—provided, Krumpelt adds, that engineers can incorporate the new materials into a system that is simple and thus cheap.

The need for a cheap way to remove sulfur from fuel gases has spurred engineers for decades. In many countries, coal-fired electric plants are required to install smokestack scrubbers to reduce emissions of sulfur dioxide, a chief component of acid rain. And many developers would like to be able to use a wide range of hydrocarbon fuels as a feedstock for generating the molecular hydrogen that powers most fuel cells. But even the trace amounts of sulfur that remain create havoc. “It’s been a big problem,” says Sossina Haile, an expert on high-temperature solid oxide fuel cells at the California Institute of Technology in Pasadena.

One option for removing sulfur has been using another spongelike ceramic called zinc oxide, which readily grabs on to sulfur, converting the zinc oxide to zinc sulfide. But it’s far from a perfect solution. Once the outer surface becomes coated with zinc sulfide, the interior of the ceramic has trouble grabbing more sulfur. And zinc sulfide is not easily converted back to zinc oxide. So zinc oxide-based

filters must be replaced regularly.

Researchers have explored using lanthanum and other rare earth oxides for years. Like zinc oxide, these ceramics also readily grab sulfur, but unlike zinc oxide they can later release it, making them reusable. In previous studies, researchers have exposed the ceramics to sulfur for long periods, allowing gases to percolate completely through the crystalline



Pure and simple. Solid-oxide fuel cells, such as the ones in this 100-kilowatt heating plant in the Netherlands, require sulfur-free hydrogen.

structure of the material. But such heavily saturated ceramics give up their sulfur too slowly to be practical for real-world use, says Flytzani-Stephanopoulos.

For their current study, the Tufts researchers tried exposing their rare earth oxides to sulfur-bearing gases for relatively brief periods, so they became coated with sulfur only on their surface. They found that lanthanum-based oxides, in particular, both grabbed and released a full surface complement of sulfur in just minutes. Moreover, they could reduce the sulfur content in fuel streams to the parts-per-billion range—good enough to protect even the most sensitive fuel-cell catalysts. When the researchers ran their materials through about 100 such charging and discharging cycles, they found little change.

An industrial plant, Krumpelt says, would use multiple filters, switching back and forth so some sop up sulfur while others discharge it. In their paper, the Tufts researchers outline such a system for use with solid oxide fuel cells, which are being developed as backup power sources for hospitals and other industrial users. If such a design can keep fuel-cell catalysts working, it could go a long way toward making such fuel cells reliable enough to succeed in the real world.

—ROBERT F. SERVICE

Polar Satellites Pared

The U.S. Department of Defense has dropped a number of climate sensors from a satellite program as part of a restructuring of the National Polar-Orbiting Operational Environmental Satellite System (NPOESS) (*Science*, 2 June, p. 1296). Along with scaling the program back from six satellites to two, with an optional two more, the Pentagon stripped sensors that measure solar and Earth electromagnetic radiation—useful for detecting long-term heat trends—and an aerosol detector to better understand how clouds affect climate. “The community was depending on NPOESS for the continuity of a number of data sets,” says Roy Spencer of the University of Alabama, Huntsville. “A lot of scientists will be disappointed.”

In a 5 June letter to lawmakers, Pentagon officials say that the instruments eliminated could fly “if the sensors are provided from outside the program.” It also says the cuts will save \$2 billion on the overall program, which has been billions over budget and years late. Although the instruments “are not [relatively] expensive,” says Berrien Moore of the University of New Hampshire, Durham, NASA’s depleted budget may make that impossible. Congress will signal its response in pending agency budgets for next year.

—ELI KINTISCH

Harvard OKs Research Cloning

Harvard University researchers have been given the go-ahead to use cloning to create disease-specific lines of human embryonic stem cells. At a 6 June press conference, scientists described plans to use somatic cell nuclear transfer—also referred to as research cloning—to study diabetes and blood and neurodegenerative diseases.

No fewer than five institutions and eight Institutional Review Boards approved the proposals. Private funding will support the work, which cannot be paid for with federal dollars. Researchers plan to use excess eggs from fertility clinics as well as fresh eggs from unpaid so-called compassionate donors.

Douglas Melton and Kevin Eggan of the Harvard Stem Cell Institute plan to create stem cell lines that will enable them to study diabetes in a dish. Eggan also plans to use the technique to study neurodegenerative diseases such as amyotrophic lateral sclerosis. George Daley of Children’s Hospital Boston is aiming for customized cell lines using skin biopsies from patients with sickle cell anemia and other blood diseases.

—CONSTANCE HOLDEN

GRADUATE TRAINING

Diversity Remains Elusive for Flagship NSF Program

LaTasha Taylor is the future of interdisciplinary graduate training, as the National Science Foundation (NSF) sees it. Since 1998, the U.S. agency has spent more than \$300 million to train a new type of graduate student who can combine knowledge from many fields to pursue challenges as diverse as space exploration and sustainable development on Earth. One of the major goals of the Integrative Graduate Education and Research Traineeship (IGERT) program is to attract more minority students and women such as Taylor into science and engineering doctoral programs.

But NSF has a long way to go. A new report by Abt Associates in Bethesda, Maryland, of this flagship program (publication nsf0617) says that minorities (defined as African Americans, Hispanics, and Native Americans) and women were underrepresented in the first three classes of IGERT students compared with the national graduate pool in science and engineering—which is itself embarrassingly unrepresentative of the nation as a whole. The IGERT numbers were 9% and 35%, respectively, compared with 12% and 38% nationwide. Moreover, one-third of the IGERT sites had no minority students. (Asians are not considered a minority in science.)

Taylor, a third-year graduate student in the astrobiology IGERT program at the University of Washington, is doing her part to broaden minority participation. “As the first African-American woman in the department, I realize that I am a pioneer,” she says, calling research and diversity her “twin passions.” In fact, Taylor says she came to Seattle only after the university agreed to work with a new coalition of eight historically black colleges and universities (HBCUs), including her alma mater, Tennessee State University in Nashville, seeking to train more minority students in astrobiology. “Minorities can sense when a research university just wants to work with them in order to get a grant,” she says. “But so far, I’ve received a lot of support from the folks here, who are genuinely interested in building capacity at HBCUs.”

IGERT has supported 2900 students with 5-year, \$3 million grants to 125 institutions. The interdisciplinary programs cover every discipline and field that NSF funds. The

traineeships, typically lasting 2 years, include a \$30,000-a-year stipend, a tuition subsidy, and money for equipment and travel. Students take additional coursework in other disciplines as well as seminars, internships, and other career-building activities. NSF is spending \$66 million a year on the program and holds a new competition every year.

The outside evaluation flagged one problem—poor recruitment—that NSF had already begun to address. In 2002, NSF spent \$2 million to create a freestanding national recruitment office to identify potential IGERT students, especially minorities and women, and steer them to IGERT sites. “Research faculty are so focused on their work, they don’t



Making a splash. LaTasha Taylor explains how a robotic fish could explore hydrothermal vents along the sea floor.

have much time to spend on recruitment,” notes Sandy Thomas, senior administrator for the Maine-based office (igert.org).

In 2003, NSF took another step to increasing minority participation by awarding its first IGERT to an HBCU, Tuskegee University in Alabama. This fall, the university’s doctoral program in materials science and engineering will have 16 students, 13 of whom are African-American. “IGERT can’t claim all the credit,” says Shaik Jeelani, vice president for research and director of the program. “But it’s given us another way to attract good students.”

NSF is also putting more emphasis on diversity in this year’s grant competition. IGERT program manager Carol Van Hartesveldt says that “each year we have been more explicit with regard to diversity. We want to lead, not be average.”

That’s not an easy task. The small number of minorities eligible for an IGERT traineeship is further diminished by student expectations that they will work with a single scientist on a well-defined question, says Jennifer Wolch, a graduate dean at the University of Southern California in Los Angeles and a co-founder of the Center for Sustainable Cities, which began with an IGERT grant program. An interdisciplinary degree can also take longer, she says, and the need to pursue a doctoral degree can scare away students who might be attracted to a master’s or certificate-level program.

A program’s location can make a big difference, too. The University of Michigan’s biosphere atmosphere research training IGERT site, for example, requires students to spend two summers at a research station near the Canadian border. It’s a wonderful experience, says Jessica Osuna, a graduate student at the University of California, Berkeley, and an IGERT fellow, but it can be a stretch for Latino students “who aren’t used to living in the forests of northern Michigan.”

Some project directors admit that they don’t have the answer to broadening participation. “In 6 years, we’ve had two underrepresented minority students,” says Stuart Fisher of Arizona State University, Tempe, whose IGERT program in urban ecology was renewed last year by NSF. “And our program should be an easy sell.”

Taylor, who is studying human-machine interfaces in autonomous robots and who this summer is working on the cockpit design of Boeing’s new Dreamliner aircraft, says none of those issues is an obstacle for her: “I did engineering and biology as an undergraduate, so having two labs and two advisers comes naturally to me.” And the semester that IGERT will add to her doctoral program “isn’t that bad.”

She believes that any serious effort to broaden participation has to start much earlier than graduate school. So in addition to taking on multiple disciplines, she has found the time to create a self-guided astrobiology tutorial for elementary and secondary school students at inner-city schools. “It’s the first of a series of CDs that I’m planning,” she says. “The point is to show kids that science and math have real applications in their lives. That’s the best way to get them hooked.”

—JEFFREY MERVIS

CREDIT: MARY LEVIN/UNIVERSITY OF WASHINGTON



Fruits of fear. France didn't take precautionary measures, such as banning consumption of fresh produce, after the Chernobyl disaster.

FRANCE

Twenty Years After Chernobyl, Legal Fallout Lingers

PARIS—Memories of Chernobyl have begun to fade in most Western European countries. But not in France, where debate still rages about the government's response to the 1986 nuclear reactor explosion in Ukraine that spread radioactive material over much of Europe. The debate reached a new pitch last week, when a judge opened a preliminary investigation against the now 82-year-old former head of a nuclear safety watchdog, who stands accused of covering up the true extent of the fallout 20 years ago.

Pierre Pellerin was director of the Central Service for Protection Against Ionizing Radiation (SCPRI) at the time. In reassuring statements issued after the disaster, SCPRI asserted that radiation had not reached dangerous levels anywhere in France. Accordingly, the French government did not adopt precautionary measures—such as banning the consumption of fresh milk, fruits, or vegetables from affected regions—implemented by neighboring countries.

Civil parties in the case against Pellerin—some 500 thyroid patients, their national association, and a group called the Commission for Independent Research and Information on Radioactivity (CRIIRAD)—charged in 2001 that Pellerin understated the risks to prevent a public backlash against nuclear energy, which provides nearly 80% of France's electricity. The result, they claim, is an increase in thyroid cancer cases, in particular in eastern France and the island of Corsica, the regions hardest hit by fallout. Other experts say there's no such effect.

An unpublished expert study conducted at the judge's request by physician Paul Genty and veterinarian and food-safety expert Gilbert Mouthon, based in part on documents seized from SCPRI, concluded that SCPRI's information at the time was “neither complete nor precise,” according to press reports. By making public average radiation measurements for France's 95 departments, the agency obscured much higher values in local hot spots, the two scientists are reported to have written.

Based on the study, the judge has charged Pellerin with “aggravated deceit.” Pellerin has denied any wrongdoing. Although the case may never go to trial, the investigation “should finally bring some clarity,” says Marcel Boiteux, a former head of France's national power company EDF, who believes at worst Pellerin may have tried to avoid panic. Boiteux, along with physicist Nobel laureate Georges Charpak and some 60 others, wrote an open letter to President Jacques Chirac in June 2005 condemning the “odious attacks” on Pellerin, whom they called “a great servant of the state.”

Even if SCPRI painted too rosy a picture, Chernobyl's potential effects on French health are hard to determine. It is well known that radioactive iodine-131 accumulates in the thyroid and can cause cancer, especially in children. And thyroid cancer is on the rise in France. But studies have shown that the rise began in 1975 or earlier, there was no upturn after 1986, and countries not affected by Chernobyl fallout have seen increases too. However, CRIIRAD president Roland Desbordes maintains that an epidemiological study ordered by the judge among people in Corsica who were under 15 in 1986—and so most vulnerable to iodine-131—will demonstrate a “Chernobyl effect.”

According to a U.N. study of Chernobyl's legacy published last year (*Science*, 14 April, p. 180), some 4000 children and adolescents in Ukraine, Belarus, and Russia did develop thyroid cancer, but it is curable in 99% of cases. An increase in France would be unexpected, says Shunichi Yamashita, a radiation expert at the World Health Organization in Geneva, Switzerland. “There is no ‘Chernobyl effect’ in France,” a group of 50 doctors and scientists wrote in an open letter to thyroid patients published in December in national newspaper *Libération*. The problem, the group said, is that French patients have become “hostages to an antinuclear and legal-medical lobby.”

—MARTIN ENSERINK

Senate Probes CDC Shuffle

A U.S. Senate panel wants to know whether a reorganization at the Centers for Disease Control and Prevention (CDC) in Atlanta, Georgia, is driving senior scientists away. Senate Finance Committee Chair Charles Grassley (R-IA) is concerned that “morale problems” are damaging CDC's “scientific capabilities,” says a spokesperson.

The concerns stem from a reorganization begun by CDC Director Julie Gerberding a year after she took office 4 years ago. CDC scientists have complained publicly about the reorganization, saying they've been shut out of management decisions and that many senior scientists have voted with their feet.

CDC spokesperson Tom Skinner acknowledges that “some employees aren't happy” but asserts that “CDC has never been in a better position to meet public health emergencies head-on.”

—JOCELYN KAISER

Australia Weighs Nuclear Power

SYDNEY—After following a nonnuclear policy for 20 years, Australia is set to reopen debate on expanding its nuclear power industry. Major issues to be explored are the expansion of the uranium industry and construction of nuclear power stations. A panel of experts will report its findings to Prime Minister John Howard in early 2007.

Some experts argue that the country could profit from a uranium enrichment and disposal industry. But others, noting that most Australian states oppose new power plant construction, say other energy sources should be explored.

—ELIZABETH FINKEL

Brain Transplant for Bonn Center

BERLIN—The Center for Advanced European Studies and Research (CAESAR), founded in Bonn in 1999, will soon join the Max Planck Society (MPG) as a new institute dedicated to neuroscience. The decision, announced last week, means that most of the center's 140 researchers will be let go.

A harsh critique from Germany's Science Council in 2004 found that CAESAR wasn't living up to expectations as a high-tech incubator, leading its governing council to seek advice from MPG. The society's surprising answer was that CAESAR should become its 79th institute, dropping current research in medical imaging, advanced materials, and bioelectronics in favor of neuroscience (*Science*, 7 April, p. 34).

MPG has said it would like to hire three director-level scientists and employ a total of 30 scientists.

—GRETCHEN VOGEL

PALEOCLIMATOLOGY

Looking Way Back for the World's Climate Future

Researchers worry that if they cannot recall the distant climatic past, the world may be condemned to repeat it. And repeating the warmth of the early Pliocene epoch of 3 million to 4 million years ago would be a shocker. With no more

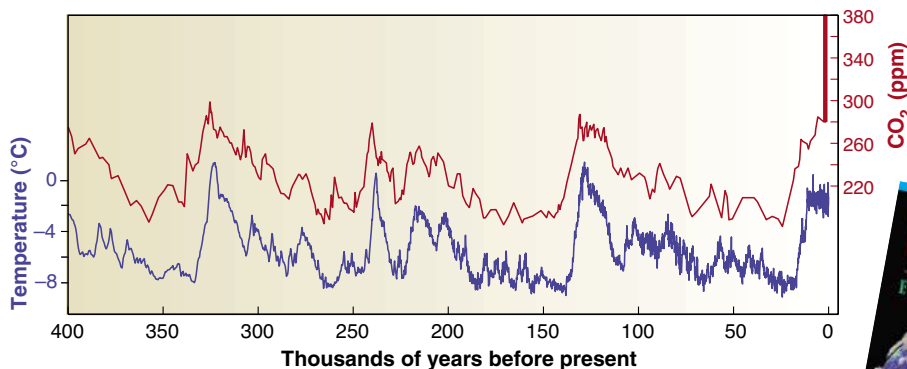
and concludes that humans may already have put the world on a path back to that epoch. "It's a very interesting period to study, a great scientific puzzle," says paleoceanographer David Lea of the University of California

occurring at mid- to high northern latitudes. Those changes might constitute a climatic switch: Throw it one way, and trigger a permanent El Niño in the Pacific Ocean capable of warming the whole world. Throw it the other way, and El Niño and La Niña alternate in a cooler world as they do today.

In an earlier study of Pliocene climate, paleoceanographer Christina Ravelo of UC Santa Cruz, a co-author of this paper, and her colleagues found continuously warm water from one end of the tropical Pacific to the other: the hallmark of an El Niño.

Then about 3 million years ago, the eastern Pacific began cooling, according to their analysis. That set up the warm-in-the-west, cool-in-the-east arrangement that typifies modern conditions. Another analysis of the same deep-sea sediment cores as Ravelo used came up with the opposite Pliocene arrangement: permanent cold in the east

(*Science*, 29 July 2005, p. 687). But Ravelo recently analyzed another kind of paleotemperature record across the Pacific and again found a permanent Pliocene El Niño, which persuades ▶



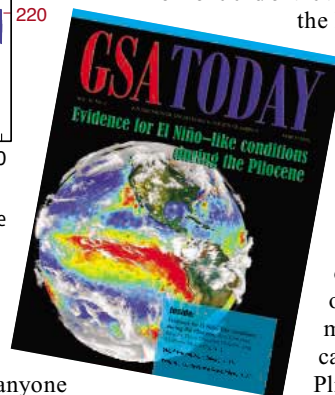
A coming switch? Atmospheric CO₂ has driven temperature change lately, and the recent CO₂ rise (vertical red line) may be triggering a permanent El Niño (red, inset).

carbon dioxide warming the greenhouse than today, the globe was a good 3°C warmer, and sea level was a whopping 25 meters higher. But how could such a modest stock of greenhouse gas fuel such warming? Unfortunately, no one knows.

On page 1485 of this issue, a group of climate researchers takes a look back at the Pliocene, pulls together models of oceanic and atmospheric behavior under those conditions,

(UC), Santa Barbara. "I like the way they're thinking." But better paleo-data and more realistic modeling will be needed before anyone knows for sure.

The key to understanding Pliocene and possibly future climate, say climate dynamist Alexey Fedorov of Yale University and his colleagues, could be the climate changes



RUSSIAN SCIENCE

Measuring the Hidden Cost of a Pay Raise

MOSCOW—A mandate to increase Russian researchers' pay could have a disastrous impact on long-term science programs, according to institute directors at the Russian Academy of Sciences (RAS). The pay mandate, issued by the government in May and made retroactive to January, aims to boost core salaries in RAS to an average of \$1000 per month. But because the government has not provided a commensurate funding boost, RAS institutes are trying to balance the books with economy measures, including a 2-year moratorium on new equipment purchases. "The recent decision just ruins the development of science," says academician Boris Ioffe, a nuclear physicist at the non-RAS Institute for Theoretical and Experimental Physics in Moscow.

RAS Vice President Alexander Nekipelov announced in May that the academy will cut research staff from 53,000 to 44,000 by 2008, beginning with a 5% reduction this year. This will help pay for some salary increases; for example, a junior researcher's pay may climb

from \$150 to \$300 per month. But the government also placed an indefinite freeze on bonus payments that often go to active researchers in recognition of factors such as scholarly achievement and high-risk work. The net result is that some top scientists will see their pay decline.

"I'm glad that some people working in the academy will get substantially bigger salaries," says Erik Galimov, director of the RAS Vernadsky Institute of Geochemistry and Analytical Chemistry. But he says this will "not solve" the main problem: the declining influx of youthful researchers. His students at Moscow State University often take part-time jobs at the institute, but "when it comes to graduation, they choose jobs with salaries dozens of times higher" than the institute pays. And the mandatory salary boost does not cover engineers, office workers, or financial staff; Galimov predicts that they will become more difficult to retain. If they leave, it would "paralyze the work of the institute," he says.

Ioffe estimates that "the only way" an RAS

institute director can implement the new salary order is to severely slash spending in nonsalary areas. "But you can't do science for nothing," he says. "You have to buy materials, new equipment."

Leonid Bezrukov, deputy head of the RAS Institute for Nuclear Research, regards the equipment purchase moratorium as the main threat. "Modern, expensive facilities are vital for us. You cannot build them on the relatively small" funds available from outside the government budget, he told *Science*. He thinks that his institute will be at a growing disadvantage against laboratories in the West: "We need funds dozens of times more than we have now." There's a risk that the institute may just "drop out," Bezrukov says. His own pay will be reduced by the salary changes; he notes that "all of our active researchers have found themselves in the same situation."

—ANDREY ALLAKHVERDOV AND
VLADIMIR POKROVSKY

Andrey Allakhverdiv and Vladimir Pokrovsky are writers in Moscow.

Lea that the weight of evidence now favors a Pliocene El Niño over La Niña.

If El Niño ruled the Pliocene, what threw the climatic switch to end its reign some 3 million years ago? To answer that and, conversely, to learn what might switch climate back to Pliocene conditions, Fedorov and his colleagues draw on several modeling studies they have published in recent years. In their scenario, the long-term cooling of the past 50 million years and accompanying drying at high latitudes in the North Atlantic would have cooled surface waters there and made them saltier. Making waters denser would have swelled the river of cold water that sinks into the depths there. That in turn would have increased the volume of cold, deep seawater. Almost all the ocean's water is near freezing, even beneath the tropics; during a permanent El Niño, cold water does not rise to the surface in the eastern Pacific.

But the overlying warm layer would have thinned as the underlying cold water expanded. In the scenario's eastern tropical Pacific, it eventually thinned enough for winds to raise cold water to the surface and break El Niño's grip on the Pacific. That, in turn, would have sharply increased the amount of low-lying clouds reflecting solar heat into space and decreased the amount of water vapor trapping heat in the atmosphere. The breakthrough of tropical cold waters would have thus accelerated global cooling roughly 3 million years ago, when ice first began growing in the north. Today, the strengthening greenhouse seems to be pushing the other way on the switch, warming high latitudes and freshening northern waters with melting ice and more rain.

Nice story, but is it true? "They might be right," says El Niño modeler Amy Clement of the University of Miami in Florida, but so far the modeling has been piecemeal. "You have all the pieces of the puzzle," she says, such as the oceans and atmosphere. But when "you put them together, the result is a lot more complicated than you expect."

Researchers agree that it's urgent to sort through the complications. If there is a climatic switch as described by Fedorov and his colleagues, humans are pushing it harder and harder toward Pliocene conditions. Carbon dioxide emissions are already raising atmospheric levels into the top of the estimated range during the Pliocene, and high northern latitudes are getting warmer and wetter. That alone, say Fedorov and his colleagues, could possibly push Earth back to a permanent, globe-warming El Niño within decades to centuries. In their scenario, all it would take would be a warm surface layer in the eastern Pacific just a few tens of meters thicker than today, and the Pliocene would be back.

—RICHARD A. KERR

PALEONTOLOGY

Ancient 'Reef' Stirs Debate Over Early Signs of Life in Australian Rocks

When paleontologists seek the roots of life, they head to rocks of the Archaean Eon, which range from 3.8 billion to 2.5 billion years old. But it's a tough task: The rocks are so battered and time-worn that any evidence of fossils is greeted with suspicion. For many years, an exception was a familiar-looking structure called a stromatolite, which has a modern analog formed by cyanobacteria. But when computer models suggested that simple chemical reactions and physical forces can mimic stromatolites, those fossils too were cast in doubt.

Now, a new study of ancient stromatolites in western Australia musters evidence that bacteria were indeed thriving 3.4 billion years ago and created an enormous reef. Australian and Canadian researchers argue this week in *Nature* that stromatolites were so diverse and complex that they must have been alive. Some



Fossil or not? New study suggests that features in rocks like this one were created by microbes 3.4 billion years ago.

paleontologists agree, but others remain dubious. Still, the detailed descriptions will be invaluable in constraining computer models of stromatolite growth—and helping determine whether life is needed to explain them, says paleontologist Bruce Runnegar, who directs the NASA Astrobiology Institute in Moffett Field, California. "This paper will be a big step forward in getting it right," he says. Some scientists hope it will also shed light on possible life forms on other planets.

The stromatolites in question were first described by Donald Lowe of Stanford University in 1980, in rocks called the Strelley Pool Chert, some 1400 kilometers northeast of Perth, Australia. Lowe pointed out their resemblance to modern forms but later had doubts. In 1996, John Grotzinger, now at the California Institute of Technology in Pasadena, and Daniel Rothman of the Massachusetts Insti-

tute of Technology in Cambridge argued in a *Nature* paper that chemical precipitation, movement of suspended sediment, and other nonbiological factors could create structures resembling at least some stromatolites.

Abigail Allwood, a graduate student at Macquarie University in Sydney, Australia, set out to see just what was in Lowe's rocks. She and colleagues studied and described stromatolites in outcrops across tens of kilometers.

Modern stromatolites are typically mounds, but Allwood found more than seven kinds in the rocks, including some shaped like intricately cusped swales and others like cones. The layers of the latter were thicker on top and thinned down the 50-degree sides, suggesting that colonies of microbes had been growing upward. "The individual grains in them could not have accumulated mechanically because

the slope of the cone is too great," says Stanley Awramik, a stromatolite expert at the University of California, Santa Barbara, who was not involved in the research. In addition, Allwood says, some of the cones had slumped, suggesting they had been covered with a mat of microbes, not a crystalline crust as in mineral formations.

Allwood and her colleagues say it's improbable that physical and chemical processes could have created such a varied, complex geometry. "It's just ridiculous," Allwood says. Runnegar is more cautious. He hasn't yet ruled out other nonbiological processes,

such as currents, but he expects the stromatolites will turn out to be real fossils.

Martin Brasier of Oxford University is less sanguine, arguing that the structures are more likely chemical precipitates. He also objects to the reasoning in the *Nature* paper. "You can't use the argument that complexity is the signature for life," he says. "The extreme variability is what we would expect from a physical mechanism."

A better indicator of life, Brasier argues, would be microfossils with a consistent shape. That would suggest DNA was at work. Brasier and colleagues may have found signs of microfossils in an older portion of the Strelley Pool Chert, which they described online 19 May in the *Philosophical Transactions of the Royal Society B*. "We've put them forward as candidates of interest," he says. Expect a healthy dose of skepticism about their origins, too.

—ERIK STOKSTAD

A solid tenet of archaeology is that civilization first sprang to life in the cities of southern Mesopotamia. But was there a parallel—or even earlier—development of urban culture to the north?

North Versus South, Mesopotamian Style

HAMOUKAR, SYRIA—They attacked from the south, flinging oval-shaped, clay bullets over the earthen walls with slingshots. After a fierce struggle, the invaders stormed the battered ramparts and set fire to the buildings. Those inhabitants of this northern Mesopotamian settlement who still survived fled, leaving behind a smoking ruin. “This was ‘Shock and Awe’ of the 4th millennium B.C.,” says Clemens Reichel, a University of Chicago archaeologist and co-director of the dig here; his team collected an astonishing 1200 small clay spheres and 120 softball-sized balls at the site last fall. After the violent confrontation 5500 years ago, pottery and other clues hint that southerners took over this site a few kilometers from the modern-day Iraqi border.

Other scholars are skeptical that Reichel’s evidence can back up this detailed battle scenario, and some even dismiss the claim that the clay balls were weapons. But there is little doubt that the settlement fell under southern influence. And the eclipse of Hamoukar and other nearby sites in the same period seems to mark an end to an emerging urban culture that existed at least as early as the one in southern Mesopotamia, say Reichel and a growing number of archaeologists. History may belong to the victors, but if Reichel’s view is correct, it would upend the long-held assumption that civilization began first in the marshes where the Euphrates and Tigris rivers flow into the Persian Gulf.

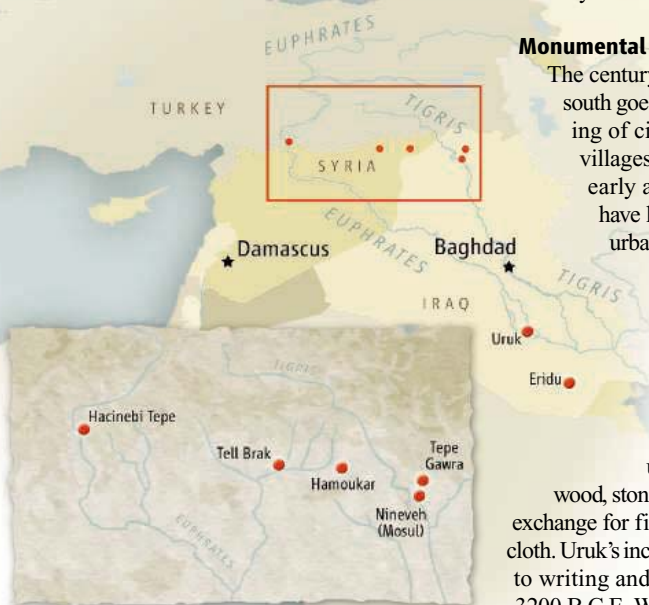
As archaeologists flock to sites in Syria (see sidebar, p. 1459), they are finding large settlements with monumental architecture and long-distance trade at the same time as the first stirrings of city life appear in southern Mesopotamia. “The possibility exists that the south was the periphery,” says Harvard

University archaeologist Carl Lamberg-Karlovsky. “It’s a heresy.”

Monumental finds

The century-old doctrine of the dominant south goes to the heart of our understanding of civilization’s origins. Although villages sprang up in the Near East as early as 10,000 B.C.E., researchers have long thought that truly complex urban areas first evolved in southern Mesopotamia in the mid- and late 4th millennium B.C.E. People from the preeminent southern city of Uruk expanded north and east after 3500 B.C.E., bringing with them the trappings of urban life, possibly in a quest for wood, stone, and other natural resources in exchange for finished goods such as grain and cloth. Uruk’s increasingly complex economy led to writing and monumental architecture by 3200 B.C.E. Within centuries, other complex societies with similar traits appeared from the Nile to the Indus.

But a handful of excavations in what is now northwestern Iraq, southeastern Turkey, and northeastern Syria haven’t borne out the story of the south’s preeminence. For example, at Turkey’s Hacinebi Tepe, archaeologists in the mid-1990s uncovered a 3-meter-wide wall



Down under. This deep trench at Tell Brak reveals monumental architecture from 4000 B.C.E.

around a central precinct dated to approximately 4000 B.C.E., along with stamp seals and sealings and infant burials with silver and copper jewelry—all signs of an entrenched hierarchy. Earlier excavators at Tepe Gawra in northern Iraq uncovered substantial homes dating back to the mid-6th millennium B.C.E.; at Tell es-Sawwan, also in northern Iraq, they found a defensive wall and moat from that era. Although a far cry from urbanism, these finds surprised archaeologists, because they predate the Uruk expansion.

More dramatic evidence with the hallmarks of urbanism is now coming out of northern Mesopotamian sites in Syria as archaeologists uncover surprising sophistication in very old layers. That apparently indigenous culture challenges fundamental ideas about how the first cities began. Rather than a dominant south bringing civilization to the primitive north, some combination of cooperation and competition between the two areas may have intensified urban evolution.

Some of the most important evidence of an early complex culture in northern Mesopotamia comes from Tell Brak, a massive mound just west of Hamoukar that rises 40 meters above the flat Mesopotamian plain. Settled as early as 6000 B.C.E., Brak's towering height is the result of thousands of years of building and rebuilding mud-brick houses, temples, and palaces in the same spot. The mound is so steep that local children hop on pieces of cardboard and ride screaming to the bottom. Previous excavations revealed that residents had built an impressive temple with hundreds of mysterious small figurines with pronounced eyes, dubbed eye idols, which are not found in the south. That temple was dated to about 3000 B.C.E. when found in the 1930s. But in the late 1990s, Cambridge University archaeologist Joan Oates (see sidebar, p. 1460) and her late husband David determined that the temple and idols were in fact 5 centuries older—from before southerners exerted control over the north.

The Oateses also began digging deeply into one side of the mound during the 1990s, exposing additional layers that predate the long reach of the powerful southern city of Uruk. Access to such levels is rare, particularly in the south, where later buildings often make it difficult to access earlier periods. But at Brak, Oates has successfully uncovered a large building with a massive basalt block at the entrance, dating to about 4000 B.C.E. That's a surprise, because most researchers assumed that monumental buildings first arose in southern cities such as Eridu and Uruk.

At Brak, Oates leads the way into the deep cut in the mound, with sheer cliffs of



Mound builders. Tell Brak looms above the Mesopotamian plain.

Syria's Open Door: Will It Last?

DAMASCUS—In spring and fall, the narrow hallway on the second floor on the back side of Syria's National Museum becomes an archaeological Grand Central Station, a peculiarly Eastern mix of frenetic activity and bureaucratic ennui. European and American excavators wander in and out of the small, high-ceilinged offices, patiently seeking permits, dropping off boxes of artifacts, or submitting reports. Bored young employees push paper and chat while their harried managers dart back and forth for meetings at the nearby Ministry of Culture.

During these busy seasons, Syria turns into what the country's chief of antiquities Bassam Jamous calls "one vast archaeological academy." More than 140 foreign and domestic teams are at work here—a far cry from the half-dozen or so expeditions of a half-century ago—and the boom is educating a rising generation of Syrian researchers.

Long an archaeological backwater, Syria is now at the center of critical debates on the origin of urbanism (see main text) and the role of trade, religion, and empire in shaping early civilization. That limelight is due in part to turbulent Middle East politics and in part to changing archaeological mores among other nations. Iraq and Iran are largely off-limits to Western scientists, strife in Israel and the Palestinian territories poses hazards, Jordan has limited sites, and Turkey and Egypt are restricting new dig permits. So Syria's rich heritage, relative domestic calm, and typically open attitude toward foreigners make it a welcome destination for many Near Eastern archaeologists. And as the researchers have come, they are making spectacular finds.

Roughly the size of North Dakota, Syria contains more than 5000 documented sites that span thousands of years of history. At Tell Sabi Abyad in the north, Peter Akkerman of Amsterdam's Rijkmuseum spearheads work at an 8500-year-old village, home to some of the oldest pottery to date in the Near East. Paolo Matthiae of the University of Rome continues digging at Ebla in western Syria; the city was conquered and burned in approximately 2200 B.C.E., fortunately baking more than 15,000 cuneiform tablets that provide rich insight into life in the 3rd millennium B.C.E. Yale University's project at Tell Leilan in the east, led by Harvey Weiss, kicked off the debate in the 1990s about the role of climate change in the ancient world. And British, U.S., and French digs at Dura-Europos on the middle Euphrates have uncovered one of the world's oldest churches as well as synagogues at this eastern limit of the Roman Empire.

But Syria's open door could swing shut. Michel Al-Maqdissi, director of excavations at the department, insists on more surveys and less digging, and he is reluctant to approve new excavations along the border with war-torn Iraq. He and Bassam also want archaeologists to spend more time and money on conserving sites that might draw tourists. Meanwhile, mounting tensions with the West following last year's assassination of a former Lebanese leader, plus stricter U.S. sanctions, make for a potentially volatile situation. For now, however, Syria's archaeological riches are helping to remake our understanding of civilization's start. The discoveries bode well for archaeology's future in this land set amid one of the world's most ancient—and tumultuous—neighborhoods.

—A.L.

At Home on a No-Frills Tell

TELL BRAK, SYRIA—Most 70-somethings quietly retire. But not archaeologist Joan Oates. Oates, who leads one of Syria's longest-standing and most productive excavations, is only now, as she nears 78, hitting her research stride. After raising three children while assisting her late husband David Oates with excavations during the past half-century, she is now returning to her original interest in the era prior to the invention of writing. Her ongoing dig of a 6000-year-old settlement is radically reshaping our understanding of early urbanism (see main text).

Oates is the prickly doyenne of Near Eastern archaeology, a dedicated excavator well into her third decade at the massive mound of Tell Brak, which dominates the Syrian plain. That effort, which she took over after the death of her husband in 2004, is now paying off. "Brak is an unusually large and early site, and we're getting not only a very good record of a major tell but also an understanding of what is happening in the region," says Tony Wilkinson, a landscape archaeologist at Durham University in the United Kingdom who has worked with Oates. "Joan has enabled that."

Oates has patiently waited for decades to return to her interest in prehistoric archaeology. After abandoning a major in chemistry while studying at Syracuse University in New York in the 1940s, she focused on archaeology. Armed with a Fulbright scholarship to the University of Cambridge, the young American worked for a time on early human shelters in what is now Israel before moving to Iraq to work on her Ph.D. on the period before Mesopotamian cities began to flourish. There she met her future husband, as well as British archaeologist Max Mallowan and his author-wife Agatha Christie, who took her under their wing.

In the 1950s and 1960s, the Oateses excavated at the Assyrian capital of Nimrud with Mallowan and then at Tell al Rimah just to the north—much later periods than those of Oates's original interest. "I was a dutiful wife and did what was dictated by what David was doing," she says. "I handled a lot of the records—drawing, writing, photographing." At Nimrud, the Oateses found and cataloged a famed collection of delicate ivories from the

In her element. After a half-century in the Near East, Joan Oates is now pursuing her first love, the roots of civilization.



1st millennium B.C.E., and at Tell al Rimah, they uncovered surprisingly sophisticated architecture in the little-known period at the start of the 2nd millennium B.C.E. Whatever Oates says, colleagues insist that she was always far more than a dutiful wife; she evolved into a leading expert in Near Eastern ceramics and was instrumental in analyzing discoveries and publishing the results.

During a tumultuous era of Iraqi revolutions and Arab-Israeli wars, she also raised three children, partly in Baghdad, partly in London, and partly at excavations. David began work at Tell Brak in 1976, and Joan followed 2 years later. In 1981, she became intrigued with one area of the massive mound, which she believed could hide very early material. "I just kept bullying him," she says, "arguing that the whole of the 4th millennium [B.C.E.] could be opened up." With limited funds and other projects, David demurred. Finally, a decade later, he relented, and she has since focused her work at that spot.

When David died, Oates assumed his mantle, along with the lifetime excavation permit granted by the Syrian authorities. Life at Tell Brak was and remains notoriously no-frills. Beds are rough cots in canvas tents, the lab is a two-room mud-brick house, and the food is basic; sardines and rice are typical fare. During a recent powerful thunderstorm, Oates's heavy tent collapsed on top of her. Undaunted, she retreated to the lab to work.

Oates has a reputation for maintaining strict control over a dig, eschewing change, and keeping a close eye on the dig purse, in contrast to the more relaxed and egalitarian approaches favored by other excavation chiefs. "She's a tough woman, and you don't want to cross her," says one archaeologist who knows her well. Nevertheless, no one disputes that Oates has given several generations of students lessons in scientific rigor. "I keep people on their toes," she says.

But despite her rough edges, Oates has learned how to win the respect of Syrian colleagues. "She knows that the only way to get access is to build good relationships with the local authorities and to be humble, helpful, and nice," says Salam Al-Quntar, a Syrian archaeologist who works at Brak. "That's her strategy, and it works."

Although Oates intends to relinquish day-to-day control over the excavation in the coming season, she can't see herself abandoning field life altogether. "Creeping up to 80, I could put my feet up a bit," she says. "But I don't think I will so long as I can keep both feet on the ground."

—A.L.

mud rising as high as 10 meters on three sides. "This is a monumental building, suggesting a relatively complex society and an organized administration at the end of the 5th millennium," she says, gesturing at the low mud-brick walls. A few centuries later, the people of Brak built a hall near the same site, 4 meters by more than 15 meters, along with a number of large ovens too big for any but communal use.

While Oates excavates in the central mound, archaeologist Henry Wright of the University of Michigan, Ann Arbor, is gathering evidence of settlement patterns in the suburbs during the same period. First, Wright and his team obtained old satellite images taken by spy satellites during the Cold War as well as civilian Landsat pictures. More recent images are confounded by development, which is crowding in on Brak. Farmers have graded nearby grazing

lands with heavy equipment to grow cotton, which requires deep plowing and large amounts of water—a deadly combination for fragile mud-brick sites. New houses and industry also creep closer to the site every year, and a wealthy landowner recently used a bulldozer to flatten a small mound just a few hundred meters from the central mound.

After examining the satellite images, Wright's team could comb the site more effi-

ciently on foot for traces of settlements. Combined, the data provide a window into a long-vanished landscape shaped by the ancient residents. Based on surveys from 2003 through 2005, Wright and his crew of techie grad students concluded that in the late 5th millennium B.C.E., 115 sites clustered within a 15-kilometer radius of Brak—a number Wright calls “astounding.” The central mound itself included more than 40 hectares, and 100 hectares if suburban sprawl is included, he adds. At least seven of the sites in the immediate vicinity are larger than villages.

Although not all the settlements likely existed at the same time, Wright’s figures impress even skeptics. “It’s bloody big—bigger than people like me thought were possible at that early time,” says anthropologist Guillermo Algaze of the University of California, San Diego, a champion of the view that southern Mesopotamia held sway over its neighbors. The new data make Brak roughly as large as Uruk in the mid-4th millennium and significantly larger than Eridu, a major southern Mesopotamian city that may have covered 10 hectares and was home to a series of early temples. Brak may have boasted a population of some 20,000, says Wright.

“There is good evidence that you have urbanism and specialized production at Brak by the middle of the 4th millennium B.C.,” he says. His work has also provided evidence of workshops devoted to ceramics and perhaps metal and stone.

Moreover, the pattern of settlement differs significantly from the dense cores of cities and evenly distributed villages and towns typical of the south. The Brak settlement resembles Mayan sites, Wright says, with large patches of empty land presumably dedicated to agriculture or animal grazing. “One suspects these were gardens, or places for nomadic relatives to camp, or spaces to separate people who didn’t trust one another,” he adds.

Site of the Kissing Bears

Some 80 kilometers away at Hamoukar, archaeologists are finding other kinds of evidence that point to a complex northern society before 3500 B.C.E. Within sight of the Iraqi border, Hamoukar is a low mound on a vast plain. A steep trench dug down one side by University of Chicago archaeologist McGuire Gibson starting in 1999 revealed a 3-meter-wide city wall which could date from as early as the first half of the 4th millennium B.C.E., before Uruk dominated the region. In recent years, Reichel and Syria’s Salam al-Quntar (see sidebar, p. 1462), who succeeded Gibson as Hamoukar co-directors, focused on a site on the other side of the mound that includes a symmetrical building with a courtyard, storage areas, and living space.



Heading for the ‘burbs. Henry Wright, with local friends, sets out to survey the outskirts of Tell Brak.

Because of erosion, the team did not have to dig far to expose the low remaining mud-brick walls dating from the mid-4th millennium B.C.E., filled with local pre-Uruk pottery and built of bricks that don’t match the typical size used in the south in that era. Also uncovered were remains of seals, used to signify ownership of jars, baskets, and storerooms. The seals carry motifs of kissing bears and lions, similar to those found at Brak and at sites in nearby Turkey but stylistically distinct from southern

seals in the same period. The excavation also revealed a series of large ovens and grinding stones that Reichel says are evidence of bread production for more than single households. Eye idols similar to ones found at Brak have been uncovered as well. Reichel says that the seals, pottery, and brick styles reveal “no signs of political or economic domination by the south.”

But Hamoukar’s location and ancient prosperity puzzles archaeologists. There is no major river, and the land, located on the edge of rain-fed agriculture, is not exceptionally fertile. The answer may lie a short walk south of the main mound in an area of low hills 280 hectares square, with pottery dating from the late 5th to early 4th millennium. Called Al Fukhar, or pottery mound, by locals, the area is even today chockfull of obsidian blades, both finished and unfinished. The obsidian comes from Turkey and was widely used in the Near East before the advent of metal blades. Some scholars assume the spot was used by passing nomads in the 4th millennium B.C.E. But al-Quntar last year excavated three 10-meter-by-10-meter squares and found a clay floor with large storage jars, a sign of permanent settlement in that period, suggesting that trade may have fueled Hamoukar’s rise.

The evidence from sites such as Hamoukar and Brak make the existence of social complexity in the north prior to the Uruk expansion “unassailable,” says Gil Stein, director of Chicago’s Oriental Institute and chief of the Hacinebi dig. Even former skeptics such as Algaze—who now says he was “entirely incorrect” about the dominance of southern influence—say they are convinced. “If you landed in



Bombarded? Chicago’s Karen Terras sorts clay balls, possible weapons from Hamoukar.



Getting dirty. Salam Al-Quntar revels in fieldwork and has little patience with bureaucracy.

A Rising Star in the Trenches

Thirty-two-year-old Salam al-Quntar discovered her first potsherds as a young child playing in the ancient olive groves surrounding her grandfather's house, which was made in part with recycled Roman stones. Today, al-Quntar is co-director of the key Hamoukar dig, where excavators are uncovering dramatic evidence of early urbanism in northern Mesopotamia (see main text).

She is also a startlingly outspoken female scientist in this predominantly Muslim country. Busy working on her Ph.D. to synthesize controversial finds at both Hamoukar and nearby Tell Brak, she splits her time among those two sites, Cambridge, Damascus, and her hometown of Suweida in southern Syria. "Her heart is really beating with archaeology, and she is uncompromising and very passionate," says Clemens Reichel, a University of Chicago archaeologist and the other co-director at Hamoukar.

A daughter of two teachers and a member of the minority Druze ethnic group, al-Quntar chose archaeology at the university because, as she admits with typical forthrightness, "my grades were not good enough" for economics. Upon graduating, she struggled to find a job for 2 years, until her family's connections landed her a position at the museum in Suweida, famed for its 4th century C.E. Roman mosaics. She watched, outraged, as local authorities built an underpass that destroyed ancient parts of the city. But she also frequented a French archaeological expedition in the area and honed her excavation skills with American and German teams

a spaceship at the start of the 4th millennium B.C., you would probably not be able to tell which would take off—northern or southern Mesopotamia," he says.

To many, the evidence suggests that northern and southern societies were distinct. Settlement patterns were different: In the south, settlements tended to be concentrated on high mounds, in part because of the danger of flooding. Southerners developed complex irrigation systems, whereas northerners generally could count on enough rain to rely on dry farming. Culturally, the eye idols found at Brak and Hamoukar hint at a religious tradition quite different from that of the south, with famed gods such as Enlil and Inanna. The very reason for the founding of cities may be different. In the south, the confluence of rivers on the flat plain spawned intensive agriculture and extensive urbanism. In contrast, fewer sites appear in the north. Places such as Hamoukar are difficult to irrigate but sit astride natural trade routes between the south and Turkey's mineral-rich mountains to the northwest. "It may be the oldest story in the world," says Reichel of the growth of Hamoukar. "Someone figured out how to make a buck."

The end of the experiment

Not all scholars are ready to concede an autonomous development in the north, however. Gibson—who dug for decades at the

Sumerian city of Nippur in the south of Iraq—argues that places such as Hamoukar and Brak got their initial push during the Ubaid



Bear pair. A stamp seal with kissing bears, dated to 3500 B.C.E., has a distinctly northern feel.

period in the 6th millennium B.C.E., when a common pottery and artifacts likely centered on southern Mesopotamia turn up throughout the Middle East, including the north. Oates and others counter that the Ubaid culture had long passed in the north when sites such as Brak began to flourish.

One problem in resolving the matter is limited evidence from the south prior to the 4th millennium B.C.E., both because of a previous lack of interest and the difficulty in excavating deep levels in the alluvium. For Gibson, the Ubaid is the next frontier in understanding the advent of

complex society, but its heartland in Iraq remains off-limits to archaeologists for the foreseeable future. A meeting this spring at the University of Durham in the United Kingdom devoted solely to the Ubaid—the first in nearly 20 years—is a sign of growing interest in that period.

In the meantime, Stein wants to see more supporting evidence to prove that the north had its own indigenous tradition. "If this is urbanism, it seems to come out of nowhere and then disappear—a failed experiment," he says. Whatever the race between north and south, agrees Algaze, "by the end of the 4th millennium B.C.E., the competition is over."

Sometime after 3500 B.C.E., Uruk colonists arrived at sites such as Brak and Hamoukar. But just how northern society fell is a source of dispute. Reichel contends that it was a violent transition at Hamoukar, but several scholars, such as Yale University archaeologist Harvey Weiss, say that Reichel's so-called bullets are actually clay blanks used for sealings. Reichel counters that the balls are similar to those flung today by local shepherd boys at Hamoukar, and the squashed ends of some—what he calls "Hershey's Kisses"—show that they were smashed against hard surfaces. The balls are associated with a layer of ash, which indicates a catastrophic fire, and Uruk-style pottery on top of that layer shows the arrival of people either from the south or influenced by its culture. Other scholars, however, say that the violence may have been the result of a nomadic attack.

elsewhere in the country. "Other people prefer to sit in their offices and stay beautiful," she says. "But I enjoy being out, and I never feel embarrassed walking around in dirty clothes."

Few Western students could boast such intensive field experience, but further study abroad, vital to advancement, at first proved elusive for al-Quntar. Her scholarship application to a German university was turned down, leaving her dejected. "I needed encouragement," she says. "I didn't know the system and wasn't sure I was qualified."

Shortly afterward, she met Augusta McMahon of the University of Cambridge, who was digging at the prehistoric northeastern site of Chagar Bazar. With McMahon's encouragement, and the active help of McMahon's mentor Joan Oates, also of Cambridge, al-Quntar won a scholarship to Liverpool University in the United Kingdom to get her master's degree. "I was afraid to apply to Cambridge; I wasn't sure they would accept me," she recalls. Then, again with the help of the old-girls' network, al-Quntar gained a place at Cambridge to work on her Ph.D., with McMahon as her immediate supervisor and Oates as a senior adviser. Last year, al-Quntar took over as co-director of the Hamoukar expedition, while also working at nearby Tell Brak under Oates's direction.

Oates praises al-Quntar's excavation skills as well as her drive and calls her a rising star in Syrian archaeology. "She is a very ambitious person who knows a lot," adds Reichel. Her ability to wear down bureaucratic intransigence complements her commitment to fieldwork, he says.

Al-Quntar's gender does create obstacles not typically encountered by foreign female scientists. For example, one young male Syrian excavator

worked without complaint for a Western female archaeologist and acknowledges al-Quntar's expertise, yet he told *Science*, "I could never take orders from a woman." Al-Quntar can be demanding and outspoken to the point of brashness, a quality that rubs some who work with her the wrong way. That assertiveness, she says, stems from years of accepting quietly whatever work the Syrian department of archaeology offered. "It was difficult at the beginning, and I wasn't allowed to say what I can say now," she recalls.

If she ever pulled punches, she doesn't now, bluntly criticizing Syrian archaeology—an unusual act in a country where dissent is typically muffled. She charges that the low pay for archaeologists coupled with a frustrating bureaucracy make it difficult for homegrown researchers. "It is a struggle; you have to be a fighter to do archaeology here," she says.

Al-Quntar is fired up about shifting the traditional focus of Near Eastern archaeology on the elite to aspects of everyday life. "It is more interesting to know how ordinary people lived and how they operated economically," she adds. "It's not all about palaces and temples."

Although satisfied that there are more women now in the field, she complains that "people still think it is strange for us to get dirty and be exposed to the sun." Overcoming the distaste of what some see as menial labor in a still largely rural culture is critical for the advancement of Syrian archaeology for both genders. Too many of the three dozen Syrians now studying abroad lack field experience, says al-Quntar, adding with her characteristic bluntness: "That's shameful."

—A.L.

And many still maintain that the Uruk expansion was a gradual acculturation based on trading rather than military aggression.

Yet there is evidence of burning in at least one area at Brak at roughly the same time as Hamoukar, says Geoff Emberling, a University

of Chicago archaeologist who was field director there until 2004. Uruk pottery thereafter appears at Brak, which also shrank in size and importance. In one room, Emberling adds, excavators found a pile of 40 fist-sized clay balls—possibly an unused ammunition dump.

On the site of Brak's old temple, the new inhabitants built a temple in the southern style of Uruk with its characteristic decorations of conical clay cones. "People didn't just move in; they took ideological control," says Emberling.

Whatever the trigger, the evolution of an indigenous urban society in northern Mesopotamia ground quickly to a halt, while southern Mesopotamia continued its evolution into the world's first literate society with large cities and a complex religious and political elite. Algaze speculates that the flat plain and myriad waterways of southern Iraq made transportation easier, giving that region the edge. And whereas many cities sprang up in the south, perhaps spurring competition and accelerating the development of technologies and trade, the north had only a few scattered urban areas that proved easy to dominate.

The Syrian finds are prompting researchers to rethink civilization's beginnings. Could the north have led the way in urbanism, passing its knowledge on to southerners? Algaze suggests that "parallel clusters" of urban growth could spur each other on, through cooperation and competition. Could the near-simultaneous bubbling of ideas about writing, monumental architecture, and trade in Egypt and Mesopotamia—and later along the Indus River—have fed one another? Such an approach could enable archaeologists to move beyond sterile questions about who was first and instead explore the complicated ingredients required for civilization to coalesce.

—ANDREW LAWLER



Burned out? Clay balls and signs of fire at these Hamoukar buildings hint at a violent end.

Golden. Shanghai's horizon reflects a growing ambition that powers China's investment in research and technology.

SCIENTIFIC MISCONDUCT

Scandals Shake Chinese Science

A spate of misconduct cases may force China's scientific leaders to clean house or watch their drive for a more innovative society sputter

For more than a decade, the Chinese government has been heaping money and prestige on its academic community in a bid to gain ground in a global technological race. In this scientific Wild East, an unprecedented number of researchers stand accused of cheating—from fudging résumés to fabricating data—to gain fame or plum positions. Buffeted by scandals and an urgent appeal for action from expatriate scientists, top scientific leaders now acknowledge the need for change in a system notorious for its high expectations and scant oversight. “Too many incentives have blurred the reasons for doing science in some people’s minds,” Lu Yongxiang, president of the Chinese Academy of Sciences (CAS), told *Science*. “We need to improve our evaluation and assessment system to establish a better culture for R&D innovation.”

The central government is taking the first tentative swipes at what will amount to a Herculean task. For starters, the Ministry of Education (MOE), which funds and oversees the nation’s universities, last month issued ethics guidelines and formed a panel to police conduct in the social sciences. “Though it is difficult to ascertain the number of misconduct cases, the negative impact of these cases should not be underestimated,” says MOE spokesperson Wang Xuming. CAS, adds Lu, “will do its best to improve oversight. Monitoring by society is also needed.” Xu Guanhua, minister of science and technology, told Chinese reporters in March that “if academic corruption exists, then we will investigate every single case, thoroughly.” That pledge notwithstanding, the Ministry of Science and Technology (MOST), with one of the largest portfolios, has not yet revealed how it plans to crack down on misconduct.

Part of the challenge, observers say, is that science in China is acutely susceptible to influence peddling. Only a small percentage of R&D funding is awarded after Western-style peer review. Success often depends more on how well

a scientist cultivates support from grant managers and politicians than on the quality of research.

In a milieu of unhealthy relationships, some question whether the government has the

“If academic corruption exists, then we will investigate every single case, thoroughly.”

—Xu Guanhua, minister of science and technology

resolve to police the scientific community strictly. “Many leaders shield misconduct; this is a serious problem,” says Chen-lu Tsou, a biophysicist at CAS’s Institute of Biophysics. Adds Liu Jixing, a retired physicist, “Without

fundamental changes, we won’t be able to buck the trend of academic corruption.”

Running to the ministries

When the late paramount leader Deng Xiaoping pronounced in late 1988 that “science and technology is the primary productive force,” it was like firing a starting gun. Since then, China has steadily ratcheted up the emphasis on R&D and innovation, setting goals such as creating 100 world-class universities in the 21st century and having science and technology contribute to 60% of the economy by 2020. The central government’s R&D appropriation has tripled in 10 years, from \$3 billion in 1996 to \$9 billion in 2006, with further increases planned for the next 15 years (*Science*, 17 March, p. 1548).

The infusion of new money, critics say, accentuated the shortcomings of a research funding system tailored to a planned economy and driven by top-down political decisions. One exception is the National Natural Science Foundation of China (NSFC), which sponsors basic research and since its founding in 1986 has used Western-style peer review to administer grants. But its 2006 budget, \$425 million, amounts to less than 5% of the central government’s R&D spending. MOST will distribute around \$1.7 billion this year, mostly for applied research at universities, CAS institutes, and occasionally, companies. The ministry relies on experts to choose and evaluate projects. “On the face of it, the process looks pretty good. But in reality, a small circle of stakeholders have already predecided where the money will go,” asserts Tang Anguo, director of East China Normal University’s Institute of Higher Education Research in Shanghai. MOST declined repeated requests for an interview.

Tang and others claim that although MOST says it relies on expert opinion in choosing which proposals to fund, grant managers can veto the advice of scientific experts, often citing political reasons for doing so. Compounding the potential for abuse, in the name of streamlining, MOST



Back to basics. Incentives have “blurred the reasons for doing science,” says academy president Lu Yongxiang.

CREDITS (TOP TO BOTTOM): NATIONAL GEOGRAPHIC/GETTY IMAGES; TORU HANA/REUTERS

has slashed its in-house staff and now routinely borrows grant managers from universities, says Liu. This creates a group of scientists-cum-managers with potential conflicts of interest.

MOST research managers wield significant power. Universities have long been engaged in *pao bu qian jin*, a pun satirizing the practice of “running to ministries to get money.” Professors’ incomes are often tied to how much grant funding they bring in; they may take up to 40% as commission, according to grant-management documents of several universities. Last year, MOST issued a directive forbidding the use of grant money as rewards, but it is not clear whether it will stop the linkage of salaries to grants.

In return for their largess, managers demand quick results to demonstrate *zheng ji*, or administrative achievements, to higher-ups. “If you don’t give them results in 3 to 5 years, your project is terminated,” grumbles Wang Yiqiu, a former vice president of Beijing University. And results are often measured in numbers. Tallies of citation-indexed papers, by individual and by institution, have become a national obsession. Nanjing University was the first to use the number of papers published in journals covered by the Science Citation Index (SCI) to evaluate faculty members in the early 1980s, and the practice has spread widely. (The Institute of Scientific and Technical Information of China publishes annual statistics ranking universities by the number of papers and by citation rates.) To earn a master’s degree, students at many universities must be first author of at least one SCI

paper, and Ph.D. students need two. Many institutions hand out cash rewards—hundreds of dollars, scaled by the journal’s reputation—for publishing an SCI paper (*Science*, 23 February 2001, p. 1477). The combination of pressure and incentives has nurtured an environment



No more Mr. Nice Guy. Chinese scientific leaders tolerate misconduct—and that’s a “serious problem,” says biophysicist Chen-lu Tsou.

that’s rife with simultaneous or serial duplicate manuscript submissions, self-plagiarized cookie-cutter papers, individual and institutional honorary authorship, and outright plagia-

ism, says Ouyang Zhongcan, director of CAS’s Institute of Theoretical Physics.

Not surprisingly, quality suffers. According to CAS, although China ranked ninth in the world in 2004 in the total number of science and technology publications, it ranked only 124th in terms of the average number of citations per paper. Former CAS president Zhou Guangzhao has long criticized an overemphasis on SCI papers, arguing that it discourages long-term or risky work. The problem, says Ouyang, is that no one seems to be listening to Zhou.

Higher political attention to a lab or a project raises the likelihood of securing ample funding. For example, in early 2000, biologist Cheng Jing gave a talk to the State Council, China’s cabinet, about the importance and applications of biochips, catching the interest of then-Prime Minister Zhu Rongji. The following September, Cheng founded a company, Capital Biochip Corp., with more than \$30 million from the State Development Planning Commission (*Science*, 15 December 2000, p. 2061). Ministries also chipped in non-peer-reviewed support, validating a popular saying among Chinese scientists: “Big grants, no review; small grants, big review.”

Crime Scene Investigation: How to Handle Misconduct

Chinese scientists aren’t the only ones who may find misconduct investigations a murky business (see main text): Confusion is the norm in much of the world, according to experts who are trying to raise global standards.

Most countries have taken an “ad hoc approach” to probing misconduct allegations, says Chris Pascal, director of the Office of Research Integrity (ORI), the overseer of investigations at biomedical labs and other facilities funded by the U.S. Department of Health and Human Services. A common experience, he says, is that officials “get an allegation and then try to figure out how to deal with it.” Without guidelines, “you don’t know what to do first, and you may end up violating legal norms.” The mistakes that often follow make it hard to reach a fair decision.

To help dispel some of the fog, Pascal and ORI consultant Nicholas Steneck, a historian at the University of Michigan, Ann Arbor, are leading a global effort to foster clear standards of conduct and encourage nations to adopt coherent policies. It’s critical, Steneck says, to create transparent systems and educate scientists and their bosses so that everyone understands where the community should draw the line. This week, ORI and the European Science Foundation (ESF)—a nongovernmental organization—announced that they will get the international ball rolling by cosponsoring the first “World Conference on Research Integrity,” scheduled for September 2007 in Lisbon, Portugal.

Interest in the project is surging, Pascal says, because of publicity over the South Korean stem cell research fraud, as well as recent news of misconduct allegations in China (*Science*, 19 May, p. 987), Japan (*Science*, 3 February, p. 595), and Norway (*Science*, 27 January, p. 448). “People used to fall asleep when I talked about educating scientists” on research integrity, Steneck says. Now they’re paying attention—and, critically, offering support. ESF adviser Anthony Mayer says the Lisbon conference got a boost from joining a new initiative proposed by Japan to compare national policies around the world, supported by the Paris-based Organisation for Economic Co-operation and Development. The European Union and others are on board.

Models of how to deal with scientific misconduct come in all shapes and sizes, Mayer says. One approach is to leave decisions to employers. The United States and the United Kingdom, for example, rely primarily on universities and research institutions for the first level of misconduct review, but the United States also has a national definition of misconduct and clear procedures for investigations, independent oversight, and appeals. The U.K. in March created a national Research Integrity Office that intends to establish guidelines and give advice. Elsewhere in Europe, Denmark has what may be the most centralized system, in which a judge oversees inquiries in all fields of science; other countries follow a variety of policies.

Organizers of the Lisbon conference say they are loath to create international rules. “We don’t want people filling out more forms on the lab bench,” says Mayer. One goal of the confab, he says, is to get people talking about practices that may spur cheating—such as using postdocs as “research slaves” or setting rigid productivity targets. That message is likely to resonate with rank-and-file scientists. —ELIOT MARSHALL

The advantage of showing off political connections was not lost on another researcher, Chen Jin, who claimed to have designed China's first homegrown digital signal processor chips. The former dean of Shanghai Jiao Tong University (SJTU) had a picture hanging outside his office of Prime Minister Wen Jiabao on a visit when Chen's star was rising. Other photos on the lab's Web site trumpeted visits of a former vice premier, a for-



Wake-up call. A letter drafted by Xin-Yuan Fu (right) calls on leaders to create a fair and open system to probe misconduct allegations. Chinese academia is rife with duplicate manuscript submissions, honorary authorship, and plagiarism, asserts physicist Ouyang Zhongcan (above).

mer MOE minister, a current vice minister of MOST, and a vice mayor of Shanghai. Chen was fired last month, after an inquiry concluded that his chips were faked (*Science*, 19 May, p. 987).

The chip scandal illustrates many shortcomings of the system. When questions surfaced about the chips' authenticity, SJTU, fearing a blow to its own reputation, asked higher authorities to step in, sources close to the investigation told *Science*. They say two inquiries were carried out: first by the Shanghai government, then by MOST. The first investigation, they say, was inconclusive partly because city officials were looking for but did not receive clear instructions from the central government on whether to punish or spare Chen. As the Chinese media continued to scrutinize the case, the main sponsor of the research, MOST, launched a second inquiry that laid the blame at Chen's feet.

Some question whether the experts who evaluated Chen's inventions—and lauded the design

as a "landmark" in China's chip-development history at the 2003 unveiling—should also bear responsibility. Politicians basked in Chen's glory when he was on the rise: Shanghai officials had organized news conferences to announce his inventions. And SJTU President Xie Shengwu eagerly took dignitaries on tours of Chen's lab. All of them are silent now. "Chen may not be as culpable as he is made out to be; he may very well be just the fall guy" for the system, veteran chip designer Alex Lee suggests. Lee worked in Silicon Valley for 20 years and was recruited in 2003 by Chen's second in command to teach at SJTU's school of microelectronics. Lee says that there are standard benchmarks for evaluating chips and wonders how experts could have been so easily fooled in the first place. He does acknowledge that "exaggerations" are widespread in academia.

War of words

Chen's case is one of several recent high-profile misconduct sagas roiling academia. In March, Qinghua University in Beijing fired an assistant dean of its medical school for falsifying work experience and



achievements in his résumé (*Science*, 14 April, p. 193). A month later, Sichuan University in Chengdu absolved biophysicist Qiu Xiaoping of a data-falsification charge (*Science*, 28 April, p. 511), although questions about the research persist. Recently aired allegations against other scientists are unresolved.

Concerned by the flurry of allegations and the government's reluctance to mount inquiries, 120 Chinese scientists, most of whom are based in the United States, called on MOST, MOE, CAS, and NSFC in a letter last month to "establish a fair, open and formal system for dealing with allegations of scientific misconduct and other issues related to integrity of research." They urged the institutions not to leave the pursuit of misconduct cases to the media (*Science*, 19 May, p. 987).

The letter unleashed a torrent of frustration and anger. A handful of prominent voices welcomed it. The letter "raises a very good issue,"

says Tsou. Others claim that the authors' prescription—a new system for addressing misconduct allegations—is naïve. Disciplinary rules exist, they say; the problem is that the rules are rarely applied. (An exception is NSFC. It established specific rules in 2005 for investigating alleged fraud in grant proposals and has prosecuted about three dozen cases so far. Punishment ranges up to indefinite debarment.) Anonymous postings on New Threads, a popular Chinese Web site for airing misconduct allegations, accused the authors of being out of touch with realities in their homeland.

Supporters of New Threads argue that official institutions can't do the job, so vigilante justice is needed. Letter drafter Xin-Yuan Fu, an immunologist at Indiana University School of Medicine in Indianapolis, believes that the Web site's popularity stems from the lack of an independent press in China. "People do not trust official media and look for alternative sources," he says. Many allegations posted are anonymous, and some are unfounded. Fu reiterates the open letter's recommendation that China establish a "rule of law" to safeguard research integrity.

Despite the mixed reaction, the open letter has reignited a debate about whether China's research system is in need of an overhaul. People may argue over whether the letter's suggestions can solve the problem of scientific misconduct, but they should keep in mind the common goal of a healthy academic environment, says Yi Rao, a neurobiologist at Northwestern University's Feinberg School of Medicine in Chicago and a letter signatory. A "proper mechanism for handling misconduct allegations is a part of that environment," he says. "Officials need to show that they are more interested in building research infrastructure than controlling funds."

The government seems to be coming around to that message. Two days after the open letter, MOE issued guidelines on "strengthening academic ethics." And late last month, it announced the formation of a committee on discipline in the social sciences; in March, more than 100 social scientists had signed an open letter calling on colleagues to behave themselves and urging the government to establish rules for combating "academic misconduct and corruption" in their field. The panel will formulate rules for universities on how to handle allegations.

It's unclear whether new rules will produce the desired results. As He Zuoxiu, a CAS physicist, notes, "the handling of misconduct cases is a matter of policy, not of mechanism"—and to date, the government has shown little appetite for cracking down. But the time may be ripe for a change. In March, Chinese Communist Party General Secretary Hu Jintao called on the country to establish a "socialist outlook on honor and dishonor" by learning "eight honors and eight shames." One of the honors is honesty.

—HAO XIN

With reporting by Gong Yidong of *China Features* in Beijing.

GENETICS

DNA's Molecular Gymnastics

The double helix has some unruly bases that get out of line, affecting its function and integrity and, sometimes, causing disease

An amusing Web site, called the Left Handed DNA Hall of Fame, catalogs the many examples in which the media and journals, including *Science*, have accidentally published a mirror-image depiction of the stereotypical DNA strand, whose double helix should twist to the right as a screw usually does. But, if a growing number of molecular biologists are correct, you may soon see more left-handed DNA—and other odd DNA structures—in journals, and it won't be by mistake.

As the Hall of Fame points out and biologists have known since 1979, DNA can actually have a left-handed twist. When the double helix untwists so that a gene's code can be read, it sometimes flips into this reverse twirl, a form called Z-DNA because the DNA backbone has a zigzag appearance. DNA's strands can also split, kink, or loop back over themselves, forming hair-

pins, crosses, and more. Biophysicists have identified about a dozen of these abnormal forms, typically finding them at repetitive or symmetrical sequences along chromosomes. Researchers have largely dismissed the alternative DNA structures as transient and without biological importance.

Yet many biologists are beginning to argue that these forms of DNA deserve greater respect and scrutiny. Molecular and cell biologists are discovering that the structures can affect transcription, revving up the activity of a gene or silencing it. In other cases, the formation of these structures gums up genetic activity and disrupts the health of cells, ultimately causing problems such as mental retardation and cancer. And other work implicates alternative structures in chromosomal weak spots called fragile sites that play a role in dozens of disorders.

Despite such evidence, many biologists remain unconvinced that DNA's alternative structures are interesting. "The origin and the importance of these effects of DNA structure is not something that everyone agrees on," says Stephen Neidle, an x-ray crystallographer at the University of London. Nonetheless, some researchers who have established links between these altered DNA states and diseases such as viral infections and cancer hope to develop drugs that target these unusual forms of DNA. Laurence Hurley, a medicinal chemist at the University of Arizona, Tucson, has become a true believer: "Alternative structures actually are biologically relevant," he says.

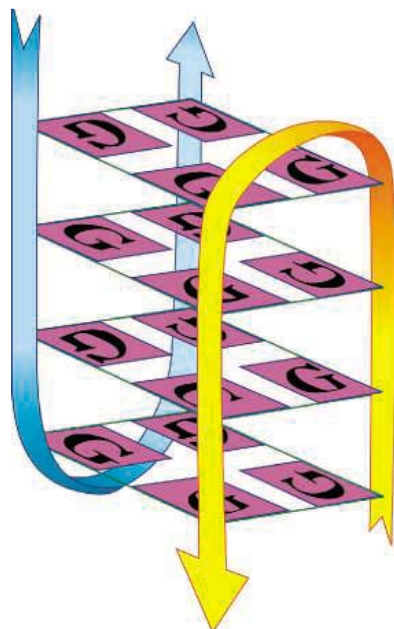
A role for Z-DNA

Biophysicist Alexander Rich of the Massachusetts Institute of Technology in Cambridge never doubted the relevance of Z-DNA, which he and colleagues unveiled in 1979 using x-ray crystallography. But it's taken until now for him and his colleagues to show that Z-DNA matters.

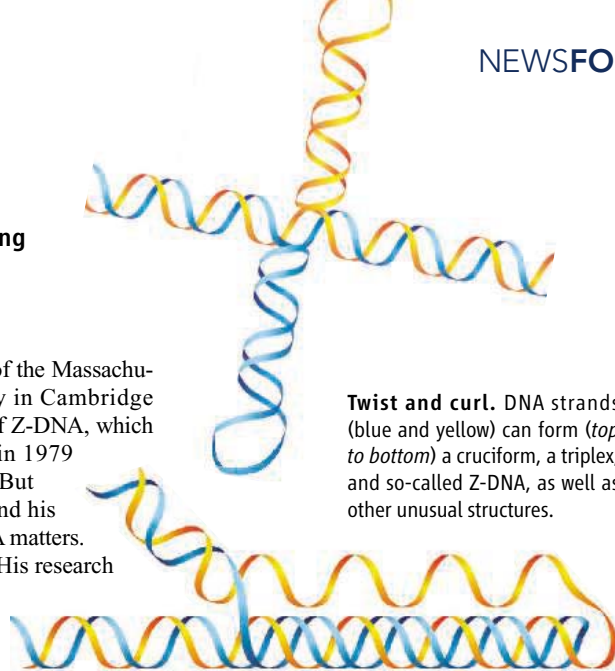
A key clue came in 2003. His research team had noticed that a poxvirus virulence factor, called E3L, mimicked a mammalian protein that binds Z-DNA. After infecting animals with mutated poxviruses, it became clear that attaching to Z-DNA was crucial to E3L's then-unknown function. If the protein lacked

the Z-DNA binding region, then mice infected by an otherwise lethal poxvirus survived, the researchers discovered.

Last year, Rich and his colleagues pinned down what E3L does for the poxvirus. When expressed in human cells, E3L increases by five- to 10-fold the production of several genes that block a cell's ability to self-destruct in response to infection, Rich's group reported in



Beyond the double helix. Like many other alternative DNA structures, this quadruplex forms when repetitive bases, in this case guanine (G), align DNA's two strands in an unusual configuration.



Twist and curl. DNA strands (blue and yellow) can form (top to bottom) a cruciform, a triplex, and so-called Z-DNA, as well as other unusual structures.

the 6 September 2005 issue of the *Proceedings of the National Academy of Sciences*. Once E3L binds to the Z-DNA in the regulatory regions of these genes and stops apoptosis, the poxvirus converts infected cells into viral production factories. "People had been very suspicious of Z-DNA," says Hurley. "This is the first really compelling data that Z-DNA does have a biological role."

Rich speculates that the Z-DNA is necessary for transcription and that E3L stabilizes the Z-DNA, thus prolonging expression of the anti-apoptotic genes. He suggests that a small molecule that interferes with the E3L binding to Z-DNA could thwart the activation of these genes and help protect people from pox infections.

Chair DNA

One step ahead of Rich, Hurley and his colleagues are already targeting alternative DNA structures with drugs they hope might fight cancer. Hurley's group discovered a particular DNA structure, called a quadruplex, that arises naturally from the regulatory sequence that controls the expression of the oncogene *cMYC*. This quadruplex, like ones formed by other DNA sequences, roughly resembles the shape of a chair.

Data from Hurley's team indicate that cells typically produce proteins that stabilize *cMYC*'s regulatory sequence into a quadruplex, preventing transcription. "Silencing [of the gene] depends on this alternative structure," he says. Cancer cells frequently have an overactive *cMYC*, and Hurley showed that if the regulatory sequence's bases are altered, the quadruplex becomes unstable and *cMYC* expression goes wild, stimulating uncontrolled cell growth. In 2002, Hurley and his colleagues reported that they could reset the brakes on such an over-expressed *cMYC* with a small molecule that stabilizes the quadruplex. And without *cMYC*'s constant prodding, cancer cells self-destructed.

Now a company Hurley helped found, Cylene Pharmaceuticals Inc. in San Diego, California, has followed through on this idea of targeting quadruplexes, although the story has taken a few twists. Instead of aiming to silence *cMYC*, Cylene researchers have developed drugs to inhibit a quadruplex that promotes the production of ribosomal RNA, which is needed to make the cell's protein factories, ribosomes. That quadruplex is still a sensible anticancer target: To have enough protein to fuel their growth, cancer cells need more ribosomes than other cells do, says Cylene President William Rice. Initial safety trials in people of the company's candidate quadruplex inhibitor should be completed by the end of the year, he notes.

When DNA breaks

Other researchers are looking at how alternative DNA structures might disrupt the genome. These unusual DNA features appear to be central to certain "fragile sites," where DNA readily breaks as it's copied, says Catherine Freudenreich, a yeast geneticist at Tufts University in Medford, Massachusetts. As DNA is replicated at these sites, parts of genes can drop out, pieces of chromosomes can swap places (translocations), or repetitive DNA can get copied multiple times—expansions that make the site even more vulnerable.

To date, researchers have implicated fragile sites in about 50 diseases, including Fragile X syndrome and several cancers. To see whether alternative structures play a role in chromosome fragility, Freudenreich focused on FRA16D, a spot on human chromosome 16. It's located inside what is likely a tumor suppressor gene; tumor cells often have broken or missing DNA at this spot. Freudenreich has recently used yeast to test whether seemingly "flexible" sections of DNA found in FRA16D's 270,000 bases were pliable enough to form alternative structures.

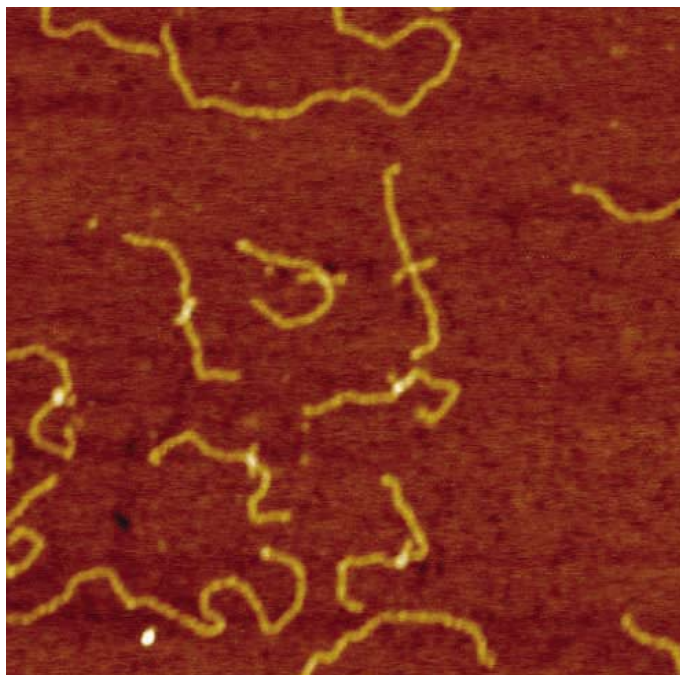
She and her graduate student Haihua Zhang pinpointed one small, 400-base-long section that contained many doublets of the bases adenine (A) and thymine (T)—a perfect setting for a crosslike alternative DNA structure known as a cruciform to form. When this DNA is spliced into yeast DNA to make a yeast artificial chromosome, cruciforms take shape, and the chromosome breaks easily, she reported in March at a DNA structure meeting in Houston, Texas.* She also found that, at least up to a

* DNA Structure, Genomic Rearrangements and Human Disease, 12–14 March, Houston, Texas.

point, the more doublets there are in a stretch of DNA, the greater the likelihood of breakage. "The presence of these motifs [explains] why the deletion breakpoints occur at these specific sites," says Hildegard Kehrer-Sawatzki of Ulm University in Germany.

The tendency of cruciforms to result in broken chromosomes may also explain why DNA is often swapped between chromosomes 11 and 22, says Hiroki Kurahashi, a molecular human geneticist at Fujita Health University in Aichi, Japan. He has found that the breaks tend to occur at the center of palindromic patterns of A's and T's on the two chromosomes, creating a window for translocations to occur. The bigger the palindrome, the greater the likelihood that DNA swapping will occur, he reported in the 17 February issue of *Science* (p. 971).

DNA sequences with repeating cytosine (C) and guanine (G) bases, which are prone to twisting counterclockwise into Z-DNA, also take a toll on the genome, particularly in mammalian cells. Karen Vasquez and her postdoc Guliang Wang of the University of Texas M. D. Anderson



Cross-up. Atomic force microscopy reveals crosslike formations of DNA (gold) that can halt replication and cause chromosomes to break.

Cancer Center in Smithville recently inserted strings of such CG repeats into mammalian cells. Others had previously shown that the repeats result in genetic instability in bacteria—a few bases were lost at the sites where the CG repeats had been introduced. Mammalian cells suffered even larger deletions, more than 50 bases at a time, Vasquez and Wang reported in the 21 February issue of the *Proceedings of the National Academy of Sciences*.

Vasquez notes that the chromosomal breaks seen in mammalian cells appear not just at the

inserted Z-DNA but as much as several hundred bases away, resulting in larger-scale deletions and translocations typical in leukemias and lymphomas. The work indicates that this breakage is not the result of stalled DNA replication but rather may occur as repair enzymes try to fix the Z-DNA, she says.

The search is on

The mounting evidence for biological relevance of alternative structures has inspired genomewide searches for DNA sequences prone to forming these odd shapes. And researchers are finding that these sequences are quite common. P. Shing Ho of Oregon State University in Corvallis has found that 70% of the regulatory regions for human genes contain sequences that could convert to Z-DNA. Hurley says he's found thousands of potential quadruplexes in a quick scan of the human genome for the appropriate DNA sequence. And Albino Bacolla of Texas A&M University Health Science Center in Houston has dug out more than 800 regions in the human genome with the DNA signature for triplexes, an alternative DNA structure in which an extra strand latches onto the double helix.

Such abundances are a tip-off that alternative DNA structures likely serve key roles in genome function, such as providing another way to fine-tune gene expression, says Hurley. And even though these structures are also sources of disease-causing alterations, it may make sense for the genome to keep them around, as these mutational hotspots also encourage the genetic diversity that underlies evolution.

Despite these roles, DNA's alternative structures still get short shrift, says Richard Bowater, a biochemist at the University of East Anglia in Norwich, U.K. Geneticists are very focused on finding mutations and other sequence changes to explain evolution and genetic disease. In contrast, alternative structures "are elusive quarry," says Rich, as they appear and disappear quickly when

DNA is copied, transcribed, or repaired. "It takes some perseverance and ingenuity to uncover them."

And although Rich and others have been chasing alternative structures for many years, their work is still at an early stage. "Currently, much of the evidence is highly suggestive," says Bowater. Providing better proof of the importance of DNA's alternative structures, he adds, "is the big challenge for this research field over the coming years."

—ELIZABETH PENNISI

POLITICS

A CLEAN SLATE. Italy's new science minister Fabio Mussi has begun his term by undoing some of his predecessor's actions. Mussi has shelved new criteria for academic assessment, guidelines for shaping curriculum and research priorities at universities, and plans for a private university.

Mussi intends to revise "unsatisfactory or erroneous" portions of these directives, he says, and has promised more funding for research and fresh measures to tackle controversial areas such as university appointments. His policies have been welcomed by university administrators.

Mussi has also withdrawn Italy from a six-nation declaration signed last year that opposes embryonic stem cell research. The move could allow such research to fit in the E.U.'s Framework VII program, currently under debate. Former minister and declaration architect Rocco Buttiglione has opposed Mussi's decision and threatened a vote to remove him from the new government of Romano Prodi.



PIONEERS

BEYOND RACE. Challenged by the 2003 U.S. Supreme Court rulings on what criteria universities may use to admit students, computer scientist Juan Gilbert decided to apply his skills



to improving diversity without using quotas. Using a technique called clustering, the 37-year-old professor at Auburn University in Alabama devised an algorithm for admissions officers that factors in academic ability, race, gender, geographic distribution, and

extracurricular activities to yield a more diverse freshman class. Gilbert says one school plans to implement the software this fall and that many others have tested it.

American Association of Collegiate Registrars and Admissions Officers official Barmak Nassirian says an organizational tool such as Application Quest "may well represent a credible model" to help universities stay within the law and still promote diversity. But he warns that software alone "is not going to be a silver bullet" that eliminates human judgment from the selection process.

INSIDE GOVERNMENT

ONE PERSON, ONE POST. Andrew von Eschenbach, 65, who has directed the National Cancer Institute (NCI) for the past 4 years, will step down from the position on 10 June. Since September 2005, von Eschenbach has also served as acting chief of the Food and Drug Administration (FDA),

for which he was nominated commissioner in March. His Senate confirmation has been stalled by FDA's stance on Plan B, the morning-after pill.

Von Eschenbach's resignation resolves conflict-of-interest concerns about his double duty heading both NCI and the agency that regulates cancer clinical trials. Taking his place at NCI as acting director will be John Niederhuber, who has been the day-to-day manager of the institute since last fall. Niederhuber has so far kept to von Eschenbach's agenda. The White House has begun a search for a permanent director, but Health and Human

Services spokesperson Christina Pearson could not comment on timing.

MOVERS

NEW MBL HEAD. Cell biologist Gary Boris is the new director and CEO of the Marine Biological Laboratory (MBL) in Woods Hole, Massachusetts. Boris, known for his discovery of the protein tubulin, comes to the 118-year-old institution from Northwestern University in Evanston, Illinois, where he worked as both a professor and a research administrator.

Boris succeeds William Speck, who is retiring next month after 5 years in the position.

Three Q's >>

There is no line between science and religion for **Shoken Miyama**. The new head of the National Astronomical Observatory (NAO) of Japan is also a Buddhist priest. At NAO, he will oversee Japan's contribution to the Atacama Large Millimeter Array (ALMA), a billion-dollar international array of 60 to 70 radio antennas being built in the Atacama Desert in Chile. Now 55, Miyama plans to retire from the observatory by age 63 and succeed his father as chief priest of a Buddhist temple in Hiroshima Prefecture.

Q: What will be the most important findings coming out of ALMA?
ALMA will clarify how planets form.

Q: Is there a connection between Buddhism and astronomy?
No. But in the cosmological view of Buddhism, space has a hierarchical structure, with the solar system as the base and three levels built upon it—something like a galaxy, a cluster of galaxies, and the whole universe. I think this similarity to the actual universe is extremely interesting. Also, in Buddhism, this universe is repeatedly emerging and disappearing



over cosmic periods of billions of years. It is something like an oscillating universe.

Q: In the West, science and religion are often seen as being in conflict. How does Buddhism avoid this?
Buddhism is an invention of the human mind; science is the effort to learn natural truths.



LETTERS

edited by Etta Kavanagh

Don't Sell Social Science Short

THE NEWS OF THE WEEK ARTICLE THAT REPORTS ON SENATOR KAY BAILEY HUTCHISON (R-TX) questioning the need to fund social science research at the National Science Foundation is alarming and shortsighted ("Senate panel chair asks why NSF funds social sciences," 12 May, p. 829). Social science research is at the fundamental core of basic research and has much to contribute to the economic viability of the United States. Twenty years of direct and jointly funded social and ecosystem science research at Colorado State University's Natural Resource Ecology Laboratory has produced deep insights into environmental and societal impacts of political upheaval, land use, and climate change in parts of Africa, Asia, and the Americas. Beyond greatly advancing our understanding of the coupled human-environmental system, the partnership of social and ecosystem science has brought scientists and decision-makers together to begin to develop solutions to difficult problems.

Insights from the social sciences about the vulnerability, sustainability, and resilience of social and environmental systems have greatly increased our understanding of the complex interactions of the world on which we depend. The contributions of social and ecological science for data analyses associated with spatial relationships, transfer of goods and services, valuation, and decision-making processes have improved our understanding of how human activities are altering environmental systems worldwide. These findings have become the core of policy and development decisions used throughout the world.

It is critical that the NSF support social science funding and that, as budget decisions are made, the social science allocation should move forward equally with increases as in other basic and applied research. Failure to do so will further hinder U.S. competitiveness in the future and will slow transfer of knowledge and usefulness to the public.

DENNIS S. OJIMA,* DIANA H. WALL,† JOHN MOORE,‡ KATHY GALVIN, N. T. HOBBS, WILLIAM H. HUNT, KEITH PAUSTIAN, DAVID SWIFT, RANDALL B. BOONE, RICHARD T. CONANT, JULIA KLEIN, LINDSEY CHRISTENSEN, MAHESH SANKARAN, JAYASHREE RATNAM, ED AYRES, HEIDI STELTZER, BREANA SIMMONS, GARY WILLIAMS

Natural Resource Ecology Laboratory (NREL), Colorado State University, Fort Collins, CO 80523-1499, USA.

*Director, NREL

†Past Director, NREL

‡Incoming Director, NREL

Photosynthetic Oxygen Production

UNDERSTANDING LIGHT-DRIVEN OXYGEN PRODUCTION from water by plants and cyanobacteria is one of the greatest challenges in molecular bioenergetics. The essential reaction step is mediated by a Mn_4CaTyr catalytic center. After photon-clocked accumulation of four

oxidizing equivalents, this center abstracts four electrons from two molecules of water in a terminal reaction that has long appeared to be a single reaction step. The hunt for the still ill-characterized intermediates of this complex reaction is on, as recently documented in *Science* (M. Haumann *et al.*, "Photosynthetic O_2 formation tracked by time-resolved x-ray experiments," Reports, 11 Nov. 2005, p. 1019) and *Nature* (1).

The sequence of states leading from the lowest oxidation state of the Mn_4CaTyr -entity, named S_0Y , to the highest, named S_3Y^{ox} , is well characterized. The chemistry from the highest state back to S_0Y under liberation of dioxygen has, however, remained enigmatic. Haumann *et al.* recorded the electron flow from water into Mn_4 by x-ray spectroscopy and found a lag phase of 250- μ s duration. It precedes the known reduction of the center, which occurs in about 1 ms. They interpreted this lag phase in terms of an intermediate, the center still in its highest oxidation state being partially deprotonated. By UV spectroscopy we previously detected a partially (twofold?) reduced Mn-intermediate. Elevated oxygen pressure ($P_{1/2} = 2.3$ bar) served to push oxygen evolution in the reverse direction (1). Instead of being contradictory, as stated by J. E. Penner-Hahn and C. F. Yocum

in their Perspective ("The photosynthesis 'oxygen clock' gets a new number," 11 Nov. 2005, p. 982), the two data sets supplement each other. Haumann *et al.* identified one non-redox intermediate lying before the rate-limiting step of the reaction cascade, and we detected one redox intermediate located after this step closer to the end (1). Further redox intermediates are expected on the path of this tetravalent electron transfer cascade, of course.

WOLFGANG JUNGE AND JUERGEN CLAUSEN

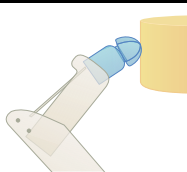
Department of Biophysics, Universitaet Osnabrueck, Room 36/132, Barbarastrasse 11, Osnabrueck D-49076, Germany.

Reference

1. J. Clausen, W. Junge, *Nature* **430**, 480 (2004).

Response

WE AGREE THAT A FULL CHARACTERIZATION OF all of the intermediates in the mechanism of photosynthetic water oxidation will represent one of the great discoveries in bioenergetics. Clausen and Junge's paper (1) was a signal achievement, providing evidence for a chemical intermediate in the formation of oxygen from water; this was modeled as B in the reaction $A \rightarrow B \rightarrow C$, where A is $S_3Y_Z^{ox}$ and C is $S_0Y_Z + O_2$. Clausen and Junge suggested that B might correspond to $S_2Y_ZH_2O_2$, although they noted that this was "only one of several choices" for B (1). Haumann *et al.*'s Report does indeed complement these earlier findings: The existence of an intermediate is confirmed by monitoring directly the redox behavior of the Mn.



Robots with feeling

1478



Oceanic nitrogen,
lost and found

1479

There is great interest in determining the chemical identity of the intermediate(s) that exist between $S_3Y_Z^{OX}$ and S_0Y_Z (i.e., the intermediate defined as *B* by Clausen and Junge). Haumann *et al.* provide important insight by defining what the intermediate is not. If the intermediate that Haumann *et al.* describe corresponded to $S_2Y_ZH_2O_2$, it would have a lower edge energy, reflecting the lower oxidation state of the Mn. It was in this context that we described the data as excluding the model put forward by Clausen and Junge; the intermediate that is seen by Haumann *et al.* does not match the properties expected of $S_2Y_ZH_2O_2$. Thus, under the parsimonious assumption that there is only one isolable intermediate between $S_3Y_Z^{OX}$ and S_0Y_Z , the recent data exclude the possibility that this intermediate is $S_2Y_ZH_2O_2$. However, as Clausen and Junge note here, it is possible that the reaction is more complex—e.g., $A \rightarrow D \rightarrow B \rightarrow C$ —with the intermediate seen by Haumann *et al.* corresponding to *D* and the intermediate seen by Clausen and Junge corresponding to *B*. In this case, *B* certainly could be $S_2Y_ZH_2O_2$. To our knowledge, there is at present no evidence for the existence of two intermediates. However, it is possible that future experiments may provide such evidence, supporting the existence of a stable partially reduced intermediate oxidation state of Mn along the route to formation of S_0 and O_2 .

JAMES E. PENNER-HAHN AND CHARLES F. YOCUM

Departments of Chemistry and Molecular, Cellular, and Developmental Biology and the Biophysics Research Division, University of Michigan, 930 North University Avenue, Ann Arbor, MI 48109-1055, USA.

Reference

1. J. Clausen, W. Junge, *Nature* **430**, 480 (2004).

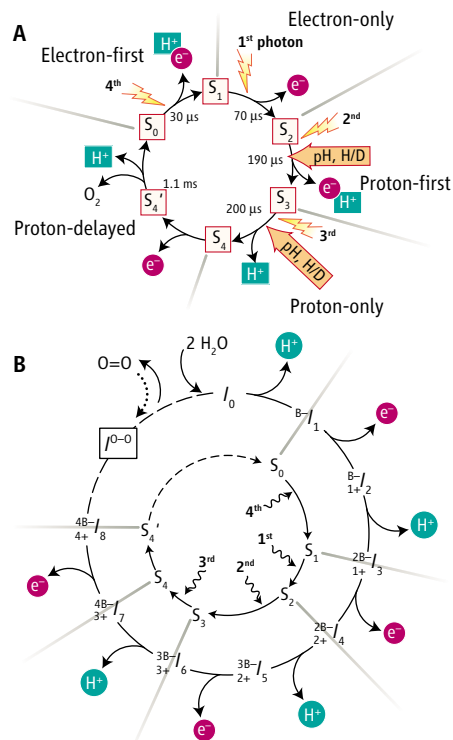
Response

THE INTERMEDIATES OF PHOTOSYNTHETIC OXYGEN evolution described by Clausen and Junge (*1*) and in our Report (Haumann *et al.*) are distinctly different. For clarification, we discuss a basic model that includes both reaction intermediates. Moreover, the proposed reaction cycle resolves inconsistencies of earlier models and provides a fresh twist in research on oxygenic photosynthesis.

The active site of dioxygen formation is a manganese complex bound to the proteins of Photosystem II (PSII). In 1970, Kok proposed a five-state reaction cycle (2) (S_0 to S_4 in Fig. 1) (Haumann *et al.*; Perspective by Penner-Hahn and Yocum). However, the simplicity of Kok's five-state charge accumulation model and of the more recent, particularly influential hydrogen-atom abstraction hypothesis (3) is generally not met by the intricate experi-

mental results (see panel A of the figure). Clarification may come from the alternative reaction cycle of panel B of the figure.

We have reported evidence for formation of the enigmatic S_4 state by deprotonation so that subsequent electron transfer leads to an additional S_4' state (Haumann *et al.*). Clausen and Junge (*1*) suggested transient formation of an intermediate state prior to dioxygen release that is stabilized at elevated oxygen partial pressure. In this state, the manganese is reduced in comparison to the S_4 state identified in our Report, and partial water oxidation may have resulted in peroxide formation. Penner-Hahn and Yocum correctly pointed out that this peroxidic intermediate cannot be identical to the S_4 state, but suggested that identity had been claimed in (*1*).



Reaction cycle of photosynthetic water oxidation in plants and cyanobacteria. (A) Irregular properties (6), and references therein] of the transitions in the classic 5-state model. A complete cycle requires sequential absorption of four photons. For each transition, it is indicated whether an electron is removed from the Mn complex, whether a proton is released from the Mn complex or its ligand environment, and whether the rate constant is sensitive to pH and H_2O/D_2O exchange. (B) Proposed sequence of alternating proton and electron abstraction from the Mn complex. The left subscript and superscript indicate the number of accumulated oxidizing equivalents and bases, respectively.

AFFYMETRIX WORKSHOP SERIES GENOTYPING

SUMMER 2006

Register to receive print and video interviews on whole-genome and targeted genotyping association studies, including:

DISCOVERIES



John Todd, Ph.D., Director, JDRF/WT Diabetes and Inflammation Laboratory, Cambridge University. Drs. Todd and Jason Cooper discuss the discovery of a new type 1 diabetes (T1D) locus identified through a genome-wide scan of ~6,000 nonsynonymous SNPs of thousands of case/control samples.



Luc Smink, Ph.D., Head of Bioinformatics, JDRF/WT DIL, Cambridge University. Dr. Smink discusses T1DBase, a community database and web resource for T1D researchers, a joint project with Dr. Nathan Goodman (ISB, Seattle). T1DBase is used at the DIL to integrate, visualize and analyze genomics and genetics data, from different sources.

SERVICES & TOOLS



Jay Kaufman, Director, DNA Analysis, Affymetrix. Mr. Kaufman discusses targeted genotyping and SNP discovery services offered through Affymetrix' service lab.

REGISTER TODAY

www.affymetrix.com/genotyping



Rather, we propose that the S_4 state is formed before peroxide formation in a sequence of events that are outwardly convoluted and irregular, but governed by a simple underlying principle: Protons and electrons are removed strictly alternately from the Mn complex. Starting in I_0 , eight successive steps of alternate proton and electron removal lead to I_8 , where four electrons and four protons have been removed. The intermediates from I_0 to I_8 are different from the peroxidic reaction intermediate formed in the $I_8 \rightarrow I_0$ transition, which in panel B of the figure is denoted as I^{O-O} . The alternate proton-electron release explains experimental results straightforwardly, thereby resolving the irregularities of the S-state model. Moreover, the I cycle explains how four successive oxidation steps can proceed without prohibitive increase in the redox potential of the manganese complex (4). A second—and equally crucial—mechanistic role of the four deprotonation events may be the accumulation of bases [Haumann *et al.*; (5)] that serve as proton acceptors in the O_2 -formation step (4).

HOLGER DAU* AND MICHAEL HAUMANN

FB Physik, Freie Universität Berlin, Arnimallee 14, D-14195 Berlin, Germany.

*To whom correspondence should be addressed. E-mail: holger.dau@physik.fu-berlin.de

References

1. J. Clausen, W. Junge, *Nature* **430**, 480 (2004).
2. B. Kok, B. Forbush, M. McGloin, *Photochem. Photobiol.* **11**, 457 (1970).
3. C. W. Hoganson, G. T. Babcock, *Science* **277**, 1953 (1997).
4. H. Dau, M. Haumann, *Photosynth. Res.* **84**, 325 (2005).
5. M. Haumann *et al.*, *Biochemistry* **44**, 1894 (2005).
6. W. Junge, M. Haumann, R. Ahlbrink, A. Mulikidjanian, J. Clausen, *Philos. Trans. R. Soc. London Ser. B* **357**, 1407 (2002).

Making Choices Without Deliberating

CONCLUDING THAT DELEGATING THINKING about complex matters to the unconscious is beneficial is, at best, misleading and, at worst, harmful to those making complex and difficult decisions in the real world (A. Dijksterhuis *et al.*, "On making the right choice: the deliberation-without-attention effect," Reports, 17 Feb., p. 1005). Dijksterhuis *et al.* make this conclusion after interpreting data from studies with small student samples making nonrisky choices that have no serious consequences; they find that not deliberating about options with more than four attributes—and yet conscious deliberation about simpler options—led to better outcomes. An equally reasonable interpretation is that conscious deliberation leads to better decisions, but there are barriers to individuals' abilities to make reasoned evaluations of options and, in these instances, unconscious processes will usually result in satisfactory choices (1). There is consid-

erable evidence from randomized controlled trials of patients making risky choices with serious health consequences that decision-aid interventions delivered by health professionals help patients make better choices about options with several attributes (2). Decision aids restructure decision information, reducing the cognitive demands of complex choices and making explicit cognitions and emotions, enabling patients to reason verbally about treatment options (3). The outcome measures used to evaluate good decisions by Dijksterhuis *et al.* are unhelpful when applied to real-world contexts; most individuals do not make choices in accord with normative theories. Decision quality should be operationalized with reference to a theoretical perspective that takes into consideration patients' reasoning about their evaluation of options in accord with their beliefs (4).

HILARY L. BEKKER

Institute of Health Sciences and Public Health Research, University of Leeds, Leeds LS2 9LT, UK.

References

1. J. Baron, *Thinking and Deciding* (Cambridge Univ. Press, Cambridge, 1994).
2. A. M. O'Connor *et al.*, *Cochrane Database Syst. Rev.*, Issue 1. Art. No.: CD001431. DOI: 10.1002/14651858.CD001431 (2003).
3. H. L. Bekker, J. Hewison, J. G. Thornton, *Patient Educ. Counsel.* **50**, 323 (2003).
4. D. Frisch, R. T. Clemen, *Psychol. Bull.* **116**, 46 (1994).

Response

BEKKER'S CONCERN IS BASED ON A GENERALIZATION of our conclusions to a situation we never suggested nor intended and on a misleading portrayal of our data. Our work is on object evaluation, and we tested our hypothesis in the domain of consumer choice. We would not want to equate such choices with a patient's dilemma in choosing (or not) a certain treatment. Patients initially have little or no relevant knowledge when they face a medical decision (they need the help of specialists), whereas consumers of CDs, clothes, or furniture are usually reasonably well informed. Our analysis is of the stage in decision-making at which choosers already have all the necessary information and only need to come to a preference and does not pertain to the earlier stage, when consciousness is necessary (1).

Bekker states that decision quality should not be judged normatively, but with reference to people's own beliefs. This is what we do in our studies. Actual decisions were investigated, and quality of decision was operationalized as postchoice satisfaction.

Bekker also states that we only base our conclusions on student samples making nonrisky choices. However, in our two studies, real decisions were investigated, and in the Report we used actual shoppers rather than students.

Finally, the alternative explanation offered for our data is contradictory in itself. Saying that "conscious deliberation leads to better deci-

sions, but there are barriers to individuals' abilities to make reasoned evaluations of options..." is like saying that consciousness is in principle a good decision-maker, but that it fails to make good decisions, because it, well, just cannot make decisions. After all, we show that unconscious thinkers suffer much less from these "barriers."

AP DIJKSTERHUIS, MAARTEN W. BOS,
LORAN F. NORDGREN, RICK B. VAN BAAREN

Department of Psychology, University of Amsterdam, Roetersstraat 15, 1018 WB, Amsterdam, the Netherlands.

Reference

1. A. Dijksterhuis, L. F. Nordgren, *Perspect. Psychol. Sci.*, in press.

CORRECTIONS AND CLARIFICATIONS

Special Section News: "A one-size-fits-all flu vaccine?" by J. Kaiser (21 Apr., p. 380). In the figure of an influenza virus on page 380, the labels for NA (neuraminidase) and HA (hemagglutinin) should have been reversed.

Reports: "Diels-Alder in aqueous molecular hosts: unusual regioselectivity and efficient catalysis" by M. Yoshizawa *et al.* (14 Apr., p. 251). Due to a nomenclature error, all references to "phthalimides" in the text and Supporting Online Material should instead refer to "maleimides." The chemical structures in the schemes and figures are all correct as drawn.

This Week in Science: "Catch, react, release" (14 Apr., p. 155). The reference to "phthalimides" should instead have read "maleimides."

Technical Comments: "Response to comment on 'ivory-billed woodpecker (*Campephilus principalis*) persists in continental North America'" by J. W. Fitzpatrick *et al.* (17 Mar., <http://www.sciencemag.org/cgi/content/full/311/5767/1555b>). In reference (11), it is stated that "[a]fter studying the evidence at length, the Bird Records Committee of the Arkansas Audubon Society voted unanimously to accept the documentation of ivory-billed woodpecker (www.arbirds.org/ivory_billed_woodpecker.html)." This is incorrect; the Committee did accept the documentation, but the vote was not unanimous.

Policy Forum: "Globalization, roving bandits, and marine resources" by F. Berkes *et al.* (17 Mar., p. 1557). In the third line of the caption on page 1558, "Baja, Mexico" should instead have read "Baja California peninsula, Mexico."

Brevia: "Genetic variation affects de novo translocation frequency" by T. Kato *et al.* (17 Feb., p. 971). The affiliation for all of the authors except Beverly S. Emanuel is incorrect. The authors are at the Division of Molecular Genetics, Institute for Comprehensive Medical Science, Fujita Health University, 1-98 Dengakugakubo, Kutsukake-cho, Toyoake Aichi 470-1192, Japan.

Letters to the Editor

Letters (~300 words) discuss material published in *Science* in the previous 6 months or issues of general interest. They can be submitted through the Web (www.submit2science.org) or by regular mail (1200 New York Ave., NW, Washington, DC 20005, USA). Letters are not acknowledged upon receipt, nor are authors generally consulted before publication. Whether published in full or in part, letters are subject to editing for clarity and space.

MATHEMATICS

A Faulty Survey of Algebra's Roots

Victor Katz

“Mathematics is, let’s face it, a dry subject, with little in the way of glamour or romance.” Thus John Derbyshire begins chapter 11 of *Unknown Quantity*, his new history of algebra. Of course, Derbyshire [a systems analyst, columnist, and writer (1)] does not really believe this, or he would not even attempt to tell the story of algebra in a manner accessible to the “curious nonmathematician.” In fact, the book demonstrates quite the opposite, that algebra in particular is a very exciting subject, developed by interesting characters and full of exciting ideas—many of which lie at the base of modern science.

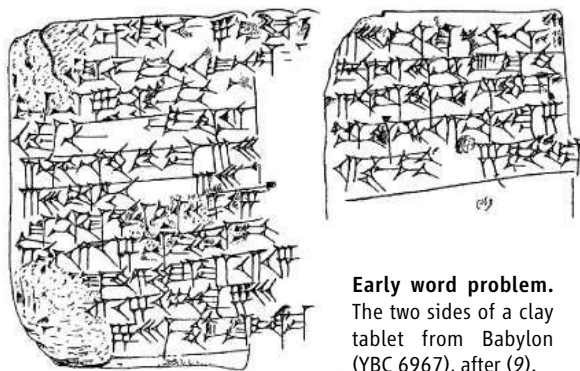
Derbyshire’s clear prose takes us from the Alexandria of Diophantus to the Baghdad of al-Khwarizmi, from the Isfahan of Omar Khayyam to the Pisa of Leonardo, from the Milan of Girolamo Cardano to the Paris of François Viète, and then on to such mathematicians as Niels Henrik Abel, Augustus De Morgan, Évariste Galois, Emmy Noether, Saunders Mac Lane, and Alexander Grothendieck. Punctuating the historical chapters, and helping readers better understand the mathematical ideas, are brief sections called “Math Primers.” In these, Derbyshire presents some basic algebraic ideas, including introductions to numbers and polynomials, cubic and quartic equations, roots of unity, vector spaces and algebras, field theory, and projective geometry.

In general, the book succeeds in its aim of enlightening the non-expert on what algebra is today, giving good summaries of recent work in such fields as algebraic topology, algebraic geometry, and even category theory. Unfortunately, Derbyshire’s history of algebra through the 17th century has many shortcomings.

First, a history of algebra should begin by telling us what algebra is. But instead of giving us a definition with some meaning, Derbyshire offers as his working definition of “algebra” in the modern American high school and early college curriculum that it is “the part of advanced mathematics that is not calculus.” As with his phrase in chapter 11, it appears that Derbyshire does not really believe what he wrote. Taken literally, this definition would include such topics

as Euclidean geometry, trigonometry, probability, and statistics—all of which are generally taught in high school and early college mathematics and none of which are, to my mind, either calculus or algebra. But in fact, through the first seven chapters (which more or less deal with the algebra currently taught in high school) Derbyshire mainly considers the solution of equations, and that topic is, I would argue, the working definition of algebra held by most high school students.

If algebra is about solving equations, then certainly both the Egyptians and Mesopotamians should get some credit. Derbyshire briefly mentions both civilizations, but he unfortunately has not read any modern research on the algebraic material in Mesopotamian civilization. He quotes Otto Neugebauer’s 1945 translation of one problem from a clay tablet (YBC 6967) without noting that recent researchers have concluded that there was a distinct geometric flavor to the instructions on the tablet, that in fact the Mesopotamians



Early word problem.
The two sides of a clay tablet from Babylon (YBC 6967), after (9).

were performing algebra by manipulating squares and rectangles (2). In other words, for them a “square” was really a geometric square and a number and its reciprocal could always be thought of as two sides of a rectangle whose area was 1. Thus, the earliest algebra had a geometric flavor. Classical Greek mathematics also contained some “geometric algebra,” of which proposition 28 from book six of Euclid’s *Elements* (referred to somewhat uncomfortably by Derbyshire) is an example. But proposition 85 of Euclid’s *Data* is easier to understand: *If two straight lines contain a given area in a given angle, and if the sum of them be given, then shall each of them be given (i.e., determined)* (3). Here

Euclid is asking simply to find two straight lines, say x and y , when their sum, $x + y$, and the area of the rectangle determined by them, xy , are known (think of the “given angle” as a right angle).

Derbyshire, however, is reluctant to call the Greek and Mesopotamian material algebra, because he believes that the key to algebra is the use of symbolism. Thus the author credits Diophantus with being the “father of algebra” on the grounds that he used some symbolism, while being “disappointed” with al-Khwarizmi’s work

in 9th-century Baghdad because that is a “sliding back” from Diophantus. Yet al-Khwarizmi was able to solve complicated algebraic problems without symbolism, and his Islamic successors (including Abū Kāmil, al-Karajī, and al-Samaw’al) were able to deal with even more sophisticated problems even though everything was written out in words. For example, if the following problem of Abū Kāmil involving three un-

knowns is not algebra, then I am not sure what is: “One says that ten is divided into three parts, and if the small one is multiplied by itself and added to the middle one multiplied by itself, it equals the large one multiplied by itself, and when the small is multiplied by the large, it equals the middle multiplied by itself” (4). Abū Kāmil was able to solve this problem using techniques of manipulation that have become standard, even though these techniques did not involve symbolism. Certainly it is easier to solve this problem using symbols, but I would venture to guess that even so today’s high school students would have trouble with it. It should also be noted that both al-Khwarizmi and Abū Kāmil gave geometric demonstrations of their methods for solving quadratic equations, the former in a naïve form similar to the Mesopotamian methods and the latter quoting from Euclid’s *Elements*.

Derbyshire also fails to mention most of the more advanced algebraic techniques developed in Islam, including polynomial algebra and the law of exponents. And in his limited treatment of Omar Khayyam’s solution of cubic equations, he claims that Omar could only solve four of the fourteen types of cubic equations by geometrical means. If Derbyshire had consulted Omar’s algebra text (5), he would have seen that Omar solved all fourteen by using the intersection of carefully selected conic sections.

Derbyshire is completely silent on the issue of whether there was algebra in India. So although the Indians knew how to solve quadratic equations by 700 CE, and even used some limited symbolism, there is no mention of these accomplishments in the book. In fact, Brahmagupta, in the 7th century, could solve $x^2 - 10x = -9$ using essentially the same algorithm we use today and, besides, made use of the negative numbers that Derbyshire claims were a “fruit of the European Renaissance.” We also find Indian mathemati-

The reviewer is at the Department of Mathematics, University of the District of Columbia, Washington, DC 20008, USA. E-mail: vkatz@udc.edu

cians working out methods for solving (in integers) what has become known as the Pell equation, $Dx^2 + b = y^2$, where D and b are given integers. For example, in the 12th century, Bhāskara showed that the smallest solution to $67x^2 + 1 = y^2$ was $x = 5967$, $y = 48,842$.

Derbyshire is on somewhat firmer ground once he moves to Europe and the developments of the 16th and 17th centuries. But even here, there are some serious errors. For example, Cardano, who wrote out the first complete study of the algebraic solution of cubic equations in his famous *Ars Magna* of 1545, did not “realize that there must *always* be three solutions” to a cubic. In fact, we read in the first chapter of that work that “if $x^3 + 6x = 20$, there is no other solution than 2” (6). For us today, this equation has two complex solutions, but Cardano, having only a very vague notion of complex numbers, certainly did not assert that a cubic equation could have one real and two complex solutions.

François Viète’s attitude toward complex numbers was hardly “retrograde.” In fact, he realized that to solve the irreducible case of a cubic (where Cardano’s procedure requires complex numbers), he could avoid complex numbers and their uncertain status by using trigonometry. And despite Derbyshire’s claim that Viète only dealt

with cubics trigonometrically, in the very book (*De equationem emendatione*) mentioned by the author, Viète presents formulas for the solution of cubic equations closely related to Cardano’s procedures (7). Viète could do this, and this needs to be emphasized, because he used letters to represent coefficients in equations, whereas Cardano could only give an algorithm and an example with specific numerical coefficients. As Derbyshire notes, Viète did understand the basics of the relationship between the coefficients and the roots of equations. It is then very curious that while Derbyshire mentions that Albert Girard, in his 1629 *New Discoveries in Algebra*, generalized Viète’s result—because he understood complex solutions—he fails to note that as part of this result, Girard states the fundamental theorem of algebra, the theorem that every polynomial equation of degree n has precisely n solutions, assuming one counts multiples (8). Derbyshire claims that Descartes was the first to state this result, in 1637, and gave it very tentatively. Girard was considerably more assertive about the result, even though (of course) neither he nor Descartes could prove their claim.

But the most serious failing of *Unknown Quantity* in dealing with the 17th century is the almost total absence of any consideration of the

development of analytic geometry by Descartes and Fermat. The realization that geometric curves could be represented by algebraic equations was a crucial step in the major developments in mathematics and in physics toward the end of that century and into the next one. Recall that Galileo showed, using Greek geometrical methods, that a projectile traveled on a parabolic curve, whereas Kepler found, through long calculations, that the planets traveled in ellipses with the sun at one focus. Neither Kepler nor Galileo used algebra at all. But once algebra in its symbolic form was brought into the service of geometry, it was easy to represent parabolas and ellipses; they could be studied and their properties developed. In fact, algebra changed dramatically at this time. Instead of just being able to give the solution to an equation as a number, one could now ask for and find the solution to a problem as a curve. And there were many problems, especially those derived from Newton’s physical principles, that required finding curves. Curiously, Newton himself used little algebra in his *Principia*, but his 18th-century successors used it extensively.

There is much good reading in *Unknown Quantity*, and the intended audience can probably learn a lot. That is why it is especially disappointing that Derbyshire failed to check his facts on so many occasions and, evidently, did not have his manuscript read by an expert in the history of the subject. I had hoped, on receiving the book, that I could recommend it to my students. Unfortunately, until the major errors are corrected in a new edition, that is not possible.

References and Notes

1. J. Derbyshire, *Prime Obsession: Bernhard Riemann and the Greatest Unsolved Problem in Mathematics* (Joseph Henry, Washington, DC, 2003). Reviewed by B. Conrey, *Science* **302**, 60 (2003).
2. J. Høyrup, *Lengths, Widths, Surfaces: A Portrait of Old Babylonian Algebra and Its Kin* (Springer-Verlag, New York, 2002). See especially pp. 55–58.
3. For information on Euclid’s *Data*, see G. L. McDowell, M. A. Sokolik, *The Data of Euclid* (Union Square, Baltimore, MD, 1993).
4. This translation from Mordecai Finzi’s Hebrew version of Abū Kāmil’s algebra appears in M. Levey, *The Algebra of Abū Kāmil* (Univ. Wisconsin Press, Madison, WI, 1966), pp. 186–192.
5. D. S. Kasir, *The Algebra of Omar Khayyam* (Columbia Teachers College, New York, 1931).
6. G. Cardano, *The Great Art: Or, the Rules of Algebra*, T. R. Witmer, Transl. (MIT Press, Cambridge, MA, 1968), p. 11.
7. F. Viète, *The Analytic Art*, T. R. Witmer, Transl. (Kent State Univ. Press, Kent, OH, 1983), pp. 286–289. The trigonometric solution can be found on pp. 174–175.
8. E. Black, Transl., *The Early Theory of Equations: Their Nature and Constitution: Translations of Three Treatises by Viète, Girard, and de Beaune* (Golden Hind, Annapolis, MD, 1986). The fundamental theorem of algebra is the first sentence of Girard’s theorem II (p. 139), and the result relating symmetric functions of roots to the coefficients is given in the remainder of the theorem.
9. O. Neugebauer, A. Sachs, *Mathematical Cuneiform Texts* (American Oriental Society, New Haven, CT, 1945), pl. 17.

BROWSINGS

100 Caterpillars. Portraits from the Tropical Forests of Costa Rica. Jeffrey C. Miller, Daniel H. Janzen, and Winifred Hallwachs. Harvard University Press, Cambridge, MA, 2006. 272 pp. \$39.95, £25.95, €36.90. ISBN 0-674-02190-8. The authors present close-ups of 100, generally ostentatious, macrocaterpillars from the estimated 9500 species inhabiting northwestern Costa Rica’s Area de Conservación Guanacaste. The species accounts include comments on behavior, range, abundance, food plants, predators, and parasites. Accompanied by an image of the adult, each highlights a relevant natural history theme. The saturniid *Automeris tridens* (above), for example, deters vertebrate predators with acetylcholine and histamine that can be injected by its hollow spines.



The Great Gypsy Moth War. The History of the First Campaign in Massachusetts to Eradicate the Gypsy Moth, 1890–1901. Robert J. Spear. University of Massachusetts Press, Amherst, MA, 2005. 326 pp. \$34.95. ISBN 1-55849-479-0.

Experimenting with silkworm production in the late 1860s, Etienne Leopold Trouvelot imported the gypsy moth to his home near Boston. Almost immediately, the European moths escaped into second-growth hardwood forests dominated by oaks, their favored food. After concentrated colonies of moths were declared a grave danger to the state and country, Massachusetts launched a campaign to exterminate the insect. Spears rebuts the myth that the moth was nearly eliminated and the efforts failed because the state irrationally terminated its funding. He shows that the entomologists in fact recognized their attempts to contain and kill the species were futile. But rather than admit defeat, they turned to political ploys and misrepresentations to maintain a facade of success and secure further appropriations. This informative account provides a useful historical perspective for anyone interested in the biology and control of invasive species.

PUBLIC HEALTH

HIV Testing in China

Zunyou Wu,^{1,2} Xinhua Sun,³ Sheena G. Sullivan,^{1,4} Roger Detels^{2*}

In the face of an infectious disease epidemic, the primary responsibility of public health is to contain and control the epidemic in order to protect the uninfected. In the area of HIV/AIDS, we have not always remembered that principle.

At the end of 2003, the United Nations and the Chinese Ministry of Health (MOH) estimated that the number of people infected with HIV in China was roughly 840,000, of whom 80,000 already had AIDS (1). Experts have expressed fear that these numbers may, in fact, be an underestimation and have warned that, left unchecked, China could have 10 million infected by 2010 (2). One of the main barriers to implementing effective prevention and control efforts in the country is that the majority of infected persons are not aware of their serostatus. At the end of 2005, Chinese authorities knew of only 141,241 confirmed HIV cases, 32,263 of whom had AIDS (3). It is important for people carrying HIV to know about their serostatus, both to prolong their own lives by accessing treatment and to prevent secondary transmission to others (4). Studies in the United States, Zambia, Kenya, Tanzania, Trinidad, Puerto Rico, and India have demonstrated that people who have learned that they are HIV-infected tend to reduce their risk behaviors and to adopt safer sex practices (5–11).

To gain a better understanding of the numbers and profile of people infected, as well as to identify those in need of treatment, the government of China launched a national program to actively seek out certain groups believed to be at high risk for HIV infection. They considered that voluntary counseling and testing (VCT), a passive approach, had failed to inform many of those who were infected, despite the fact that testing was free. Under the new policy, community health workers invite members of targeted high-risk groups to come for testing through outreach. In institutional settings (such as prisons), HIV testing is conducted as part of a routine health check-up. In communities or institutions, refusal is permissible. Testing is accompanied by a social marketing campaign instead of individual counseling. The campaign promotes HIV awareness and addresses misconceptions through various mechanisms, including slogans

on posters and banners, newspaper and television commercials, public announcements by celebrities, and community events.

The increased use of routine testing to identify HIV carriers as part of antiretroviral treatment (ART) scale-up has been controversial and was the subject of debate at last year's International Conference on AIDS in Asia and the Pacific (12). Some would argue that the traditional approach to HIV case ascertainment—one that follows a genetic counseling model rather than an infectious disease model and that emphasizes protecting the rights of the infected—is no longer appropriate in this age of ART (13). Indeed, we believe that an overemphasis on privacy in the early years of the HIV epidemic in the United States (14) may have resulted in HIV infection of thousands of persons receiving unscreened blood, even before an HIV test was available, and overlooked the need to protect the uninfected (15).

The Chinese approach has been criticized by the international community and was debated at length at the Third Conference on HIV/AIDS International Cooperation Projects in China, held on 3 to 4 September 2005 (16). At that meeting, a representative of the United Nations presented a summary of discussions on surveillance, HIV testing, and VCT programs in China and voiced concerns about the new testing policy.

The principal issue of contention was whether active testing of risk groups violates human rights, because it may not always be entirely voluntary and may involve little counseling. The position of the Joint U.N. Programme on HIV/AIDS (UNAIDS) and the World Health Organization (WHO) on HIV testing is that it should be accompanied by informed consent and counseling to promote prevention practices (17). The new testing policy theoretically follows the model of voluntary testing, but there is often significant social pressure not to refuse. Pressure comes from local authorities and health workers in the form of the public announcements mentioned above, which strongly encourage HIV testing, and also from other community members who have already undergone testing. For those receiving a routine annual health check-up, such as government workers and detention center inmates, informed consent for the entire health exam is taken, but not specifically for the HIV test and, therefore, no standard HIV pretest counseling is given.

Active testing for HIV among high-risk groups in China, although controversial, is in the best interests of public health.

Posttest counseling is preferentially provided to those testing positive and includes information about disease progression, treatment, and preventing transmission to partners.

The new testing policy was initially implemented in Henan province, where it was becoming apparent that increasing numbers of former commercial plasma donors who had been infected with HIV by contaminated plasma through donation practices in the 1990s were progressing to AIDS. From June to August 2004, the provincial government of Henan identified and registered 280,307 former plasma donors and invited them to receive HIV-1 antibody testing. It is likely, however, that some former donors hid their identity. Almost 8% of those acknowledging plasma donation refused testing. Of the 258,237 (92.1%) individuals actu-



Yijuan Duan, Deputy Director of Ruili CDC in Yunnan, takes a blood sample from a male drug user for HIV testing.

ally tested, 23,157 (9.9%) were identified as HIV-positive (18). The number of HIV infections identified over the 3 months of active testing was almost six times that of the previous 10 years. Importantly, among the 23,157 HIV infections, 12,159 were HIV-serodiscordant couples, the uninfected members of which are now able to protect themselves from infection.

From September to December 2004, the government of Yunnan province launched its own active testing initiative among drug users, spouses of HIV-infected individuals, children under 10 years of age whose mothers were HIV-positive, sexually transmitted disease (STD) patients, sex workers, former plasma donors, pregnant women, patients suffering from infections, and other groups. They invited 424,000 individuals to be tested, of whom 1.3% refused. Of the 418,630 individuals tested, 13,486 (3.2%) were positive for HIV (19). This is essentially equivalent to the total number identified in the previous 18 years.

Following these provincial models, the MOH announced plans to implement active testing of

¹National Center for AIDS/STD Control and Prevention, Chinese Center for Disease Control and Prevention, Beijing 100050, PR China. ²School of Public Health, University of California at Los Angeles, Los Angeles, CA 90095, USA. ³Division of AIDS, Department of Disease Prevention and Control, Ministry of Health, Beijing, 100044, PR China. ⁴Centre for Human Genetics, Edith Cowan University, Joondalup, Perth, WA 6207, Australia.

*Author for correspondence. E-mail: detels@ucla.edu



Cartoon educational posters are used for an AIDS campaign in a rural community in China.

all former plasma donors in the country from October 2004 to June 2005. Nationwide testing of other high-risk groups using the strategy implemented in Yunnan continues among sex workers, intravenous drug users, men who have sex with men, and STD clinic patients. In coordination with the Ministry for Justice, inmates in detention centers and detoxification centers are also being tested.

China is attempting to provide free health care to its HIV-infected, particularly the impoverished. In December 2003, the Chinese government announced the ambitious “Four Free and One Care” policy, which entails (i) free ART to rural residents and urban residents without insurance; (ii) free VCT; (iii) free prevention of mother-to-child transmission (20); and (iv) free schooling for children within families with HIV/AIDS (1, 2). People testing positive are assessed for CD4⁺ to determine eligibility for the free ART program. Thus, testing is not purely for information gathering and reduction of HIV transmission, but also acts as a gateway to services for those identified with the disease.

At the end of 2005, the free ART program served 20,453 AIDS patients, including approximately 17,000 former plasma donors, 600 drug users, and 100 men who have sex with men. In addition to the social welfare support described above for infected individuals and their families, individuals may also receive a monthly living allowance from their local government, which varies among the different provinces (1). Therefore, the Chinese approach benefits both those tested and found to be infected and those at risk for becoming infected.

A major barrier to agreeing to have VCT is the fear of stigma and discrimination. The Chinese government has commissioned several campaigns to reduce stigma and discrimination (2) and has introduced new laws to protect the rights and confidentiality of the HIV-infected in an effort to ease their concerns and to increase VCT (21, 22). In particular, Article 3 of the new *Regulations on AIDS Prevention and Control* (1 March 2006), pledges to

“protect the legal rights of people living with HIV/AIDS and their relatives. This includes the rights to marriage, employment, medical treatment and education. Any institution or individual shall not discriminate against people living with HIV/AIDS and their relatives (21).”

However, stigma and discrimination remain significant obstacles. Routine testing programs implemented on a wider scale—such that most people in the risk groups are tested—can potentially normalize HIV testing and lessen the stigma and discrimination associated with it. Although no formal evaluation of the testing campaigns has been undertaken, certainly, the ancillary effects of wide-scale testing—increased access to VCT, raised public awareness about HIV, as well as normalizing the procedure of HIV testing—may have had a positive effect on reducing stigma in communities where HIV is prevalent. For example, in Henan, the number accepting VCT has increased since active testing was implemented.

Additional benefits that we believe accrue from active testing and its accompanying education campaigns include increased awareness of HIV among the general population, increased use of condoms by discordant couples, and increased availability of HIV and CD4⁺ testing resulting from the infrastructure that was established to implement the campaigns. In 2006, the MOH, together with UNAIDS and WHO, released a new HIV estimate of 650,000. Nationwide testing contributed in part to this more accurate revision by allowing a better understanding of the epidemic in certain high-risk groups, particularly plasma donors (3).

China cannot risk allowing complacency and low reception of VCT among at-risk groups to hinder control of the epidemic. If those at risk remain unaware, they cannot take steps to prevent further transmission of HIV and to seek treatment. China's responsibility for control of the HIV/AIDS epidemic is to protect the uninfected through identifying those who are HIV-infected and providing treatment and social and economic support for the

infected and their families.

References and Notes

1. State Council AIDS Working Committee Office, U.N. Theme Group on HIV/AIDS in China, *A Joint Assessment of HIV/AIDS Prevention, Treatment and Care in China* (Beijing, 2004).
2. J. Watts, *Lancet* **362**, 1983 (2003).
3. Ministry of Health of China, UNAIDS, and WHO, *2005 Update on the HIV/AIDS Epidemic and Response in China* [Chinese Center for Disease Control and Prevention (China CDC), Beijing, 2006].
4. M. J. Rotheram-Borus, P. A. Newman, M. A. Etzel, *J. Acquir. Immune Defic. Syndr.* **25** (suppl. 2), S105 (2000).
5. The Voluntary HIV-1 Counseling and Testing Efficacy Study Group, *Lancet* **356**, 103 (2000).
6. S. Allen *et al.*, *AIDS* **17**, 733 (2003).
7. H. Amaro, A. C. Morrill, J. Dai, *J. Health Psychol.* **10**, 287 (2005).
8. M. E. Bentley *et al.*, *AIDS* **12**, 1869 (1998).
9. R. Fox, N. J. Odaka, R. Brookmeyer, B. R. Polk, *AIDS* **1**, 241 (1987).
10. J. A. Inciardi, H. L. Surratt, S. P. Kurtz, J. C. Weaver, *AIDS Care* **17** (suppl. 1), S88 (2005).
11. R. R. Robles, T. D. Matos, H. M. Colon, C. A. Marrero, J. C. Reyes, *Drugs Soc. (New York)* **9**, 173 (1996).
12. A. Erikson *et al.*, *Correspondent* **15**, 24 (2006).
13. T. Frieden *et al.*, *N. Engl. J. Med.* **353**, 2397-2402 (2005).
14. R. Bayer, *N. Engl. J. Med.* **334**, 1540 (1996).
15. L. B. Leveton, H. C. Sox, M. A. Stoto, Eds. *HIV and the Blood Supply: An Analysis of Crisis Decision-Making* (Institute of Medicine, National Academies Press, Washington, DC, 1995).
16. Chinese Ministry of Health, U.N. Theme Group on HIV/AIDS in China, The Third Conference on HIV/AIDS International Cooperation Projects in China, Kunming, 3 to 4 September 2005.
17. UNAIDS-WHO, “Policy statement on HIV testing” (www.who.int/entity/rpc/research_ethics/hivtestingpolicy_en.pdf).
18. Ministry of Health Expert Consultation Committee, “Report on HIV screening among key populations in Henan province” (Ministry of Health, Beijing, 2005).
19. Ministry of Health Expert Consultation Committee, “Report on HIV screening among key populations in Yunnan Province” (Ministry of Health, Beijing, 2005).
20. HIV-positive mothers are given the options of abortion or ART perinatally, cesarean delivery (where available), and free formula milk for 12 months.
21. State Council Regulations on AIDS Prevention and Treatment, Articles 3, 10, 39, 41, 55, 56.
22. The Infectious Diseases Control Act of the People's Republic of China, Articles 12, 16, 68, 69.
23. We thank S. Korenman, Associate Dean for Ethics at the UCLA School of Medicine, for reviewing this manuscript, W. W. Cao for review of relevant publications, and W. Aft for editorial assistance.

CLIMATE CHANGE

Evolutionary Response to Rapid Climate Change

William E. Bradshaw and Christina M. Holzapfel

Over the past 40 years, species have been extending their ranges toward the poles and populations have been migrating, developing, or reproducing earlier in the spring than previously (1–4). These range expansions and changes in the timing of seasonal events have generally been attributed to “phenotypic plasticity”—that is, the ability of individuals to modify their behavior, morphology, or physiology in response to altered environmental conditions (5, 6). Phenotypic plasticity is not the whole story. However, recent studies show that over the recent decades, climate change has led to heritable, genetic changes in populations of animals as diverse as birds, squirrels, and mosquitoes (see the first figure).

These genetic changes in animal populations (7) have involved adaptation to the timing of seasonal events or to season length. For example, Canadian red squirrels are reproducing earlier in the spring, thereby capitalizing on earlier spruce cone production (8). Blackcaps (birds) in central Europe have been increasingly overwintering in Britain rather than Iberia; the genetically distinct British subpopulation arrives earlier at the nesting grounds and thus obtains superior territories or mates (9, 10). European great tits (birds) depend on caterpillars to feed their young. With earlier springs, the caterpillars have been maturing earlier, before the tit chicks hatch, leading to a decline in lifetime reproductive success of the birds. Among the tits, there is genetic variation in the ability to adjust egg-laying date. The individual birds most able to modify the timing of egg laying in response to the earlier springs are the ones that maintain the greatest lifetime reproductive success (11).

Insects are also adapting to recent, longer growing seasons. In European (12), North American (13), and Australian (14) populations of fruit flies, the frequencies of different alleles and of chromosomal inversions have been shifting toward the frequencies of more southern populations. With longer growing seasons, populations of North American mosquitoes that live in pitcher plants have shown a genetic shift toward the use of shorter, more southern day lengths to cue the initiation of larval dormancy (15).

Although the specific adaptations of these animals to climate change are as diverse as the organisms themselves, they all involve genetic



Adaptive animals. The Yukon red squirrel (*Tamiascurus hudsonicus*) (left), the pitcher-plant mosquito (*Wyeomyia smithii*, shown descending into its carnivorous host, *Sarracenia purpurea*) (middle), and the European blackcap (*Sylvia atricapilla*) (right) show genetically based shifts in the timing of their seasonal reproduction, dormancy, or migration during recent, rapid climate warming.

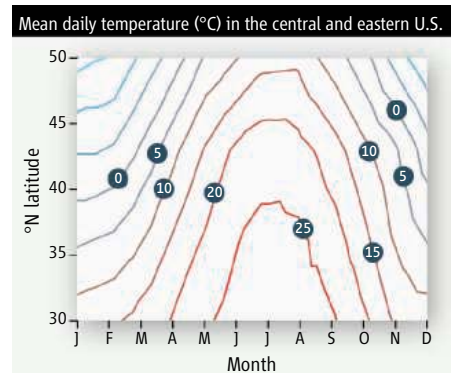
changes relating to season: earlier or more flexible timing of reproduction in squirrels and birds, later arrival of winter in mosquitoes, and a longer growing season for fruit flies.

None of these studies provides evidence that there have been genetic changes in response to higher temperature alone. Moreover, when northern mosquitoes were experimentally transplanted to a simulated southern climate, a huge loss of fitness occurred; 88% of this fitness loss was due to experiencing the incorrect seasonal cues (day length), whereas the warmer summer temperature of the more southern locality was not a factor (16). Hence, the correct interpretation of cues that correspond to seasonality, rather than to hotter temperatures, is of primary importance. We

are not aware of any examples of genetic changes in animal populations toward either higher thermal optima or greater heat tolerance that are correlated with recent climate warming.

A consideration of the seasonal profiles of temperature in eastern and central North America shows why recent climate change is imposing seasonal rather than thermal selection on natural populations (see the second figure). The latitudinal variation in climate is less a matter of summer warmth (the July isotherms are far apart) than it is of winter cold (the January isotherms are close together), and northern populations experience shorter growing seasons than southern populations. For example, mean daily temperatures are above 10°C all year at 30°N but are above 10°C for only 2.5 months at 50°N. Global warming is proceeding fastest at the most northern latitudes, where the gradient in winter cold is steepest (17, 18), thereby expanding the growing season while alleviating winter cold stress without imposing summer heat stress (16). Hence, northern climates are becoming more like those in the south.

At least within insect species, northern populations use longer day lengths to cue the initiation of dormancy earlier in the fall than do southern populations (18), and recent climate warming has resulted in a genetic shift toward the use of shorter, more southern day lengths (16). By contrast, within insect species, the upper limits of heat tolerance do not change with latitude (20), because the latitudinal variation in North American surface temperature is more a matter of winter cold than of summer heat (see the second figure). Hence, adaptive shifts in the timing of seasonal events should precede adaptive shifts of



Winter cold versus summer heat. The isotherms for mean daily temperature in the central and eastern United States (from the Gulf of Mexico to the Canadian border) are close together in the winter but spaced far apart in the summer. Thus, changes to seasonal length or the timing of spring have a greater effect on animal populations than changes in temperature by themselves. Data are for 1931–1960 (16), before rapid climate warming occurred.

CREDIT: (TOP) PHOTO OF SQUIRREL, C. KOLACZ/UNIVERSITY OF ALBERTA; CANADA; PHOTO OF BLACKCAP BIRD/MAX PLANCK INSTITUTE FOR ORNITHOLOGY, VOGELWART RADOLFZELL, GERMANY

The authors are at the Center for Ecology and Evolutionary Biology, University of Oregon, Eugene, OR 97403, USA. E-mail: mosquito@uoregon.edu

thermal optima or increased heat tolerance over evolutionary time, and that is the pattern that is emerging.

Studies providing evidence for genetic change in response to recent, rapid climate change have come from research groups that have focused their efforts on one or a few species over several decades. These studies have involved retrospective comparisons in flies, mosquitoes, and black-caps or have used pedigree analysis through multiple generations in squirrels and great tits. The time scales over which genetic changes are detectable cover a wide range. In mosquitoes, a clear change could be seen over 5 years (15). Moderate changes were detectable over 10 years in red squirrels (8). In great tits, even after 30 years, only the portion of the population that is most able to modify the timing of egg laying in response to earlier springs has changed genetically (11). Despite both phenotypic and genetic changes in the ability of great tits to track the seasonal availability of caterpillars, the average lifetime reproductive success of the population as a whole is declining. The population cannot keep pace with environmental change and may be vulnerable to extinction (11). Hence, the ability to evolve in response to recent climate warming does not, in itself, ensure that a population will survive (2, 11, 21).

As these examples show, the effects of rapid climate warming have penetrated to the level of

the gene in a diverse group of organisms. These genetic changes in populations affect the timing of major life history events: when to develop, when to reproduce, when to enter dormancy, and when to migrate. Small animals with short life cycles and large population sizes will probably adapt to longer growing seasons and be able to persist; however, populations of many large animals with longer life cycles and smaller population sizes will experience a decline in population size or be replaced by more southern species. Questions remain about the relative rates of environmental and evolutionary change (5, 11, 21, 22). But it is clear that unless the long-term magnitude of rapid climate change is widely acknowledged and effective steps are taken to mitigate its effects, natural communities with which we are familiar will cease to exist (2, 22–24).

References and Notes

1. C. Parmesan, G. Yohe, *Nature* **421**, 37 (2003).
2. R. Warren, in *Avoiding Dangerous Climate Change*, H. J. Schellnhuber et al., Eds. (Cambridge Univ. Press, Cambridge, 2006), chap. 11.
3. D. Berteaux et al., *Integr. Comp. Biol.* **44**, 140 (2004).
4. T. L. Root et al., *Nature* **421**, 57 (2003).
5. L. Hughes, *Trends Ecol. Evol.* **15**, 56 (2000).
6. G.-R. Walther et al., *Nature* **416**, 389 (2002).
7. Evidence for genetically-based shifts in a population include differences between populations of animals reared under identical conditions after years or decades of selection (flies, mosquitoes); pedigree analysis, which establishes the genetic basis of phenotypic change based

8. on resemblance between relatives in succeeding generations (squirrels, great tits); and differences between subpopulations in migratory patterns that persist in lab-reared offspring (blackcaps).
8. D. Réale et al., *Evolution* **57**, 2416 (2003).
9. S. Bearhop et al., *Science* **310**, 502 (2005).
10. P. Berthold et al., *Nature* **360**, 668 (1992).
11. D. H. Nussey, E. Postma, P. Gienapp, M. E. Visser, *Science* **310**, 304 (2005).
12. F. Rodríguez-Trelles, M. A. Rodríguez, *Evol. Ecol.* **12**, 829 (1998).
13. M. Levitan, *Evol. Ecol. Res.* **5**, 597 (2003).
14. P. A. Umina, A. R. Weeks, M. R. Kearney, S. W. McKechnie, A. A. Hoffmann, *Science* **308**, 691 (2005).
15. W. E. Bradshaw, C. M. Holzapfel, *Proc. Natl. Acad. Sci. U.S.A.* **98**, 14509 (2001).
16. W. E. Bradshaw, P. A. Zani, C. M. Holzapfel, *Evolution* **38**, 1748 (2004).
17. Intergovernmental Panel on Climate Change, *Climate Change 2001: The Scientific Basis*, J. T. Houghton et al., Eds. (Cambridge Univ. Press, Cambridge, 2001).
18. T. R. Karl, K. E. Trenberth, *Science* **302**, 1719 (2003).
19. A. S. Danilevskii, *Photoperiodism and Seasonal Development of Insects* (Oliver & Boyd, Edinburgh, 1965).
20. A. Addo-Bediako et al., *Proc. R. Soc. London Ser. B* **267**, 739 (2000).
21. M. Lynch, in *Conservation Genetics: Case Histories from Nature*, J. C. Avise, J. L. Hamrick, Eds. (Chapman & Hall, New York, 1996), chap. 15.
22. C. D. Thomas et al., *Nature* **427**, 145 (2004).
23. A. van Vliet, R. Leemans, in *Avoiding Dangerous Climate Change*, H. J. Schellnhuber et al., Eds. (Cambridge Univ. Press, Cambridge, 2006), chap. 12.
24. E. Kolbert, *Field Notes from a Catastrophe: Man, Nature, and Climate Change* (Bloomsbury, New York, 2006).

10.1126/science.1127000

APPLIED PHYSICS

Toward Robots That Can Sense Texture by Touch

Richard Crowder

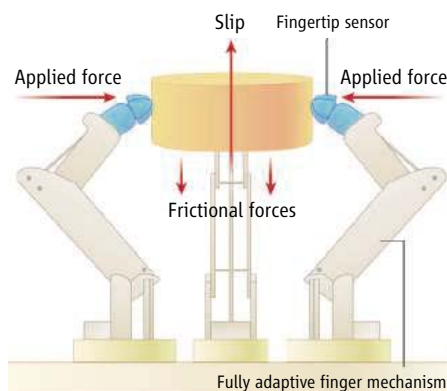
Today's state-of-the-art dexterous robotic hands cannot achieve tasks that most 6-year-old children can do without thinking, such as tie a shoelace or build a house of cards. The improvement of the manipulative capabilities of robotic hands requires advances in a wide range of technologies, including mechanics, actuators, sensors, and artificial intelligence. Many robots—such as NASA's Robonaut (1)—have the dexterity required to perform some of the tasks that we take for granted, but replication of the full manipulative capabilities of the human hand is still years away.

A key advance needed for these new robots is the development of a sensor or set of sensors that can replicate the human sense of touch. Most robotic systems incorporate binary touch

sensors—that is, sensors that can distinguish between touch or no touch. Many more sophisticated sensors have been discussed in the literature, but their take-up by industry is hampered by manufacturing challenges, in particular, the assurance of protection against the wear and tear found in the real world. In contrast, vision sensors are almost commonplace in many robotic systems (2).

The development of tactile sensors is one of the most difficult aspects of robotics. (A tactile sensor measures force and spatial information, whereas touch is technically just the force at a single point.) Many technologies have been explored, including a carbon-loaded elastomer, piezoelectric materials, and micro-electromechanical systems (3). Many designs exist, but few have moved from the research laboratory to become a commercial success. Those that have tend to be robust and easy to construct, but provide poor spatial resolution.

A compact, high-resolution touch sensor has been developed from a thin film. Incorporation of this sensor into robotic hands may substantially improve their dexterity.



A three-fingered gripper. The fingertips are designed to allow a wide variety of objects to be grasped and manipulated. The addition of a fingertip sensor will not only allow the applied force to be controlled, but will also (with a suitable controller) minimize the object's slip in any direction.

The author is in the School of Electronics and Computer Science, University of Southampton, Southampton SO17 1BJ, UK. E-mail: rmc@ecs.soton.ac.uk

On page 1501 of this issue, Maheshwari and Saraf (4) report the development of a compact, high-resolution touch sensor. The thin-film design permits the authors to produce a single tactile sensor that is larger than a typical human fingertip, with similar resolution. However, as with most sensors of this resolution and size, the challenge is to extract the sensor's information efficiently—something that the human nervous system does with supreme efficiency.

The new sensor responds to an applied force either with electroluminescent emissions or with a change in current density. The electroluminescent response can be considered the high-resolution mode. The authors use a charge-coupled device (CCD) camera to capture the electroluminescent emissions from the sensor. This vision-based approach allows the high-resolution tactile image to be easily obtained and manipulated. The current density measurement, although of lower resolution, could also be used in a dexterous robot hand, either as a lower resolution sensor or for protection. Given that the sensing element is a film, it should be possible to use it to coat the fingertip or palm of a robot, although the CCD camera will need to be integrated with the sensing film.

The detection of texture at the resolution reported by Maheshwari and Saraf will allow not only object texture and local forces to be determined; slip can also easily be detected though examination of the tactile image over time. The early detection of slip is used in the control of many multifingered hands.

To appreciate the advantages of having a single sensor for both slip and texture, it is worth considering how it can be integrated into robotic hands that need to restrain and manipulate a wide range of objects under a wide range of conditions. To achieve a satisfactory grasp, optimal force control is required. Any movement of a robotic hand may result in the grasped object slipping and possibly being dropped; hence, the sensors on the hand have to register any slippage and adjust the applied forces to bring the object back to rest (see the figure).

The problem of defining the required grasp force is crucial and can be posed as an optimization problem (5). A range of techniques have been used to solve this problem. Some approaches are analytic solutions and cannot be easily implemented in real-time applications, particularly when dynamic adaptation to external disturbances is required. Also, analytic approaches cannot be used if variables such as object weight and hand acceleration are unknown. To overcome this situation, advanced control techniques have been developed, which use tactile sensors to measure the applied force to the object and its slip as required by the controller (6). Controllers that can optimize the applied force in response to slip have been successfully implemented (7, 8).

To achieve satisfactory control of a dexterous hand, a sensor requires a wide dynamic range,

typically up to 1000 Hz; the reported sensor is capable of achieving this. Dynamic application of the sensor is thus of considerable interest in the robotic community, and the high resolution of the tactile information will be of interest in medical robotics, particularly in minimal access (or keyhole) surgery.

The development of tactile sensors is one of the key technical challenges in advanced robotics and minimal-access surgery. The unique sensor developed by Maheshwari and Saraf could prove to be a key advance in technology, for reasons including relatively simple construction, apparent robustness, and high resolution. The next stage in the development of this sensor is to look at its robustness and performance characteristics over time. Once these issues are resolved, the sensor can be integrated into a dexterous hand, hopefully leading to an improvement in dexterity.

ECOLOGY

Getting a Better Picture of the Ocean's Nitrogen Budget

Zbigniew S. Kolber

The most common nitrogen-fixing cyanobacterium in the oceans is more abundant than previously estimated and can therefore account for at least a portion of the apparent oceanic nitrogen deficit.

The deficit in the biologically available nitrogen supply required to support new production (photosynthetic activity that results in permanent carbon fixation) in tropical and subtropical oceans represents one of the most intriguing conundrums in oceanography. Upwelling of the deep, nutrient-rich waters through mechanisms of winter mixing due to storm activity, eddy pumping, and diffusion can supply only a fraction (40 to 60%) of the necessary nitrate (1). The remainder must be provided by reduction of atmospheric dinitrogen (N_2), which requires breaking the ultrastable triple nitrogen-nitrogen bond. In the ocean, most of this process is performed by a nonheterocystous photosynthetic prokaryote, *Trichodesmium* sp. The estimates of nitrogen fixation by this diazotroph average ~ 90 Tg N year⁻¹ (2), which represents less than 50% of the required new nitrogen (3) (1 Tg = 10^{12} g). During the past 10 years, a substantial effort has been expended to account for the missing part in the ocean's nitrogen budget. Researchers have sought to reassess the diazotrophic activity of *Trichodesmium* or to identify other organisms that may fix the "miss-

The author is at the Monterey Bay Aquarium Research Institute, 7700 Sandholdt Road, Moss Landing, CA 95039, USA. E-mail: zkolber@mbari.org

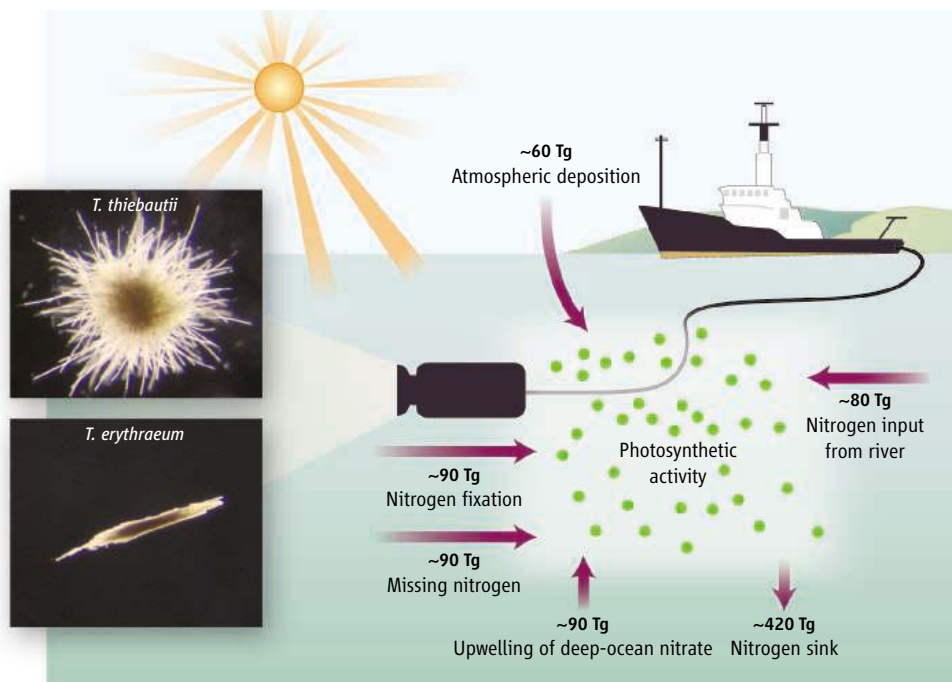
References

1. G. Huang, *New Scientist* **46** (4 February 2006).
2. M. Lee, *Int. J. Robot. Res.* **19**, 636 (2000).
3. R. Crowder, in *Handbook of Industrial Automation*, R. Shell, E. Hall, Eds. (Dekker, New York, NY, 2000), pp. 377–392.
4. V. Maheshwari, R. F. Saraf, *Science* **312**, 1501 (2006).
5. A. Bicchi, V. Kumar, in *Proceedings of IEEE International Conference on Robotics and Automation* (IEEE, San Francisco, 2000), pp. 328–353.
6. M. Brown, C. Harris, *Neurofuzzy Adaptive Modelling and Control* (Prentice Hall International, Hemel Hempstead, UK, 1994).
7. J. Dominguez-Lopez, R. Crowder, R. Damper, C. Harris, in *2004 IEEE International Conference on Systems, Man and Cybernetics* (IEEE, The Hague, Netherlands, 2004), vol. 4, pp. 3193–3198.
8. O. Fuentas, R. Nelson, in *IEEE/SICE/RSJ International Conference on Multisensor Fusion and Integration for Intelligent Systems* (IEEE, Washington, DC, 1996), pp. 342–348.

10.1126/science.1129110

ing" nitrogen. Although new, single-cell diazotrophic bacteria have been identified (4), their potential contribution to nitrogen fixation has been difficult to quantify. On page 1517 of this issue, Davis and McGillicuddy (5) decided to have another "look" at this problem, literally. Using a towed undulating video camera, they captured images of *Trichodesmium* colonies (in puff and tuft morphologies; see the figure) over large areas of the Sargasso Sea. On the basis of the unexpectedly high abundance of these colonies, they postulate that the apparent nitrogen deficit in the world's oceans is simply due to an accounting error.

The video images of colonies paint a picture of *Trichodesmium* distribution in the water column very different from that described in the existing literature. Conventional net tows and bottle sample data indicate that *Trichodesmium* colonies generally congregate at the surface of the ocean, with their abundance sharply decreasing at depth. Such patterns of vertical distribution are consistent with (i) the prevalence of gas vacuoles within colonies of these cyanobacteria, which make them buoyant; (ii) the high energy requirements for bacterial nitrogenase to catalyze nitrogen fixation, which are met in well-lit surface waters; and (iii) independence from dissolved nitrate, which allows



The ocean's nitrogen. Shown are the approximate fluxes of bioavailable nitrogen in the ocean. There is an apparent deficit of about ~ 90 Tg required to support the existing level of oceanic new production. Using a towed video camera, Davis and McGillicuddy observed *Trichodesmium*, the most common oceanic nitrogen-fixing diazotroph, with abundance exceeding the known estimates by a factor of 2 to 3. The authors have reassessed the rates of nitrogen fixation by this organism, substantially narrowing the nitrogen deficit.

Trichodesmium to thrive just below the water surface (where other phytoplankton species are severely nutrient-limited). The images captured by Davis and McGillicuddy, however, show a much more uniform distribution of puffs and tufts colonies, sometimes extending over the entire depth of light penetration in the water column (the euphotic zone). The authors argue that their findings reflect the fact that net tows destroy a substantial portion of the colonies recovered from the lower portion of the water column (6). Using the new estimates of *Trichodesmium* abundance, the authors reassess the rates of nitrogen fixation at a level two to three times that provided by the existing estimates, wiping out the perplexing nitrogen deficit in the ocean.

Although a better picture of *Trichodesmium* abundance will provide new insights into global biogeochemical cycles, the reassessment of the nitrogen fixation based on these observations should be considered with caution. The authors assume rates of nitrogen fixation at the ocean surface of about $0.7 \text{ nM N colony}^{-1} \text{ hour}^{-1}$. This value represents the high end of the reported nitrogen fixation rate, which generally ranges from 0.03 to 0.8 for puffs and tufts (7), far exceeding the average colony-specific nitrogenase activity (8). Based on the existing literature, a more conservative estimate of about 0.25 to $0.35 \text{ nM N colony}^{-1} \text{ hour}^{-1}$ is more representative of average colony performance. Also, the assumed relationship between nitrogen fixation and irradiance, based on the Michaelis-Menten

relationship (as described by the authors), is not applicable in situations where the available energy, rather than substrate concentration, limits the rate of nitrogen fixation. Such an approach could potentially lead to overestimation of nitrogen fixation rates at depths below 50 m. Arguably, the reported increase in abundance of *Trichodesmium* colonies in the euphotic zone will raise the overall estimates of nitrogen fixation, but the gain is likely to be much smaller than that postulated by the authors.

Certainly, the new technique presented by Davis and McGillicuddy allows a much more precise assessment of *Trichodesmium* presence over large spatial scales. It has been argued that this presence is controlled to a large extent by iron availability (9). Iron is a cofactor in the nitrogenase enzyme complex, and nitrogenase activity requires high energy input that must be satisfied by an equally iron-dependent photosynthetic apparatus. On the other hand, nitrogen self-reliance allows *Trichodesmium* to control the nitrogen-to-phosphorus ratio in areas of the ocean where iron is plentiful. Better assessment of *Trichodesmium* distribution should clarify the relationships between nitrogen, iron, and phosphorus over large portions of the oceans.

The unusually high iron requirement makes *Trichodesmium* dependent on aeolian dust supply. The potential changes in prevailing wind patterns, land aridity, and land use following the warming of oceans and land masses are likely to modify the spatial patterns of aeolian iron fluxes, potentially altering the abundance and spatial dis-

tribution of *Trichodesmium*. If so, the patterns of photosynthetic production will change as well, modifying the ocean's ability to draw atmospheric carbon and introducing a gamut of ill-defined feedback mechanisms into the system of carbon exchange between the atmosphere and the ocean (10). *Trichodesmium* abundance could serve as one of the critical state variables in this system—a variable that Davis and McGillicuddy made easy to observe and quantify.

Plugging the global nitrogen deficit, however, may require effort beyond counting the *Trichodesmium* colonies. Their nitrogen-fixing performance must be calibrated with respect to irradiance regime, physiological conditions, and basin-scale variability in diazotrophic activity. To that end, it will be necessary to complement the imaging techniques with methods of measuring the energy fluxes into the nitrogen-fixing apparatus; assessing the local, incredibly high variability in the colony-specific nitrogen fixation rates; and quantifying the spatial and temporal patterns in gene expression for the nitrogenase complex in *Trichodesmium*. Whether such measurements can be performed at resolution and time scales comparable to that of the video-imaging techniques is limited only by the existing methods, techniques, and technology. Given enough effort, these barriers will fall.

Davis and McGillicuddy may indeed hold one of the keys to solving the nitrogen deficit in the world's oceans. They have found a brilliant approach toward basin-scale three-dimensional measurements of *Trichodesmium* abundance. As research activities on the oceanic nitrogen cycle accelerate, the remaining elements of the nitrogen puzzle will hopefully fall into place. There may be a few surprises along the way. Take the recent discovery of anammox activity (in which ammonium is oxidized with nitrite to nitrogen gas) by bacteria found below the euphotic zone (11)—this finding may again widen the gap between nitrogen sources and sinks. Or we may discover new oceanic diazotrophs. Image by image, we'll find out.

References

1. D. Karl *et al.*, *Nature* **388**, 533 (1977).
2. V. J. Coles, R. R. Hood, M. Pascual, D. G. Capone, *J. Geophys. Res.* **109**, C06007 (2004).
3. C. Mahaffey, A. F. Michaels, D. G. Capone, *Am. J. Sci.* **305**, 546 (2005).
4. J. P. Zehr *et al.*, *Nature* **412**, 635 (2001).
5. C. S. Davis, D. J. McGillicuddy Jr., *Science* **312**, 1517 (2006).
6. J. Chang, *J. Exp. Mar. Biol. Ecol.* **245**, 215 (2000).
7. K. M. Orcutt *et al.*, *Deep Sea Res. II* **48**, 1583 (2001).
8. D. G. Capone *et al.*, *Global Biogeochem. Cycles* **19**, 10.1029/2004GB002331 (2005).
9. I. J. Berman-Frank *et al.*, *Limnol. Oceanogr.* **46**, 1249 (2001).
10. P. G. Falkowski, *Nature* **387**, 272 (1997).
11. M. M. M. Kuypers, *Proc. Natl. Acad. Sci. U.S.A.* **102**, 6478 (2005).

MATERIALS SCIENCE

Multiferroics as Quantum Electromagnets

Yoshinori Tokura

The term “electromagnetism” comes from the fact that the electric and magnetic fields are generally not independent of one another. A changing magnetic field produces an electric field (electromagnetic induction), whereas the motion of electric charges, or electric current, generates a magnetic field (the Biot-Savart law). Typically, electromagnets are wire coils or loops, which tend to be bulky and difficult to fabricate. Would it be possible to devise an electromagnet made from a nano- or micrometer-scale material (not in the form of a coil) that could be activated by simply applying an electric field or current? The answer is perhaps yes, but the issue is not straightforward at all. The magnetoelectric (ME) effect in a solid—that is, the induction of a magnetization (M) by means of an electric field and the induction of an electric polarization (P) by means of a magnetic field—was presumed to exist by Pierre Curie (1), who considered the analogy of the electromagnetic phenomena in a vacuum and in a solid. This analogy is important today from the standpoint of applications: The highly efficient control of magnetism by an electric field or electric current in a solid may advance the technology of spin-electronics (spintronics) technology, such as magnetic storage and magnetic random-access memory. Since the ME effect was first confirmed in the 1960s by Russian scientists, many magnetic materials have been shown to produce this effect (2). Nevertheless, the magnitude of the observed ME effect has been too small for practical devices.

Multiferroics, the materials in which both ferromagnetism and ferroelectricity can coexist, are the prospective candidates that can potentially host what might be called a giant ME effect. Here, the prefix “ferro” originally refers to iron, which shows a spontaneous M controlled by a weak magnetic field. Likewise, ferroelectricity refers to the spontaneous P controllable with an electric field. In multiferroics, the coexistent spontaneous M and P may respond to relatively weak magnetic and electric fields, respectively. Thus, a naïve expectation is that the large ME effect may be driven

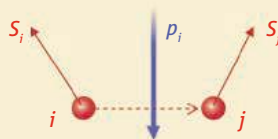
by weak electric or magnetic fields, if the M and P are closely coupled. The problem is how to design such a multiferroic material and how to enhance its M - P coupling. In the recent literature there have been reports of some polar (that is, having built-in P) crystals that can also show the spontaneous M of ferromagnetism, particularly the perovskite structure involving Bi^{3+} or Pb^{2+} ions as well as magnetic ions. In general, these polar ferromagnets can show very interesting linear and nonlinear optical

properties arising from the ME response in the optical frequency region (2, 3), yet the coupling between M and P at the electronic ground state has remained very small.

A useful hint for designing strong M - P coupling has recently been obtained by the discovery of ferroelectricity in the spiral-spin magnets (4–6), as schematically shown in the figure. There are many possible spin arrangements in magnetic materials. For example, when the spins on the adjacent atomic sites are canted from each

other (see the figure, first panel), the horizontal mirror-plane symmetry is lost, and polarization can be generated along the vertical direction. Recently, it has also been theoretically shown (7) that the overlap of the electronic wave function between the two atomic sites with canted spins generates a genuine electronic polarization via the relativistic quantum-mechanical effect called the spin-orbit interaction. When the spins form a spiral modulation along a specific crystallographic direction (see the figure, second panel), then every nearest-neighbor pair produces a unidirectional P and hence should generate a macroscopic P of electronic (spin) origin. The direction of the polarization can be completely determined by the clockwise or counterclockwise rotation of the spin along the spiral propagation axis, called the spin helicity. In those compounds, the spontaneous polarization can be easily controlled by an external magnetic field of specific direction (4, 5), which may be viewed as a giant ME effect. The multiferroics based on this mechanism are in what is called the conical spin state (see the figure, third panel), where the transverse spiral component coexists with the uniform magnetization component along the cone axis. These spiral and conical spin states are widely seen in complex transition-metal compounds like spinels and perovskites, where competing exchange interactions of the

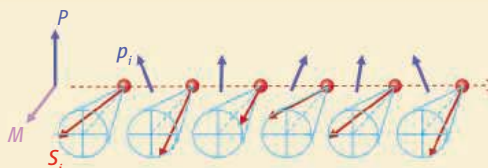
Canted spins on neighboring atomic sites can produce an electronic polarization (p) due to overlap of the electronic wave functions (the spin-exchange interaction) and the spin-orbit interaction.



Spiral spin structure can produce a uniform overall polarization P , which is the sum of individual polarizations (p_i).



Conical spin structure allows both uniform magnetization M and polarization P , producing a multiferroic state of purely magnetic origin.



Clamping of ferromagnetic and ferroelectric domain walls may allow electric (or magnetic) field-induced reversal of magnetization (or polarization).



Designing better magnets. Possible spin superstructures in the multiferroics with strong coupling between magnetism and electricity.

The author is in the Department of Applied Physics, University of Tokyo, 7-3-1Hongo, Bunkyo-ku, Tokyo 113-8656, Japan and in the Spin Superstructure Project, Exploratory Research for Advanced Technology Office, Japan Science and Technology Corporation, Tsukuba 305-8562, Japan. E-mail: tokura@ap.t.u-tokyo.ac.jp

neighboring spins can cause such a periodically modulated spin structure.

With the existence of ferroelectricity of magnetic origin, a new aspect is expected to emerge in the ME effect. Such a multiferroic state may in most cases compete with another ME phase, say a paraelectric-antiferromagnetic phase. Therefore, the application of a magnetic (or electric) field may induce a first-order phase transition between those ME phases, resulting in the magnetic (or electric) control of the ME phases and hence control of the P (or M). In fact, this is the microscopic origin of the magnetic P -control as observed for some magnetic ferroelectrics (4, 5). The critical tuning of the ME phase competition may

produce the giant ME phenomena, such as the electric-field induction of the ferromagnetic phase, that is, a quantum “electromagnet.”

An even more remarkable characteristic expected for the multiferroics is the electric (magnetic) reversal of the M (P) vector. As shown in the fourth panel of the figure, the multiferroics of purely spin origin may exhibit the clamping of the ferromagnetic and ferroelectric domain walls, and this fixes the relative direction of M and spin helicity (or equivalently P) across the domain wall. This may provide a low energy-consuming way of achieving electrical M -reversal in future spintronics. All these fundamental investigations on the multiferroics have just started in the

research community, including the effort to explore the tailor-made multiferroics made with magnetic-dielectric superlattices as well as nanoscale self-organized materials. The fast pace of this research effort promises an exciting time ahead for multiferroic materials.

References

1. P. Curie, *J. Phys.* **3**, 393 (1894).
2. M. Fiebig, *J. Phys. D Appl. Phys.* **38**, R123 (2005).
3. J. H. Jung *et al.*, *Phys. Rev. Lett.* **93**, 037403 (2004).
4. T. Kimura *et al.*, *Nature* **426**, 55 (2003).
5. N. Hur *et al.*, *Nature* **429**, 392 (2004).
6. G. Lawes *et al.*, *Phys. Rev. Lett.* **95**, 087205 (2005).
7. H. Katsura, N. Nagaosa, A. V. Balatsky, *Phys. Rev. Lett.* **95**, 057205 (2005).

10.1126/science.1125227

PLANT SCIENCE

Microtubules Make Tracks for Cellulose

Clive Lloyd

In a remarkable series of biological transformations, green plants convert carbon dioxide into cellulose fibers stronger than steel. These thin threads of polymeric glucose are wrapped around growing cells, lending structural support to the plant as it extends further into the environment. The fibers are not simply secreted into the plant cell wall in a haphazard fashion

but are deposited in ordered layers that still allow the cell to expand. For more than 40 years, it has been known that the alignment of these cellulose fibers (microfibrils) in the cell wall often coincides with cytoskeletal microtubules tethered to the cytoplasmic side of the plasma membrane (see the figure). Despite this coincidence, there has never been direct proof that microtubules provide a guidance mechanism for the alignment of cellulose microfibrils. Now, on page 1491 of this issue, Paredes *et al.* (1) provide that proof.

Plants explore the environment, not by cell movements, but by massive cell expansion that is driven by influx of water into a central vacuole. The resulting cellular swelling exerts a force that is nondirectional. As explained by Green in 1962 (2), such a force can be channeled along an axis by “hoop-reinforcement” caused by the winding of cellulose microfibrils

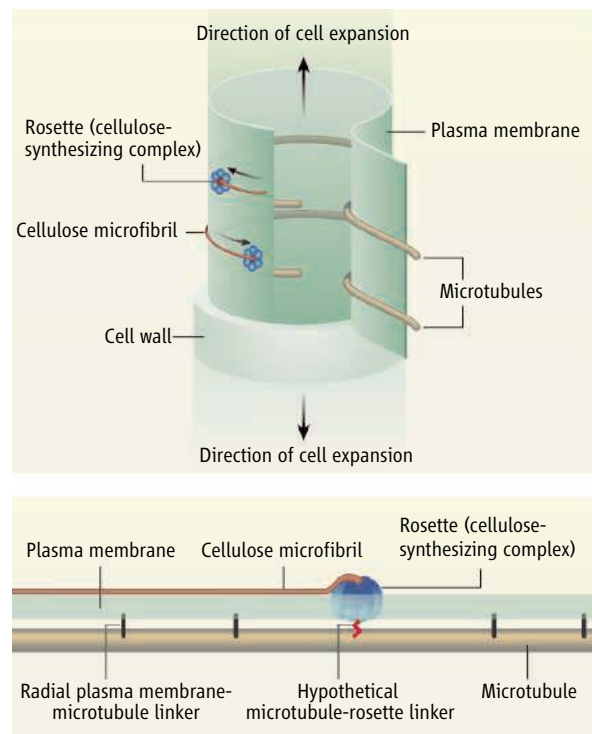
around the cell, perpendicular to the direction of expansion. In the early 1960s, before the discovery of microtubules, the anti-mitotic drug colchicine was known to dissolve the “spindle fiber protein” comprising the mitotic spindle. Because Green found that the hoop-like order of fibers in the plant cell wall was also destroyed by colchicine, he predicted that a form of “spindle fiber protein” in the cyto-

plasm would provide a template for the orderly placement of cellulose in the cell wall. Soon after, Ledbetter and Porter (3) published their landmark paper on the electron microscopy of plant cells, revealing the presence of cytoplasmic cortical microtubules. These colchicine-sensitive structures appeared as long filaments that circumnavigated the cell, just beneath the plasma membrane, in hundreds of transverse

hoops that mirrored the organization of cellulose microfibrils in the cell wall. This parallelism between the two systems marked the beginning of the so-called microtubule-microfibril syndrome, but instead of heralding a period of consensus, the field has been largely divided in its interpretation ever since.

Missing from this relationship between microtubules and microfibrils was the cellulose-synthesizing machinery itself, but another technical advance

Microtubule railroad. Microtubules that lie beneath the plant cell's plasma membrane serve as tracks for membrane-associated cellulose synthases (rosette structures) to travel along. As it moves, the synthase deposits a cellulose microfibril into the adjacent cell wall. It is not yet known if there is a direct link between cellulose synthase and microtubule.



The author is in the Department of Cell and Developmental Biology, John Innes Centre, Norwich NR4 7UH, UK. E-mail: clive.lloyd@bbsrc.ac.uk

located the putative enzyme complexes in the plasma membrane. By fracturing frozen cells, the two-layered lipid membrane could be split apart, revealing large, embedded protein particles. In terrestrial plants, these putative cellulose-synthesizing particles occurred in groups of six, forming hexagonal rosettes (4). Heath (5) proposed unifying models of how microtubules at the inner face of the plasma membrane could influence cellulose microfibrils on the outer face. In the indirect version of the model, a cellulose-synthesizing rosette moves within the plasma membrane as it extrudes in its wake a rigid microfibril that incorporates into the cell wall. Here, the cellulose synthesizing rosette is self-propelled and moves along the plasma membrane, but within the channels formed between pairs of microtubules that lie just inside the inner face of the plasma membrane. In contrast to this model, in which microtubules are seen as passive “bumper rails,” a “monorail” model suggests that the motive force is provided by direct attachment of a rosette to a microtubule or to a cytoskeletal actin filament lying alongside the microtubule.

Although numerous (but not all) studies confirmed microtubule-microfibril parallelism, a steady drip of findings questioned the role of microtubules in cellulose deposition. An early objection was that a criss-cross pattern formed by layer upon layer of cellulose in some plant cell walls resembled the layering patterns of exoskeleton components in insects. Because these cuticles were thought to form by

spontaneous crystallization, it was argued that plant cell walls formed analogously, independently of microtubules (6). We now know, however, that plant microtubules are much more dynamic than the static transverse “hoops” that were originally envisaged, and can switch their orientation (7) to mirror all patterns of cellulose deposition. More cogent concerns about the role of microtubules came from a new generation of studies showing that alignment of microtubules and cellulose can be uncoupled. For example, in one mutant strain of the flowering plant *Arabidopsis thaliana*, cellulose microfibrils retain their parallel order despite disruption of the cortical microtubules (8).

Most investigators have studied either microtubules or cell walls. Few have tried to amalgamate the two views, and no-one has been able to track cellulose biosynthesis in living cells. Paredez *et al.* have made a breakthrough by tandemly expressing fluorescent versions of one cellulose synthase component (CESA6) and the microtubule protein, tubulin (TUA1), in *Arabidopsis* plants. The synthase was seen to move along the plasma membrane in lines that largely coincided with fluorescent cortical microtubules. The colinearity was preserved even when the microtubules reoriented, showing a primary role for microtubules in alignment. The fact that synthases continued to move for a while after their co-aligned microtubules had depolymerized showed that synthase movement is powered by cellulose polymerization and not by micro-

tubules. However, such unguided enzyme complexes soon dissipated, prompting Paredez *et al.* to hypothesize that synthases may be stabilized by some lateral interaction with microtubules. Interactions on either side of a microtubule, for example, could account for the bidirectional movement of synthases along microtubules.

Beyond the microtubule-microfibril parallelism is the question of how microtubules come to be oriented perpendicular to the axis of growth and how they then reorient while building the cross-ply patterns of some multi-layered cell walls. It will be some time before we understand how hormones, the biophysical forces of growth, and environmental factors all impinge upon the machinery controlling cell shape, but it is likely that the present study will be seen to represent one of the first significant steps in this quest.

References

1. A. R. Paredez, C. R. Somerville, D. W. Ehrhardt, *Science* **312**, 1491 (2006) published online 20 April 2006 (10.1126/science.1126551).
2. P. B. Green, *Science* **138**, 1404 (1962).
3. M. C. Ledbetter, K. R. Porter, *J. Cell Biol.* **19**, 239 (1963).
4. S. C. Mueller, R. M. Brown, *J. Cell Biol.* **84**, 315 (1980).
5. I. B. Heath, *J. Theor. Biol.* **48**, 445 (1974).
6. A. C. Neville, D. C. Gubb, R. M. Crawford, *Protoplasma* **90**, 307 (1976).
7. M. Yuan, P. J. Shaw, R. M. Warn, C. W. Lloyd, *Proc. Natl. Acad. Sci. U.S.A.* **91**, 6050 (1994).
8. K. Sugimoto, R. Himmelsbach, R. E. Williamson, G. O. Wastneys, *Plant Cell* **15**, 1414 (2003).

10.1126/science.1128903

APPLIED PHYSICS

Can a Fraction of a Quantum Be Better Than a Whole One?

Colin M. Pegrum

Small-scale superconducting devices have unique analog and digital applications, and understanding how they work provides insight into some basic quantum-mechanical principles. In a superconductor, current is carried by electron pairs that are all described by a single wave function with a coherent phase. This process has remarkable consequences for closed, ringlike structures. Because the phase must be well defined at all points, if a path is followed around the loop and back to its starting point, the phase can only change by an integer multiple of 2π . Phase and magnetic flux are closely related, thus the flux

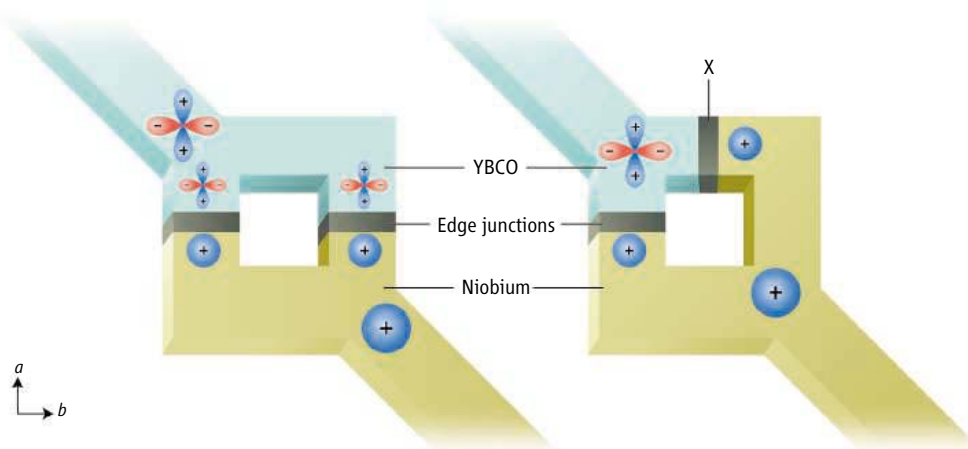
Φ threading a loop is quantized in integer units n of the flux quantum Φ_0 , so that $\Phi = n\Phi_0$, a relation that was verified experimentally in 1963 (1, 2). On page 1495 of this issue, Ortlepp *et al.* report a method to use the unusual properties of flux quanta to perform digital logic operations (3).

Useful and active thin-film superconducting devices, such as the one described by Ortlepp *et al.*, contain tunnel junctions. These have a very thin nonsuperconducting barrier through which electron pairs can tunnel quantum mechanically. Below a certain critical value, current can flow without electrical resistance, but a current-dependent phase difference is created across the junction. This effect was predicted by Josephson in 1962 (4) and verified soon after (5). If just two junctions

are added to a loop to form a superconducting quantum interference device (SQUID), and if a suitable steady bias current is applied, the interplay of circulating current, phase, and flux results in a device with unprecedented sensitivity for analog measurements of magnetic flux or field (6).

But the ring-plus-junction structure is also the building block for advanced digital devices combining ultra-low heat dissipation and astonishing speed, far outstripping their semiconducting counterparts (7). Digital technology based entirely on niobium, a low-temperature superconductor, is well developed [see, for example (8)]. Ortlepp *et al.* have taken a major step forward by combining niobium with yttrium barium copper oxide (YBCO), a high-temperature superconductor. But their work

The author is in the Department of Physics, University of Strathclyde, Glasgow G4 0NG, UK. E-mail: colin@phys.strath.ac.uk



The π -SQUID principle. SQUID loops with zero phase shift (left) and with a π phase shift (right). The red (–) and blue (+) lobes represent the wave function phases in YBCO, and the blue sphere represents the symmetrical s -wave for niobium. Josephson junctions are formed on the edge of the YBCO film. The π phase difference in the right-hand loop is created across the Josephson junction at X, where the coupled wave functions in the YBCO and niobium have phases with opposite signs.

involves fractional, not integer flux quanta. How can fractional flux quantization arise?

Again, it has to do with the quantum wave function and its phase. In niobium, electron pairs have opposite spins and zero angular momentum; therefore, niobium is an s -wave superconductor, with properties that are isotropic (that is, independent of direction). But in most high-temperature superconducting materials, pairing is between equal spins, and the resulting nonzero angular momentum state is d -wave, with a symmetry known as $d_{x^2-y^2}$. In addition, YBCO is a layered anisotropic material. Thin films are grown epitaxially, usually with their a and b axes parallel to the surface, by using a single-crystal substrate such as SrTiO_3 , which has a unit cell of size similar to that of YBCO, thus promoting epitaxy.

It is now well established that the phases in the orthogonal a and b directions have opposite signs; that is, they differ by a factor of π . An initial verification used a tricrystal substrate (9), which was fused together from three pieces of SrTiO_3 with suitably different crystallographic orientations. A thin-film ring of YBCO straddling all the substrate subsections will have segments with differing phases. This introduces a permanent π phase change around the loop, even in the absence of applied field or current. A phase change of 2π is equivalent to $1\Phi_0$, so the π phase change creates a spontaneous and permanent flux of $\Phi_0/2$ in the loop (10). This has been verified by SQUID microscopy, which is a scanning technique that uses a SQUID coupled to a micrometer-size sensing loop (11) and is a direct proof of the $d_{x^2-y^2}$ state of YBCO.

But specialized tricrystal substrates are not well suited to practical device development. Ortlepp *et al.* use a single layer of YBCO with just one crystallographic orientation on a plain,

single-crystal SrTiO_3 substrate. Junctions are formed on the edge of the YBCO film, and closed loops are completed by tracks of niobium. Most junctions are grown on edges parallel to the a axis, and loops containing these behave conventionally (see the left panel of the figure). But some loops contain junctions on edges parallel to both the a and b axes. The wave functions emerging from these orthogonal edges have opposite phases and this creates a so-called π -SQUID (see the right panel of the figure), which is a loop with a built-in fractional phase bias that approaches π for large-inductance loops. This works because the phase in niobium is independent of orientation, because it has s -wave symmetry. A similar concept was used for a demonstration of d -wave symmetry in high-temperature superconducting materials (12). To exploit this technique, Ortlepp *et al.* first had to perfect a process for growing high-quality YBCO-niobium ramp-edge junctions, which is a major achievement in itself (13).

Their complete device is a little more complex than a simple two-junction π -SQUID, with extra junctions and drive and readout circuitry. It functions as a bistable flip-flop, which is a crucial universal circuit element that can divide digital pulse trains by two and can also act as a binary storage element. The core of the π -SQUID version is self-biasing, thanks to the spontaneously generated flux (sustained by a persistent circulating current). Therefore it needs no external connections, which simplifies design and operation, makes it more tolerant to random parameter spreads, and most importantly, reduces its size, making it much smaller than its all-niobium counterpart. This fits in well with current trends in digital development: smaller, faster, and cooler. It is, of course, also a very elegant demonstration of

fundamental quantum-mechanical principles.

So where is superconducting digital technology heading? A clear niche is emerging for superconducting digital devices in ultrafast digital-to-analog conversion or in direct digital processing, where semiconductor technology can run out of speed, or dissipation becomes excessive. An example of this application is receiver systems for radar or cellular phone networks (14). And dependable, compact, low-cost cooling is now no longer a serious issue.

There are other ways to engineer and use phase shifts. Devices fabricated entirely from high-temperature superconductors can be made by creating neighboring regions in a film where the a and b axes are rotated, without recourse, to multicrystal substrates (15). Or, junctions themselves can be given a permanent internal phase shift by adding a ferromagnetic layer (16). Another approach uses a normal metal junction barrier (17); a current in a channel connected to the barrier can switch the phase from 0 to π . More speculatively, a role is emerging for high-temperature superconducting π junctions in “quiet” phase qubits, which are one possible building block for quantum computers (18), where the permanent phase offers a way to minimize dephasing interactions with the environment.

References

1. B. S. Deaver Jr., W. M. Fairbank, *Phys. Rev. Lett.* **7**, 43 (1961).
2. R. Doll, M. Näbauer, *Phys. Rev. Lett.* **7**, 51 (1961).
3. T. Ortlepp *et al.*, *Science* **312**, 1495 (2006); published online 20 April 2006 (10.1126/science.1126041).
4. B. D. Josephson, *Phys. Lett.* **1**, 251 (1962).
5. P. W. Anderson, J. M. Rowell, *Phys. Rev. Lett.* **10**, 230 (1963).
6. R. Kleiner, D. Koelle, F. Ludwig, J. Clarke, *Proc. IEEE* **92**, 1534 (2004).
7. D. K. Brock, E. K. Track, J. M. Rowell, *IEEE Spectrum* **37**, 40 (December 2000).
8. O. A. Mukhanov, D. Gupta, A. M. Kadin, V. K. Semenov, *Proc. IEEE* **92**, 1564 (2004).
9. C. C. Tsuei *et al.*, *Phys. Rev. Lett.* **73**, 593 (1994).
10. C. C. Tsuei, J. R. Kirtley, *Rev. Mod. Phys.* **72**, 969 (2000).
11. J. R. Kirtley, *Physica C* **368**, 55 (2002).
12. D. J. Van Harlingen, J. E. Hilliard, B. L. T. Plourde, B. D. Yanoff, *Physica C* **318**, 410 (1999).
13. H.-J. H. Smilde, H. Hilgenkamp, G. Rijnders, H. Rogalla, D. H. A. Blank, *App. Phys. Lett.* **80**, 4579 (2002).
14. J. Rosa, *RF Design* (March 2005), pp. 40–46; available at www.rfdesign.com.
15. F. Tafuri, J. R. Kirtley, F. Lombardi, T. Bauch, A. Barone, *Physica C* **404**, 367 (2004).
16. V. M. Krasnov *et al.*, *Physica C* **418**, 16 (2005).
17. J. J. A. Baselmans, B. J. van Wees, T. M. Klapwijk, *Phys. Rev. B* **65**, 224513 (2002).
18. G. Blatter, V. B. Geshkenbein, L. B. Ioffe, *Phys. Rev. B* **63**, 174511 (2001).

The Pliocene Paradox (Mechanisms for a Permanent El Niño)

A. V. Fedorov,^{1*} P. S. Dekens,^{2†} M. McCarthy,² A. C. Ravelo,² P. B. deMenocal,³ M. Barreiro,⁴ R. C. Pacanowski,⁵ S. G. Philander⁴

During the early Pliocene, 5 to 3 million years ago, globally averaged temperatures were substantially higher than they are today, even though the external factors that determine climate were essentially the same. In the tropics, El Niño was continual (or “permanent”) rather than intermittent. The appearance of northern continental glaciers, and of cold surface waters in oceanic upwelling zones in low latitudes (both coastal and equatorial), signaled the termination of those warm climate conditions and the end of permanent El Niño. This led to the amplification of obliquity (but not precession) cycles in equatorial sea surface temperatures and in global ice volume, with the former leading the latter by several thousand years. A possible explanation is that the gradual shoaling of the oceanic thermocline reached a threshold around 3 million years ago, when the winds started bringing cold waters to the surface in low latitudes. This introduced feedbacks involving ocean-atmosphere interactions that, along with ice-albedo feedbacks, amplified obliquity cycles. A future melting of glaciers, changes in the hydrological cycle, and a deepening of the thermocline could restore the warm conditions of the early Pliocene.

The early Pliocene was similar to and also very different from the world of today. The intensity of sunlight incident on Earth, the global geography, and the atmospheric concentration of carbon dioxide (I) were close to what they are today, but surface temperatures in polar regions were so much higher that continental glaciers were absent from the Northern Hemisphere, and sea level was ~25 m higher than today (2–5). This apparent paradox—that conditions today and those during the early Pliocene are two different climate states in response to practically the same external forcing—can be addressed with information from such sources as the Pliocene Research Interpretations and Synoptic Mapping Project (PRISM) (2). Although there are some inconsistencies in the information concerning tropical ocean temperatures (6), most of the discrepancies can be eliminated by considering Pliocene observations in the broader context of earlier and subsequent climate changes, rather than in isolation.

Over the past 65 million years, since the beginning of the Cenozoic when temperatures in polar regions were in the neighborhood of 10°C, Earth experienced erratic global cooling (Fig. 1A). This was a consequence primarily of the drifting of the continents, accompanied by changes in ocean-basin geometry, mountain

building, volcanic eruptions, and other phenomena that affect the two factors that determine globally averaged surface temperatures: the

albedo of the planet and the atmospheric concentration of greenhouse gases. Superimposed on the global cooling were periodic climate cycles in response to Milankovitch forcing. This term refers to modest, periodic variations in the distribution of sunlight because of periodic variations in orbital parameters such as the angle of tilt (obliquity) of Earth’s axis.

The response to Milankovitch forcing involves not only glaciers that wax and wane, but also tropical sea surface temperatures (SSTs) that rise and fall (7–10). These phenomena could be separate to some degree, each involving its own physical processes and feedbacks, in the same way that the response to seasonal variations in sunlight involves several different phenomena such as the Indian monsoons, coastal upwelling off southwest Africa, and severe winter storms in central Canada. In other words, an explanation for the monsoons does not explain the other features of the seasonal cycle. It is similarly unlikely that processes involving ice sheets alone can explain all aspects of the response to Milankovitch forcing. The important additional processes are likely to include biogeochemical cycles such as the carbon cycle, as well as tropical ocean-atmosphere interactions.

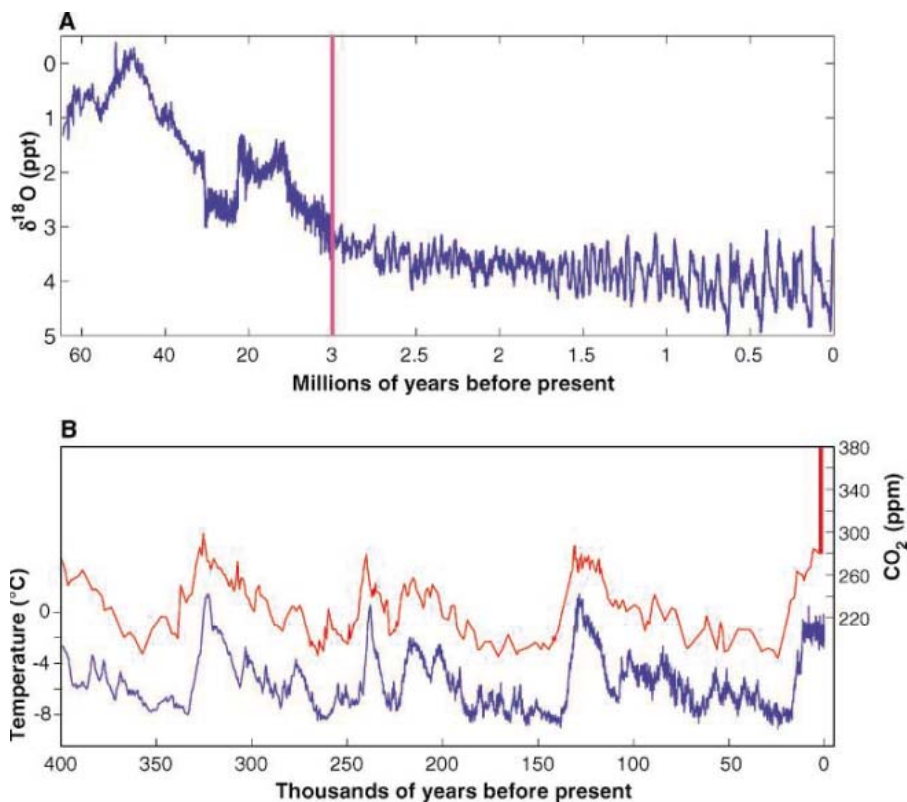


Fig. 1. (A) Variations in $\delta^{18}\text{O}$ over the past 60 million years. Higher values of $\delta^{18}\text{O}$ indicate colder climate (greater global ice volume). The gradual cooling over the past ~50 million years is evident. Note that the time scale changes at 3 Ma. The Milankovitch cycles are modest in amplitude up to ~3 Ma but then start amplifying (23). (B) Fluctuations in temperature and in the atmospheric concentration of carbon dioxide over the past 400,000 years as inferred from Antarctic ice-core records (45). The vertical red bar is the increase in atmospheric carbon dioxide levels over the past two centuries and before 2006.

¹Department of Geology and Geophysics, Yale University, New Haven, CT 06520, USA. ²Ocean Sciences Department, University of California, Santa Cruz, CA 95064, USA. ³Lamont-Doherty Earth Observatory of Columbia University, Palisades, NY 10964, USA. ⁴Department of Geosciences, Princeton University, Princeton, NJ 08544, USA. ⁵Geophysical Fluid Dynamics Laboratory, National Oceanic and Atmospheric Administration, Princeton, NJ 08540, USA.

*To whom correspondence should be addressed. E-mail: alexey.fedorov@yale.edu

†These authors contributed equally to this work.

Although Milankovitch forcing has been relatively constant over the past several million years, the amplitude of the climatic response underwent remarkable changes as the long-term global cooling introduced different climate feedbacks. The Pliocene is of special interest because the feedbacks that came into play during that epoch, around 3 million years ago (Ma), started an amplification of the response of climate to orbital forcing. Over the past ~1 million years, this process culminated in drastic oscillations between prolonged glaciations, or ice ages, and brief, warm interglacials (Fig. 1). During the warm interglacial periods—including the current one, which began some 10,000 years ago—conditions approach those of the early Pliocene. Will the present warm conditions terminate soon, to be followed by the next ice age? Or will the onset of the next ice age be inhibited by the current rise in the atmospheric concentration of greenhouse gases induced by humans (Fig. 1B)? Will that rise restore the warm conditions of the early Pliocene? Answers to these questions require identification of the processes that maintained warm conditions in the early Pliocene and then terminated them. Many studies focus on high-latitude processes associated with the appearance of northern continental ice sheets at ~3 Ma. More recently, attention has turned to the tropics after the discovery that El Niño was a continual (rather than intermittent) phenomenon up to ~3 Ma (6, 11, 12).

A Polar Perspective

The global cooling that started around 50 Ma led to the appearance of large ice sheets, first on Antarctica around 35 Ma and subsequently on northern continents at ~3 Ma (13). In sediments from a site in the North Pacific Ocean, ice-rafted debris appears abruptly at ~2.7 Ma, indicating that the warm conditions of the early Pliocene had come to an end (14). Did this happen because of the increase in Earth's albedo when Northern Hemisphere ice sheets appeared?

This hypothesis has been tested with the use of general circulation models (GCMs) of the atmosphere. The results indicate that removal of the northern ice sheets increases temperatures only in the regions initially covered with ice (4). If, in addition, SSTs are specified to be high in high latitudes but unchanged in

low latitudes, then the atmosphere is warmer over much larger regions, with some effects extending into the tropics (15).

These results suggest that high SSTs in high latitudes, more than low albedo, helped maintain the warm conditions of the early Pliocene, but what processes maintained those high SSTs? One possibility is a larger poleward transport of heat by oceanic currents during the early Pliocene. Presumably the closure of the Panamanian Seaway in the early Pliocene reorganized the oceanic circulation and ultimately altered the poleward transport of heat. However, an open Panamanian Seaway could not explain the early Pliocene high-latitude warmth because the closure at the end of the warm period would have intensified the deep, thermohaline circulation in the Atlantic sector (16, 17), thus transporting more, not less, heat northward. It is conceivable that what mattered most was the northward transport not of heat, but of moisture

that promoted the growth of the glaciers and hence a cooling trend (18). One problem with this argument is that the timing of the closure between 4.5 and 4.0 Ma (19) was much earlier than the onset of cold high-latitude conditions. Furthermore, this still leaves the warm conditions of the early Pliocene unexplained.

Another puzzle concerns the amplification of the Milankovitch cycles that started around 3 Ma. At high latitudes, the appearance of northern glaciers at that time introduced ice-albedo feedbacks that could have caused the amplification. Those feedbacks depend on variations in the intensity of solar radiation at high latitudes in summer (13). The precession of the equinox and changes in Earth's obliquity make comparable contributions to high-latitude summer solar radiation. Why then, in the global ice volume records (Fig. 1), is the obliquity signal dominant over the precession signal (13)?

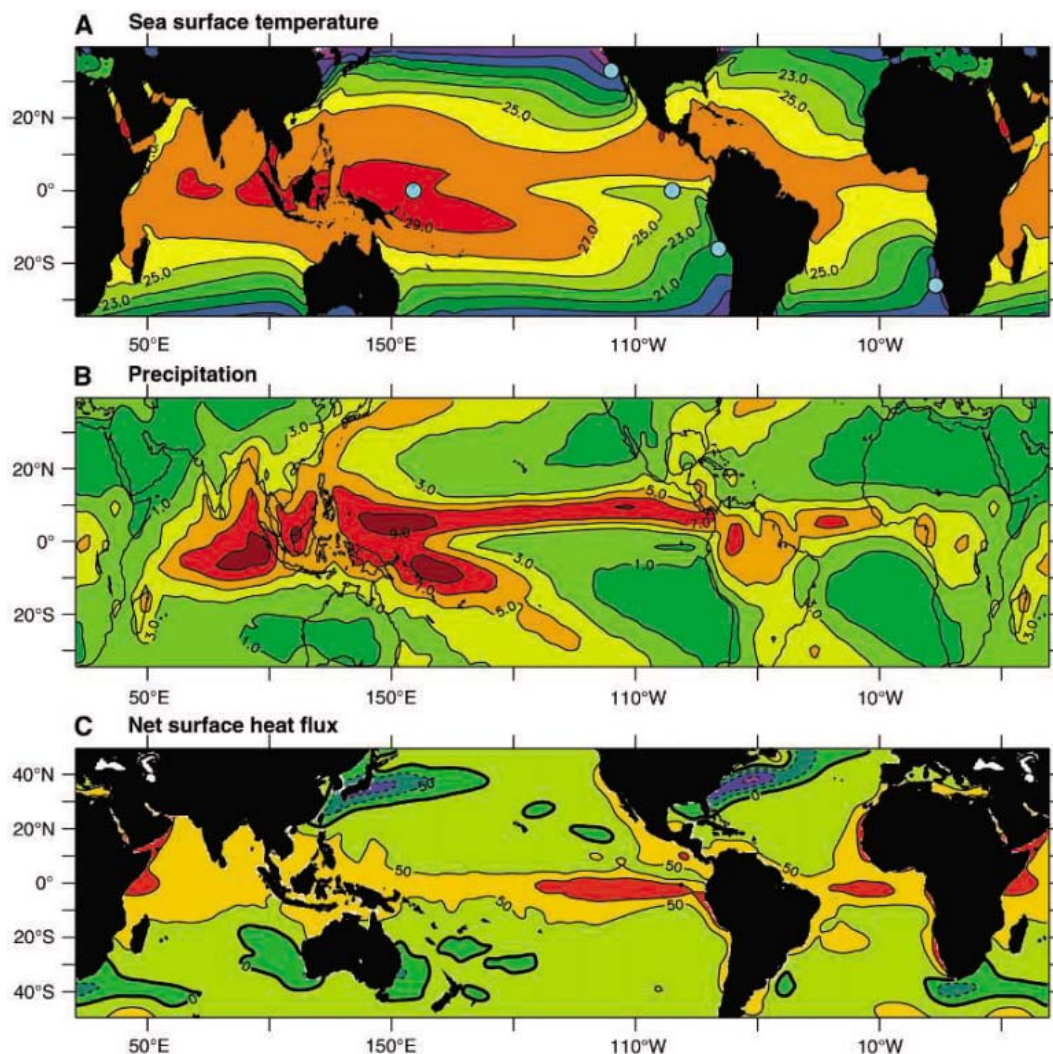


Fig. 2. (A) Annual mean SST pattern ($^{\circ}\text{C}$). The dots show approximate locations of the deep cores used to calculate the time series of SSTs displayed in Fig. 3. (B) Annual mean rainfall pattern (mm/day). Note the maximum in precipitation in the tropics associated with the ITCZ. (C) Annual mean heat flux (W/m^2) into the ocean at low latitudes and out of the ocean at higher latitudes (46). The contour interval is $50 \text{ W}/\text{m}^2$. Note a slightly different latitudinal extent of (C) as compared to (A) and (B).

Variation in the equator-to-pole gradient of solar heating is dominantly controlled by obliquity. This gradient becomes a key parameter if the focus is not on the poleward transport of heat, which involves a negative feedback, but instead on the transport of moisture from low latitudes, which can amplify the waxing and waning of ice sheets (20). This argument brings conditions in the tropics into play but cannot explain recent findings that Milankovitch cycles of both ice volume and equatorial Pacific SSTs became amplified around 3 Ma. Obliquity stands out as the dominant signal, with the SST changes leading those in ice volume by several thousand years (7, 21). Even if ice-albedo feedbacks came into play before changes in ice volume, how could they have caused variations in the tropics? What are the tropical processes that could have contributed to climate variations associated with ice ages?

Tropical Perspective

Previous studies based on sparse data suggested that tropical and subtropical SSTs during the early Pliocene were essentially the same as those of today (2). Recent data from regions not covered by PRISM indicate otherwise. Apparently the salient features of SST patterns in low latitudes—the cold surface waters off the western coasts of Africa and the Americas (Fig. 2)—were absent until ~3 Ma. This is evident in Fig. 3, which shows that up to ~3 Ma, the SST difference between the eastern and western equatorial Pacific was very small, and cold surface waters were absent from the coastal upwelling zones off the western coasts of Africa and the Americas (11, 12, 22–24). Today, a large reduction in the east-west temperature gradient along the equator in the Pacific occurs only briefly during El Niño, which in effect was continual rather than intermittent up to 3 Ma. Corroborating evidence for a continual (or “permanent”) El Niño is available in land records (25) that document the distinctive regional climate signatures associated with El Niño. Up to 3 Ma there was a persistence of mild winters in central Canada and the northeastern United States, droughts in Indonesia, and torrential rains along the coasts of California and Peru and in eastern equatorial Africa. The onset of dry conditions in the latter region around 3 Ma may have been important in the evolution of African hominids (26, 27).

Persistent El Niño conditions would have had a huge impact on the global climate, given

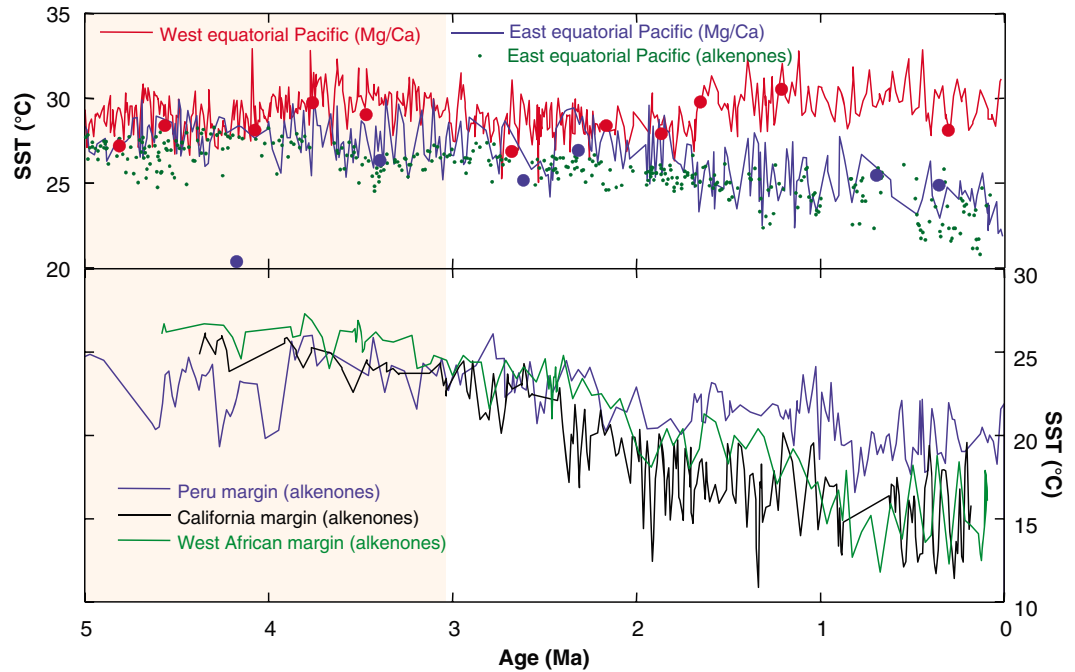


Fig. 3. (Top) SST records in the western equatorial Pacific (red line, ODP site 806) and in the eastern equatorial Pacific (blue line, site 847), both based on Mg/Ca and adapted from (11), and that for the eastern Pacific based on alkenones (green dots, site 847) and adapted from (24). Larger circles are for the data based on Mg/Ca but from (44) for ODP sites 806 (red) and 847 (blue). Pink shading denotes the early Pliocene. For discussion, see (6). (Bottom) Alkenone-based SST records for the California margin (black, ODP site 1014) (24), the Peru margin (blue, site 1237) (24), and the West African margin (green, site 1084) (22). The locations of the ODP sites are shown in Fig. 2; for the exact geographical locations, see (47).

that today even brief El Niño episodes can have a large influence. The reasons are evident in Fig. 2, which shows a remarkably high correlation between tropical SSTs and rainfall patterns. Tall, rain-bearing, convective clouds cover the warmest waters, but highly reflective stratus decks that produce little rain cover the cold waters. During El Niño, the warming of the eastern equatorial Pacific reduces the area covered by stratus clouds, thus decreasing the albedo of the planet, while the atmospheric concentration of water vapor—a powerful greenhouse gas—increases. Calculations with a GCM of the atmosphere indicate that this happened during the early Pliocene and contributed significantly to the warm conditions at that time (28).

The appearance of cold surface waters around 3 Ma in regions remote from each other (Figs. 2 and 3A) can be explained in terms of a global shoaling of the oceanic thermocline. [A contributing factor could have been the northward drift of Australia that restricted flow from the equatorial western Pacific into the Indian Ocean (29).] A shallower thermocline must involve changes in the oceanic heat budget shown in Fig. 2 (30, 31). In a state of equilibrium, the loss of heat in high latitudes—mainly where cold continental air masses flow over the warm Gulf Stream and Kuroshio Current in winter—balances the gain, mostly in low-latitude upwelling regions where cold water rises to the surface.

An increase in the loss of heat in high latitudes must be accompanied by an increase in the gain of heat, which requires a shallower equatorial thermocline (30). A decrease in the heat loss, and associated reduction in the poleward heat transport by the ocean, would imply a deeper equatorial thermocline.

The oceanic heat transport is affected by the meridional overturning of the oceanic circulation. A freshening of the surface waters in the extratropics, which reduces the surface meridional density gradient between low and high latitudes, can reduce the heat transport. This is true for the deep, slow thermohaline component of the circulation whose changes affect mainly the climate of the northern Atlantic (32), as well as for the rapid, shallow wind-driven component whose changes affect mostly the tropics. Sufficiently large freshening in the extratropics can induce a perennial El Niño (33).

Idealized calculations with an ocean GCM (Fig. 4) show that such a freshening can reduce the zonal SST gradient along the equator, reduce the poleward heat transport, and deepen the equatorial thermocline (33). As the freshwater flux increases from one experiment to the next, the different parameters are seen to change slowly at first and then to change rapidly as the flux approaches a critical value. When the freshwater forcing exceeds a threshold, the zonal SST gradient vanishes and permanently warm conditions prevail in the

tropics. Thus, these calculations represent one potential mechanism for maintaining a permanent El Niño.

Our arguments suggest that, during (and probably before) the early Pliocene, when El Niño was continual, oceanic heat gain at low latitudes and heat loss at high latitudes were minimal, and the thermocline was deep. The theory that the gradual global cooling during much of the Cenozoic (Fig. 1) and the associated decrease in the temperature of the deep ocean (34) caused the thermocline to shoal has corroborating evidence (11). A threshold was reached around 3 Ma when the thermocline became so shallow that the winds could bring cold waters to the surface in the various upwelling zones (31). With the transition to this colder climate, the mean SSTs in the eastern equatorial Pacific should have become asymmetric with respect to the equator, possibly resembling the present-day structure in which warmer water and the Intertropical Convergence Zone (ITCZ) stay north of the equator while colder water stays south of it (Fig. 2B).

The appearance of cold surface waters in the equatorial upwelling zones introduced feedbacks that affected the response of tropical SSTs to Milankovitch forcing. The winds influence SSTs and also depend on those temperatures because they blow from the cold toward the warm regions along the equator where the Coriolis force vanishes. This circular argument implies a positive feedback between the ocean and the atmosphere first described by Jacob Bjerknes (35). (Another positive feedback involves low stratus clouds.) In the case of El Niño, the SST-wind feedback depends on an adiabatic redistribution of warm surface waters (Fig. 5A). On much longer time scales it involves diabatic, vertical movements of the thermocline (Fig. 5B) and influences the climatic response to obliquity variations (31). During times when obliquity and solar heating in high latitudes have maxima, reduced oceanic heat loss to the atmosphere can induce a deepening of the equatorial thermocline and a tendency toward El Niño conditions. This is possible only on time scales sufficiently long for the tropical oceans to adjust to changes in higher latitudes.

Obliquity causes annually averaged sunlight to vary for such prolonged periods (thousands of years) that the tropical response is practically

in phase with the extratropical forcing (7). The precession of the equinox, by contrast, has too short a time scale for an adjustment in the oceanic heat budget to be possible. It induces seasonal changes in sunlight but has no effect on the annually averaged sunlight. These arguments explain why tropical Pacific temperature records are dominated by obliquity variations and are nearly in phase with high-latitude rather than local solar variations (21, 31), and why

Pacific; it contributed to global warming by causing the absence of stratus clouds from the eastern equatorial Pacific, thus lowering the planetary albedo, and by increasing the atmospheric concentration of water vapor, a powerful greenhouse gas. Today the atmospheric concentration of another greenhouse gas, carbon dioxide, is comparable to what it was in the early Pliocene, but the climate of the planet is not yet in equilibrium with those high values. It

is possible that a persistence of high carbon dioxide concentrations could result in a return to a globally warm world if it were to increase temperatures and precipitation in high latitudes, and as a consequence cause the tropical thermocline to deepen by a modest amount, a few tens of meters. (Near the date line at the equator, the thermocline is already so deep that its vertical excursions leave surface temperatures unaffected.)

A deepening of the tropical thermocline requires a reduction in the oceanic heat loss in the extratropics (30). However, in certain atmospheric models, warm conditions in high latitudes depend on the atmosphere gaining heat from the oceans (36). This is also the case in the coupled ocean-atmosphere climate model that was recently used to simulate the early Pliocene (37). In that model, the oceanic heat loss in the extratropics is balanced by the gain of heat in the eastern equatorial Pacific. This gain is possible despite higher SSTs in low latitudes because temperature gradients along the equator, and presumably the depth of the equatorial thermocline, do not change significantly. This means that, in the model, maximum SSTs in the western tropical Pacific rise significantly above 30°C. This is inconsistent with observations indicating that at no time in the past 10 million years were SSTs much higher than 30°C. Are the models at fault, or is there a problem with the observations?

More data from the western tropical Pacific (and also from currently warm regions to the west of upwelling zones) are needed to determine the maximum temperatures over the last millions of years, and to determine whether observations of perennial El Niño are robust. If the information available at present should prove accurate, then temperatures in excess of 30°C in some models, and problems in their ability to simulate a perennial El Niño, could be indicative of flaws in the models—for example, in the parameterization of clouds. Models are

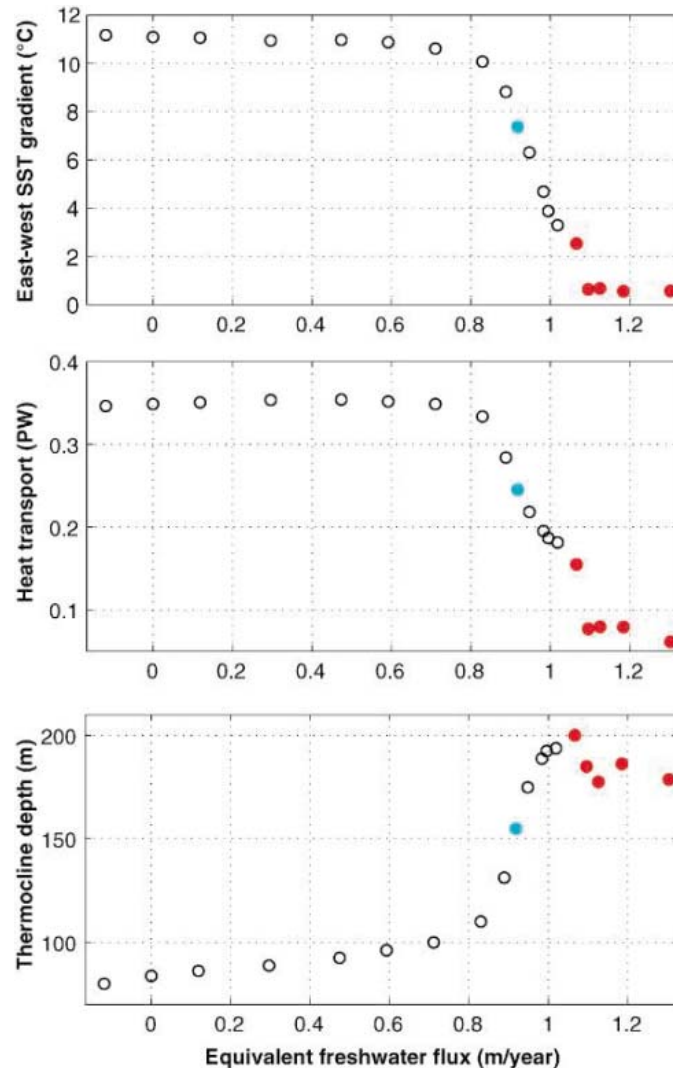


Fig. 4. Changes in the zonal SST gradient along the equator (top), the poleward heat transport across a fixed latitude (middle), and the equatorial thermocline depth (bottom) in an idealized ocean GCM as the flux of fresh water onto the surface near the northern boundary of the basin increases. Blue dots correspond to the conditions of today; red dots indicate the equatorial thermocline collapse (33).

they become amplified over the long term (7) when the thermocline shoals (11) and air-sea feedbacks are strengthened.

Discussion

A major factor in the warmth of the early Pliocene was the persistence of El Niño in the

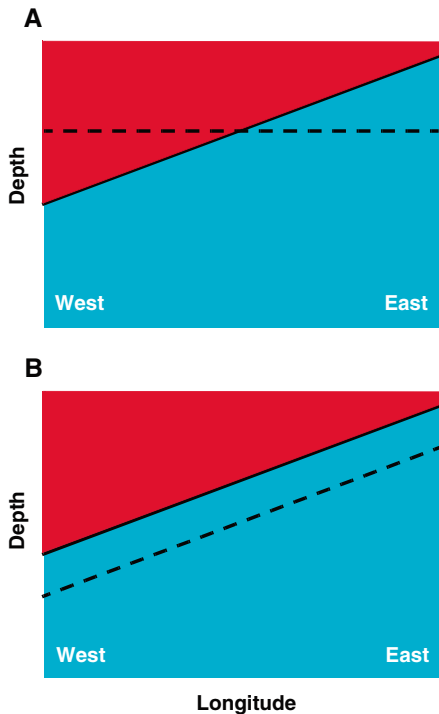


Fig. 5. A sketch of the change (from solid to dashed line) in the thermocline along the equator for (A) an adiabatic, horizontal redistribution of warm water that characterizes the interannual oscillations between El Niño and La Niña, and (B) a slow diabatic increase in the volume of warm water that can lead to a perennial El Niño. An increase in obliquity will correspond to a combination of (B) and (A) because tropical ocean-atmosphere interactions will modify the slope of the thermocline as well. At present, the mean thermocline depth in the equatorial Pacific is ~ 120 m.

designed to reproduce the world of today, but it is unclear how much confidence we should have in simulations of very different climates.

Efforts to predict future global warming could benefit enormously from a better understanding of past climates, especially of the Milankovitch cycles for which the forcing functions are known precisely. The obliquity cycles are of special interest because they started increasing in amplitude around 3 Ma and then changed character again around 1 Ma. Initially, it was thought that the latter change involved a shift of the dominant period from 40 K to 100 K (13). However, recent analyses indicate that the shift could have been from 40 K to multiples of 40 K,

specifically 80 K and 120 K (38). Apparently obliquity continued to play a dominant role, up to the present, in pacing glacial terminations and also in equatorial Pacific variables (21, 39). To determine the relative importance of feedbacks involving ice albedo, tropical ocean-atmosphere interactions, and biogeochemical cycles, it will be valuable to have a detailed description of the obliquity signal over the past several million years, inferred from a synthesis of the diverse measurements (productivity, SST, thermocline depth, ice volume, atmospheric gas concentration, etc.). Explaining the remarkable changes in the climate response to solar forcing that itself did not change significantly is a major challenge for both paleoclimatologists and climate modelers.

References and Notes

- Estimates of the concentration of carbon dioxide in the atmosphere during the early Pliocene range from 340 to 380 ppm (5, 40) to 280 to 300 ppm (41). Today the concentration has been in excess of 330 ppm for only a few decades, and has been elevated above 280 ppm for only 2000 to 3000 years (42).
- H. J. Dowsett, J. Barron, R. Poore, *Mar. Micropaleontol.* **27**, 13 (1996).
- H. J. Dowsett, M. A. Chandler, T. M. Cronin, G. S. Dwyer, *Paleoceanography* **20**, 10.1029/2005PA001133 (2005).
- T. Crowley, *Mar. Micropaleontol.* **27**, 3 (1996).
- M. E. Raymo, B. Grant, M. Horowitz, G. H. Rau, *Mar. Micropaleontol.* **27**, 313 (1996).
- Geochemical and faunal-based estimates of SST in the equatorial Pacific over the past 5 million years are in basic agreement with each other, as is evident in Fig. 3 (11, 12, 23, 24), and with the $\delta^{18}\text{O}$ record from planktonic foraminifers (12, 31, 43). The recent contradictory finding that the eastern tropical Pacific was relatively cool in the early Pliocene (44) is based on two questionable data points, one of which is shown in Fig. 3 (the large blue circle at ~ 4.1 Ma) and the other one lying outside the time range of this figure. For further discussion, see (43). Higher resolution time series of tropical SSTs that resolve Milankovitch cycles are now also available (7–10).
- K. Lawrence, Z. Liu, T. Herbert, *Science* **312**, 79 (2006).
- D. W. Lea, D. K. Pak, H. J. Spero, *Science* **289**, 1719 (2000).
- M. Medina-Elizalde, D. W. Lea, *Science* **310**, 1009 (2005); published online 13 October 2005 (10.1126/science.1115933).
- T. de-Garidel-Thoron, Y. Rosenthal, F. Bassinot, L. Beaufort, *Nature* **433**, 294 (2005).
- M. Wara, A. C. Ravelo, M. L. Delaney, *Science* **309**, 758 (2005); published online 23 June 2005 (10.1126/science.1112596).
- A. C. Ravelo, D. H. Andreason, M. Lyle, A. O. Lyle, M. Wara, *Nature* **429**, 263 (2004).
- J. Zachos, M. Pagani, L. Sloan, E. Thomas, K. Billups, *Science* **292**, 686 (2001).
- G. H. Haug, D. M. Sigman, R. Tiedemann, T. F. Pedersen, M. Sarnthein, *Nature* **401**, 779 (1999).
- L. C. Sloan, T. J. Crowley, D. Pollard, *Mar. Micropaleontol.* **27**, 51 (1996).
- G. H. Haug, R. Tiedemann, *Nature* **393**, 673 (1998).
- A. Klockner, M. Prange, M. Schulz, *Geophys. Res. Lett.* **32**, 10.1029/2004GL021564 (2005).
- N. W. Driscoll, G. H. Haug, *Science* **282**, 436 (1998).
- G. H. Haug, R. Tiedemann, R. Zahn, A. C. Ravelo, *Geology* **29**, 207 (2001).
- M. E. Raymo, K. Nisancioglu, *Paleoceanography* **18**, 10.1029/2002PA000791 (2003).
- Z. Liu, T. Herbert, *Nature* **427**, 720 (2004).
- J. R. Marlow, C. B. Lange, G. Wefer, A. Rosell-Melé, *Science* **290**, 2288 (2000).
- A. M. Haywood, P. Dekens, A. C. Ravelo, M. Williams, *Geochem. Geophys. Geosyst.* **6**, 10.1029/2004GC000799 (2005).
- P. S. Dekens, A. C. Ravelo, M. McCarthy, in preparation.
- P. Molnar, M. Cane, *Paleoceanography* **17**, 10.1029/2001PA000663 (2002).
- P. B. deMenocal, *Science* **270**, 53 (1995).
- S. J. Feakins, P. B. deMenocal, T. I. Eglinton, *Geology* **33**, 977 (2005).
- M. Barreiro, S. G. Philander, R. C. Pacanowski, A. V. Fedorov, *Clim. Dyn.*, 10.1007/s00382-005-0086-4 (2006).
- M. Cane, P. Molnar, *Nature* **411**, 157 (2001).
- G. Boccaletti, R. Pacanowski, S. G. Philander, A. V. Fedorov, *J. Phys. Oceanogr.* **34**, 888 (2004).
- S. G. Philander, A. V. Fedorov, *Paleoceanography* **18**, 1045 (2003).
- S. Manabe, R. J. Stouffer, *Nature* **378**, 165 (1995).
- A. V. Fedorov, R. C. Pacanowski, S. G. Philander, G. Boccaletti, *J. Phys. Oceanogr.* **34**, 1949 (2004).
- C. H. Lear, H. Elderfield, P. A. Wilson, *Science* **287**, 269 (2000).
- H. A. Dijkstra, J. D. Neelin, *J. Clim.* **12**, 1630 (1999).
- M. Winton, *J. Clim.* **16**, 2875 (2003).
- A. M. Haywood, P. J. Valdes, *Earth Planet. Sci. Lett.* **218**, 363 (2004).
- P. Huybers, C. Wunsch, *Nature* **434**, 491 (2005).
- L. Beaufort, T. de Garidel-Thoron, A. C. Mix, N. G. Pisias, *Science* **293**, 2440 (2001).
- J. Van Der Burgh, H. Visscher, D. L. Dilcher, V. M. Kürschner, *Science* **260**, 1788 (1993).
- M. Pagani, K. H. Freeman, M. A. Arthur, *Science* **285**, 876 (1999).
- A. Indermühle *et al.*, *Nature* **398**, 121 (1999).
- A. C. Ravelo, P. S. Dekens, M. McCarthy, *GSA Today* **3**, 10.1130/1052-5173 (2006).
- R. E. M. Rickaby, P. Halloran, *Science* **307**, 1948 (2005).
- J. R. Petit *et al.*, *Nature* **399**, 429 (1999).
- A. Da Silva, A. C. Young-Molling, S. Levitus, *Atlas of Surface Marine Data* (NOAA, Silver Spring, MD, 1994), vol. 6.
- Locations and depths of the Ocean Drilling Program (ODP) sites used for Fig. 3: ODP site 806 (0°N, 159°E, 2520 m); ODP site 847 (0°N, 95°W, 3373 m); ODP site 1014 (33°N, 120°W, 1165 m); ODP site 1237 (16°S, 76°W, 3212 m); ODP site 1084 (26°S, 13°E, 1192 m).
- Supported in part by NSF grants OCE-0550439 (A.V.F.) and OCE-081697 and ATM-0222383 (A.C.R.), U.S. Department of Energy Office of Science grant DE-FG02-06ER64238 (A.V.F.), NOAA grant NA16GP2246 (S.G.P.), and Yale University. We thank two anonymous reviewers and T. Herbert, K. Lawrence, P. Huybers, Z. Liu, D. Sigman, J. Severinghaus, and M. Bender for fruitful discussions.

10.1126/science.1122666

The Breakup of a Main-Belt Asteroid 450 Thousand Years Ago

David Nesvorný,^{1*} David Vokrouhlický,¹ William F. Bottke¹

We selected 264,403 asteroids from the Lowell Observatory catalog (*I*) that have observational arcs longer than 10 days, and we used the hierarchical clustering method (HCM) (*2*) to search for groups. The HCM selects groups of orbits in (semimajor axis *a*, eccentricity *e*, inclination *i*, perihelion longitude ϖ , nodal longitude Ω) space based on distances between two neighbor orbits. We used the standard definition of distance in (*a*, *e*, *i*) space, various definitions of distance in (ϖ , Ω) space, and different cut-off values to test the sensitivity of the method on these parameters. One new and two previously known asteroid families were found. The Iamini and Karin clusters, known to be 1 to 5 million years (My) old and ≈ 5.8 My old (*3*, *4*), respectively, showed up as several groups with five to ten members, each representing a small part of the two families that has maintained a coherent distribution of osculating orbits until the present epoch.

The newly identified family is a group of six 1- to 2.5-km-diameter asteroids, whose orbits are very tightly clustered near the inner main belt of the ≈ 10 -km-diameter object 1270 Datura (Table 1). It is extremely unlikely that such a concentration of orbits is a random fluctuation. The small dispersion of orbits in *a*, *e*, and *i* indicates velocity perturbations $\delta V \approx 2 \text{ m s}^{-1}$ relative to Datura, except for (89309) 2001VN36, which has $\delta V \approx 5 \text{ m s}^{-1}$. These values are comparable to the expected escape speed from a 10-km-diameter asteroid ($\approx 5 \text{ m s}^{-1}$)

Table 1. Values of ϖ and Ω for asteroids in the Datura cluster on mean Julian date (MJD) 2453700.5. Time-averaged (proper) orbital elements of 1270 Datura are *a* = 2.23468 AU, *e* = 0.15341, and $\sin(i)$ = 0.09230. All remaining members except (89309) 2001 VN36 have the average orbital elements within 3×10^{-4} AU, 10^{-4} , and 10^{-4} to these values, respectively. (89309) 2001 VN36 has a displacement in *a*, *e*, and $\sin(i)$ that is ≈ 3 times larger. All members of the Datura cluster are tightly clustered in ϖ and Ω . Absolute magnitudes *H* were taken from (*1*).

Asteroid	<i>H</i> (mag)	ϖ (°)	Ω (°)
(1270) Datura	12.5	356.58	97.90
(60151) 1999UZ6	16.3	357.58	96.80
(89309) 2001VN36	16.3	359.78	93.00
(90265) 2003CL5	15.4	357.71	95.70
2001WY35	17.0	357.29	96.89
2003SQ168	16.9	356.72	97.49
2003UD112	17.9	358.62	95.47

and are much smaller than typical asteroid orbital speeds at 2.235 astronomical units (AU) ($\approx 20 \text{ km s}^{-1}$). Moreover, the size frequency distribution of Datura cluster members, which include one large and numerous small asteroids, is also characteristic of impact-generated debris. Given these results, we propose that the Datura cluster is the remnant of a larger parent asteroid that was disrupted by a collision with a \approx km-sized asteroid.

To determine the age of the Datura cluster, t_{age} , we numerically tracked the present orbits of four Datura cluster members backward in time. We did not use (89309) 2001VN36, which is strongly chaotic due to effects of the 9:16 orbital resonance with Mars, nor did we use 2003 SQ168 and 2003 UD112, which have large orbital uncertainties. A total of 840 alternative orbit histories

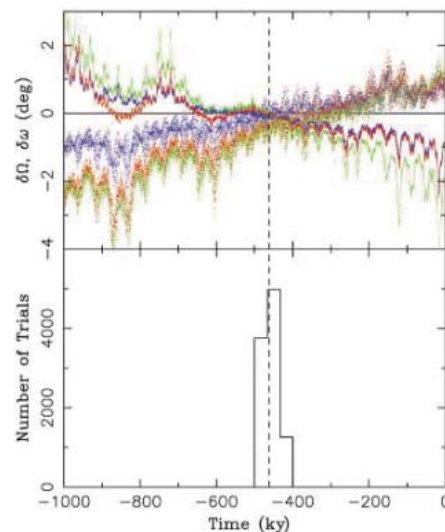


Fig. 1. Convergence of orbits suggests that the Datura cluster formed 450 ± 50 ky ago. **(Top)** Past evolutions of ϖ (ascending lines) and Ω (descending lines) for (60151) 1999UZ6 (red), (90265) 2003CL5 (blue), and 2001WY35 (green). Values relative to 1270 Datura are shown. The dashed vertical line denotes time $t = -467$ ky, when smallest dispersion of ϖ and Ω occurred for this trial. Here we used semimajor axis drift rates $daldt = -2.8 \times 10^{-5}$, -2.3×10^{-4} , 1.5×10^{-5} , and -6.2×10^{-5} AU My^{-1} for 1262 Datura, (60151) 1999UZ6, (90265) 2003CL5, and 2001WY35, respectively. These values are within the range of $daldt$ suggested by the theory of the Yarkovsky effect (*5*). **(Bottom)** The histogram of plausible t_{age} determined from 10^7 different orbital histories of Datura cluster members. Plotted here are all t_{age} for which $\delta V < 5 \text{ m s}^{-1}$.

were produced for each of the four asteroids that differed by the starting orbit (chosen randomly within the orbit uncertainty range for each asteroid) and magnitude of Yarkovsky thermal drag (*5*). We randomly selected one orbital history for each Datura member asteroid and determined t_{age} for this trial by requiring that the dispersion in ϖ and Ω at t_{age} corresponds to $\delta V < 5 \text{ m s}^{-1}$. Such a convergence is expected at the time of the breakup. For comparison, the dispersion of ϖ and Ω at the current epoch corresponds to $\delta V \approx 40 \text{ m s}^{-1}$. The range of plausible t_{age} values was determined from 10^7 trials. The result shows that the Datura cluster is 450 ± 50 thousand years (ky) old (Fig. 1), considerably younger than other known asteroid families.

Existing color data indicate that 1270 Datura has a taxonomic type within the asteroidal S complex, which is thought to be compositionally related to the ordinary chondrite meteorites. 1270 Datura has a short, ≈ 3.3 hours rotation period, possibly as a result of momentum transfer occurring during the family-forming collision. Based on impact simulations with a hydrodynamic code, we estimate that the disrupted parent body was ≈ 15 km in diameter. Apparently, a substantial fraction of the parent body's mass was ejected to space as fragments ranging in size down to micrometer-sized dust particles.

The production of these particles implies that the Datura cluster may be a source of some of the material in the circumsolar (zodiacal) dust cloud. Based on the Datura cluster's inclination ($\approx 5.3^\circ$), we speculate that it might be the source for the E/F dust band pair discovered by the infrared astronomical satellite (IRAS) in 1983 (*6*). We estimate that micrometer-sized Datura particles migrate by radiation effects from 2.235 AU to 1 AU in only ≈ 2000 years. Therefore, a wave of micrometer-sized Datura particles may have reached Earth only a few thousand years after the formation of the Datura cluster. Signs of this event may be found by analyzing tracers of extraterrestrial dust in deep ocean sediments and Antarctic ice cores.

References and Notes

1. E. Bowell, K. Muinonen, L. H. Wasserman, in *Asteroids, Comets and Meteors*, A. Milani *et al.*, Eds. (Kluwer, Dordrecht, 1994), pp. 477–481.
2. V. Zappalà, A. Cellino, P. Farinella, Z. Knežević, *Astron. J.* **100**, 2030 (1990).
3. D. Nesvorný, W. F. Bottke, H. F. Levison, L. Dones, *Nature* **417**, 720 (2002).
4. D. Nesvorný, W. F. Bottke, H. F. Levison, L. Dones, *Astrophys. J.* **591**, 486 (2003).
5. W. F. Bottke, D. Vokrouhlický, D. P. Rubincam, M. Broz, in *Asteroids III*, W. F. Bottke, A. Cellino, P. Paolicchi, R. Binzel, Eds. (Univ. of Arizona Press, Tucson, 2002), pp. 395–408.
6. M. V. Sykes, *Astrophys. J.* **334**, L55 (1988).
7. This manuscript is based upon work supported by NASA's Planetary Geology and Geophysics program and the Czech Grant Agency.

13 February 2006; accepted 3 April 2006
10.1126/science.1126175

¹Department of Space Studies, Southwest Research Institute, 1050 Walnut Street, Suite 400, Boulder, CO 80302, USA.

*To whom correspondence should be addressed. E-mail: davidn@boulder.swri.edu

Visualization of Cellulose Synthase Demonstrates Functional Association with Microtubules

Alexander R. Paredez,^{1,2} Christopher R. Somerville,^{1,2} David W. Ehrhardt^{2*}

Expression of a functional yellow fluorescent protein fusion to cellulose synthase (CESA) in transgenic *Arabidopsis* plants allowed the process of cellulose deposition to be visualized in living cells. Spinning disk confocal microscopy revealed that CESA complexes in the plasma membrane moved at constant rates in linear tracks that were aligned and were coincident with cortical microtubules. Within each observed linear track, complex movement was bidirectional. Inhibition of microtubule polymerization changed the fine-scale distribution and pattern of moving CESA complexes in the membrane, indicating a relatively direct mechanism for guidance of cellulose deposition by the cytoskeleton.

Cellulose is synthesized in vascular plants by a plasma membrane-localized enzyme, cellulose synthase, that has been visualized by freeze fracture of plasma membranes as 25- to 30-nm-diameter symmetrical rosettes with six resolved subunits (1). From measurements of the dimensions of cellulose microfibrils, it has been inferred that each of the six subunits of a rosette synthesizes approximately six β -1,4-glucan chains, which hydrogen bond with each other to form a microfibril of about 36 chains that is extruded into the extracellular space and can reach more than 7 μ m in length (2). The only known components of cellulose synthase in higher plants are a family of 10 CESA proteins. Genetic studies of cellulose synthesis during secondary cell wall formation have shown that at least three different CESA proteins must be simultaneously present to support cellulose synthesis (3).

The deposition of cellulose fibrils is generally oriented perpendicular to the axis of cellular expansion in growing tissue, a feature that has been postulated to facilitate directional, or anisotropic, cell growth. Disruption of microfibril organization by the anti-spindle fiber drug colchicine, and accompanying isodiametric cell expansion, led Green to propose that spindle fibers might play a role in orienting the deposition of cellulose microfibrils and constraining the pattern of cell expansion (4). Soon thereafter, cortical microtubules were discovered (5) and were frequently observed to lie parallel to the cellulose fibrils [reviewed in (6)]. The alignment hypothesis for cellulose deposition has since evolved into two

major forms: Microtubules have been proposed to act as molecular rails, directly guiding cellulose synthase rosettes as they synthesize microfibrils (7); alternatively, microtubules have been proposed to serve as passive constraints, forming channels that confine the lateral movement of synthesizing complexes such that a net coorientation of microfibrils and microtubules results (8), a model that has been popularized in current textbooks (9). The alignment hypothesis, under either model, makes two predictions: that microtubules and microfibrils should be coaligned, and that changes in microtubule organization should cause changes in microfibril arrangement (10). However, many inconsistencies between the orientation of microtubules and cellulose alignment have been observed, and a role for microtubules in cellulose alignment remains controversial (10–14). Here we test the alignment hypothesis by simultaneous and dynamic visualization of cellulose synthase and microtubules in living plant cells.

Visualization of dynamic CESA6 complexes in the cell membrane. Until recently, the only way to simultaneously visualize microtubules and cellulose synthase was by electron microscopy of fixed tissue, where the dynamic relationship between molecules cannot be observed and only a very limited region of the cell can be viewed at a time. Thus, transient states of molecular association could not be examined, and global patterns of organization and association were difficult to observe. Other methods to visualize the outcome of cellulose synthase activity, such as polarization microscopy or dye labeling of material in the cell wall (11), do provide global views of accumulated cellulose organization, but they do not report on the activity and distribution of cellulose synthase during the process of cell wall creation. To visualize cellulose synthase, we produced transgenic *Arabidopsis*

plants in which an N-terminal fusion of citrine yellow fluorescent protein (YFP) (15) to the CESA6 protein was expressed under control of the native *CESA6* promoter in a *cesa6*-null mutant background [*prc1-1* (16)]. This construct complemented the mutant phenotypes of reduced hypocotyl elongation and radialized cell expansion, indicating that the fusion protein was functional (table S1). A similar construct for the *CESA7* gene was previously shown to complement a mutation affecting secondary cell wall synthesis in the vasculature (17).

Observation of expanding hypocotyl cells by spinning disk confocal microscopy revealed YFP:CESA6 fluorescence in three subcellular locations (Fig. 1). First, the label was detected in the focal plane of the plasma membrane as discrete particles at or below the resolution limit of the microscope (Fig. 1, A and B). These particles were not randomly dispersed, but tended to be organized into linear arrays (Fig. 1, A and B). Imaged over time, these particles were also observed to be motile (Movie S1), tracing roughly linear trajectories along the axes of the particle arrays. These trajectories were visualized in static images by averaging the frames of the time series (Fig. 1C). In kymograph analysis, particle motions described straight traces that were parallel to each other, indicating that velocities were steady and highly similar from particle to particle (Fig. 1D). The cross-hatching of traces in the kymographs indicates that particle movement was bidirectional within the tracks defined by particle translocation. Thus, particle motility does not show polarity relative to individual tracks nor to the cell axis. The slopes of these traces revealed an average velocity of 330 nm/min, with a range of 150 to 500 nm/min and a standard deviation of 65 nm/min (Fig. 1E). These rates of movement correspond to the addition of ~300 to 1000 glucose residues per glucan chain per minute, values roughly one-third of those previously predicted for in vivo synthetic rates in algal cells (18). Labeled particles were seen to appear de novo in optical sections and to begin translation immediately (Movie S6), indicating a very short lag time (<10 s) for particle motility to commence after appearance at the cell membrane. A short lag time for the initiation of particle motility is also supported by frame averaging analysis, where evidence for stationary particles was seldom observed (Figs. 1 and 2). Particle lifetimes have not yet been accurately determined because the high density of the particles, the limited field of view, and loss of signal over extended observation due to photobleaching make it difficult to obtain compelling numbers. However, we have observed individual particles moving at a constant rate for at least 15 min.

Citrine-YFP fluorescence was also seen to accumulate in cytoplasmic compartments (Fig. 1G). Organelles labeled by a prominent

¹Department of Biological Sciences, Stanford University, ²Carnegie Institution, Department of Plant Biology, 260 Panama Street, Stanford, CA 94305, USA.

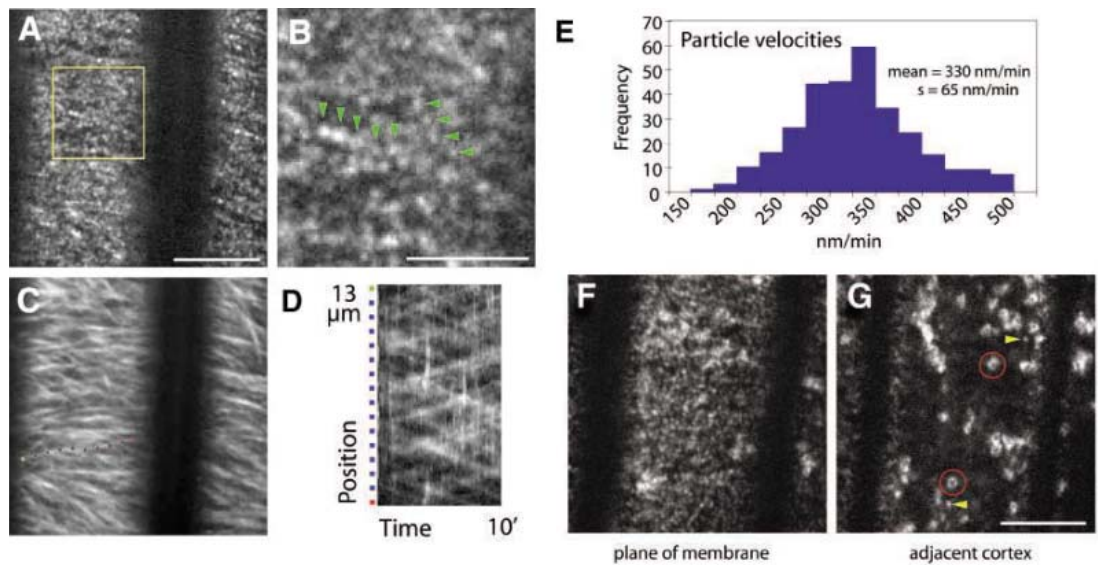
*To whom correspondence should be addressed. E-mail: ehrhardt@stanford.edu

ring of fluorescence were confirmed to be Golgi by colocalization with a cyan fluorescent protein (CFP):MANNOSIDASE marker (fig. S1) (19). Labeling of the Golgi by YFP:CESA6 was nonuniform and characterized by formation of distinct puncta (Fig. 1G). The relative brightness of these puncta suggests a higher concentration of labeled protein than is observed in puncta at the plasma membrane, perhaps representing the package of Cesa6 protein into secretory vesicles (20). It is also possible that assembly of CESA rosettes in the Golgi could contribute

to the punctate appearance of label in the Golgi, consistent with previous observations by electron microscopy (20). In addition to particulate localization at the cell membrane and to the Golgi, YFP:CESA6 also labeled a population of small organelles, at or near the resolution limit of the imaging system (Fig. 1G). These organelles were distinguished from the particles in the membrane by their focal plane (Fig. 1, F and G), higher fluorescent intensities, and faster and less steady patterns of movement (Movie S3).

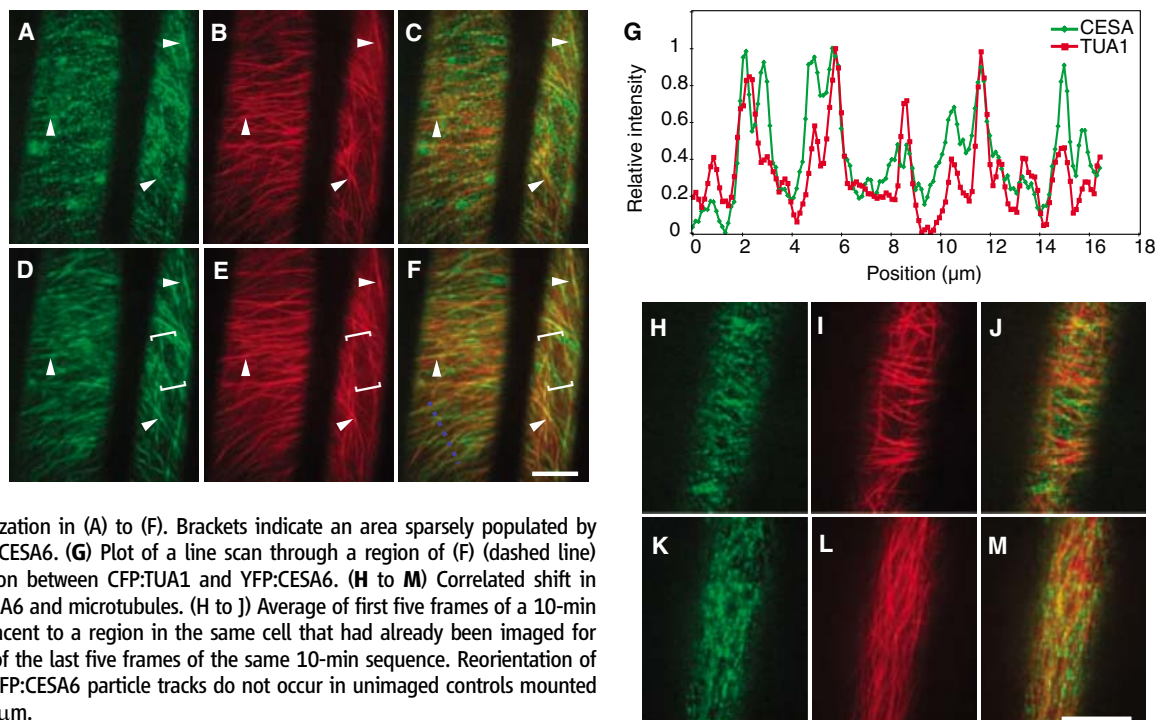
The herbicide isoxaben specifically inhibits cellulose synthesis in plants. Missense mutations in *CESA3* and *CESA6* confer resistance to isoxaben, suggesting that these subunits are direct targets (21, 22). However, the residues affected are remote from the presumed active site of the enzyme, suggesting that the mode of action is not direct inhibition of catalysis. Treatment of seedlings with 100 nM isoxaben resulted in the rapid loss of YFP:CESA6 particles from the plasma membrane (fig. S2, Movie S2). Within 5 min, a de-

Fig. 1. YFP:CESA6 localization and motility in etiolated hypocotyl cells. Optical sections of plasma membrane (A, B, C, and F) and adjacent cytoplasm (G) in upper hypocotyl cells of etiolated *prc1-1* seedlings expressing YFP:CESA6 (3 days old). Images in all figures were acquired by spinning disk confocal microscopy. (A) Average of five frames (10-s intervals) acquired at the plane of the cell membrane. (B) Enlarged region of (A) corresponding to the yellow frame showing arrays of CESA particles marked with green arrowheads. (C) Average of 61 frames showing movement of labeled particles along linear tracks during 10 min. (D) Kymograph of region highlighted in (C), displaying steady, consistent, and bidirectional particle translocation. (E) Histogram of particle velocities calculated from kymograph analysis of 303 particles in 32 tracks measured in seven cells from six seedlings. (F) and



(G) Adjacent focal planes of the same cell showing YFP:CESA6 particles in the cell membrane, Golgi [red circles in (G)], and a particulate cytosolic compartment [yellow arrowheads in (G)]. Scale bars: 10 μm (A and G), 5 μm (B).

Fig. 2. Colocalization of microtubules and YFP:CESA6 in etiolated hypocotyl cells. YFP:CESA6 labeling is in green, microtubules labeled with CFP:TUA1 are in red, and combined images are on the right. Image acquisition interval was 10 s. (A to C) Average of five image frames showing colocalization of YFP:CESA6 particles and microtubules. (D to F) Average of 30 frames reveals YFP:CESA6 particle paths along microtubules and microtubule bundles. Arrowheads mark prominent areas of colocalization in (A) to (F). Brackets indicate an area sparsely populated by either microtubules or YFP:CESA6. (G) Plot of a line scan through a region of (F) (dashed line) showing a strong correlation between CFP:TUA1 and YFP:CESA6. (H to M) Correlated shift in orientation of both YFP:CESA6 and microtubules. (H to J) Average of first five frames of a 10-min image sequence taken adjacent to a region in the same cell that had already been imaged for 10 min. (K to M) Average of the last five frames of the same 10-min sequence. Reorientation of the microtubules and the YFP:CESA6 particle tracks do not occur in unimaged controls mounted for 20 min. Scale bar, 10 μm .



crease in particle density was observed, and within 20 min most of the plasma membrane YFP:CESA6 was lost (fig. S2). The ability of the YFP:CESA6 construct to rescue the mutant, together with its localization pattern, dynamic behavior, velocity of movement, and sensitivity to drug treatment, suggest that the observed YFP-labeled particles at the cell cortex were individual cellulose synthase biosynthetic complexes. The fluorescence intensities of the individual YFP:CESA6 particles within a given cell were not uniform (Fig. 1, Movie S1), suggesting either that the stoichiometry of CESA subunits within a complex is not fixed, or that individual particles may be composed of a variable number of rosette complexes.

Dynamic colocalization with cortical microtubules. To observe the spatial relationship between microtubules and membrane-localized cellulose synthase, we crossed a CFP:TUA1 α -tubulin marker into the YFP:CESA6 line. Two-channel confocal imaging of expanding hypocotyl cells revealed extensive overlap between the two patterns of label distribution (Fig. 2), and labeled CESA particles were observed to move along tracks defined by microtubules (Fig. 2, D to F, and Movie S3; ~60% of pixels labeled with YFP:CESA6 above the local background were also labeled with CFP:TUA1 above the local background). Although most microtubules in these growing cells had an orientation that was roughly transverse to the cell axis, there were regional

differences within cells for net array orientation, and many microtubules exhibited discordant angles and curved configurations. The high coincidence of YFP:CESA6 label with regional microtubule organization and with discordant and curved microtubules (Fig. 3) further indicate that the observed degree of colocalization was not due to coincidental overlap of two linear arrays with similar orientation. Furthermore, bidirectional tracking of labeled rosettes along curved and discordant microtubules is not expected if rosettes are simply passively channeled between the visually resolved spaces between elements of the cortical microtubule array.

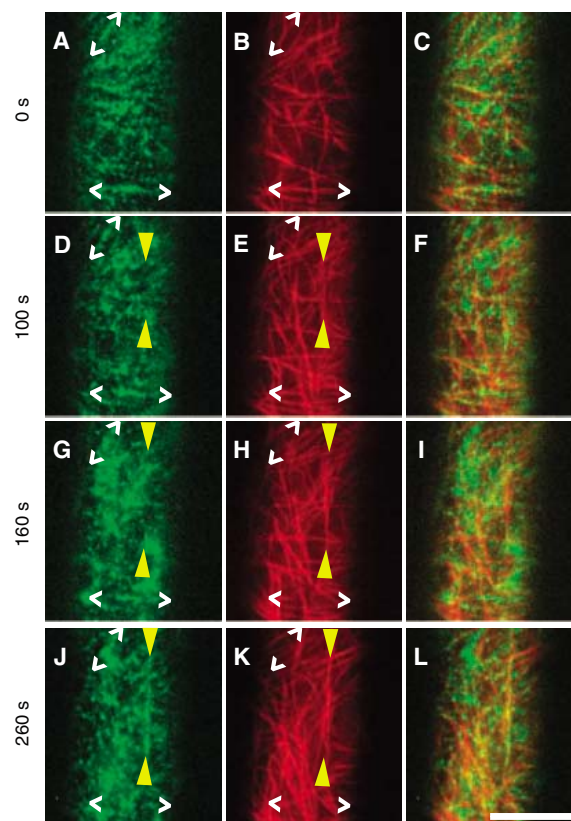
Despite the widespread colocalization of YFP:CESA6 and cortical microtubules, there was not complete overlap between the two distributions. Time-lapse observation revealed that the dynamics of these two interacting molecular systems contributes to the observed degree of colocalization. For example, cortical microtubules migrate by polymer treadmilling at rates that are roughly four times the mean velocity of membrane-localized particles (23). Microtubule catastrophe can occur at up to 75 times this velocity (23). Thus, microtubules are considerably more dynamic than is cellulose synthase. Frequently, microtubules with associated YFP:CESA6 were observed to depolymerize rapidly while the YFP:CESA6 persisted and continued to translocate along their original trajectories, producing a local YFP:CESA6 linear array without the presence of a co-

linear microtubule (Fig. 3, Movie S5). Once complexes are set in motion, the rigidity of crystalline cellulose may be enough to maintain an initial trajectory (12). Linear arrays of YFP:CESA6 were observed to persist for as long as 4 min after their associated microtubules had depolymerized; these arrays eventually dissipated (Fig. 3, Movie S5), suggesting that the microtubules not only predict the localization of YFP:CESA6, but also stabilize the linear arrays of dynamic CESA6 complexes. Events in which microtubule polymerization outpaced the establishment of related YFP:CESA6 linear arrays were also observed (Fig. 3, Movie S5). Single treadmilling microtubules are the most dynamic elements of the cortical cytoskeleton (23) and were frequently observed in time-lapse movies (Movie S3), but YFP:CESA6 seemed to be primarily associated with the brighter and more stable elements of the microtubule cytoskeleton that correspond to microtubule bundles.

Microtubules guide cellulose synthase distribution and behavior. We investigated the causal relation between microtubules and organization of cellulose deposition by two methods: observation of dynamic patterns of colocalization during organizational transitions and disruption of the cytoskeleton with the drug oryzalin. In hypocotyl cells just below the hook, microtubules are organized into dense arrays of transverse bands, and the YFP:CESA6 complexes show the same orientation (Fig. 2, A to F, H to J; fig. S3, A to C). About 20 min after stimulation of these cells with blue light (488-nm excitation laser), a marked reorganization of CFP-labeled microtubules was observed, from a net transverse to a net longitudinal orientation (~30 observations in 30 plants) (Fig. 2, I and L); this response is consistent with previous observations of blue light-stimulated reorientation of the cortical microtubule array in pea hypocotyls (24). Reorientation was not observed in control specimens mounted for observation but kept in the dark. This stimulated rearrangement of microtubules allowed us to examine the coupling between the cytoskeletal and cellulose synthase arrays. Dual label imaging revealed that the arrays of microtubules and YFP:CESA6 changed orientation concurrently (recordings of eight cells in eight plants) (Fig. 2, H to M) (Movie S4). Assembly of new microtubule tracks was observed to precede the appearance of linear arrays of YFP:CESA6 protein at the same position (Fig. 3). Correlated changes in the arrangement of microtubules and YFP:CESA6 localization were also observed along the axis of the hypocotyl in the course of normal development (fig. S3).

If cortical microtubule organization plays a role in establishing YFP:CESA6 organization, then global disruption of microtubules by destabilizing drugs should change the patterns of YFP:CESA6 distribution and move-

Fig. 3. Dynamic relation between YFP:CESA6 and CFP:TUA1. In all images YFP:CESA6 labeling is in green, CFP:TUA1 labeling is in red, and combined images are on the right. Each image is the average of three frames. Image acquisition rates are as in Fig. 1. Carets mark two regions where distinct microtubule bundles are decorated with CESA6 at the first time point (A to C). At subsequent time points (D to L), microtubule bundles marked by carets have depolymerized and YFP:CESA6 remains. Yellow arrowheads mark a newly assembled microtubule bundle (E and F) that persists over the remaining course of the experiment (H and I, K and L). Corresponding CESA label is not detected in this position (D and F, G and I) until after the new bundle is created (J and L). Scale bar, 10 μ m.



ment. Treatment of intact seedlings with 10 μM oryzalin for 3 hours abolished the microtubule arrays in hypocotyl cells and caused marked changes in YFP:CESA6 organization and behavior, but did not deplete the CESA particles from the membrane (~ 100 cells observed in 20 plants) (Fig. 4). YFP:CESA6 particles continued to translocate, but particles aggregated and moved in swarms that were not seen in untreated cells. Most of the “resistant” YFP:CESA6 tracks overlapped with oryzalin-resistant microtubules. In some cases, YFP:CESA6 tracks could be seen continuing past the end of microtubules (Fig. 4H). We infer that microtubules confer orientation on the movement of the CESA complexes but are not required for CESA motility per se. When microtubules were nearly completely depopulated from the cortex of etiolated hypocotyl cells (20 μM oryzalin for 7 hours; ~ 30 cells observed in 16 plants), the pattern of CESA distribution changed. Rather than accumulating in dense swarms after partial loss of the cortical array, YFP:CESA6 was much more uniformly dispersed (compare Fig. 4, A and I). Notably, rosettes in these cells moved in roughly linear and parallel tracks set at oblique angles to the cell axis (Fig. 4I). Thus, in the course of disrupting the cortical cytoskeleton with oryzalin, the pattern of YFP:CESA6 distribution and trajectories in the membrane makes a transition through three distinct states. In the absence of oryzalin, YFP:CESA6 is distributed in a highly organized state defined by the organization of the intact cortical microtubule array. As the cytoskeleton becomes partially disrupted, YFP:CESA6 distribution and trajectories change markedly, but continue to be dominated by the influence of a small number of microtubules. When the cortical array is nearly completely disassembled, YFP:CESA6 acquires a second state of high organization in which particles are again more uniformly dispersed and trajectories appear to be more uniformly aligned.

Conclusions and discussion. Taken together, these observations demonstrate that cellulose synthase complexes containing CESA6 are organized in the cell membrane by a functional association with cortical microtubules. The distribution and movement of YFP:CESA6 along trajectories defined by discordant and curved microtubules, and the high level of coordination between YFP:CESA6 and microtubules observed during reorganization events, show that CESA localization and guidance display tight spatial and temporal coupling to microtubules, and therefore, that the two arrays of molecules are likely to be in intimate contact with each other. These observations effectively rule out a model in which CESA complexes are guided solely by passive channeling between the optically resolved microtubules of the cortical array. One possibility is that each cortical microtubule, or microtubule bundle, allows for lateral interaction with the cytosolic domains of

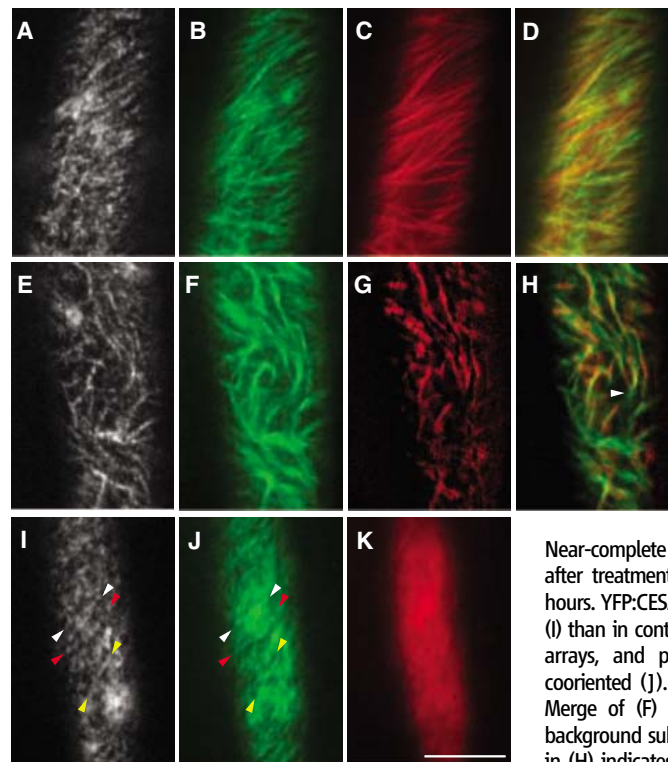


Fig. 4. Microtubule depolymerization changes YFP:CESA6 organization. Gray images: YFP:CESA6, average of 5 frames; green images: YFP:CESA6, average of 30 frames; and red images: CFP:TUA1, average of 30 frames. Image acquisition rates are as in Fig. 1. (A to D) Control treatment with 0.02% methanol for 3.5 hours. (E to H) Treatment with 10 μM oryzalin (in 0.02% methanol) for 3.6 hours causes loss of microtubule organization with correlated changes in YFP:CESA6 localization (E) and trajectories (F). (I to K)

Near-complete loss of cortical microtubules after treatment with 20 μM oryzalin for 7.6 hours. YFP:CESA6 is more uniformly dispersed (I) than in controls or cells with partial cortical arrays, and particle trajectories are highly cooriented (J). (D) Merge of (B) and (C). (H) Merge of (F) and (G), where (G) has been background subtracted (31). White arrowhead in (H) indicates CESA label extending beyond a defined microtubule track. Colored arrow-

head in (I) and (J) highlight organized tracks of YFP:CESA6 in the absence of microtubules. Scale bar, 10 μm .

CESA complexes, leading to organization of two linear arrays of CESA, one on either side of the microtubule. This model is consistent with freeze-etching experiments that revealed rosettes to lie alongside, but not directly on top of, cortical microtubules (8). The arrangement of rosettes into two linear arrays along each microtubule also suggests possible mechanisms to account for bidirectional movement along individual CESA tracks. Our observations of normal rates of rosette movement following microtubule depolymerization demonstrate that any interactions with microtubules, whether by direct contact of CESA protein or through linker proteins, are not required for cellulose synthase motility and further support the idea that the motive force for complex motility is provided primarily by cellulose polymerization (25, 26). Our results also show that, although cortical microtubules have a defining influence on the distribution and guidance of CESA rosettes if they are present, in the absence of cortical microtubules, the movement of CESA complexes does not appear to be random, suggesting an intrinsic capacity to self-organize (12) or the action of a second extrinsic organizational mechanism. This surprising observation may explain previous experiments that did not support a causal relation between microtubules and the orientation of cellulose deposition (14, 27).

Previous experiments that challenged the microtubule alignment model for CESA guidance should be reexamined with live-cell

confocal microscopy and with careful attention paid to the physiological and developmental stage of the tissue. In this respect, we emphasize that we have examined the localization of only a single type of CESA protein in one tissue type. It could be that other CESA proteins do not have localization patterns that are so tightly coupled to the cytoskeleton, that the behavior of CESA proteins varies within different organs, or that only a subset of the microtubules is involved in guidance in some cell types and that these were overlooked in some previous studies.

In vitro measurements of cellulose synthesis have been fraught with technical difficulties, and substantial effort is required to demonstrate enzyme activity in tissue extracts (28). The methods and results described here create new opportunities to assay the effects of genetic, developmental, and environmental variation on cellulose synthesis. In principle, improved single-molecule optical methods may be used to measure not only the rate of synthesis but also the duration and orientation of deposition—factors that have profound effects on the physical properties of cellulose. Such assays may facilitate an understanding of the roles of genes such as *COBRA* and *KORRIGAN*, whose effects on cellulose synthesis and cell-grown anisotropy are poorly understood (29, 30).

References and Notes

1. S. Kimura *et al.*, *Plant Cell* **11**, 2075 (1999).
2. C. Somerville *et al.*, *Science* **306**, 2206 (2004).

3. N. G. Taylor, R. M. Howells, A. K. Huttly, K. Vickers, S. R. Turner, *Proc. Natl. Acad. Sci. U.S.A.* **100**, 1450 (2003).
 4. P. B. Green, *Science* **138**, 1404 (1962).
 5. M. Ledbetter, K. Porter, *J. Cell Biol.* **19**, 239 (1963).
 6. P. K. Hepler, B. A. Palevitz, *Annu. Rev. Plant Physiol. Plant Mol. Biol.* **25**, 309 (1974).
 7. I. B. Heath, *J. Theor. Biol.* **48**, 445 (1974).
 8. T. Giddings, L. Staehelin, in *The Cytoskeletal Basis of Plant Growth and Form*, C. W. Lloyd, Ed. (Academic Press, New York, 1991), pp. 85–99.
 9. B. Alberts *et al.*, *Molecular Biology of the Cell* (Garland, New York, ed. 4, 2002).
 10. T. I. Baskin, *Protoplasma* **215**, 150 (2001).
 11. T. I. Baskin, G. T. S. Beemster, J. E. Judy-March, F. Marga, *Plant Physiol.* **135**, 2279 (2004).
 12. A. M. C. Emons, B. M. Mulder, *Trends Plant Sci.* **5**, 35 (2000).
 13. R. Himmelspach, R. E. Williamson, G. O. Wasteneys, *Plant J.* **36**, 565 (2003).
 14. G. O. Wasteneys, *Curr. Opin. Plant Biol.* **7**, 651 (2004).
 15. O. Griesbeck, G. S. Baird, R. E. Campbell, D. A. Zacharias, R. Y. Tsien, *J. Biol. Chem.* **276**, 29188 (2001).

16. M. Fagard *et al.*, *Plant Cell* **12**, 2409 (2000).
 17. J. C. Gardiner, N. G. Taylor, S. R. Turner, *Plant Cell* **15**, 1740 (2003).
 18. H. D. Reiss, E. Schnepf, W. Herth, *Planta* **160**, 428 (1984).
 19. A. Nebenfuhr, J. A. Frohlich, L. A. Staehelin, *Plant Physiol.* **124**, 135 (2000).
 20. C. H. Haigler, R. M. Brown, *Protoplasma* **134**, 111 (1986).
 21. W. R. Scheible, R. Eshed, T. Richmond, D. Delmer, C. R. Somerville, *Proc. Natl. Acad. Sci. U.S.A.* **98**, 10079 (2001).
 22. T. Desprez *et al.*, *Plant Physiol.* **128**, 482 (2002).
 23. S. L. Shaw, R. Kamyar, D. W. Ehrhardt, *Science* **300**, 1715 (2003).
 24. M. Yuan, P. J. Shaw, R. M. Warn, C. W. Lloyd, *Proc. Natl. Acad. Sci. U.S.A.* **91**, 6050 (1994).
 25. C. Lloyd, *Int. Rev. Cytol.* **86**, 1 (1984).
 26. D. G. Robinson, H. Quader, *Eur. J. Cell Biol.* **25**, 278 (1981).
 27. K. Sugimoto, R. Himmelspach, R. E. Williamson, G. O. Wasteneys, *Plant Cell* **15**, 1414 (2003).
 28. J. Lai-Kee-Him *et al.*, *J. Biol. Chem.* **277**, 36931 (2002).
 29. F. Roudier *et al.*, *Plant Cell* **17**, 1749 (2005).
 30. S. Robert *et al.*, *Plant Cell* **17**, 3378 (2005).

Supporting Online Material

www.sciencemag.org/cgi/content/full/1126551/DC1

Materials and Methods

Figs. S1 to S3

Table S1

Movies S1 to S8

References

22 February 2006; accepted 12 April 2006

Published online 20 April 2006;

10.1126/science.1126551

Include this information when citing this paper.

REPORTS

Flip-Flopping Fractional Flux Quanta

T. Ortlepp,^{1*} Ariando,² O. Mielke,¹ C. J. M. Verwijs,² K. F. K. Foo,² H. Rogalla,² F. H. Uhlmann,¹ H. Hilgenkamp²

The *d*-wave pairing symmetry in high-critical temperature superconductors makes it possible to realize superconducting rings with built-in π phase shifts. Such rings have a twofold degenerate ground state that is characterized by the spontaneous generation of fractional magnetic flux quanta with either up or down polarity. We have incorporated π phase-biased superconducting rings in a logic circuit, a flip-flop, in which the fractional flux polarity is controllably toggled by applying single flux quantum pulses at the input channel. The integration of π rings into conventional rapid single flux quantum logic as natural two-state devices should alleviate the need for bias current lines, improve device symmetry, and enhance the operation margins.

Superconducting Josephson electronics are based on the storage and transmission of magnetic flux quanta, and make use of one of the unique aspects of superconductivity: its macroscopic phase coherence. To comply with the requirement that the superconducting wave function is single valued, its phase ϕ can only vary by multiples of 2π when going around a closed superconducting ring structure. In the standard case, contributions to phase variations $\Delta\phi$ can arise from magnetic flux Φ that is enclosed by the ring (through $\Delta\phi = 2\pi\Phi/\Phi_0$) and from the phase drop over Josephson junctions incorporated in the ring [through $\Delta\phi = \arcsin(I_f/I_c)$], where I_f and I_c are the supercurrent and the critical current of the junction, respectively, and $\Phi_0 = 2.07 \times 10^{-15}$ Wb is the magnetic flux quan-

tum. The resulting periodic dependence of the maximum supercurrent that can pass through the ring on the applied magnetic flux forms the basis for the superconducting quantum interference device (SQUID), which is the prime

building block for superconducting electronics and sensors.

The introduction of additional phase-shifting elements in such superconducting loops leads to remarkable effects. For example, by incorporating a π phase shift, the ring is set to the twofold degenerate state that otherwise would be obtained by the application of a magnetic flux of exactly $(1/2)\Phi_0$ (Fig. 1) (1, 2). To compensate for this built-in π phase shift, a spontaneous circulating current flows in the ring in either the clockwise or counterclockwise direction. The magnetic flux associated with this persistent circulating current is a fraction of a flux quantum, growing asymptotically to a half flux quantum in the large inductance limit (3). The polarity of this spontaneous flux can be used to store information.

In isolated π rings that are fabricated with high-critical temperature (T_c) grain boundaries

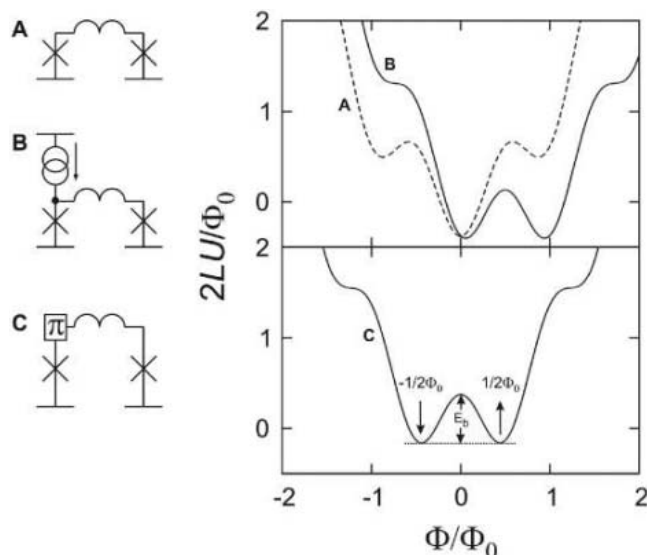


Fig. 1. Potential energy U as a function of enclosed magnetic flux for three different superconducting loop configurations. (A) A standard two-junction SQUID loop. (B) A conventional RSFQ storing loop, composed of a SQUID with an external current source. (C) The new configuration with an intrinsic π phase shift.

¹Institute of Information Technology, Rapid Single-Flux Quantum (RSFQ) Design Group, University of Technology Ilmenau, Post Office Box 100565, D-98684 Ilmenau, Germany. ²Faculty of Science and Technology and MESA+ Institute for Nanotechnology, University of Twente, Post Office Box 217, 7500 AE Enschede, Netherlands.

*To whom correspondence should be addressed. E-mail: thomas.ortlepp@tu-ilmenau.de

(4) or with connections between high- T_c and low- T_c superconductors (5), the generation and manipulation of fractional flux quanta has already been demonstrated with scanning SQUID microscopy. An important step toward applications of π rings in electronic circuitry is their incorporation in superconducting logic gates, where a controlled operation on an electronically applied input signal leads to a predefined output signal (6, 7).

Here we report on the realization of a toggle flip-flop (TFF) based on Josephson contacts between high- T_c and low- T_c superconductors, where the polarity of the fractional flux quantum provides the internal memory. We discuss

the benefits of incorporating such elements in rapid single flux quantum (RSFQ) superconducting electronic circuitry (8).

Figure 2 shows a schematic of the device and an optical micrograph of the chip, which was taken just before the deposition of an Nb ground plane. The state of the flip-flop is represented by polarity of the flux in the storage loop, with an inductance of $L_{\text{store}} \approx 10$ pH and junctions J_2 and J_3 with a critical current of $I_c = 90$ μ A. The ring with junctions J_4 and J_5 will carry a current in the opposite direction to L_{store} , and its main role is to enhance the stability of the device. In the initial state, one of the stable flux states is generated by the built-in π phase

shifts. The flip-flop toggles between both stable states when a single flux quantum (SFQ) pulse is applied through it. These pulses are generated by a direct current (dc)/SFQ converter on the rising ramp of an input current I_{in} and transferred via a Josephson transmission line (JTL) to the input junction J_1 of the flip-flop. To clarify the device operation, let us presume that the flip-flop is in the state with a clockwise current in the storage loop. The flip-flop is designed so that when an SFQ pulse enters through J_1 , the associated currents give rise to a switching of J_3 and J_4 , causing the flux state in L_{store} to reverse. If a second pulse arrives at the input, it causes a switching of J_2 and J_5 , which toggles the flip-flop back to the original state. The flip-flop internal state can be read out with a two-junction SQUID loop, which is a sensitive sensor for magnetic fields and is nested in the middle of the storing loop. The operating point of the SQUID loop can be adjusted to create a voltage signal for an upward fractional flux and no voltage for a downward fractional flux inside the loop.

The flip-flop is fabricated by connecting the d -wave superconductor $\text{YBa}_2\text{Cu}_3\text{O}_{7-\delta}$ and the s -wave superconductor Nb separated by an Au barrier layer in a thin-film ramp-type Josephson junction configuration (9, 10). The measurements were performed in a well-shielded flow cryostat at a temperature of $T = 5.3$ K.

To demonstrate the correct operation, SFQ pulses were generated in a standard dc/SFQ converter and were fed to the flip-flop via a JTL. An SFQ pulse is generated by the dc/SFQ converter circuit every time the current in the input loop is increased exceeding a value corresponding to a flux quantum Φ_0 in the dc/SFQ inductance. Figure 3A shows the triangular input signal to the dc/SFQ converter and the output voltage over the read-out SQUID as a function of time, clearly demonstrating the toggling of the flip-flop at every incoming SFQ pulse generated at the rising edge of the periodic input signal. Several experiments with the generation of multiple input pulses at any ramp of an enlarged input signal confirm the correct operation, with the

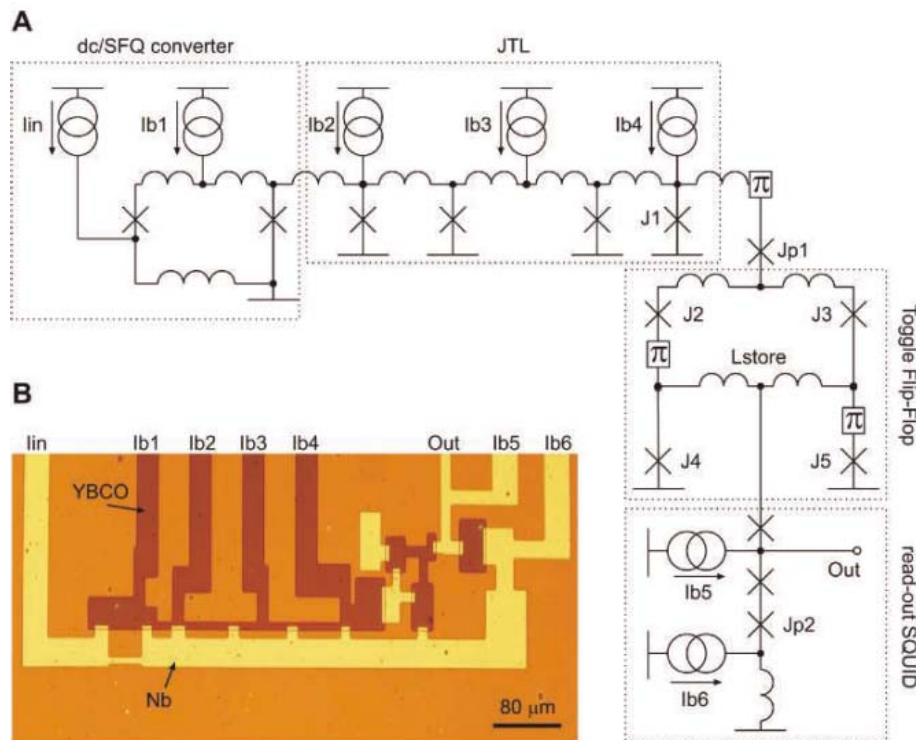
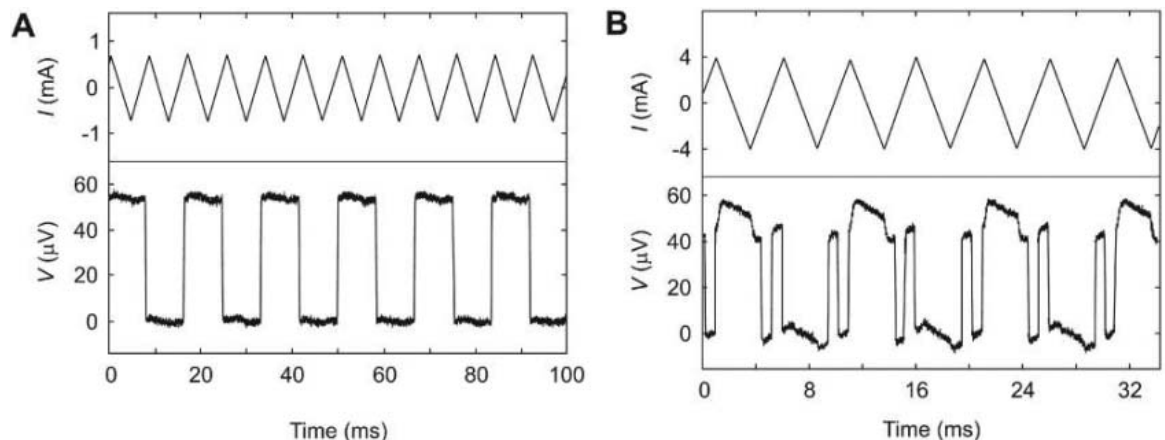


Fig. 2. (A) Schematic and (B) optical micrograph of the π shift toggle flip-flop. The Josephson junctions have designed critical currents between 90 and 130 μ A controlled by the width between 7.5 and 11 μ m. All lines to ground are connected in a phase-coherent manner by a superconducting ground plane, not shown here.

Fig. 3. Measurement results for (A) a triangular input current of about 1-mA amplitude. On each rising ramp of this input signal, an SFQ pulse is generated, transferred to the TFF, and its internal state is toggled. (B) A triangular input current of about 4-mA amplitude with three SFQ pulses is generated on each rising ramp of the input signal.



corresponding number of output switchings as shown in Fig. 3B. In this figure, the amplitude of the input current is increased to generate three SFQ pulses on the rising ramp. When the TFF for each of these pulses was subjected to switching, the output showed a transition between its voltage states. Small deviations in the voltage level in this oversteered mode of operation are caused by a parasitic coupling between adjacent lines in the experimental setup.

The maximum frequency of the circuit is similar to conventional RSFQ circuits with a comparable characteristic voltage $I_c R_n$, where I_c is the critical current and R_n is the normal resistance. This specific sample shows an $I_c R_n$ of about 110 μV , which limits the output voltage to 55 μV . In this sample, an extra ground plane layer was introduced for the first time to the standard fabrication process, which may influence the $I_c R_n$ products and still needs to be optimized. Nevertheless, $I_c R_n$ values up to 0.7 mV have been shown by using a similar fabrication process (9). This corresponds to a Josephson frequency of 340 GHz, which sets the scale for the speed of digital operation.

The operation of RSFQ circuits is based on three different elementary blocks for transport, decision, and storage of information bits (11). In the design process, the mode of RSFQ digital operation is defined by creating topological schemes with the three mentioned functional elements and by specifying their parameters. A complication in standard RSFQ is that superconducting ring structures without built-in π phase shifts have one lowest energy state, i.e., the zero-flux state, and a degenerate first-order state with a flux of $\pm\Phi_0$ (Fig. 1). To reach an operating point with a twofold degenerate lowest energy state, a bias current must be asymmetrically injected (Fig. 1B). However, this requires additional bias lines and control over these currents. In principle, the flip-flop can

work without this bias current (12), but this requires an even higher asymmetry in the critical currents of the junctions. This asymmetry imposes strict margins on the design parameters, such as the junction critical currents and the inductance values. These factors have until now strongly hampered the development of large-scale RSFQ logic circuits.

The spontaneous generation of fractional flux in the π shift device eliminates the need for the asymmetrically injected bias current, which reduces the amount of connections to external control electronics and allows for symmetry in the design parameters. Figure 4 shows an exemplary π TFF configuration with improved parameters, a design based on the initial experimental results presented above. This is of great benefit in the design process and fabrication, and also leads to denser circuitry; our first realization needed only a quarter of the size of a standard TFF in established Nb technology with the same feature size of 2.5 μm .

To study the influence of parameter variations on the circuit performance, a Monte Carlo yield analysis was performed. Several thousand parameter sets, which had normally distributed random values for all adjustable parameters (critical currents, inductances, and bias currents), were assigned to the π shift circuit, and its operation was checked by automatic circuit simulation runs. The π shift devices show a strongly improved stability against possible parameter variations. This was also observed experimentally; the TFF showed correct operation even when the bias current I_{b4} was varied by $\pm 18\%$ from its operation point. By further optimizing critical currents and inductances, this operation range can be increased to $\pm 55\%$ deviation from the mean value.

The bistability of π phase shift devices is of relevance for all logic cells with internal states. This also includes all Boolean operations

(AND, OR, etc.), because RSFQ is pulse-driven logic, input and sometimes output buffer stages are required for the temporary storage of information. There is no strong advantage in using π loops in a JTL, splitter, or confluence buffer, because these cells do not have an internal state and therefore the bistable character of π loops is dispensable.

The results above are obtained by exploiting the π phase shift associated with the $d_{x^2-y^2}$ symmetry in the high- T_c superconductors. However, it can easily be adapted to other technologies providing the π phase shift, such as superconductor-ferromagnet-superconductor Josephson junctions (13, 14).

We realized SFQ operation of a logic circuit with a twofold degenerate ground state created by using intrinsic π phase shifts. By incorporating π phase shifters in RSFQ circuits, we found a strongly improved stability against spread, a compact circuit realization because of the decreased size of large inductances, and a reduction in bias current supplies. This enables a simplification in the RSFQ circuit design, with relaxed requirements to the fabrication process. The realization of a natural bistable system addresses one of the most challenging tasks for the superconducting electronics: the setting up of memory. Our TFF realization needs only a quarter of the size of a typical TFF in established Nb technology with the same feature size of about 2.5 μm .

References and Notes

1. C. C. Tsuei, J. R. Kirtley, *Rev. Mod. Phys.* **72**, 969 (2000).
2. R. R. Schulz *et al.*, *Appl. Phys. Lett.* **76**, 912 (2000).
3. J. R. Kirtley, K. A. Moler, D. J. Scalapino, *Phys. Rev. B* **56**, 886 (1997).
4. C. C. Tsuei *et al.*, *Phys. Rev. Lett.* **73**, 593 (1994).
5. H. Hilgenkamp *et al.*, *Nature* **422**, 50 (2003).
6. E. Terzioglu, M. R. Beasley, *IEEE Trans. Appl. Supercond.* **8**, 48 (1998).
7. A. V. Ustinov, V. K. Kaplunenko, *J. Appl. Phys.* **94**, 5405 (2003).
8. K. K. Likharev, V. K. Semenov, *IEEE Trans. Appl. Supercond.* **1**, 3 (1991).
9. H. J. H. Smilde, H. Hilgenkamp, G. Rijnders, H. Rogalla, D. H. A. Blank, *Appl. Phys. Lett.* **80**, 4579 (2002).
10. Materials and methods are available as supporting material on Science Online.
11. D. K. Brock, E. K. Track, J. M. Rowell, *IEEE Spectr.* **37**, 40 (2000).
12. S. V. Polonsky *et al.*, *IEEE Trans. Appl. Supercond.* **3**, 2566 (1993).
13. V. V. Ryazanov *et al.*, *Phys. Rev. Lett.* **86**, 2427 (2001).
14. T. Kontos *et al.*, *Phys. Rev. Lett.* **89**, 137007 (2002).
15. This work was supported by the Netherlands Organization for Scientific Research, the Dutch Foundation for Research on Matter, the Dutch Stichting Technische Wetenschappen NanoNed program, the European Science Foundation PiShift program, and the University of Technology Ilmenau Promotion of Excellency. Helpful discussions with S. Karthikeyan are gratefully acknowledged.

Supporting Online Material

www.sciencemag.org/cgi/content/full/1126041/DC1
Materials and Methods

9 February 2006; accepted 6 April 2006

Published online 20 April 2006;

10.1126/science.1126041

Include this information when citing this paper.

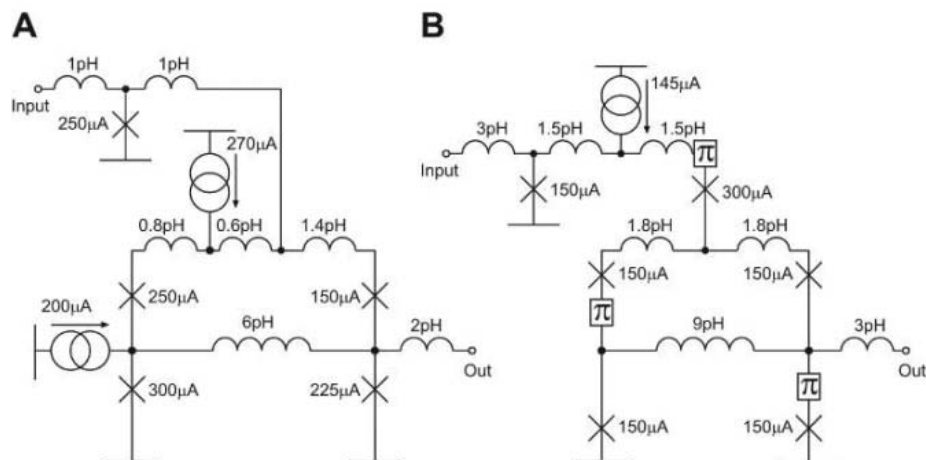


Fig. 4. Comparison of the circuit parameters for (A) a conventional and (B) an exemplary symmetric π shift toggle flip-flop.

Coherent State Evolution in a Superconducting Qubit from Partial-Collapse Measurement

N. Katz,¹ M. Ansmann,¹ Radoslaw C. Bialczak,¹ Erik Lucero,¹ R. McDermott,¹ Matthew Neeley,¹ Matthias Steffen,¹ E. M. Weig,¹ A. N. Cleland,¹ John M. Martinis,^{1*} A. N. Korotkov²

Measurement is one of the fundamental building blocks of quantum-information processing systems. Partial measurement, where full wavefunction collapse is not the only outcome, provides a detailed test of the measurement process. We introduce quantum-state tomography in a superconducting qubit that exhibits high-fidelity single-shot measurement. For the two probabilistic outcomes of partial measurement, we find either a full collapse or a coherent yet nonunitary evolution of the state. This latter behavior explicitly confirms modern quantum-measurement theory and may prove important for error-correction algorithms in quantum computation.

The wave-particle duality in quantum mechanics originates from two distinct ways in which a quantum state may change: a linear (unitary) evolution according to the Schrödinger wave equation and a nonlinear (projective or “collapse”) evolution due to measurement (1). In recent years, it has been understood that an interesting combination of wave and particle dynamics can be observed by using partial measurements, in which the quantum state both partially collapses and coherently evolves at the same time (2). In quantum optics, continuous quantum measurement back-action was harnessed to control state evolution, leading to the generation of squeezed

states (3). Also, partial measurement is predicted to be useful as a form of quantum-error correction, in which continuous feedback is used for correction (4). We present full experimental verification of a partial measurement on a solid-state qubit (5–9) that is also a macroscopic quantum system (10, 11). The simplicity of our partial measurement presents a clear demonstration of this phenomenon (12), shedding light on the physics of quantum measurements.

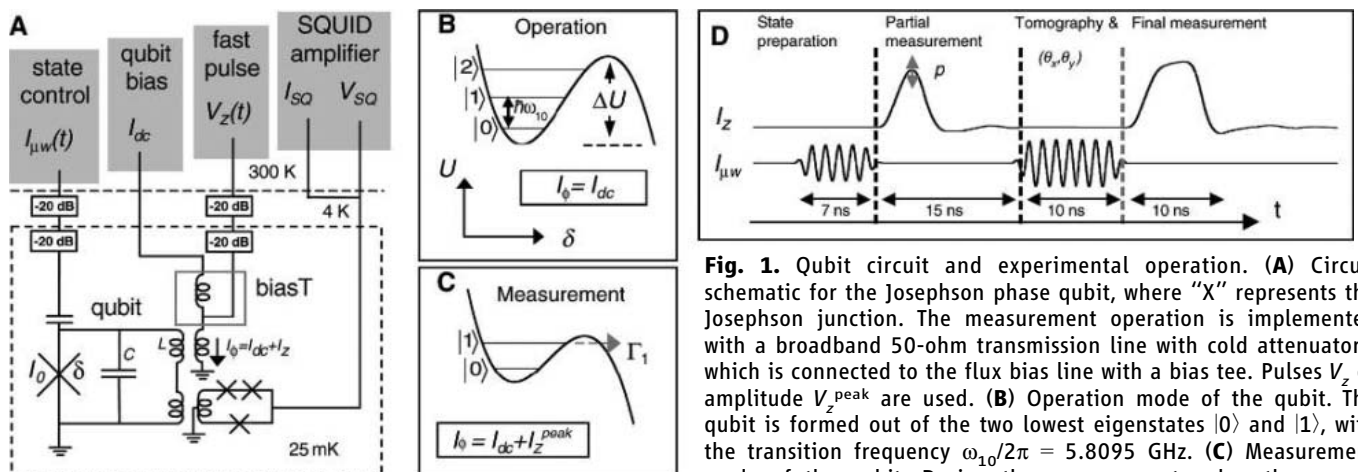
Recent experiments (13–16) with superconducting circuits, fabricated using lithographic techniques, have provided an intriguing link between microscopic quantum states and macroscopic quantum phenomena. Many important coherent effects, familiar from quantum optics and nuclear magnetic resonance explorations, have been reproduced in such devices. Energy relaxation and dephasing of these Josephson qubits have also been extensively studied (6, 7, 17, 18), leading to the

development of various techniques to further enhance the lifetime of the qubit state. However, the delicate issue of measurement (19) and the subsequent evolution of the qubit have received less attention (16, 20–23). Substantial progress has been made to overcome low measurement visibilities (16, 20, 21, 23), measurement back-action (17, 20), short lifetimes of superposition states (5, 16, 23), and difficulties in integrating complex pulse sequences with arbitrary phase and amplitude. Many of these problems are now resolved in the Josephson phase qubit. By using our recent improvements in rapid measurements (16, 22), quantum state tomography (23, 24), and measurement fidelity, we can now explicitly demonstrate the coherent aspects of nonunitary state evolution during a partial measurement. This further places the phase qubit as a major candidate for scalable quantum-information processing in the solid state.

In a schematic of the phase qubit (16, 25) circuit (Fig. 1A), the superconducting phase difference across the Josephson junction (with critical current I_0) is δ , which serves as our quantum variable. A control flux bias is introduced into the inductor L , and the total current $I_\phi = I_{dc} + I_z(t)$ [where I_{dc} is a constant current and $I_z(t)$ is a time-dependent current pulse] biases the junction and adjusts the cubic potential (Fig. 1, B and C). This, in turn, determines the height of the energy-potential barrier ΔU and the transition frequency $\omega_{10}/2\pi$. The qubit state is coherently manipulated by on-resonant microwave-frequency (μW) pulses $I_{\mu\text{w}}$ (in the 5- to 10-GHz range) that drive transitions between the basis states. Smooth control pulses I_z on the bias line (generated from room temperature voltage pulses V_z and a cold μW bias tee) are used to vary the frequency difference ω_{10} adiabatically,

¹Department of Physics and California NanoSystems Institute, University of California, Santa Barbara, CA 93106, USA. ²Department of Electrical Engineering, University of California, Riverside, CA 92521, USA.

*To whom correspondence should be addressed. E-mail: martinis@physics.ucsb.edu



barrier ΔU is lowered so that the tunneling probability of $|1\rangle$ increases. (D) Timing of the experiment. The microwave sequence $I_{\mu\text{w}}(t)$ includes the initial preparatory pulse and the later tomographic pulse. The bias current $I_\phi(t)$ is held at the constant value I_{dc} during the microwave pulses and is pulsed to higher values $I_{dc} + I_z(t)$ for the partial and full measurements. The experimental bias current is shown, including a $\sim 3\%$ ringing after the pulses.

leading to the accumulation of a controlled phase between the $|0\rangle$ and $|1\rangle$ states. When the bias current is pulsed to higher values $I_{dc} + I_{z}^{peak}$ (Fig. 1C), the rate of tunneling Γ_1 of the $|1\rangle$ state out of the metastable qubit potential becomes large. Tunneling is a selective measurement of the $|1\rangle$ state because the rate from the $|0\rangle$ state is typically slower by a factor of about 200. Furthermore, Γ_1 is exponentially sensitive to ΔU , and we may vary the amplitude of the measurement pulse I_{z}^{peak} to tunnel a controlled fraction p of the $|1\rangle$ state population out of the well. Once tunneled, the state decays rapidly to an external ground state. The coherence with the wavefunction component remaining in the qubit well is lost in less than 0.3 ns (25) and constitutes the partial collapse. The two components are distinguished at a later time by

the on-chip superconducting quantum interference device (SQUID) amplifier and read-out circuitry.

The timeline of the experimental sequence is shown in Fig. 1D. We first apply a microwave pulse (typically 7 ns in duration) to prepare the qubit in a known state. This is followed by a short (3.2-ns full-width at half maximum) partial-measurement pulse. The remaining qubit state is then analyzed by a second tomographic microwave pulse (10 ns in duration) followed by a final full-measurement ($p \cong 1$) pulse. For a given initial state and partial measurement, the complete tomographic determination of a state involves scanning over all phases and a range of amplitudes of the tomographic pulse (Fig. 2). For each pixel in the two-dimensional scan of tomography pulses, data are taken 200 times to acquire

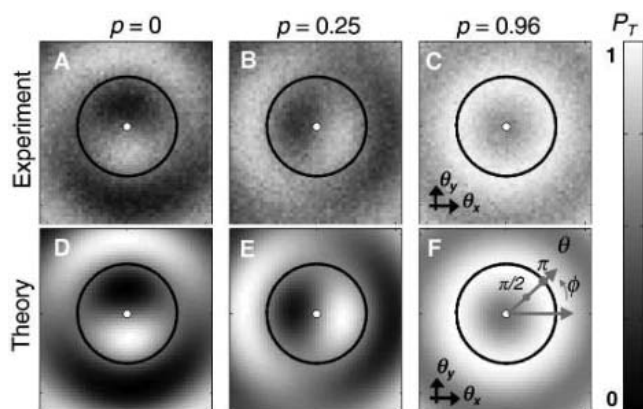
sufficient statistics to determine the resulting qubit populations.

Ideally, the initial qubit state prepared by the first microwave pulse can be described as a superposition $|\psi_0\rangle = \cos(\theta_0/2)|0\rangle + e^{-i\phi_0} \sin(\theta_0/2)|1\rangle$, where θ_0 and ϕ_0 are polar and azimuthal angles on the Bloch sphere (12) in the rotating frame. This pulse is used to define the initial phase $\phi_0 = 0$.

A partial measurement leads to a non-trivial evolution of the quantum state (2, 12), with the net probability for each eventuality on the right,

$$|\psi_0\rangle \rightarrow \begin{cases} |\psi_M\rangle = \frac{1}{N} [\cos(\theta_0/2)|0\rangle + e^{-i\phi_M} \sqrt{1-p} \times \sin(\theta_0/2)|1\rangle] & 1 - p \sin^2(\theta_0/2) \\ \text{tunnel out of qubit well} & p \sin^2(\theta_0/2) \end{cases} \quad (1)$$

Fig. 2. Tomographic scan of the qubit state, initially at $\theta_0/\pi = 0.53 (\pm 0.02)$, following partial measurements. The central spots mark $\theta = 0$ and the circles correspond to $\theta = \pi$. (A to C) Experimental tomographic probabilities P_T for $p = 0, 0.25$, and 0.96 . We observe a clear change in P_T from an antisymmetric ($p = 0$) to a nearly symmetric ($p = 0.96$) distribution. (D to F) Fitted distributions for the data of (A) to (C). The distributions are in marked agreement, given the simplicity of the model. The primary difference is the reduced visibility of the experimental data, which is quantified in Fig. 3C.



where $N = [\cos^2(\theta_0/2) + (1-p)\sin^2(\theta_0/2)]^{1/2}$ is the normalization and ϕ_M is an acquired phase (M indicates measured). Casting $|\psi_M\rangle$ into a normalized form $|\psi_M\rangle = \cos(\theta_M/2)|0\rangle + e^{-i\phi_M} \sin(\theta_M/2)|1\rangle$, we find

$$\theta_M = 2 \tan^{-1} \left[\sqrt{1-p} \tan(\theta_0/2) \right] \quad (2)$$

For the subset of events that do not tunnel from the partial measurement, the change from θ_0 to θ_M constitutes the coherent and non-unitary evolution of the qubit state due to partial measurement. As p approaches unity, the state is fully projected into the state $|0\rangle$, as expected. Notably, because of the normalization factor, the amplitude of the state $|0\rangle$ increases even though this state is not explicitly

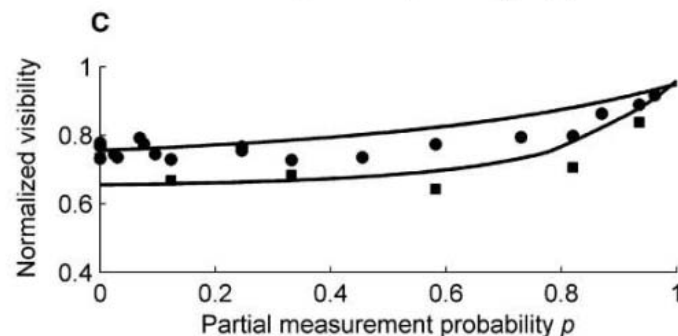
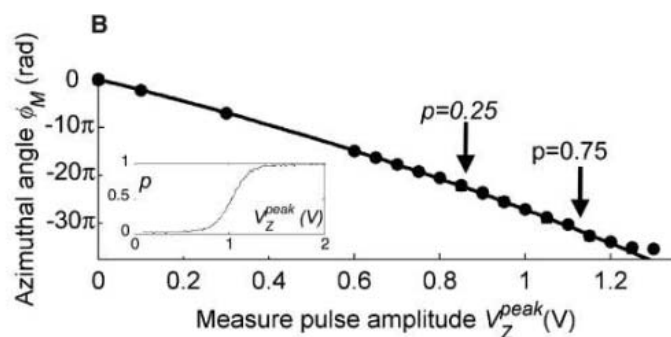
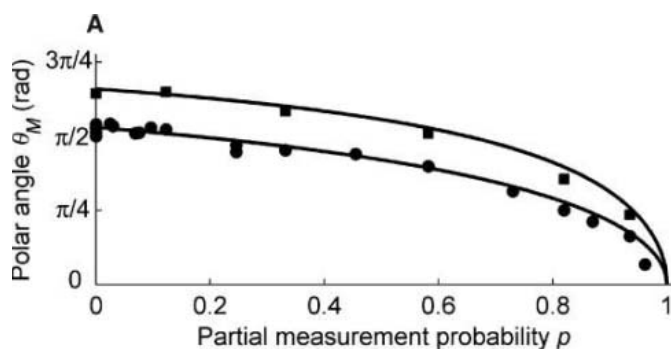


Fig. 3. State evolution, due to partial measurement, for two initial states $\theta_0/\pi = 0.53 (\pm 0.02)$ (circles) and $\theta_0/\pi = 0.66 (\pm 0.02)$ (squares). (A) The evolution of the polar angle θ_M due to a partial measurement with probability p . The experimental measurement is shown to be in close agreement with the ideal partial measurement (solid lines). (B) The evolution of the measurement phase angle ϕ_M as a function of pulse height for both initial states. The phase accumulates in agreement with a simple model integrating over the time-dependent qubit frequency during the pulse (solid line). The initial polar angle θ_0 does not influence this rotation. (Inset) Calibration of the measurement probability p of the $|1\rangle$ state versus pulse amplitude V_z^{peak} . (C) Visibility of the tomographic scan v_{meas} normalized to ideal visibility $v_{ideal} = 1 - p \sin^2(\theta_0/2)$, versus measurement probability p . Data compare well with an optical Bloch equations simulation (solid lines) that uses experimental values for decoherence.

measured. Because these events did not undergo any tunneling or subsequent decay, the accumulated phase ϕ_M can be calculated (in this simple model) from the frequency dependence on the time-varying bias current and is given by $\int_0^{T_p} [\omega_{10}(I_\phi(t)) - \omega_{10}(I_{dc})] dt$, for a pulse of duration T_p .

The resulting state $|\psi_M\rangle$ is determined with the tomographic microwave pulse, which only changes $|\psi_M\rangle$ and does not influence the tunneled population outside the qubit well. The tomography pulse, with components θ_x and θ_y , in the xy plane of the Bloch sphere, rotates the qubit state by an angle $\theta = \sqrt{\{\theta_x^2 + \theta_y^2\}}$ around the direction $\phi = \tan^{-1}(\theta_y/\theta_x)$ (Fig. 2F). The resulting state is therefore given by

$$|\psi_T\rangle = [\cos(\theta_M/2)\cos(\theta/2) - \sin(\theta_M/2)\sin(\theta/2)e^{i(\phi-\phi_M)}]|0\rangle + [\cos(\theta_M/2)\sin(\theta/2) + \sin(\theta_M/2)\cos(\theta/2)e^{i(\phi-\phi_M)}]|1\rangle \quad (3)$$

The final measurement pulse causes tunneling of the $|1\rangle$ state component of $|\psi_T\rangle$ (T indicates tomography). This results in the total measured probability of tunneling

$$P_T = p\sin^2(\theta_0/2) + [1 - p\sin^2(\theta_0/2)]|\langle 1|\psi_T\rangle|^2 = 1 - \frac{1 - p\sin^2(\theta_0/2)}{2} \times [1 + \cos(\theta_M)\cos(\theta) - \sin(\theta_M)\sin(\theta)\cos(\phi - \phi_M)] \quad (4)$$

which includes the original $p\sin^2(\theta_0/2)$ probability from the partial-measurement pulse summed with the additional probability from the final measurement.

The measured distributions of P_T are shown in Fig. 2, A to C, as a function of the tomographic parameters (26). We saw a change in the symmetry of the distributions from an antisymmetric pattern (Fig. 2A) to a symmetric one (Fig. 2C), demonstrating the evolution of the qubit state due to the partial measurement, as θ_M changes continuously from the initial state value of $\sim\pi/2$ to ~ 0 . In addition to the change in θ_M , we observed a rapid and repeatable rotation of the distribution of P_T due to the expected coherent accumulation of phase ϕ_M (Fig. 2B). Theoretical fits to P_T are used to determine θ_M and ϕ_M , with p , θ_0 , ϕ_0 , θ , and ϕ calibrated separately. Fitted distributions, displayed in Fig. 2, D to F, capture the main features of the data.

In the plots of θ_M and ϕ_M versus probability p and pulse amplitude V_z^{peak} (Fig. 3, A and B), the measurements were carried out for two different initial states (\pm SD) $\theta_0/\pi = 0.53 (\pm 0.02)$ and $\theta_0/\pi = 0.66 (\pm 0.02)$. We

observed convincing agreement between Eq. 2 and experiment with no fit parameters, indicating the validity of the nonunitary description of the partial measurement operator in Eq. 1. The agreement (25) of the measured ϕ_M with the expected phase calculated from $\omega_{10}(I_\phi)$ indicates that rapid pulsing of the flux bias can also be used as a high-fidelity z -gate.

This idealized picture of state evolution is not fully realized in our experiment because of energy relaxation and dephasing. Ideally, the measured probabilities in Fig. 2 should oscillate between $p\sin^2(\theta_0/2)$ and unity, leading to a visibility $v_{\text{ideal}} = 1 - p\sin^2(\theta_0/2)$ in P_T . In practice, the experimental visibility is less. Figure 3C shows the measured visibility v_{meas} of the experiment divided by v_{ideal} . We calculated the expected visibility by solving the optical Bloch equations (12) with the use of the experimental parameters of energy relaxation time ($T_1 = 110$ ns) and dephasing time ($T_2 = 80$ ns) obtained in a separate experiment. In the calculation, the measurement is taken to be an instantaneous change of the Bloch vector according to the generalized quantum description of the partial measurement operator acting on a density matrix state (12). The good agreement between experiment and simulation, with no fit parameters, shows that the partial measurement is indeed applying a rapid evolution of the state, in full agreement with Eq. 1, with very little added decoherence (less than 4%). The slight asymmetries in the experimental patterns, barely visible on Fig. 2, A to C, are traced to the effect of the off-resonant state $|2\rangle$ (Fig. 1B), with a population that is measured to never exceed 2% during the entire experiment. Further enhancements in qubit lifetimes and careful shaping of the microwave pulses will allow us to reduce this unwanted occupation even further.

Measurement is a critical component of fault-tolerant quantum computation as it is widely used in quantum error-correction algorithms (27). Instantaneous measurement of a qubit state is typically used to project the remaining encoded qubits to the correct state. This experiment shows in detail that the evolution of the quantum state with measurement is obeying the quantum mechanical predictions. In any realistic, experimental implementation, slow and incoherent measurements will rapidly degrade the success of error correction by adding uncontrolled decoherence. Our measurement scheme is thus attractive because it is both fast and coherent.

Rapid pulsing of the bias for a phase qubit has been shown to be a well-defined quantum operator of partial measurement and high-fidelity z -rotation. The speed, visibility, and

coherence of this measurement technique are expected to be well suited for determining multiple qubit states, including violation of Bell inequalities for two qubit states, and for use in quantum error-correction codes.

References and Notes

- M. Schlosshauer, *Rev. Mod. Phys.* **76**, 1267 (2004).
- J. Dalibard, Y. Castin, K. Mølmer, *Phys. Rev. Lett.* **68**, 580 (1992).
- J. M. Geremia, J. K. Stockton, H. Mabuchi, *Science* **304**, 270 (2004).
- C. Ahn, H. M. Wiseman, G. J. Milburn, *Phys. Rev. A* **67**, 052310 (2003).
- Y. Nakamura, Y. A. Pashkin, J. S. Tsai, *Nature* **398**, 786 (1999).
- D. Vion *et al.*, *Science* **296**, 886 (2002).
- J. M. Martinis, S. Nam, J. Aumentado, C. Urbina, *Phys. Rev. Lett.* **89**, 117901 (2002).
- I. Chiorescu, Y. Nakamura, C. J. P. M. Harmans, J. Mooij, *Science* **299**, 1869 (2003).
- J. Q. You, F. Nori, *Phys. Today* **58**, 42 (2005).
- J. M. Martinis, M. H. Devoret, J. Clarke, *Phys. Rev. Lett.* **55**, 1543 (1985).
- J. R. Friedman, V. Patel, W. Chen, S. K. Tolpygo, J. E. Lukens, *Nature* **406**, 43 (2000).
- M. A. Nielsen, I. L. Chuang, *Quantum Computation and Quantum Information* (Cambridge Univ. Press, Cambridge, 2000).
- A. Wallraff *et al.*, *Nature* **431**, 162 (2004).
- I. Chiorescu *et al.*, *Nature* **431**, 159 (2004).
- W. D. Oliver *et al.*, *Science* **310**, 1653 (2005).
- K. B. Cooper *et al.*, *Phys. Rev. Lett.* **93**, 180401 (2004).
- P. Bertet *et al.*, *Phys. Rev. Lett.* **95**, 257002 (2005).
- J. M. Martinis *et al.*, *Phys. Rev. Lett.* **95**, 210503 (2005).
- A. N. Korotkov, *Phys. Rev. B* **63**, 115403 (2001).
- A. Wallraff *et al.*, *Phys. Rev. Lett.* **95**, 060501 (2005).
- A. Lupascu, E. F. C. Driessen, L. Roschier, C. J. P. M. Harmans, J. E. Mooij, *Phys. Rev. Lett.* **96**, 127003 (2006).
- R. McDermott *et al.*, *Science* **307**, 1299 (2005).
- M. Steffen *et al.*, *Cond. Mater.*, in press; preprint (<http://arxiv.org/abs/cond-mat/0602432>).
- G. M. D'Ariano, M. G. A. Paris, M. F. Sacchi, *Adv. Imaging Electron Phys.* **128**, 205 (2003).
- Materials and methods are available as supporting material on *Science* Online.
- The quantum-state tomography shown here can be implemented in different ways. Typically, only three high-precision measurements are needed for a single qubit. For multiple qubit-state tomography, of course, such a simplified scheme becomes mandatory. However, the full two-dimensional scan allows us to resolve the rotation angle with high precision, determine the visibility shown in Fig. 3C, easily avoid any calibration errors in the microwave frequency, and fully test for proper state rotations.
- P. W. Shor, *Phys. Rev. A* **52**, R2493 (1995).
- We acknowledge S. Waltman and the National Institute for Standards and Technology for support in building the microwave electronics. Devices were made at the University of California at Santa Barbara and Cornell Nanofabrication Facilities, a part of the NSF-funded National Nanotechnology Infrastructure Network. N.K. acknowledges support of the Rothschild fellowship. This work was supported by Advanced Research and Development Activity under grant W911NF-04-1-0204 and NSF under grant CCF-0507227.

Supporting Online Material

www.sciencemag.org/cgi/content/full/312/5779/1498/DC1
Materials and Methods
Fig. S1

21 February 2006; accepted 20 April 2006
10.1126/science.1126475

High-Resolution Thin-Film Device to Sense Texture by Touch

Vivek Maheshwari¹ and Ravi F. Saraf^{1,2*}

Touch (or tactile) sensors are gaining renewed interest as the level of sophistication in the application of minimum invasive surgery and humanoid robots increases. The spatial resolution of current large-area (greater than 1 cm²) tactile sensor lags by more than an order of magnitude compared with the human finger. By using metal and semiconducting nanoparticles, a ~100-nm-thick, large-area thin-film device is self-assembled such that the change in current density through the film and the electroluminescent light intensity are linearly proportional to the local stress. A stress image is obtained by pressing a copper grid and a United States 1-cent coin on the device and focusing the resulting electroluminescent light directly on the charge-coupled device. Both the lateral and height resolution of texture are comparable to the human finger at similar stress levels of ~10 kilopascals.

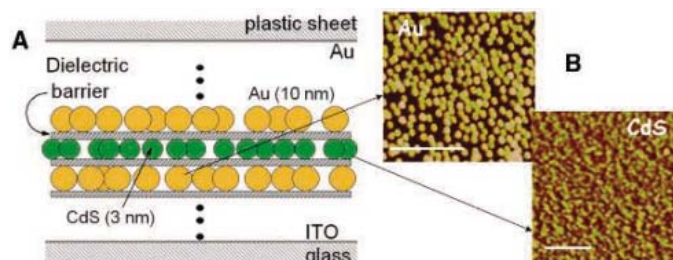
Sensation of touch, primarily the determination of stress distribution over the area of physical contact between the sensor and the object surfaces (1), is a critical component to advance minimum invasive surgical procedures by giving the surgeon a “touch sensation” (2–6) to decipher, for example, cancer tissue (3) and gallstone (2) using the signal from tactile sensor (7). Moreover, there is great interest in developing humanoid robots (8, 9) that can sense shapes (10, 11), textures (12, 13), and hardness (14) and manipulate complex objects (11), which are not readily possible by vision alone. Touch (or tactile) sensors are usually made as micro-electromechanical systems composed of micromachined deformable components (15) or by integrating chip with electronic circuit and strain sensitive materials, such as magento-resistive ceramics (16), piezoelectric polymers (17, 18), and strain sensitive conducting elastomers (19, 20). Tactile sensors from optical data have been demonstrated in which the contact stress distribution is calculated from the change in shape of the deformable sensor surface obtained by a camera (21). For small-area devices, such as an 8 by 8 array of capacitance sensors, spatial resolution of 100 μm is demonstrated (22). However, for large-area devices, ~1 cm² or larger, the spatial resolution for stress distribution is, at best, in the ~2 mm range (20) compared with the ~40-μm resolution achieved by the surface of a human finger (23).

We report a ~100-nm-thick, 2.5-cm² device, based on the principle of electron tunneling, capable of imaging stress distribution with spatial resolution of ~40 μm. The height resolution is <5 μm, comparable to the ~2 μm for a human finger (24). Our device, composed of metal and semiconducting nanoparticles, directly converts local stress into electrolumi-

nescent light and modulation in local current density. Both the electroluminescence intensity and current density are linearly proportional to the local stress.

To demonstrate the high-resolution capability, we image stress by directly focusing the electroluminescent light signal on a charge-coupled device (CCD) camera. The sensitivity or minimum stress required for direct imaging of touch on CCD is ~9 kPa, which is well within the 10 to 40 kPa range that a human finger applies to sense texture and shape (25). To demonstrate the spatial resolution of the device, we use a copper grid to hold the specimen for transmission electron microscope (TEM) analysis. When the Cu grid composed of free-standing 40-μm-wide lines at a pitch of 220 μm is pressed on the sample, the stress distribution from the features produces spatial variation in electroluminescent light that is directly imaged on the CCD. Furthermore, we press a U.S. 1-cent coin against the device and image the stress distribution from the embossing on the coin directly onto the CCD. The fabrication requires no lithography, and the transduction of stress distribution is virtually continuous at 100-nm scale. A simple model based on electron tunneling between the nanoparticle layers and ionic conductivity through the dielectric medium explains the characteristics of the device.

Fig. 1. Multilayer structure of electro-optical device. (A) Schematic of the unit structure of the device showing nanoparticle monolayers spaced by an organic DL composed of polyelectrolytes PSS and PAH. A total of three Au and two CdS



and two CdS nanoparticle monolayers with dielectric barriers are deposited. The top Au electrode is coated with flexible plastic, and the bottom transparent Indium-Tin Oxide (ITO) electrode is on glass. The electroluminescent light from the CdS is measured through the bottom electrode. (B) AFM topography (i.e., height) image after deposition of first Au layer and the first CdS layer after that. The scale is 50 nm.

The device (Fig. 1) consists of alternating layers of Au (10 nm thick) and CdS (3 nm thick) nanoparticles separated by dielectric layers (DL), composed of stacked alternating layers of poly(styrene sulfonate) (PSS) and poly(allylamine hydrochloride) (PAH). All the monolayers of polymer and nanoparticles are deposited from solution using layer-by-layer self-assembly (26, 27). The particular device described here has three Au layers and two CdS layers, with four layers each of PAH and PSS as the interlying DL [see details of structure and process in (28)]. The atomic force microscope (AFM) images in Fig. 1B indicate that the nanoparticles do not form long-range, (electrically) percolating clusters. Consistent with the AFM image, the film is insulating in the in-plane direction, as independently confirmed by measuring two-point electrical continuity using spring-loaded flat Au (pogo) pins.

In the vertical direction, the film is conducting due to tunneling between the Au and CdS layers. Figure 2A shows the current density J through the film as a function of bias V between the bottom ITO and top Au electrode under a uniform compressive stress σ . The uniform stress is applied by placing an optically flat quartz disk on the flexible Au electrode. The nonlinear J - V curve is fit based on a model combining the field-assisted electron tunneling current [i.e., the Fowler-Nordheim equation (29–31)] through the nanoparticles and the ionic (leakage) current due to ions in the polyelectrolyte. According to the relation $J_{\text{tunneling}} = P \exp(-aK/V)$, where a is the (vertical) interparticle distance, K is a critical field for activated tunneling that depends on the work functions of the particles, and P at constant temperature is proportional to V^2 and the number density of carriers for conduction (29, 32). The ionic leakage-current, $J_{\text{leakage}} = V/R$, is due to mobile ions (H^+ , Na^+ and OH^- , Cl^-) in the polyelectrolytes, where R , the ohmic resistance, is proportional to the distance between the electrodes. A three-parameter (i.e., R , aK , and P) fit for three sets of data, with corresponding straight line due to leakage I - V , is an excellent match to the experiment for the whole range of

¹Department of Chemical Engineering, University of Nebraska, Lincoln, NE 68588, USA. ²Edward Via Virginia College of Osteopathic Medicine, Blacksburg, VA 24060, USA.

*To whom correspondence should be addressed. E-mail: rsaraf@unlnotes.unl.edu

V and σ studied (Fig. 2A). The three fitting parameters are self-consistent as applied stress increases (Fig. 2B); R from the fit decreases linearly with σ , implying that the film deforms linearly. The estimated resistivity of $\sim 1.6 \times 10^8 \Omega\text{-m}$ is reasonable for ion conductivity in PSS and PAH under ambient humidity (33, 34). The linear decrease in Ka with σ indicates that the interparticle spacing (i.e., a) also decreases linearly with σ , which is consistent with linear deformation of overall thickness. Assuming a (at $\sigma = 0$) ~ 5 nm, the critical field K of $\sim 10^9$ V/m is reasonable (29, 32). Because P depends on the carrier density, at fixed V , the linear increase in P may be attributed to a linear increase in the number of percolating channels between the electrodes as the film is deformed. Furthermore, although not shown, consistent with the Fowler-Nordheim equation, $P \sim V^2$ (at constant load) for the complete range of operating conditions (>8 V). The curve fit in Fig. 2A indicates that the tunneling process becomes important beyond ~ 8 V (indicated as a box). Electroluminescence will occur only when tunneling through CdS occurs. Hence, the electroluminescence intensity I_{EL} should be

measurable above the bias of $\sim 8 \pm 1$ V. I_{EL} as reported is intensity (in arbitrary units) per 16 by 16 μm pixel of the CCD camera. The noise level based on imaging a blank sample (i.e., dark current) is 1 arbitrary unit. The I_{EL} threshold at ~ 8 V further supports the charge-transport model (Fig. 2C). The average I_{EL} per pixel is limited to 80 kPa because the electroluminescence from the edge of the disk is enhanced as a result of “square-edge-punch” stress concentration (35). Furthermore, as $J_{\text{tunneling}}$ increases exponentially with stress compared with a linear increase for J_{leakage} , at larger bias (i.e., >18 V) tunneling dominates over leakage current. The deformation is reversible with nominal hysteresis (Fig. 2D).

To assess the capabilities of the device for measuring surface topography and texture, a TEM specimen holder from Electron Microscopy Sciences (i.e., a Cu grid) and a U.S. 1-cent coin was pressed against the flexible Au electrode of the device, and the resulting electroluminescent light from the device was focused on the CCD camera below the ITO/glass substrate (Fig. 3A). The embossing of President Lincoln’s head on the coin is apparent

in the stress image obtained on the CCD. The overall intensity of the stress image increases with average stress σ (Fig. 3A). The TEM grid lines have a trapezoidal cross-section with a top base of 40 μm that is in contact with the device, a width of 80 μm at half height, and interline spacing of 230 μm (Fig. 3B, inset, and Fig. 3C). Lines of the Cu grid (seen in the optical microscope image) are clearly resolved in the stress image (Fig. 3B). Comparison between the topography and I_{EL} scan of the TEM Cu grid shows that the flat surface of 40- μm line width in contact with the device is well resolved, leading to a lateral spatial resolution of at least 40 μm .

The remarkable correspondence between the optical microscope image and the stress image seen in Fig. 3, A, D, and E, indicates that the variation in stress distribution caused by the embossing on a U.S. 1-cent coin leads to significant change in local current density, which in turn is manifested as modulation in I_{EL} . The device can decipher fine features, such as wrinkles on the clothing of President Lincoln and the letters “TY” in “LIBERTY,” observed in the optical microscope and the stress image (Fig. 3D). Because the electroluminescence intensity from the device is virtually continuous, the resolution of the stress image is determined by the optics and the CCD camera. For the CCD with a 512 by 512 array of $\sim 16\text{-}\mu\text{m}$ pixels, the I_{EL} is well over noise level (Fig. 3, C, E, and F), indicating that the electroluminescence is enough to achieve lateral spatial resolution of at least $\sim 20 \mu\text{m}$ (as the area of chip and disk are comparable). However, the stress will be “smeared” as a result of the thickness of the flexible Au electrode, leading to higher resolution. Furthermore, from Fig. 3, E and F, height modulation of $\sim 10 \mu\text{m}$ is measurable, indicating that the device is fairly deformable. The high compliance is perhaps due to some interpenetration among the nanoparticle layers. The inset in Fig. 3F shows that the embossing is rough at the micron scales. This local roughness will cause nonuniformity in the surface charge distribution, leading to “hot spots” of high electric field strength. The “pointillist” pressure images are attributed to these hot spots.

The relationship between the optical (i.e., I_{EL}) and electronic (i.e., J) signal from the device pressed by the quartz disk is linear (Fig. 4A), implying that the stress image from either signal would be similar. Above, we have demonstrated the tactile sensor principle by measuring I_{EL} . Extension to a fully electronic device by measuring J , required for certain applications (such as surgery), is possible using standard microelectronic circuitry. For example, an electronic device could be made by self-assembling the multilayer thin-film between mutually perpendicular parallel lines of Au (electrodes) on flexible plastic backing (i.e., flex-circuit). The stress distribution would be

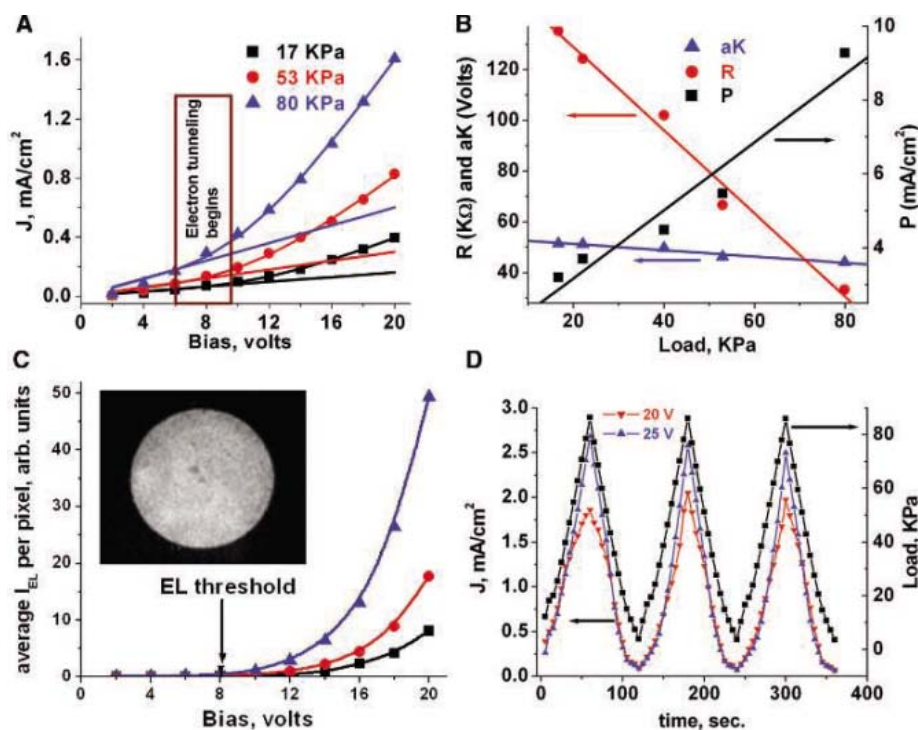


Fig. 2. Electro-optical characteristics of the device and electron-transport mechanism. The device is compressed using an optically flat quartz disk on the flexible Au electrode. (A) J - V data points at various σ . The fitted line is based on a model combining charge transport by electron tunneling and ions. The straight line corresponds to J_{leakage} . The box indicates the expected onset of electroluminescence. (B) The three fitting parameters estimated from fitting the J - V curve show linear dependence, indicating that the deformation is linear with respect to load. (C) The electroluminescence from the CdS nanoparticles for σ in 17 to 80 kPa range commences at ~ 8 V. The inset is the electroluminescence image on the CCD camera below the ITO corresponding to the 1.1-cm-diameter quartz disk pressing the top electrode (Fig. 3A). Uniform light indicates uniform load distribution. The data symbols correspond to Fig. 2A. (D) The current J monitored under dynamic loading of the device at a fixed bias of 20 and 25 V indicates reasonably low hysteresis. The line is to guide the eye.

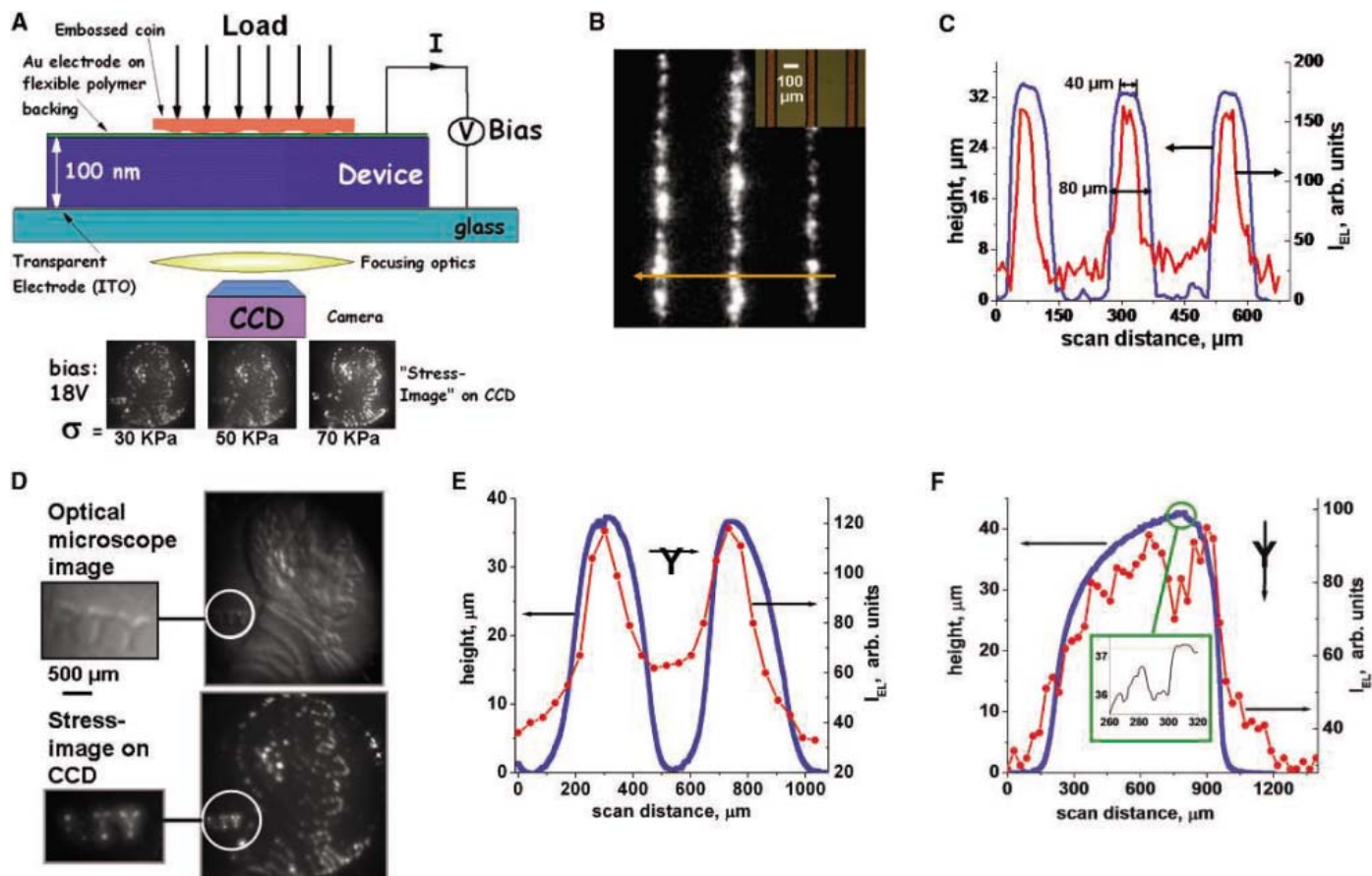


Fig. 3. Characteristics of the pressure imaging device. **(A)** Schematic of the setup to image texture of a metal coin; also shown are the pressure images taken on CCD camera at three different compressive stresses. The diameter of the coin is ~ 2 cm, and the device is a 2.5-cm square. The bias between the coin and the ITO electrode is fixed at 18 V. **(B)** Comparison between optical microscope (inset) and pressure image (at $V = 18$ V and $\sigma = 40$ kPa) of a TEM Cu grid. The horizontal line in the pressure image is the I_{EL} scan

shown in Fig. 3C. **(C)** Comparison between the topographic and I_{EL} scans across the TEM Cu grid. **(D)** Comparison between optical microscope and pressure image (at $V = 18$ V and $\sigma = 30$ kPa) of the coin, showing the finer structure. The magnified image shows the letters "RTY" of the word "LIBERTY" on the coin. **(E)** and **(F)** Comparison between the topographic and I_{EL} scan across letter "Y" of "LIBERTY." The inset of **(F)** shows the local roughness of the coin.

imaged by mapping J at the intersection points of the top and bottom electrode lines (similar to a display device). Both I_{EL} and J increase linearly with σ ; however, the sensitivity to bias for an optical device is larger (by a factor of about 3), which implies that the latter has a larger dynamic range (Fig. 4B). For $I_{EL} \sim 5$ (corresponding to a signal-to-noise ratio of 5) the sensitivity of the optical device is ~ 9 kPa at a bias of 25 V. Assuming a minimum measurable current signal of 1 nA for the electronic device proposed in the inset of Fig. 4A, for the intersection point of $\sim 20 \mu\text{m}^2$ (36) a sensitivity of ~ 10 kPa would be possible. Because the resolution of $20 \mu\text{m}$ is comparable to the CCD pixel size used in the optical device, a spatial resolution of $\sim 50 \mu\text{m}$ at a sensitivity of 10 kPa should be possible for the electronic device.

There are two practical advantages of the described tunneling-based device compared with the reported tactile imaging devices based on deformable membranes or stress-sensitive materials. First, we achieve high sensitivity

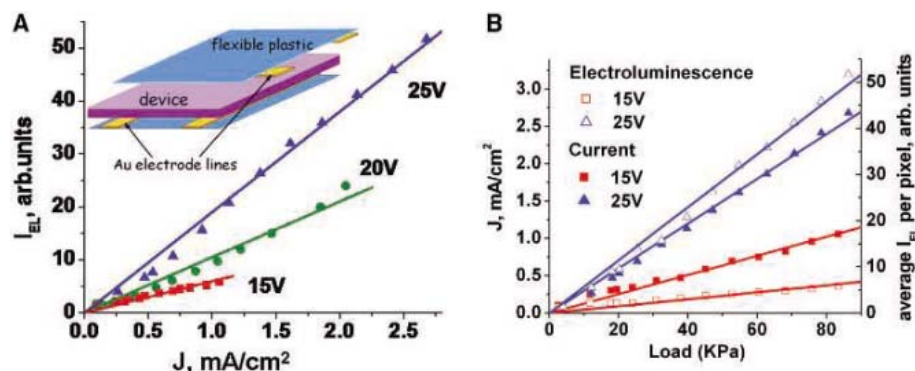


Fig. 4. Comparison of electronic (i.e., current) and optical (i.e., electroluminescence) signals. **(A)** I_{EL} is linearly proportional to J . Each data point is at fixed bias with varying σ . The slope at the three biases are 6.0, 10.5, and 19.0 (arbitrary units) cm^2/mA . The efficiency of the device to convert current to photoluminescence increases with bias as indicated by the slope. **(B)** Both J and I_{EL} increase linearly with σ (i.e., load) for the 15 to 25 V bias range studied. The change in slope as bias increases from 15 to 25 V for J and I_{EL} is 2.34 and 7.63, respectively.

because tunneling depends exponentially on displacement (i.e., strain). Second, the self-assembly process involves no complex lithog-

raphy, making it easier to build the device directly on surfaces of large area and complex shapes.

References and Notes

- G. Robles-De-La-Torre, V. Hayward, *Nature* **412**, 445 (2001).
- S. Matsumoto *et al.*, *Surg. Endosc. Ultrasound Intervent. Tech.* **11**, 939 (1997).
- N. Sakai, M. Tatsuta, H. Yano, H. Iishi, S. Ishiguro, *Gastrointest. Endosc.* **51**, 69 (2000).
- O. Tohyama, S. Maeda, H. Itoh, *IEEE J. Sel. Top. Quant. Electron.* **5**, 115 (1999).
- P. K. Plinkert, I. Baumann, E. Flemming, *Laryngorhinootologie* **76**, 543 (1997).
- P. N. Brett, R. S. Stone, *Proc. Inst. Mech. Eng. [H.]* **211**, 309 (1997).
- The tactile signal may be displayed on a monitor as a digital hardness score (2), or a virtual reality tool similar to the NanoManipulator (37) may be developed. In the NanoManipulator, the force from the manipulator performing nanoscale displacement of molecules is transmitted to a joy stick, giving the operator a "touch sensation" during the manipulation.
- P. Dario, E. Guglielmelli, C. Laschi, *J. Robot. Syst.* **18**, 673 (2001).
- Y. Okumura *et al.*, *Adv. Robot.* **18**, 699 (2004).
- Y. B. Jia, *IEEE Trans. Robot.* **21**, 726 (2005).
- M. Kaneko, K. Tanie, *IEEE Trans. Rob. Autom.* **10**, 355 (1994).
- A. M. Okamura, M. R. Cutkosky, *Int. J. Robot. Res.* **20**, 925 (2001).
- R. Tajima, S. Kagami, M. Inaba, H. Inoue, *Adv. Robot.* **16**, 381 (2002).
- M. Shikida, T. Shimizu, K. Sato, K. Itoigawa, *Sens. Actuators A Phys.* **103**, 213 (2003).
- J. Engel, J. Chen, C. Liu, *J. Micromech. Microeng.* **13**, 359 (2003).
- R. D. Howe, M. R. Cutkosky, *IEEE Trans. Rob. Autom.* **9**, 140 (1993).
- D. De Rossi, F. Carpi, E. P. Scilingo, *Adv. Colloid Interface Sci.* **116**, 165 (2005).
- C. Domenici, D. Derosi, *Sens. Actuators A Phys.* **31**, 97 (1992).
- S. P. Lacour, C. Tsay, S. Wagner, *IEEE Electron Device Lett.* **25**, 792 (2004).
- T. Someya *et al.*, *Proc. Natl. Acad. Sci. U.S.A.* **101**, 9966 (2004).
- N. J. Ferrier, R. W. Brockett, *Int. J. Robot. Res.* **19**, 795 (2000).
- B. L. Gray, R. S. Fearing, *IEEE Int. Conf. Robot. Autom.* **1**, 1 (1996).
- J. W. Morley, A. W. Goodwin, I. Darian-Smith, *Exp. Brain Res.* **49**, 291 (1983).
- R. S. Johansson, R. H. LaMotte, *Somatosens. Res.* **1**, 21 (1983).
- As a finger touches a surface, the fingernail color begins to redden above a threshold force of ~ 0.3 N and completely reddens at ~ 1 N. For ordinary grabbing and sensing operations, the force at the fingertip ranges from 1 to 4 N. Assuming a contact area of ~ 1 cm², a reasonable threshold stress to determine texture by human finger would be in the 10 to 40 kPa range (38).
- G. Decher, *Science* **277**, 1232 (1997).
- C. Y. Jiang, S. Markutsya, Y. Pikus, V. V. Tsukruk, *Nat. Mater.* **3**, 721 (2004).
- Alternating monolayers of Au (10 nm) and CdS (3 to 4 nm) nanoparticles (NP), spaced by a dielectric layer (DL) composed of PSS and PAH, are deposited using a layer-by-layer assembly process by sequentially dipping (26) in four solutions: The 0.1% (by weight) solutions of PSS and PAH of molecular weights 70 and 15 kD have a pH of 8 and 4.2, respectively. The anionic Au and CdS deposition solutions with 10^{12} and 10^{16} particles/ml have a pH of 6 and 4.5, respectively. The deposition time for the polymer monolayer is 30 min each; for the Au and cationic CdS nanoparticles, it is 24 hours and 1 hour, respectively. All the solutions are in DI water (filtered through 20 μ Millipore filter), and each deposition step is followed by a rigorous wash in DI. The chemical structure of DL between Au and CdS nanoparticle monolayers is Au(NP)/PAH/(PSS/PAH)₃/PSS/CdS(NP). The process is initiated by cleaning the 1-inch by 1-inch ITO-coated (400 nm) glass surface in piranha solution (H₂SO₄/H₂O₂; 3:1 by volume) to make the electrode surface negatively charged. The final structure of the device is glass/ITO/DL[Au-NP/DL/CdS-NP/DL]₂/Au-NP/DL/Au-electrode/plastic. The structure of the flexible electrode is Au (200 nm)/Cr (70 nm)/Al (12 μ m)/siloxane rubber (~ 5 μ m). The Au is sputter-deposited on the Al foil with Cr as the adhesion layer. Poly(dimethyl siloxane) is spincoated on the other side for the electrode, followed by UV cross-linking. The resultant free-standing electrode is physically placed on the device with the Au side in physical contact with the device surface.
- R. H. Fowler, L. Nordheim, *Proc. R. Soc. London A* **119**, 173 (1928).
- T. Cassagneau, T. E. Mallouk, J. H. Fendler, *J. Am. Chem. Soc.* **120**, 7848 (1998).
- J. Y. Ouyang, C. W. Chu, C. R. Szmanda, L. P. Ma, Y. Yang, *Nat. Mater.* **3**, 918 (2004).
- S. O. Kasap, in *Principles of Electrical Engineering Materials and Devices, Revised Edition*, S. O. Kasap, Ed. (McGraw Hill, New York, 2000), pp. 284–288.
- D. M. DeLongchamp, P. T. Hammond, *Chem. Mater.* **15**, 1165 (2003).
- M. F. Durstock, M. F. Rubner, *Langmuir* **17**, 7865 (2001).
- K. L. Johnson, *Contact Mechanics* (Cambridge Univ. Press, Cambridge, 1985).
- Recently, 20- μ m device features have been demonstrated on flexible circuits (39).
- A. Seeger *et al.*, *J. Vac. Sci. Technol. B* **19**, 2717 (2001).
- S. A. Mascaro, H. H. Asada, *IEEE Trans. Robot. Autom.* **17**, 698 (2001).
- T. W. Kelley *et al.*, *Chem. Mater.* **16**, 4413 (2004).
- We thank the Office of Naval Research (N00014-01-1-0977) and the National Science Foundation (534812) for financial support.

14 February 2006; accepted 7 April 2006
10.1126/science.1126216

Converting Ceria Polyhedral Nanoparticles into Single-Crystal Nanospheres

Xiangdong Feng,^{1*}† Dean C. Sayle,² Zhong Lin Wang,^{3,4,5*} M. Sharon Paras,⁶ Brian Santora,¹ Anthony C. Sutorik,⁶ Thi X. T. Sayle,² Yi Yang,¹ Yong Ding,³ Xudong Wang,³ Yie-Shein Her¹

Ceria nanoparticles are one of the key abrasive materials for chemical-mechanical planarization of advanced integrated circuits. However, ceria nanoparticles synthesized by existing techniques are irregularly faceted, and they scratch the silicon wafers and increase defect concentrations. We developed an approach for large-scale synthesis of single-crystal ceria nanospheres that can reduce the polishing defects by 80% and increase the silica removal rate by 50%, facilitating precise and reliable mass-manufacturing of chips for nanoelectronics. We doped the ceria system with titanium, using flame temperatures that facilitate crystallization of the ceria yet retain the titania in a molten state. In conjunction with molecular dynamics simulation, we show that under these conditions, the inner ceria core evolves in a single-crystal spherical shape without faceting, because throughout the crystallization it is completely encapsulated by a molten 1- to 2-nanometer shell of titania that, in liquid state, minimizes the surface energy. The principle demonstrated here could be applied to other oxide systems.

For large-scale, wafer-level fabrication of nanodevices and their integration with silicon technology, the surface of a wafer needs to be perfectly flat (on the order of less than 2 to 4 nm) and free from defects. Ceria nanoparticles are a key abrasive nanomaterial for chemical-mechanical planarization (CMP) of ad-

vanced integrated circuits. CMP using nanoparticles accounted for 60% of the \$1 billion market for nanomaterials in 2005 (1, 2). As the size of the integrated circuit architecture decreases for chip miniaturization and nanorization, defects must be reduced by at least 50% to make chip mass-manufacturing viable for each generation.

Crystalline ceria nanoparticles have been synthesized by means of a variety of methods, including room temperature solution precipitation (3, 4), microwave-assisted hydrothermal route (5), hydrothermal crystallization (6), microemulsion (7), mechanochemical processing (8), thermal decomposition (9), aerosol pyrolysis (10, 11), sol-gel method (12), thermal hydrolysis (13), and solvothermal synthesis (14). But ceria nanoparticles synthesized by these techniques are faceted and possess sharp edges, corners, and apexes (15, 16), which are more prone to scratch the silicon wafers and limit the CMP rates. For superior performance, spherical nanoparticles would be ideal because they can act like ball bearings and can polish the silicon surface without scratching it. However, this is a challenge because spherical single-crystal nanoparticles must have energetically unfavorable high-index surfaces.

We produced nanospheres of CeO₂ and Ce_{1-x}Ti_xO₂ (0 ≤ x ≤ 0.25) with a liquid-phase flame spray pyrolysis of solutions of cerium and titanium precursors dissolved in a flammable solvent (i.e., an alcohol) (17, 18) (fig. S1). The alcohol solution of metal precursors is pumped at a rate of 150 g/min into an atomization device that sprays a fine mist into the combustion chamber. The mist is directly ignited by pilot torches in the line of the spray, leading to instantaneous combustion of the metal precur-

sors and generation of the desired metal oxide as a nanoparticulate “smoke.” Depending on experimental conditions, combustion occurs in the range of 1200° to 2500°C. Temperatures are rapidly quenched downstream from the initial combustion zone, leading to a measure of kinetic control over the chemical reaction, crystallization, phase evolution, and particle growth. Due to the short particle residence time, atomic diffusion and particle growth end rapidly after initial particle formation. The product stream (powder plus CO₂ and water vapor) is drawn from the combustion chamber by exhaust fans into powder collectors. The apparatus used for this study can generate nanoparticles at a rate as high as about 300 g/hour.

Pure ceria nanoparticles without doping were synthesized through liquid-phase flame spray pyrolysis of a solution made from dissolving cerium carbonate into propionic acid (19). The nondoped CeO₂ nanoparticles show faceted and occasionally irregular shapes (Fig. 1A), and have a large size variation. Transmission electron microscopy (TEM) images show that each nanoparticle is a single crystal (Fig. 1B). Electron diffraction patterns acquired from dozens of nanoparticles indicate that they are cubic ceria phase with the fluorite (CaF₂)-type structure (Fig. 1C). High-resolution TEM clearly shows that the nanoparticles are dominated by {111} and {001} type of facets and some of them exhibit octahedral and truncated octahedral shape (Fig. 1D). For cubic structured ceria, {111} and {001} are the dominant facets, possibly resulting from low surface energy. The surfaces of the nanoparticles are atomically sharp, abrupt, and clean without visible contaminant (fig. S2). In comparison to image simulation, the (001) surface is likely terminated with oxygen (see the simulated image in fig. S2).

Ceria nanospheres doped with varied amounts of titanium were synthesized through liquid-phase flame spray pyrolysis (L-FSP) of a solution made by dissolving cerium carbonate into propionic acid with stoichiometric amounts of titanium (IV) (triethanolaminate) isopropoxide (20). The cerium oxide containing 6.25 atomic % of Ti is dominated by spherical shapes (Fig. 1E and fig. S3), and each particle is a single crystal (Fig. 1F). High-resolution

TEM shows that each particle is a single crystal with visible {111}, {001}, and high-index facets (Fig. 1G and figs. S4 to S6), and the particle shape is close to being an ideal sphere. The smaller size particles are single crystals and more spherical (Fig. 1H). For larger size nanospheres, the facets are a little more pronounced, and {110} facets can also be identified (Fig. 1I). The crystal lattice extends to the surface of the nanosphere and the surfaces are fairly clean and atomically sharp.

For the ceria nanosphere doped with 12.5 atomic % Ti, the particles are dominated by spherical shape and single crystals (Fig. 2A). High-resolution TEM clearly shows that a large particle is nearly spherical and its surface is covered with a uniform amorphous thin layer (1 to 2 nm) (Fig. 2B). The area of the {111} and {001} facets are largely reduced with an increased formation of high-index planes, conditions required for forming a spherical shape. The characteristics displayed by a smaller size particle are similar to those of the bigger ones (Fig. 2C). Nanospheres of different sizes can be separated by a centrifugal (fig. S7).

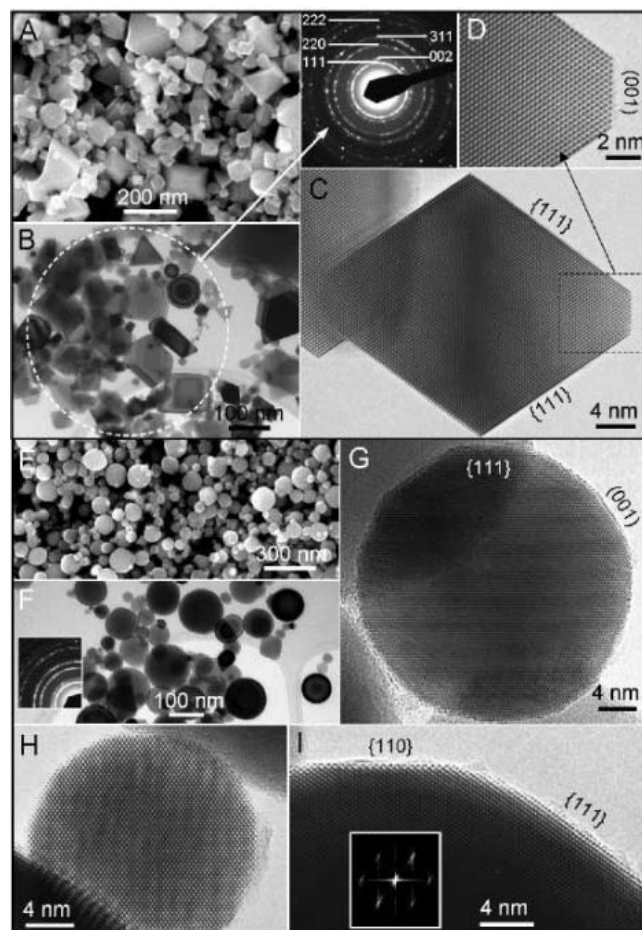
To identify the nature of the surface amorphous layer, chemical maps of Ce and Ti were acquired for the 12.5 atomic % Ti-doped nanospheres with the use of a scanning TEM (STEM) with a probe size of ~1 nm. The mor-

phology and distribution of the nanospheres is displayed in the bright-field STEM image (Fig. 2D), and corresponding maps for Ce and Ti acquired with the use of the x-ray signal emitted from the sample as the probe was scanned across the sample are shown in Fig. 2, E and F, respectively. Ti atoms are distributed at the surface of the particles, and some TiO₂ particles were also found. The data show that the surface amorphous layer is TiO₂.

We performed molecular dynamics (MD) simulations using the DL_POLY code (21) and potential parameters taken from (22, 23) to understand the formation process of the nanospheres. Most atomistic simulations start by proposing a structural model; however, this has the disadvantage of requiring the simulator to choose or design a potentially erroneously structural model. Our strategy involved the simulation of crystallizing nanoparticles in flame by constructing an amorphous/molten precursor that was then crystallized at high temperatures and quenched to room temperature.

At the beginning of the simulation, two identical “cubes” of CeO₂, comprising 15,972 atoms (5324 Ce and 10,648 O), were generated. One cube was doped with 25 atomic % Ti (1330 substitution atoms, located at the surface), whereas the other nanoparticle remained “pure.” Both cubes were first amorphized

Fig. 1. (A to D) Microstructure of CeO₂ nanoparticles without Ti doping. (A) Scanning electron microscopy (SEM) image, (B) low-magnification TEM image, and [(C) and (D)] high-resolution TEM images of the ceria nanocrystals with faceted shapes. The inset between (A) and (D) is an electron diffraction pattern from the area circled in (B). (E to I) Microstructure of CeO₂ nanospheres doped with 6 atomic % of Ti. (E) SEM image, (F) low-magnification TEM image, and [(G) to (I)] high-resolution TEM images of the ceria nanocrystals, showing their spherical shape and single-crystal structure. The inset in (F) is an electron diffraction pattern recorded from the area, showing the cubic ceria structure of the sample. The inset in (I) is a fast Fourier transform of the high-resolution TEM image.



¹Ferro Corporation, 7500 East Pleasant Vally Road, Independence, OH 44131, USA. ²Cranfield University, Defense Academy of the United Kingdom, Shrivenham, Swindon SN6 8LA, UK. ³School of Materials Science and Engineering, Georgia Institute of Technology, Atlanta, GA 30332-0245, USA. ⁴Department of Advanced Materials and Nanotechnology, College of Engineering, Peking University, 100871 Beijing, China. ⁵National Center for Nanoscience and Technology, Beijing 100080, China. ⁶Nanocerex, Inc., 712 State Circle, Ann Arbor, MI 48108, USA.

*To whom correspondence should be addressed. E-mail: shawn.feng@jhresearchusa.com (X.D.F.); zhong.wang@mse.gatech.edu (Z.L.W.)

†Present address: James Hardie Building Products, 10901 Elm Avenue, Fontana, CA 92337, USA.

and then recrystallized at high temperature during the simulation. Further simulation details can be found in (24, 25).

Figure 3A shows a series of images for the cooling of the Ti-doped particle. Figure 3, B to H, shows the (room temperature) structure of the nanoparticles at the end of the simulations. The undoped nanoparticle has an octahedral shape and morphology with $\{111\}$ surfaces, truncated with $\{100\}$ facets, and includes sharp edges and corners. Conversely, the Ti-doped CeO_2 nanoparticle is effectively spherical. Both structures are in accord with our experimentally synthesized nanoparticles (Figs. 1 and 2).

The crystallization process, starting from the amorphous precursor to the final crystalline structure, was then studied by analyzing a movie of the crystallization simulations. In the undoped system, a single, fluorite-structured (CaF_2), crystalline “seed” was observed to evolve “naturally” within the amorphous sea of ions (Ce and O) during the MD simulation. Ce and O surrounding this seed then started to condense onto its surface, propagating the crystallization front, which traverses through the nanoparticle. Moreover, as the crystallization front impinged the surface, the crystallization was observed to evolve energetically stable $\{111\}$ surfaces, resulting in a fluorite-structured single crystal of CeO_2 with $\{111\}$ and $\{100\}$ facets (Fig. 3, B to D). The simulations also revealed that energy was liberated during this process, which reflects the latent heat of crystallization.

Similar to the undoped CeO_2 nanoparticle, the Ti-doped system also evolved a fluorite-structured crystalline seed (Fig. 3A), and the amorphous sea of ions (Ti, Ce, and O) started to condense onto its surface. The amorphous layer has a short-range ordering but lacks a long-range ordering (figs. S8 and S9). The crystallization front traversed through the nanoparticle emanating spherically from the crystalline seed (Fig. 3A) and continued until it consumed the entire CeO_2 core. As the crystallization front impinged on the outer surfaces of the CeO_2 , it did not start to evolve $\{111\}$ and $\{100\}$ because it was enveloped by the amorphous TiO_2 shell. Moreover, as the crystallization front moves out to the surface (TiO_2 region), the TiO_2 does not crystallize; rather, it remains amorphous. This enables the nanoparticle to retain its sphericity, which is driven by the system minimizing its surface energy to facilitate an energetically more stable nanoparticle. This is in contrast to the faceted surfaces, including sharp edges and corners, associated with the undoped CeO_2 nanoparticles.

Our synthetic strategy of generating the nanoparticles in flame at about 2500°C facilitates the crystallization of the cerium oxide (CeO_2 , melting point 2400°C), while maintaining the TiO_2 in a molten state (TiO_2 melting point 1843°C). In particular, the CeO_2 occupies the core region of the nanoparticle and is encapsulated by a TiO_2 shell; limited Ti(IV) is incorporated into the lattice. Here, in contrast to

the undoped CeO_2 system, the CeO_2 core crystallizes while enveloped by a TiO_2 shell. Crucially, because the CeO_2 surfaces are

covered with amorphous TiO_2 as they evolve, the energy difference between different surfaces is no longer notable. Therefore, it is the flame

Fig. 2. Microstructure of CeO_2 nanospheres doped with 12 atomic % of Ti. **(A)** Low-magnification TEM image and **(B and C)** high-resolution TEM images of the ceria nanocrystals, showing their spherical shape and single-crystal structure as well as the amorphous layer on the surface. The inset in **(A)** is an electron diffraction pattern recorded from the area, proving the cubic ceria structure of the sample. **(D to F)** STEM images of the nanocrystals doped with 12 atomic % of Ti, showing the morphology, corresponding Ce distribution map, and Ti distribution map. The nanospheres are dominated by Ce, and the Ti is distributed at the surfaces. The bright clusters seen in **(F)** are precipitated TiO_2 particles. The yellow, red, and green circles represent three corresponding particles that are rich in Ti.

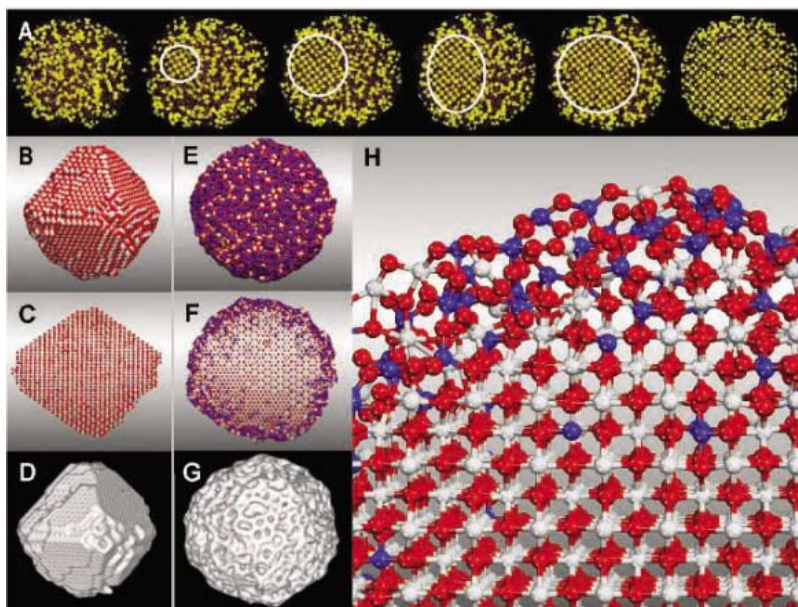
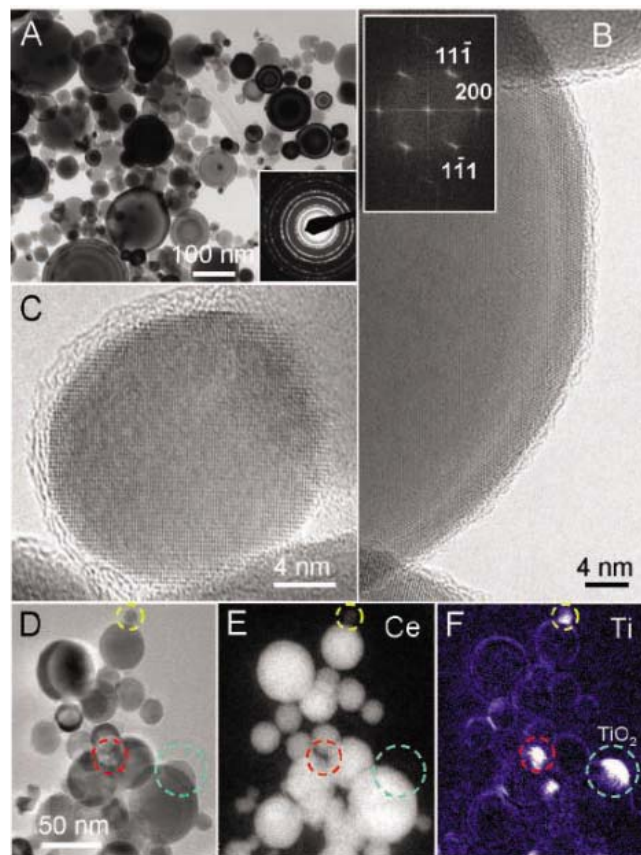
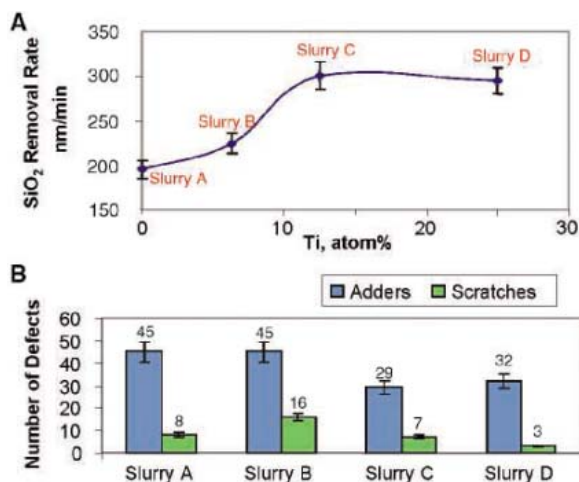


Fig. 3. **(A)** Images taken during a crystallization simulation (Ti-doped CeO_2), showing the initial amorphous precursor (left), evolution, and growth of the seed (circled) to the fully crystalline nanoparticle with amorphous shell (right). **(B to D)** Nondoped nanoparticle. **(E to G)** Ti-doped CeO_2 nanosphere. **(H)** Enlarged segment of the Ti-doped nanosphere. **(B)** and **(E)** Sphere model representation of the atom positions. **(C)** and **(F)** Side view with smaller spheres to view through the nanoparticle. **(D)** and **(G)** Surface rendered model. Cerium is colored white; Ti(IV) is blue, and oxygen is red. The nanoparticles are about 7 to 8 nm in diameter. All images show actual atom positions and are not schematics.

Fig. 4. Chemical-mechanical planarization performance of single-crystal nanospheres of $Ce_{1-x}Ti_xO_2$ ($x = 0 - 0.25$). (A) A comparison of the thermal oxide, SiO_2 , removal rates among the four CMP slurries. (B) A comparison of the defect rates in terms of the total number of the adders that adhere to the pattern wafers after CMP testing and the number of scratches observed. Error bars show means \pm SD.



temperature that facilitates sphericalization of the Ti-doped CeO_2 nanoparticles.

The $Ce_{1-x}Ti_xO_2$ ($0 \leq x \leq 0.25$) nanospheres can be used as an abrasive material for CMP of advanced integrated circuits because of its special spherical and crystalline structure characteristics. The primary function of CMP is to smooth a nominally macroscopically flat wafer at the feature (or microlevel), i.e., planarize features. Therefore, two of the important parameters to evaluate a CMP slurry are the uniform material removal rate across the wafer and the defect concentration of the wafer. Cerium oxide particles have been used in the oxide or silicon wafer polishing because of its selectivity and good oxide-removal rate. The cerium oxide particles have always been crystalline and cubic in structure. It is believed that the relatively sharp edges of the cubic-shaped ceria particles (Fig. 1) may gouge and/or scratch wafer surfaces that are being planarized.

Four CMP slurries were prepared by mixing 1.0 weight % of the spherical single-crystalline $Ce_{1-x}Ti_xO_2$ powders (as synthesized without any particle-size separation) with a chemical additive, proline (table S1) (26). The CMP efficiency is characterized by the removal rate of thermal oxide, SiO_2 (27), which is shown in Fig. 4A and table S1. The rate for the undoped CeO_2 nanoparticles of slurry A is 195 nm/min. The SiO_2 removal rates gradually increased to 224 and 301 nm/min as the Ti content in the nanoparticles $Ce_{1-x}Ti_xO_2$ increased to $x = 0.0625$ and 0.125, respectively. The CMP rate decreased back to 295 nm/min as the Ti content further increased to $Ce_{0.75}Ti_{0.25}O_2$.

The defects generated during CMP are detrimental to the chip production yield, and in the production of advanced integrated circuits the CMP process is used many times. Each successive generation of advanced chips requires at least a 50% reduction in defect rate in order to make the chip mass-manufacturing viable in accommodating the reduced feature sizes and increased number of interconnects in each chip. The adders and, more importantly, the scratches are substantially reduced as the nanoparticles become more spherical and

contain higher Ti contents (Fig. 4B). This can be easily understood in terms of the lack of sharp edges and corners as well as the ability to roll freely on the wafer surface during polishing as the nanoparticles become more spherical.

We report the synthesis of spherical, single-crystal, Ti-doped CeO_2 nanoparticles at large scale (up to 300 g/hour). This was achieved by synthesizing Ti-doped CeO_2 nanoparticles in flame temperatures that facilitate crystallization of the CeO_2 yet retain the TiO_2 in a molten state. The (molten) titanium oxide shell encapsulates the inner ceria core and accommodates a spherical morphology, which minimizes its surface energy, and the nanoparticles become more perfect (spherical) with increasing TiO_2 content. For CMP, spherical, single-crystal Ti-doped CeO_2 nanoparticles are shown to facilitate an 80% reduction in defects and a 50% increase in the silica removal rate. This technology will impact the development of high-quality and high-precision microelectronics and nanoelectronics over large-size wafers. The methodology demonstrated here for synthesizing spherical single-crystal inorganic particles might offer unlimited possibilities in a broad range of fields such as chemical mechanical planarization, photonics, magnetics, catalysis, and inorganic pigment where spherical nanoscale inorganic particles are pivotal.

References and Notes

- R. K. Singh, R. Bajaj, *Mater. Res. Soc. Bull.* **27**, 743 (2002).
- CMP is a process that is used in the semiconductor industry to isolate and connect individual transistors on a chip. The CMP process has been the fastest growing semiconductor operation in the past decade, and its future growth is expected to be equally explosive because of the introduction of copper-based interconnects in advanced microprocessors and other applications of CMP for next-generation nanoscale devices. The CMP slurries typically contain particle-based abrasives, which constituted nearly 60% of the total \$1 billion worldwide market for nanopowders in 2005.
- H. Chen, H. Chang, *Ceram. Int.* **31**, 795 (2005).
- F. Zhang *et al.*, *Appl. Phys. Lett.* **80**, 127 (2002).
- F. Bondioli *et al.*, *J. Mater. Chem.* **15**, 1061 (2005).
- P. Shuk, M. Greenblatt, *Solid State Ionics* **116**, 217 (1999).
- A. Bumajdad, M. I. Zaki, J. Eastoe, L. Pasupulety, *Langmuir* **20**, 11223 (2004).
- T. Tsuzuki, J. S. Robinson, P. G. J. McCormick, *J. Australas. Ceram. Soc.* **38**, 15 (2002).
- Y. Wang, T. Mori, J. Li, T. Ikegami, *J. Am. Ceram. Soc.* **85**, 3105 (2002).
- E. Lopez-Navarrete, A. Caballero, A. R. Gonzalez-Elipe, M. Ocana, *J. Mater. Res.* **17**, 797 (2002).
- T. T. Kodas, M. J. Hampden-Smith, *Aerosol Processing of Materials* (Wiley-VCH, New York, 1999).
- A. Hartridge, A. K. Bhattacharya, *J. Phys. Chem. Solids* **63**, 441 (2002).
- M. Hirano, Y. Fukuda, H. Iwata, Y. Hotta, M. Inagaki, *J. Am. Ceram. Soc.* **83**, 1287 (2000).
- S. Yabe *et al.*, *Kidorui* **34**, 124 (1999).
- Z. L. Wang, X. D. Feng, *J. Phys. Chem. B* **107**, 13563 (2003).
- F. Zhang, Q. Jin, S.-W. Chan, *J. Appl. Phys.* **95**, 4319 (2004).
- C. Bickmore, K. Waldner, D. Treadwell, R. M. Laine, *J. Am. Ceram. Soc.* **79**, 1419 (1996).
- A. C. Sutorik, M. S. Bialist, *Mater. Sci. Forum* **386**, 371 (2002).
- To prepare a ceria stock solution, 3100 g of Propionic Acid (Food Grade, Univar) was heated in a 12-liter round-bottom flask. Once refluxing, a total of 740 g cerium carbonate (99.9995%, Pacific Industrial Development Corporation) was added. The solution was turbid due to insoluble cerium sources and impurities. Once the solution cooled to room temperature, 620 g of deionized water was added, and the solution was vacuum filtered through a 0.2 μ m filter. This stock solution (9 to 10 weight % CeO_2 as determined by mass loss on heating) was then diluted with a mixture of methanol:water (5.2:1 weight ratio) to a final solution of about 5 weight % ceria before flame pyrolysis. The L-FSP operating parameters are pumping rate at 120 g/min, the atomizer oxygen flow at 3.4 m³/hour, and supplemental oxygen flow at 7.0 m³/hour.
- To prepare titanium-doped ceria, $Ce_{1-x}Ti_xO_2$, with $x = 0.0625$, 0.125, and 0.25, stoichiometric amounts of titanium (IV) (triethanolaminato) isopropoxide (TYZOR-TE) from Dupont were added to the ceria stock solution prepared above (23), and the combined solution was diluted to 4 to 5 weight % oxide with methanol:water (5.2:1 weight ratio). The liquid-phase flame spray pyrolysis operating parameters are the same as (23).
- DL-POLY, W. Smith and T. R. Forester, copyright by the council for the Central Laboratory of the Research Councils, Daresbury Laboratory, Daresbury, Warrington, UK, 1996 (www.cse.clrc.ac.uk/msi/software/DL-POLY/).
- T. X. T. Sayle, S. C. Parker, C. R. A. Catlow, *Surf. Sci.* **316**, 329 (1994).
- D. C. Sayle, C. R. A. Catlow, M. A. Perrin, P. Nortier, *J. Phys. Chem. Solids* **56**, 799 (1995).
- T. X. T. Sayle, S. C. Parker, D. C. Sayle, *Chem. Commun.* **21**, 2438 (2004).
- For the Ti-doped nanoparticle, constant volume MD simulation was performed for 7000 ps at 3750 K. The nanoparticle was then quenched: MD simulation was performed for 400 ps at 273 K. Each simulation required about 100 hours with the use of 96 processors of a SunFire Galaxy-class supercomputer.
- W. G. America, S. V. Babu, *Electrochem. Solid-State Lett.* **7**, G327 (2004).
- The SiO_2 film layer for CMP testing was a 1000-nm thermal oxide film on a silicon wafer (of size 200 mm). The wafers were polished with the use of a Strasbaugh 6EC polisher, a Rodel IC1000 pad with Suba IV backing at a down pressure of 3164 kg/m², and a table and head rotation speed of 130 rpm, and slurry flow rate of 150 ml/min. The defect study was performed on patterned Massachusetts Institute of Technology-mask silica wafers by polishing the wafer for 60 s using the above mentioned polishing conditions. The defects were examined under an Applied Materials WF736 defect inspection station. The polishing slurry mixture was adjusted to pH 4 with the use of nitric acid and was then subjected to high-shear mixing for 30 min before polishing. The defect was examined by optical detection techniques. A laser beam illuminated the surface, and the surface roughness was retrieved from the reflected

signals received by several detectors. Our defect detection tool had a minimum size of detection of ~ 0.1 μm in the lateral direction. For the CMP experiments, pre-CMP defect wafer maps were subtracted from post-CMP wafer maps in order to determine the defect adders. Then the wafers were characterized for scratching by means of optical technique.

28. Z.L.W. thanks the NSF (DMR 9733160), the NASA Vehicle Systems Program and Department of Defense Research and Engineering, and the Defense Advanced Research Projects Agency for support. D.C.S. thanks the Cambridge-Cranfield High Performance Computing Facility, Engineering and Physical Science Research Council (GR/S48431/01, GR/S48448/01, and GR/S84415/01) for support.

Supporting Online Material

www.sciencemag.org/cgi/content/full/312/5779/1504/DC1
Figs. S1 to S9
Table S1

3 February 2006; accepted 10 April 2006
10.1126/science.1125767

Regenerative Adsorption and Removal of H_2S from Hot Fuel Gas Streams by Rare Earth Oxides

Maria Flytzani-Stephanopoulos,* Mann Sakbodin, Zheng Wang

Sorbent materials that allow for high-temperature, regenerative desulfurization of fuel gas streams for the anode of a solid oxide fuel cell have been developed. Reversible adsorption of H_2S on cerium and lanthanum oxide surfaces is demonstrated over many cycles at temperatures as high as 800°C , on both fresh or presulfided sorbents, and at very high space velocities. The adsorption and desorption processes are very fast, and removal of H_2S to sub-parts per million levels is achieved at very short (millisecond) contact times. Any type of sulfur-free gas, including water vapor, can be used to regenerate the sorbent surface. Preferably, the anode off-gas stream is used to sweep the desorbed H_2S to a burner.

Conversion of heavy fuels to a hydrogen-rich gas mixture to power solid oxide fuel cells (SOFC) is a cleaner and more efficient way to generate energy than the direct combustion of the fuel, but heavy liquid fuels and coal contain organosulfur compounds that are difficult and expensive to fully remove before fuel reformation. Critical developments will include sulfur-resistant catalysts for the reformers as well as sulfur sorbents that can be regenerated and that operate at temperatures in the range of 650° to 800°C without any performance degradation. Installed upstream of the SOFC anode, the sorbent will protect the nickel-based anode material from sulfidation, which causes irreversible fuel cell power losses.

Sorbents that can be used at SOFC temperatures regenerate poorly, which is a serious drawback that has plagued each of the single- or mixed-oxide combinations that has been considered for hot fuel gas desulfurization. Because of the deterioration of the sorbent structure over time, none of the proposed sorbent materials has become commercially viable (1).

The rare earth oxides, especially lanthanum and Ce(III) oxides, have excellent sulfidation thermodynamics in realistic reformat gas compositions, such as the ones produced by steam reforming, autothermal reforming, or partial oxidation of heavy oils, diesel, jet fuels, or by coal gasification (1–4). However, if bulk or deep sulfidation of the sorbent is allowed to proceed, the cyclic performance is quickly

degraded because of complexities in regeneration, most notably structural changes occurring during the transformation of the sulfided sorbent back to the oxide phase (5–13).

We report on a different approach to this problem: We used only the surface of the sorbent in sulfidation and regenerated only the surface of the sorbent upon saturation. By using very high space velocities or short contact times of the gas with the sorbent in regeneration (14), bulk regeneration of the sorbent with its attendant structural complexities is prevented. An added benefit of this approach is a very small footprint of the sorber and regenerator

units, which is highly desirable for small-scale applications of fuel cells, such as those used in confined locations and for auxiliary power units.

Figure 1A shows the changes in H_2S concentration for the cyclic sulfidation-regeneration of presulfided lanthanum oxide sorbent particles (<53 μm) loaded in a packed-bed reactor run isothermally at 800°C and at a gas hourly space velocity of $400,000$ hour^{-1} at standard temperature and pressure (STP). An expanded view of the H_2S concentration profile in one cycle of sulfidation/regeneration is shown in Fig. 1B. The sorbent had a surface area ($\pm\text{SD}$) of 3.5 ± 0.6 m^2/g at the test conditions (Table 1). The gas mixture composition was chosen to simulate the exit gas stream of a catalytic partial oxidation reformer of a heavy fuel oil, such as JP-8. An exaggerated amount of H_2S (0.1 volume %) was used to shorten the length of each cycle. The carrier gas was He rather than N_2 , but this did not affect the results. We also found that substituting H_2 and H_2O , respectively, for CO and CO_2 in the fuel gas had no effect on the adsorption efficiency and sulfur capacity of the sorbent.

Regeneration was conducted in the same fuel gas mixture by switching off the H_2S feed gas. Other gas mixtures can be used to regenerate the sorbent surface equally efficiently (14, 15). The breakthrough time at 1 part per million (ppm) H_2S was the same for all 15 cycles shown in Fig. 1C. The surface sulfur capacity at breakthrough of 1 ppm of H_2S was 0.9 mg sulfur per gram sorbent ($\text{S}/\text{g}_{\text{sorbent}}$). Thus, lanthanum oxide can be used to

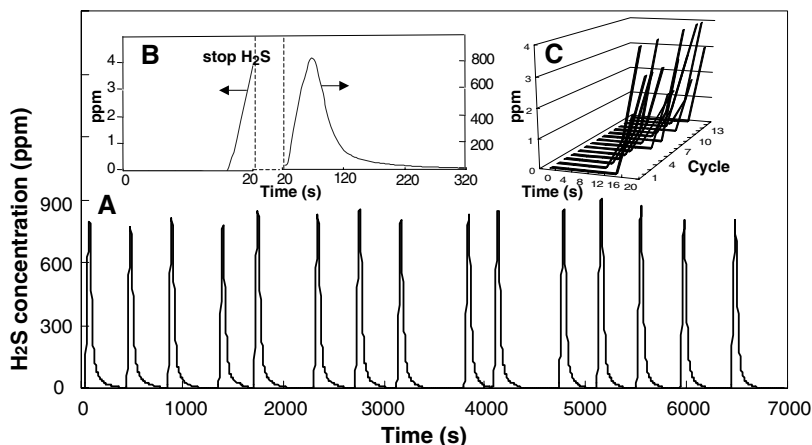


Fig. 1. (A) Consecutive sulfidation and regeneration of presulfided La_2O_3 in a packed-bed reactor with the use of simulated reformat gas at 800°C . Switch to desorption at 4 parts per million by volume (ppmv) H_2S . Sulfidation: 0.1% H_2S –20% H_2 –20% CO –1% CO_2 –10% H_2O –He, space velocity = $400,000$ hour^{-1} . Regeneration: 20% H_2 –20% CO –1% CO_2 –10% H_2O –He, space velocity = $400,000$ hour^{-1} . (B) Expanded view of the H_2S concentration profile in one cycle of sulfidation and regeneration of presulfided La_2O_3 . (C) H_2S breakthrough curves in successive sulfidation cycles of presulfided La_2O_3 .

Department of Chemical and Biological Engineering, Tufts University, Medford, MA 02155, USA.

*To whom correspondence should be addressed. E-mail: maria.flytzani-stephanopoulos@tufts.edu

reversibly and very efficiently adsorb H_2S from reformat gas mixtures at 800°C to protect the anode of an SOFC. Similar results were obtained with ceria, doped ceria, mixtures of lanthana and ceria, and copper-containing ceria (1, 15).

Temperature-programmed desorption (TPD) of H_2S from the surface of the same presulfided lanthana sample (Fig. 2) shows that the H_2S adsorption takes place over a wide temperature range. Of importance to the SOFC application, we found reversibly bound H_2S on this material in the temperature range of 650° to 800°C , which matches the operating temperature of the SOFC. The total amount of H_2S (~ 1.5 mg $\text{S}/\text{g}_{\text{sorbent}}$) desorbed in TPD is higher than the amount adsorbed in each sulfidation half-cycle at the conditions of Fig. 1, because the latter took place in the presence of 10% water vapor. These results demonstrate that presulfided lanthana sorbents actually retain reversible surface sulfur adsorption capacity over a wide temperature window. Similar data were obtained with ceria-rich sorbents (15). As indicated by the TPD analysis, lanthana can also be used at lower temperatures as a regenerable sulfur sorbent. Cyclic performance data at 400°C are shown in figs. S5 and S6 (15). Rare earth oxides should prove a good sorbent choice for regenerative fuel gas desulfurization over the extended temperature range of 350° to 800°C , and for all types of fuel cells.

Stable sulfur loadings at 1 ppm H_2S breakthrough (Table 1) were measured at different sulfidation space velocities, but the same regeneration space velocity [$80,000$ hour $^{-1}$ (STP)], over three different presulfided sorbents. The surface area (10.2 ± 0.4 m $^2/\text{g}$) of the presulfided CeO_2 was about three times as high as that of the presulfided lanthana, but its sulfur capacity did not scale with the surface area, indicating an effect of sorbent surface composition on the H_2S adsorption equilibrium. Of greater practical importance is the observation that a variation of the gas hourly space velocity in the range of $80,000$ to $400,000$ hour $^{-1}$ had no effect on the sulfur capacity of any of the sorbents listed in Table 1. Only the breakthrough time changed, inversely proportional to the space velocity. Thus, adsorption of H_2S is indeed a very fast process limited only by the supply of the adsorbate.

Table 1. Stabilized surface sulfur capacities at 1 ppm H_2S breakthrough for different sulfidation space velocities (S.V.). Presulfidation: 0.25% H_2S –50% H_2 –He, S.V. = 12,000 hour $^{-1}$, $T = 800^\circ\text{C}$. Sulfidation: temperature $T = 800^\circ\text{C}$, 0.1% H_2S –50% H_2 –10% H_2O –He. Regeneration: $T = 800^\circ\text{C}$, 50% H_2 –10% H_2O –He, S.V. = 80,000 hour $^{-1}$. Surface areas are shown \pm SD.

Sorbents	Sulfur loading at 1 ppmv H_2S breakthrough (mg $\text{S}/\text{g}_{\text{sorbent}}$) at sulfidation S.V. =		Surface area (m $^2/\text{g}$)	
	80,000 hour $^{-1}$	160,000 hour $^{-1}$ or 400,000 hour $^{-1}$	After presulfidation	After cyclic tests
CeO_2	1.00	1.20*	10.2 ± 0.4	9.8 ± 0.2
Ce70\%LaO_x	1.20	1.30†	9.2 ± 0.3	8.5 ± 0.2
La_2O_3	0.80	0.90†	3.5 ± 0.6	3.4 ± 0.5

*S.V. = 160,000 hour $^{-1}$ (STP). †S.V. = 400,000 hour $^{-1}$ (STP).

The regeneration times in each of the 15 cycles shown in Fig. 1A are 8 to 10 times as long as the sulfidation times. At first glance, this is a drawback, because it would require multiple beds for a continuous cyclic process. However, delayed regeneration was due to re-adsorption of the eluted H_2S on the subsequent layers of sorbent in the packed bed.

The desorption rate of H_2S from the sorbent surface is actually very fast. To compare the time constants of adsorption and desorption, we used another reactor setup that avoids re-adsorption of eluted H_2S on subsequent sorbent layers as occurs in a packed bed reactor. Here, a thermogravimetric analyzer (TGA) was used with a few milligrams of the sorbent powder loaded as a thin layer on quartz wool in the quartz pan of the TGA. The weight change of the sorbent was recorded as a function of the gas composition. After sulfidation was carried out for 100 s, H_2S was switched off and the 50% H_2 –3% H_2O –He gas mixture continued to be supplied at the same flow rate, effectively removing the adsorbed H_2S (Fig. 3A). Alternatively, both the H_2S and H_2 were switched off and water vapor in He was used for sorbent regeneration in Fig. 3B. The total gas flow rate was 500 ml/min (STP) for both sulfidation and regeneration. The gas mixtures used in the TGA tests contained no CO or CO_2 , and only $\sim 3\%$ water vapor was carried in by saturation of the feed gas at ambient conditions, simplifying the operation of the TGA. These choices do not affect the sorbent's ability to regenerate. If water competes with H_2S for adsorption sites, the use of a lower concentration of water will slightly improve the rate of adsorption and the sulfur loading. Indeed, the stable sulfur capacity of the sorbent in the TGA tests is twice as high (1.8 mg $\text{S}/\text{g}_{\text{sorbent}}$) as the one measured at the conditions of Fig. 1 or Table 1. The important key finding from the TGA tests, however, is the demonstration that the time constants of sulfidation and regeneration are similar and very short (<1 ms) (Fig. 3). Hence, with proper choice of sorber design—for example, by using thin wall coatings of sorbent on a honeycomb monolith—re-adsorption of H_2S will be greatly suppressed, and just two units of sorbent alternating between the H_2S adsorption and desorption modes would suffice.

The sulfided lanthanide oxide sorbents can be regenerated with an oxidative gas mixture (1). Notably, however, any gas composition can be used to regenerate the saturated sorbent surface, including water vapor, a hydrogen-rich gas, inert gases, and water vapor and air mixtures (fig. S2) (15). When an oxidizing gas is used to regenerate the sorbent, some of the eluted sulfur from a packed-bed of sorbent is in the form of SO_2 (1, 15) (fig. S2).

Water vapor alone can be used to remove the H_2S from the lanthana sorbent (Fig. 3B). The use of water to sweep away the desorbed H_2S in the regeneration step is practical for many power-generation systems. In the case of an SOFC, a simple and very attractive regeneration scheme would be to pass the anode off-gas (largely composed of water vapor and some unconverted fuel gas) over the saturated sorbent to sweep away H_2S . This gas stream is typically taken to a combustor where any unconverted fuel is fully burned and the heat is supplied to the primary fuel reformer. In the burner, H_2S will be oxidized to SO_2 , which would be emitted with the exhaust gases if it met the required emission standards or

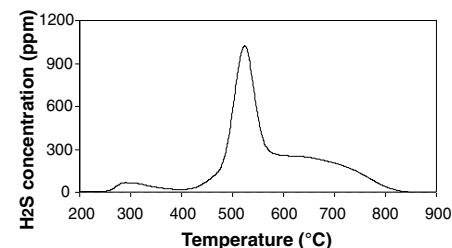


Fig. 2. TPD of H_2S from presulfided La_2O_3 . Adsorption gas: 0.25% H_2S –50% H_2 –He, flow rate = 50 ml/min. Desorption gas: 50% H_2 –He, flow rate = 50 ml/min, heating rate = $10^\circ\text{C}/\text{min}$.

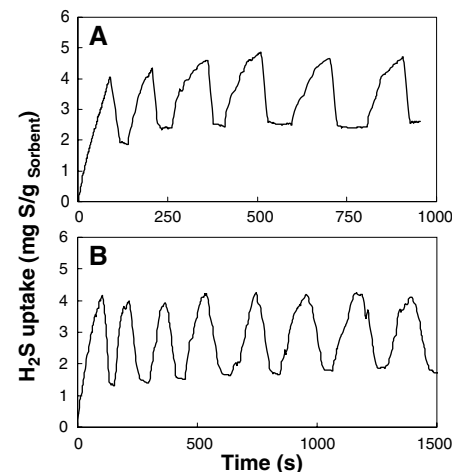


Fig. 3. Cyclic sulfidation and regeneration of presulfided La_2O_3 in a thermogravimetric analyzer at 800°C . Sulfidation gas composition: 0.1% H_2S –50% H_2 –3% H_2O –He. Regeneration gas in (A) is 50% H_2 –3% H_2O –He and in (B) is 3% H_2O –He.

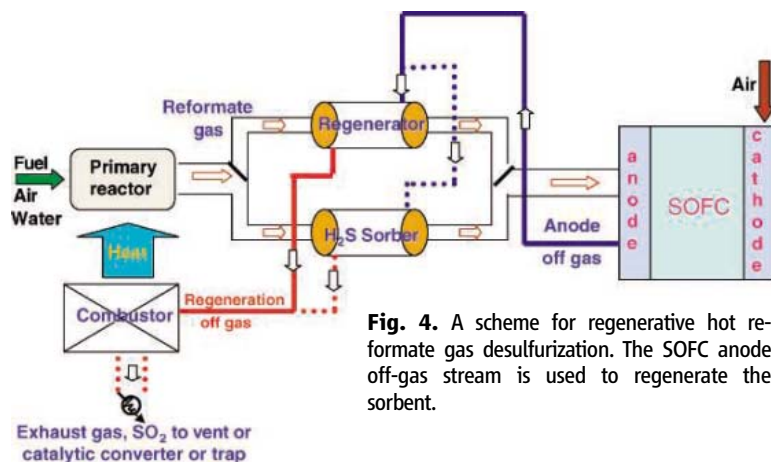


Fig. 4. A scheme for regenerative hot reformat gas desulfurization. The SOFC anode off-gas stream is used to regenerate the sorbent.

otherwise would be trapped or converted as appropriate.

Figure 4 shows a conceptual flowchart of fuel reforming for SOFC use, including regenerative desulfurization over a lanthanide oxide sorbent in the temperature range of 650° to 800°C. This shows that all of the SOFC anode off-gas stream can be used to regenerate the sorbent surface. That is, no split streams are required, because regeneration can take place at high space velocity that corresponds to using the whole anode off-gas stream over the saturated sorbent. This design also avoids the use of a new gas stream, such as air and its attending compressor equipment, for the regeneration step. The dual sorber and regenerator units can be made as small as desired for different applications. In certain designs, some of the anode off-gas may be directed straight to the reformer to add steam to the fuel-reforming process. In such cases, a split stream of the anode off-gas would be used to regenerate the sorbent units.

Various configurations of reactors can be envisioned for the desulfurization system. Because of its low pressure drop, a ceramic honeycomb monolith with the sorbent coated as a thin layer on the channel walls is considered a suitable choice. Sizing the reactor volume for a 5-kilowatt electric (kWe)-rated SOFC, at a 400,000 hour⁻¹ space velocity, a 0.2-liter monolith (0.02-liter sorbent) can be used in each of the two (sorber and regenerator) units (16). The corresponding switch time for a gas containing 500 to 50 ppm H₂S would be 0.5 to 5 min, respectively (16). For a first-order process, the lower the content of H₂S in the fuel gas, the lower the sulfur capacity will be. This was not considered in the above estimate because a compensating effect can come from the use of sorbents with much higher surface area than the one used here. The flexibility that this design entails should be of interest to any scale of power generation, but more importantly to limited-footprint applications, such as auxiliary power units, portable fuel cells, and confined-space installations.

References and Notes

- Z. Wang, M. Flytzani-Stephanopoulos, *Energy Fuels* **19**, 2089 (2005).
- I. Barin, F. Sauert, E. Schultze-Rhönhof, S. S. Wang, *Thermochemical Data of Pure Substances Part I/Part II* (Verlag Chemie, Weinheim, Germany, 1993).
- I. Barin, O. Knacke, *Thermochemical Properties of Inorganic Substances* (Springer-Verlag, New York, 1973).
- I. Barin, O. Knacke, O. Kubaschewski, *Thermochemical Properties of Inorganic Substances: Supplement* (Springer-Verlag, New York, 1977).
- S. Lew, A. F. Sarofim, M. Flytzani-Stephanopoulos, *Ind. Eng. Chem. Res.* **31**, 1890 (1992).
- Z. Li, M. Flytzani-Stephanopoulos, *Ind. Eng. Chem. Res.* **36**, 187 (1997).
- M. Kobayashi, M. Flytzani-Stephanopoulos, *Ind. Eng. Chem. Res.* **41**, 3115 (2002).
- J. H. Swisher, J. Yang, R. P. Gupta, *Ind. Eng. Chem. Res.* **34**, 4463 (1995).
- R. V. Siriwardane, J. A. Poston, G. Evans, *Ind. Eng. Chem. Res.* **33**, 2810 (1994).

- M. Kobayashi, H. Shirai, M. Nunokawa, *Ind. Eng. Chem. Res.* **41**, 2903 (2002).
- E. Garcia, J. M. Palacios, L. Alonso, R. Moliner, *Energy Fuels* **14**, 1296 (2000).
- K. W. Yi, E. Podlaha, D. P. Harrison, *Ind. Eng. Chem. Res.* **44**, 7086 (2005).
- W. J. W. Bakker, F. Kapteijn, J. A. Moulijn, *Chem. Eng. J.* **96**, 223 (2003).
- M. Flytzani-Stephanopoulos, Z. Wang, M. Sakbodin, PCT Patent Application No. PCT/US05/40488; filed 8 November 2005.
- Materials and methods are available as supporting material on Science Online.
- Approximately 50 liters/min H₂ (STP) per 5 kWe is required for a Polymer Electrolyte Membrane (PEM) fuel cell (17). Taking this as the basis for an SOFC, a flow rate of 125 liters/min reformat gas with 40% H₂ will be required to power a 5-kWe SOFC. At space velocity = 400,000 hour⁻¹, about 20 cm³ of sorbent or 200 cm³ monolith volume (larger by a factor of 10) will be required. For two units, 400 cm³ would be required. The switching time, *t*, is estimated for a sorbent density of 2 g/cm³ and for a surface sulfur capacity of 1 mg S/g_{sorbent}. Based on the mass balance, the following equation can be established: (500 or 50 × 10⁻⁶) × 125 liters/min × *t* = [1 mg S/g_{sorbent} (2 g/cm³ × 20 cm³)]/32,000 mg/mol × 22.4 liters/mol. Thus, *t* = 0.5 min for 500 ppm H₂S or 5 min for 50 ppm H₂S-laden fuel gas.
- F. Barbir, *PEM Fuel Cells Theory and Practice* (Elsevier Academic Press, Burlington, MA, 2005).
- This work was supported by the Army Research Laboratory, Power and Energy Collaborative Technology Alliances (CTA) program.

Supporting Online Material

www.sciencemag.org/cgi/content/full/312/5779/1508/DC1

Materials and Methods

Figs. S1 to S6

Table S1

References

1 February 2006; accepted 13 April 2006

10.1126/science.1125684

Near-Synchronous Interhemispheric Termination of the Last Glacial Maximum in Mid-Latitudes

Joerg M. Schaefer,^{1*} George H. Denton,² David J. A. Barrell,³ Susan Ivy-Ochs,^{4,5} Peter W. Kubik,⁶ Bjorn G. Andersen,⁷ Fred M. Phillips,⁸ Thomas V. Lowell,⁹ Christian Schlüchter¹⁰

Isotopic records from polar ice cores imply globally asynchronous warming at the end of the last glaciation. However, ¹⁰Be exposure dates show that large-scale retreat of mid-latitude Last Glacial Maximum glaciers commenced at about the same time in both hemispheres. The timing of retreat is consistent with the onset of temperature and atmospheric CO₂ increases in Antarctic ice cores. We suggest that a global trend of rising summer temperatures at the end of the Last Glacial Maximum was obscured in North Atlantic regions by hypercold winters associated with unusually extensive winter sea ice.

Terminations of asymmetric 100,000-year glacial cycles represent one of the most fundamental climate signals of late Quaternary time (1). Isotopic compositions in Antarctic ice cores and in benthic foraminifera from marine sediment cores show well-defined changes beginning between about 19 × 10³ to 17 × 10³ years ago (ka) (2), interpreted to

represent the onset of the termination of the Last Glacial Maximum (LGM) (3–7). In contrast, Greenland ice cores register continued stadial cold conditions between 17 ka and 14.7 ka (8, 9). At the same time, North Atlantic sediments reveal a major pulse of iceberg discharge (10) accompanied by a near-shutdown of the meridional overturning circu-

lation (MOC) (11). We used ^{10}Be chronologies of mid-latitude moraines to investigate this puzzle of asynchrony between Antarctic and Greenland climate signals early in the last termination. We focused on mid-latitude mountain valley glaciers and outlet glaciers of localized ice caps, rather than continental glaciers (e.g., the Cordilleran and Laurentide ice sheets). Moraines formed by glacier advance and retreat, reflecting variations in temperature and precipitation, sensitively record climate change [e.g., (12, 13)]. Mid-latitude glacial deposits afford an opportunity to constrain interhemispheric comparisons of climate change. The LGM is represented in formerly glaciated regions by a prominent set of morphologically distinct moraines (Fig. 1 and figs. S1 and S2). Within the last decade, surface exposure dating (SED), by measurement of in situ-produced cosmogenic nuclides in boulders on moraine surfaces, has afforded new capabilities for quantifying glacial histories (14).

We present a compilation of new and published ^{10}Be data from deposits formed at the start of the termination of the LGM, focusing on a comparison of the inner LGM moraines in southern and northern mid-latitudes. Buildup of ^{10}Be in surface boulders is assumed to have commenced as soon as glaciers retreated from these inner moraines. In each region, we infer that such recession marks the onset of the last termination. The key questions we investigate are as follows: (i) When did the LGM termination begin in the mid-latitudes of both hemispheres? (ii) How does the timing of this termination compare to events recorded in polar ice cores? (iii) Do the mid-latitudes yield evidence that may help to solve the puzzle of inter-polar asynchrony during the early part of the last termination?

From southern mid-latitudes, we present a glacial geomorphology map (Fig. 1) and ^{10}Be chronology (table S1) from Lake Pukaki, Southern Alps, New Zealand. We then compare the ^{10}Be results with previously published moraine chronologies from southeastern Australia (15, 16) and Lago Buenos Aires in northern Patagonia (17). The moraine chronologies from northern mid-latitudes include new ^{10}Be data from Bloody Canyon on the

eastern flank of the Sierra Nevada (fig. S2 and table S2), together with published chronologies from the Fremont Lake basin in the Wind River Range of Wyoming (18), the Wallowa Mountains in Oregon (19), and the northern Yellowstone ice cap in Montana (20), all in the United States of America. We also discuss published ^{10}Be dates from moraines in northern Switzerland (21). For details of all field sites, see Supporting Online Material (SOM) Text.

Characteristically, mid-latitude LGM glacial sequences were deposited by large, low-gradient valley glacier systems that formed well-preserved moraine belt(s) that are several kilometers wide. Substantial lakes commonly lie inboard of the inner LGM moraine(s), attesting to notable glacier retreat at the LGM termination. In these settings, the most precise moraine chronology records are from New Zealand (Fig. 1 and fig. S1), southeastern Australia (15, 16), Wind River Range (18), and Wallowa Mountains (19). Other

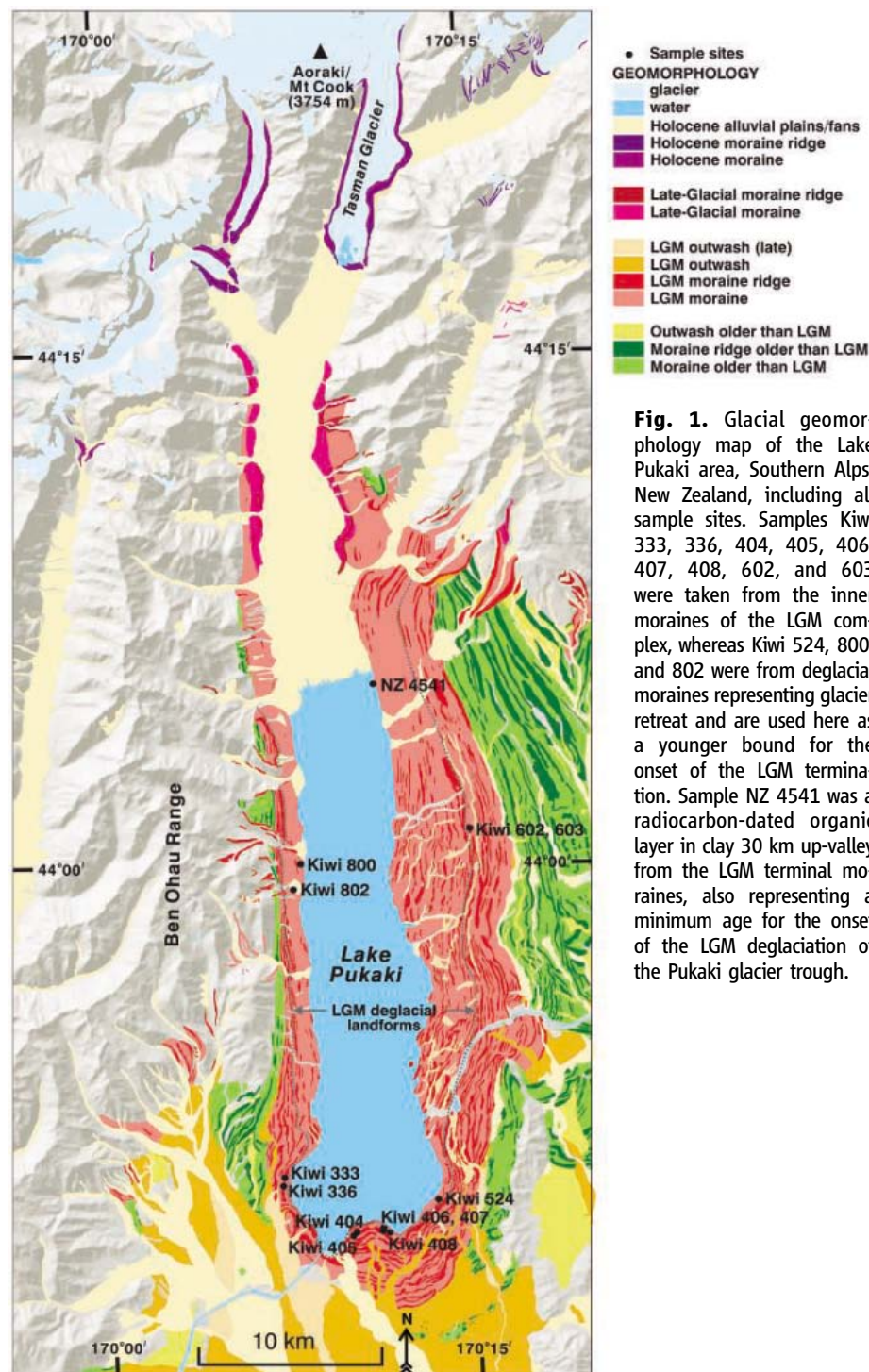


Fig. 1. Glacial geomorphology map of the Lake Pukaki area, Southern Alps, New Zealand, including all sample sites. Samples Kiwi 333, 336, 404, 405, 406, 407, 408, 602, and 603 were taken from the inner moraines of the LGM complex, whereas Kiwi 524, 800, and 802 were from deglacial moraines representing glacier retreat and are used here as a younger bound for the onset of the LGM termination. Sample NZ 4541 was a radiocarbon-dated organic layer in clay 30 km up-valley from the LGM terminal moraines, also representing a minimum age for the onset of the LGM deglaciation of the Pukaki glacier trough.

¹Lamont-Doherty Earth Observatory (L-DEO), Palisades, NY 10964, USA. ²Department of Earth Sciences and Climate Change Institute, University of Maine, Orono, ME 04469, USA. ³GNS Science, Dunedin, New Zealand. ⁴Institute of Particle Physics, Eidgenössische Technische Hochschule (ETH) Hoenggerberg, 8093 Zürich, Switzerland. ⁵Geographisches Institut, Universität Zürich-Irchel, CH-8057 Zürich, Switzerland. ⁶Paul Scherrer Institute, c/o Institute of Particle Physics, ETH-Hoenggerberg, 8093 Zürich, Switzerland. ⁷University of Oslo, 0316 Oslo, Norway. ⁸New Mexico Tech, Socorro, NM 87801, USA. ⁹University of Cincinnati, Cincinnati, OH 45221, USA. ¹⁰Universität Bern, Geologisches Institut, CH-3012 Bern, Switzerland.

*To whom correspondence should be addressed. E-mail: schaefer@ldeo.columbia.edu

locations discussed here display either closely clustered moraines [e.g., Yellowstone Ice Cap (20)] or a single prominent moraine representing the late LGM [e.g., Bloody Canyon (fig. S2)]. In the latter case, LGM moraine formation was predominantly by vertical accretion, with the earlier LGM tills lying buried in the moraine core and the youngest LGM tills forming the ground surface. For all sites except northern Switzerland, the sampled boulders lie on the inner moraines adjacent to an LGM glacier trough that was evacuated by ice at the beginning of the termination. The Swiss study (21) provided a chronology for an outermost LGM moraine, thus yielding a maximum age constraint on the last termination.

The 64 ¹⁰Be dates used for this mid-latitude review are summarized in Table 1 and Fig. 2 (the dates are listed individually in tables S1 to S3, the latter including an additional 41 ¹⁰Be dates from tropical regions). The internal consistency between the ¹⁰Be chronologies from the various mid-latitude inner LGM moraines is striking on the basis of both mean values and oldest values of the respective age populations (14). The Southern Hemisphere mean SED ages for the onset of the LGM termination are 16.8 × 10³ years (ky) [southeastern Australia (15, 16)], 17.4 ky [Lago Buenos Aires, Patagonia (17)], and 17.4 ky (Lake Pukaki, New Zealand). The Patagonian study is based on only two samples and thus is complemented by the LGM chronology from the nearby Chilean Lake District (42°S, 73°W) (13). On the basis of geomorphic mapping and a detailed radiocarbon chronology of glacial deposits, we dated the beginning of the last termination in the Chilean Lake District at 14,700 carbon-14 years before the present (¹⁴C yr B.P.) (22), corresponding to about 17,900 calendar years (IntCal04). The overall mean of these ages is 17.3 ky.

The ¹⁰Be exposure ages of inner LGM moraines in the Northern Hemisphere range from 16.3 ky [northern Yellowstone Ice Cap (20)] to 17.8 ky (Bloody Canyon, Sierra Nevada). The ¹⁰Be ages from the terminal LGM moraine at Bloody Canyon, the Tioga 3 moraine, agree with earlier ³⁶Cl chronologies given in (23) (table S4). The northern Yellowstone data afford the youngest ages in this survey. However, recently published ¹⁰Be dates from eastern Yellowstone Ice Cap moraines yield ages that are 5 to 10% older (24). For the conclusions drawn below it is not critical whether the northern Yellowstone data are included, but we consider it appropriate for consistency to retain them in the evaluation. Compatible with the geomorphic position of the sampled boulders, the ¹⁰Be dates from the outer LGM moraines of the Rhone Glacier system at Wangen an der Aare, northern Switzerland (21), yield the oldest mean age of 19.3 ± 1.8 ky, representing an older bound for the termination. A close minimum age for the last termination of 14,600 ¹⁴C yr B.P., corresponding to 17,700 calendar years, was reported by Lister

Table 1. Comparison of ¹⁰Be data for the inner LGM moraines in southern and northern mid-latitudes. Means are nonweighted; uncertainties are 1σ standard deviation. The SH mean and the NH mean represent the mean and the 1σ standard deviation of the mean ages of each individual study in the respective hemisphere. We include the oldest age of the age populations from each locality as a conservative maximum for the formation age of the respective moraine (14).

Site	Position	Mean age (ky)	"Oldest" age (ky)	Comment	Reference
<i>Southern Hemisphere</i>					
Lake Pukaki, New Zealand	44°S/170°E 550–770 m	17.4 ± 1.0	19.3 ± 1.0	Seven samples (table S1)	This study
Southeastern Australia	36°–43°S/145°–148°E 600–2000 m	16.8 ± 1.3	19.1 ± 1.8	19 samples	(15, 16)
Lago Buenos Aires, Patagonia	46.5°S/71°W 430–455 m	17.4 ± 1.9	18.8 ± 1.5	Two samples	(17)
Chilean Lake District	41°S/73°W	17.9 ± 0.4		72 ¹⁴ C calibrated ¹⁴ C age	(22)
SH mean		17.3 ± 0.5	19.1 ± 0.3		
<i>Northern Hemisphere</i>					
Bloody Canyon, Sierra Nevada	38°N/119°W 2350–2450 m	17.8 ± 1.5	19.7 ± 1.2	Four samples (table S2)	This study
Fremont Lake Basin, Wind River Range, Wyoming	43°N/109°W 2250–2400 m	17.6 ± 0.8	18.7 ± 0.6	10 samples	(18)
Wallowa Mountains, Oregon	45°N/117°W 1400–1560 m	16.8 ± 0.8	18.0 ± 0.8	9 samples out of 15	(19)
Northern Yellowstone Ice Cap, Montana	45°N/111°W 1530–1560 m	16.3 ± 1.2	18.8 ± 1.6	Nine samples	(20)
Northern Switzerland	47°N/8°E 580–610 m	19.3 ± 1.8	20.9 ± 0.9	Four samples	(21)
NH mean		17.1 ± 0.7	18.8 ± 0.7	Including Yellowstone (Excluding Yellowstone)	
		(17.4 ± 0.5)	(18.8 ± 0.9)		

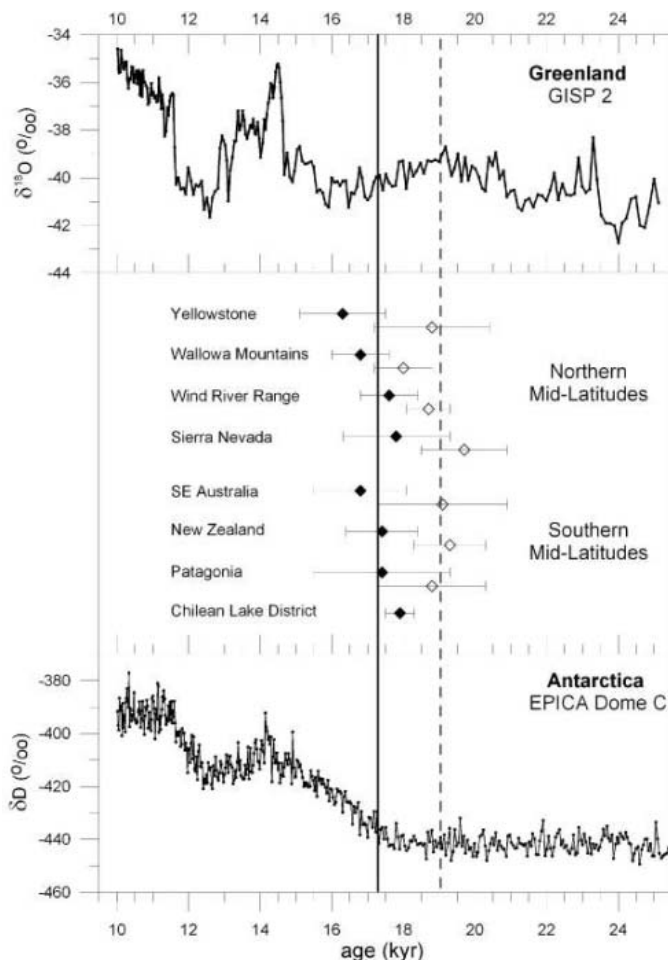
et al. (25) from a sediment core in nearby Lake Zurich on the basis of a twig recovered just above an ice-rafted sediment layer deposited when the ice evacuated the basin. The Northern Hemisphere mean of SED ages for the onset of the termination, including the northern Yellowstone data, is 17.1 ky. Excluding the northern Yellowstone data, the mean is 17.4 ky: Both are indistinguishable from the Southern Hemisphere mean of 17.3 ky.

The timing of the beginning of the LGM termination of mid-latitude glaciers shows remarkable regional, hemispheric, and inter-hemispheric consistency despite the varied geographic, geological, glaciological, and micro-climatic settings. Therefore, we conclude that the climate change driving the termination was of interhemispheric character. A recent study from the tropics further strengthens this conclusion. Smith *et al.* (26) reported ¹⁰Be dates of moraines in Peru (5°S) and Bolivia (15°S). They showed an early LGM maximum extent before marine isotope stage 2, but the innermost LGM termination moraines yielded a nonweighted mean of 17.3 ± 1.9 ky (41 of 50 samples from six moraines, i.e., nine outliers excluded; table S3), indistinguishable from the mid-latitude data (Table 1).

Although reduced annual precipitation could have triggered LGM glacier retreat, large spatial and temporal variabilities in precipitation patterns imply that very complex changes in atmospheric circulation are needed to account for a uniform interhemispheric change in precipitation. However, glacier mass balance is highly sensitive to temperature during the summer ablation season and much less responsive to winter temperatures [e.g., (27)]. A striking consistency between temperature rise since the middle of the 19th century and retreat of 169 different glacier systems from Little Ice Age moraines (28) highlights glacier sensitivity to temperature changes. The retreat of LGM ice and abandonment of LGM moraines had many morphological similarities, albeit on a much larger scale, to the present-day glacier recession from Little Ice Age moraines. We conclude that global rise in summer temperatures provides a straightforward explanation for the observed synchronous interhemispheric, mid-latitude glacier retreat at the end of the LGM.

The onset of the LGM termination in mid-latitude moraines and in polar ice core records is compared in Fig. 2. A warming trend began in Antarctica sometime between 19 ky and 17 ky ago (2, 5). The start of mid-latitude LGM glacier termination in both hemispheres is

Fig. 2. Comparison of the onset of the mid-latitude glacier LGM termination with polar ice core records. Plotted for each moraine record are (i) the mean age (solid diamonds) and (ii) the oldest ^{10}Be boulder age of each moraine set (open diamonds). Error bars indicate 1σ standard deviation and 1σ analytical uncertainty, respectively. The solid vertical line is the mean of all individual mean ages (17.2 ky); the dotted vertical line is the mean age of all the oldest ^{10}Be ages [19 ky, see text and (14)]. No substantial warming was indicated in the isotopic record from Greenland at that time (8), whereas isotopes implied that temperatures started to rise in Antarctica (5) in near-synchrony with the onset of mid-latitude glacier LGM termination.



concordant with steadily rising temperatures recorded in Antarctica and also correlates well with the onset of the glacial-interglacial transition defined by benthic foraminifera records [e.g., (7)]. In near-synchrony with temperature increase, Antarctic ice core greenhouse gas concentrations also started to rise [e.g., (29)], implying that CO_2 could have been the globalizer of the LGM termination.

The paleoclimate records in the North Atlantic region tell a very different story during the glacial-interglacial transition (Fig. 2). Slight temperature rise may have begun in Greenland as early as 24 ka (30), but the dramatic warming event at the onset of the Bölling occurred at 14.7 ka (31), unambiguously later than the mid-latitude glacier termination of the LGM. Similarly, marine sediment records show that the MOC in the North Atlantic almost shut down between 17.5 ka and 14.7 ka (11), which is consistent with sea surface cooling [e.g., (32)] and a continuation of cold stadial conditions in Greenland (9) during this interval. Thus, the Greenland ice cores do not express the inter-hemispheric summer temperature rise at the beginning of the last termination, evident in mid-latitude moraine records.

On the basis of our data, we extend the reasoning given in (33) and suggest the following

hypothesis to explain this anomaly. During the LGM, large volumes of ice were stored in Northern Hemisphere ice sheets. A global summer temperature warming initiated mid-latitude glacier retreat and also destabilized the Northern Hemisphere ice sheets, particularly the seaward-draining ice streams, triggering large-scale iceberg discharge into the North Atlantic commencing at about 17.5 ka (10). The resulting freshwater input to the North Atlantic zone of deep-water formation slowed and almost stopped MOC (11), resulting in a substantial spread of North Atlantic sea winter ice. As a consequence of an extensive sea-ice cover, the North Atlantic climate between about 17.5 and 14.7 ka (i.e., early in the LGM termination) was characterized by hypercold winters (33), which markedly reduced mean-annual temperatures and obscured the global summer temperature increase registered by mid-latitude glacier recession. By this scenario, the Greenland isotopic records attest to regional North Atlantic conditions during a termination that was nearly global in character.

References and Notes

1. W. S. Broecker, J. van Donk, *Rev. Geophys. Space Phys.* **8**, 169 (1970).
2. Because of the use of different age models, the onset of the last termination in Antarctic ice cores has been assigned

ages of about 19 ky for Byrd [Greenland Ice Sheet Project (GISP) 2 chronology] (3), 18 ky for the Byrd core [Greenland Ice Core Project (GRIP) chronology] (4), 17.5 ky for European Project for Ice Coring in Antarctica (EPICA) Dome C (EDC1 time scale) (5), and 17 ky for Vostok (GT4 time scale) (6).

3. T. Blunier, E. J. Brook, *Science* **291**, 109 (2001).
4. T. Blunier *et al.*, *Nature* **394**, 739 (1998).
5. J. Jouzel *et al.*, *Geophys. Res. Lett.* **28**, 3199 (2001).
6. J. R. Petit *et al.*, *Nature* **399**, 429 (1999).
7. N. J. Shackleton *et al.*, *Nature* **335**, 708 (1988).
8. M. Stuiver, P. M. Grootes, *Quat. Res.* **53**, 277 (2000).
9. This period is called Greenland Stadial 2a by (34) and corresponds to the European Oldest Dryas interval.
10. G. C. Bond, R. Lotti, *Science* **267**, 1005 (1995).
11. J. F. McManus, R. Francois, J.-M. Gherard, L. D. Keigwin, S. Brown-Leger, *Nature* **428**, 834 (2004).
12. C. M. Clapperton, *Quat. Sci. Rev.* **9**, 299 (1990).
13. G. H. Denton, Ed., *Geogr. Annal.* **81A**, 105 (1999).
14. Materials and methods are available as supporting material on Science Online.
15. T. T. Barrows, J. O. Stone, L. K. Fifield, R. G. Cresswell, *Quat. Sci. Rev.* **21**, 159 (2002).
16. T. T. Barrows, J. O. Stone, L. K. Fifield, R. G. Cresswell, *Quat. Res.* **55**, 179 (2001).
17. M. R. Kaplan, R. P. Ackert, B. S. Singer, D. C. Douglass, M. D. Kurz, *Geol. Soc. Am. Bull.* **116**, 308 (2004).
18. J. C. Gosse, J. Klein, E. B. Evenson, B. Lawn, R. Middleton, *Science* **268**, 1329 (1995).
19. J. M. Licciardi, P. U. Clark, E. J. Brook, D. Elmore, P. Sharma, *Geology* **32**, 81 (2004).
20. J. M. Licciardi *et al.*, *Geology* **29**, 1095 (2001).
21. S. Ivy-Ochs, J. M. Schaefer, P. W. Kubik, H.-A. Synal, C. Schlüchter, *Eclogae Geol. Helv.* **97**, 47 (2004).
22. G. H. Denton *et al.*, in (13), p. 107.
23. F. M. Phillips *et al.*, *Science* **274**, 749 (1996).
24. J. M. Licciardi, K. L. Pierce, M. D. Kurz, R. C. Finkel, *Geol. Soc. Am. Abstr. Prog.* **37**, 41 (2005).
25. G. Lister, *J. Quat. Sci.* **7**, 187 (1988).
26. J. A. Smith, G. O. Seltzer, D. L. Farber, D. T. Rodbell, R. C. Finkel, *Science* **308**, 678 (2005).
27. J. Oerlemans, *Glaciers and Climate Change*, A. A. Balkema Publishers, Ed. (Lisse, Netherlands, 2001), pp. 148.
28. J. Oerlemans, *Science* **308**, 675 (2005); published online 3 March 2005 (10.1126/science.1107046).
29. E. Monnin *et al.*, *Science* **291**, 112 (2001).
30. R. B. Alley, E. J. Brook, S. Anandakrishnan, *Quat. Sci. Rev.* **21**, 431 (2002).
31. J. P. Severinghaus, E. J. Brook, *Science* **286**, 930 (1999).
32. E. Bard, F. Rostek, J.-L. Turon, S. Gendreau, *Science* **289**, 1321 (2000).
33. G. H. Denton, R. B. Alley, G. C. Comer, W. S. Broecker, *Quat. Sci. Rev.* **24**, 1159 (2005).
34. M. J. C. Walker *et al.*, *Quat. Sci. Rev.* **18**, 1143 (1999).
35. J.M.S. thanks the Comer Science and Educational Foundation and the Lamont Climate Center for support of this study. GNS Science contributed to the glacial geomorphic mapping in New Zealand and the participation of Barrell. NOAA supported the participation of G.H.D., B.G.A., and T.V.L. C.S. thanks the Schweizer Nationalfonds. We are grateful to V. Rinterknecht and R. Schwartz for help with the ^{10}Be samples from New Zealand and California and thank J. Licciardi, G. Winckler, B. Newton, and two anonymous reviewers for constructive comments. This is L-DEO contribution number 6898.

Supporting Online Material

www.sciencemag.org/cgi/content/full/312/5779/1510/DC1

Materials and Methods

SOM Text

Figs. S1 to S3

Tables S1 to S4

References

21 November 2005; accepted 25 April 2006
10.1126/science.1122872

Changes in North Atlantic Radiocarbon Reservoir Ages During the Allerød and Younger Dryas

Stein Bondevik,^{1*} Jan Mangerud,² Hilary H. Birks,³ Steinar Gulliksen,⁴ Paula Reimer⁵

Estimates of the radiocarbon age of seawater are required in correlations between marine and terrestrial records of the late Quaternary climate. We radiocarbon-dated marine shells and terrestrial plant remains deposited in two bays on Norway's west coast between 11,000 and 14,000 years ago, a time of large and abrupt climatic changes that included the Younger Dryas (YD) cold episode. The radiocarbon age difference between the shells and the plants showed that sea surface reservoir ages increased from 400 to 600 years in the early YD, stabilized for 900 years, and dropped by 300 years within a century across the YD-Holocene transition.

The difference between the ¹⁴C age of the ocean and that of the atmosphere is called the marine reservoir age. It varies over time as a result of changes in the ¹⁴C production rates in the atmosphere (1), the circulation of the oceans (2), and the ventilation between the ocean and the atmosphere (3, 4). Any radiocarbon age of a marine organism has to be corrected for a marine reservoir age in order to compare it with terrestrial and ice-core records. Today, the sea surface reservoir age along Norway's western coast is 360 ± 20 years (5).

For the final millennia of the last glaciation, ¹⁴C ages of dated marine sequences commonly conflict with those from ice-core records. It has been suggested that this discordance reflects changes in the reservoir ages (6, 7). However, for the period from 14,000 to 11,000 years ago, only a few reservoir ages have been measured in the North Atlantic. These have been obtained by the use of tephra layers to correlate between ¹⁴C dated-marine and terrestrial sequences (3, 8–10).

We calculated a sequence of reservoir ages from the relatively warm Bølling/Allerød period, through the cold Younger Dryas (YD), and into the present interglacial by dating terrestrial plant fragments and marine shells from the same sediment cores (Fig. 1). The cores were collected from two basins, which are now bogs 7 to 10 m deep, on the outermost western coast of Norway, at Kulturmyra (62°20'N, 5°39'E) and Kvaltjern (60°25'N, 4°59'E). These were marine bays in the late-glacial period. Distinct changes in lithology are seen at the Preboreal-YD-Allerød transitions (Fig. 1) (9, 11). The mud from the cores contained both terrestrial plant

fragments, either blown or washed in from adjacent land, and in situ marine shells (Fig. 1 and fig. S1).

We limited ¹⁴C dating to the best material. For terrestrial dates, we selected delicate plant fragments identified as terrestrial plants (tables S1 and S2), such as moss stems and leaves (fig. S1), that are unlikely to have been reworked or in transit across the land's surface before deposition in the basins (11). Most of the marine samples selected were articulated or whole individual shells to avoid problems with re-orientation and were from suspension feeders to avoid species that consumed organic matter from the underlying sediments (5, 12). However, some intervals contained only shell fragments. As a test, we dated shell fragments that were spatially close to the articulated shells and found that some of the shell fragments were significantly older, indicating redeposition, whereas other fragments yielded ages similar to those of the articulated shells (Fig. 2A).

Both the δ¹³C (table S1 and S2) and δ¹⁸O measurements (11) showed that the shells calcified in marine water of high salinity, with very little addition of fresh water. The obtained reservoir ages are thus representative of the open ocean (11). Hydrographic stations near the studied sites show that modern salinity in the area stays between 31 and 33 parts per thousand throughout the year (13). There is no relationship between the δ¹³C measurements and the observed changes in reservoir ages (fig. S2).

The distance between the marine ¹⁴C age-depth curve and the terrestrial ¹⁴C age-depth curve in Fig. 2 shows the main changes of the reservoir ages. Before the YD, the curves are approximately 300 to 400 years apart, but the separation of the curves increases to a maximum of 600 years in the mid-YD, close to the age of the Vedde Ash Bed. From there and into the Preboreal, the curves approach each other to a distance of about 350 years. Our smoothed terrestrial curve in Fig. 2A resembles the tree-ring curve (black curve in Fig. 3A) but has too few dates to show the important plateaus around 10,000 and 11,000 radiocarbon years

before the present (¹⁴C yr B.P.) and other rapid fluctuations. Figure 2B thus shows only the major changes in the reservoir ages. However, to see the detailed picture of these changes in the reservoir ages, we wiggle-matched our sequences of terrestrial dates to those of the tree-ring record, as described below.

The part of the new calibration curves that relies on tree-ring evidence (IntCal04) dates back to 12,410 calendar (cal) yr B.P. (14). Beyond that and back to 14,700 cal yr B.P., IntCal04 is mainly constructed from ¹⁴C dates of foraminiferas from Venezuela's Cariaco basin that are corrected for a constant reservoir age of 405 years (14). However, it has been proposed that the latter increased up to 650 years during the Bølling/Allerød (15, 16). We therefore replaced that part of IntCal04 with a new, floating tree-ring curve composed of 1382 rings between 10,650 and 12,000 ¹⁴C yr B.P. These tree rings were anchored to the Cariaco basin varves starting at 12,825 cal yr B.P. by Kromer *et al.* (15). Thus our tree-ring record from IntCal04, combined with the new, floating tree-ring curve (15), represents a true terrestrial curve that extends across most of the studied interval.

To correlate our sequences of terrestrial ¹⁴C dates with the tree-ring curve, we varied position and sedimentation rates to find the best possible match with wiggles in the curve (17). For this wiggle-matching, we assumed constant sedimentation rates within each sedimentary unit. As independent time controls, we used established ages for the YD-Preboreal boundary (11,530 to 11,630 cal yr B.P.) (18–20), the Vedde Ash Bed (12,050 to 12,170 cal yr B.P.), and the Allerød-YD boundary (12,800 to 13,000 cal yr B.P.) (21) evident in the lithology. With the terrestrial ¹⁴C dates positioned, we calculated the reservoir ages as the difference between the ¹⁴C age of the marine samples and the corresponding ¹⁴C age of the tree-ring curve (Fig. 3, A and C).

The combined tree-ring curve (Fig. 3A) was then used as input to the same global ocean-atmosphere box diffusion model used to derive the Holocene mixed-layer Marine04 curve (16, 22). The resulting curve (blue line, Fig. 3A) shows the expected ¹⁴C ages of the surface ocean for circulation and ventilation between the ocean-atmosphere interface similar to that of the present day along Norway's west coast. The offset between a marine ¹⁴C age and the output of this box model is defined as ΔR (1). We have calculated this offset of ΔR values for our late-glacial sequence (Fig. 3D). For surface water today in this area, ΔR is equal to -3 ± 22 years (5), a negligible offset to the box model in Fig. 3A.

In the earliest period (13,800 to 14,500 cal yr B.P.), the reservoir age is 300 to 400 years, which is similar to the output from the box model and to present-day values (Fig. 3, A and C). The small plateau in the tree-ring record at 11,800 ¹⁴C yr B.P. (Fig. 3A) is mirrored in the marine ¹⁴C dates. This agreement sug-

¹Department of Geology, University of Tromsø, N-9037 Tromsø, Norway. ²Department of Earth Science and Bjerknes Centre for Climate Research, ³Department of Biology and Bjerknes Centre for Climate Research, University of Bergen, Allégaten 41, N-5007 Bergen, Norway. ⁴Radiological Dating Laboratory, Sem Sælandsvei 5, N-7034 Trondheim, Norway. ⁵School of Archaeology and Palaeoecology, Queen's University Belfast, Belfast BT7 1NN, UK.

*To whom correspondence should be addressed. E-mail: stein.bondevik@ig.uit.no

gests that the exchange of CO₂ between the atmosphere and the surface ocean at that time was comparable to that of the present. Paleoclimatological reconstructions show surface water temperatures in the Norwegian Sea to be almost the same as those of today, but the bottom water was colder (23–25). The small reservoir ages indicate that the first inflow of warm Atlantic water in the late-glacial period was shallow and brought no old water to the surface. However, a small increase in reservoir ages at ~14,000 cal yr B.P. corresponds in time to the Older Dryas cold event (23–25).

During a short interval (13,200 to 13,500 cal yr B.P.), we found higher reservoir ages of 500 to 600 years, with ΔR values reaching

185 years. This coincides with lower total organic carbon and loss-on-ignition in our cores (9, 11) and with the timing of the Gerzensee/Killarney oscillation (also known as the Intra-Allerød cold period), a fluctuation seen in the marine records that was associated with reduced inflow of Atlantic water and increased sea-ice cover (23–25).

Reservoir ages increased gradually from 400 years to more than 600 years in the early YD (Fig. 3C). This increase forms a 700-¹⁴C yr-long plateau in the marine ¹⁴C ages that is centered at 11,000 ¹⁴C yr B.P. (Fig. 3A) and is related to a strong decline in radiocarbon activity (Δ¹⁴C) from 12,700 to 12,100 cal yr B.P. (Fig. 3B). To match this decline of Δ¹⁴C in

our YD data, the air-sea gas exchange parameter in the box model had to be reduced from 19 to 14 mol m⁻² year⁻¹ (16, 22), a reduction of 25% compared to that of modern conditions (CO₂ concentration was set to 220 parts per million for the YD).

A high reservoir age during the YD could be explained by a combination of increased sea-ice cover and reduced advection of surface water to the North Atlantic (3, 4). The rapid decline in Δ¹⁴C accompanies increased sea-ice cover in the Norwegian Sea, reaching a maximum of 7 months/year (26) right after the Vedde Ash tephra, which would have gradually reduced the rate of CO₂ exchange between the atmosphere and the sea surface. Bard *et al.* (3) modeled half a

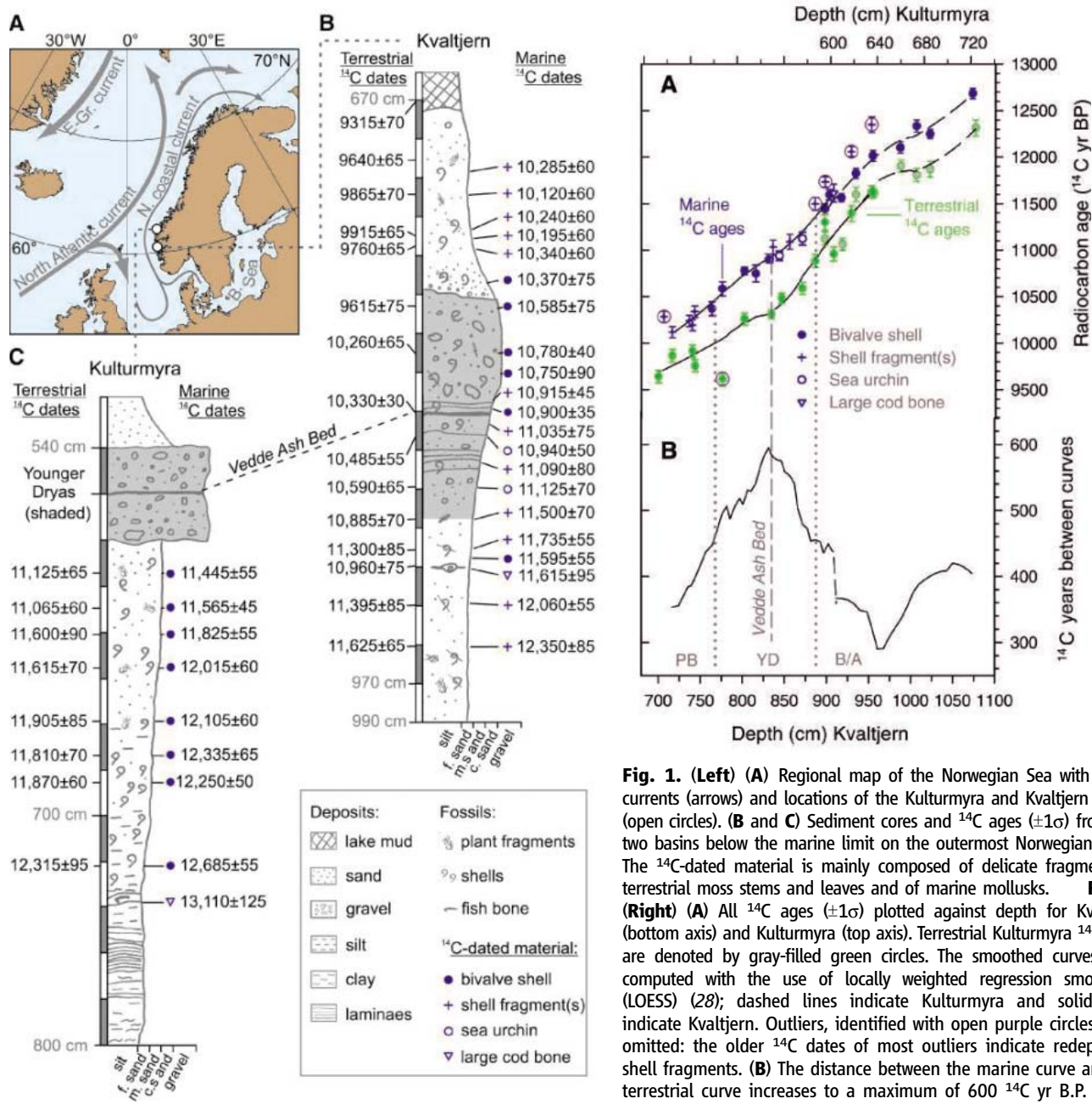


Fig. 1. (Left) (A) Regional map of the Norwegian Sea with ocean currents (arrows) and locations of the Kulturmyra and Kvaltjern basins (open circles). **(B and C)** Sediment cores and ¹⁴C ages (±1σ) from the two basins below the marine limit on the outermost Norwegian coast. The ¹⁴C-dated material is mainly composed of delicate fragments of terrestrial moss stems and leaves and of marine mollusks. **Fig. 2. (Right) (A)** All ¹⁴C ages (±1σ) plotted against depth for Kvaltjern (bottom axis) and Kulturmyra (top axis). Terrestrial Kulturmyra ¹⁴C ages are denoted by gray-filled green circles. The smoothed curves were computed with the use of locally weighted regression smoothing (LOESS) (28); dashed lines indicate Kulturmyra and solid lines indicate Kvaltjern. Outliers, identified with open purple circles, were omitted; the older ¹⁴C dates of most outliers indicate redeposited shell fragments. **(B)** The distance between the marine curve and the terrestrial curve increases to a maximum of 600 ¹⁴C yr B.P. in the mid-YD (solid line). PB, Preboreal; B/A, Bølling/Allerød.

year of sea ice north of 50°N in the North Atlantic to correspond to an increase of reservoir ages of ~100 years. However, mollusks in the Barents Sea, which is covered by sea ice for 10 months/year, did not show higher reservoir ages (12), presumably because of the exchange of carbon between the air and seawater in the summer when the sea ice cracks open. Nevertheless, we believe that a reduction of the northward flow of warm and young subtropical surface water to the North Atlantic is probably the most important factor to explain the increase in reservoir age during the YD (3). Such a reduction must have persisted for the last two-thirds of the YD, with stable high reservoir ages around 600 years and ΔR between 250 and 300 years (Fig. 3, C and D).

A large and rapid change took place at the end of the YD, when the reservoir ages and ΔR

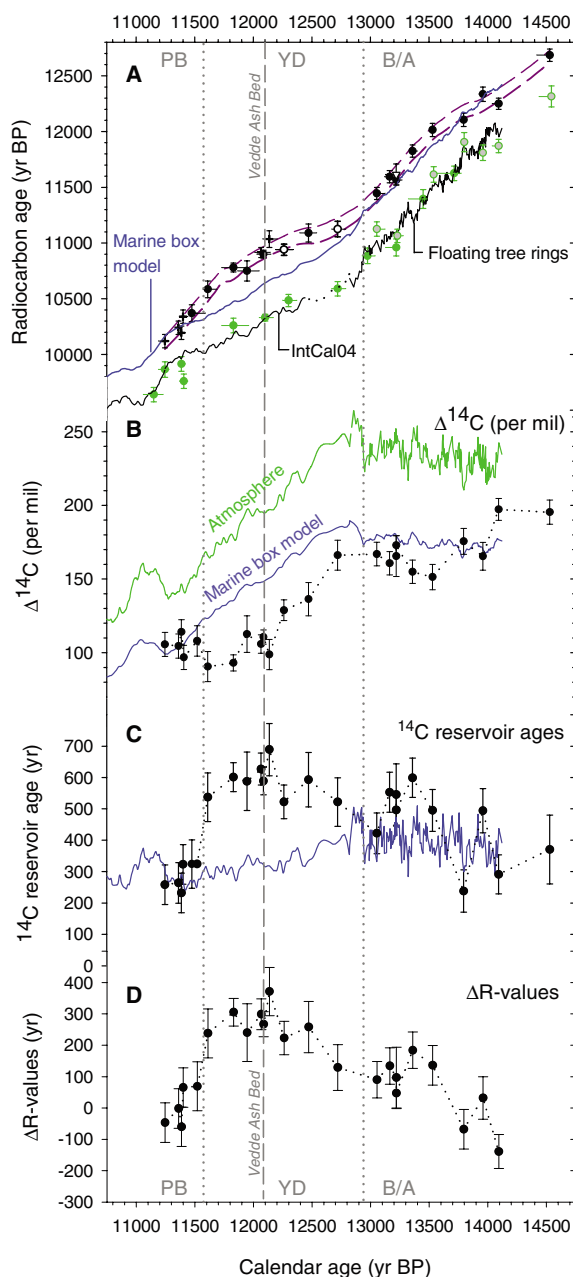
dropped by 300 years (Fig. 3C) within a century. At that time, a rapid decline in atmospheric $\Delta^{14}\text{C}$ (Fig. 3B) caused the well-known 10,000 ^{14}C yr B.P. plateau (Fig. 3A) in terrestrial dates and marine varves from low latitudes (14, 16). Our dates show that the opposite happened in the North Atlantic, where a rise in marine $\Delta^{14}\text{C}$ corresponds to rapidly decreasing marine ^{14}C ages from 10,600 to 10,100 ^{14}C yr B.P. This steep slope opens possibilities for higher resolution of calibrated marine ^{14}C dates at the YD-Preboreal transition, in contrast to the low resolution in terrestrial ^{14}C dates on the 10,000 ^{14}C yr B.P. plateau. Overall, this result indicates increased outgassing of aged ^{14}C from the North Atlantic into the atmosphere at the end of the YD due to increased ocean circulation, possibly in combination with more efficient CO_2

exchange across the ocean surface as sea ice melted (4).

The changes we see in our late-glacial record of sea surface reservoir ages are thus closely related to circulation changes in the North Atlantic, with lower reservoir ages during the warmer periods (Preboreal and Bølling/Allerød) and higher reservoir ages during the colder periods (YD and Gerzensee/Killamey–Intra-Allerød cold period). Our curve of marine ^{14}C ages (Fig. 3A) demonstrates previously unidentified ^{14}C plateaus at some times, such as the first half of the YD, and diverges from such plateaus at other times, as seen for the time around the terrestrial 10,000 ^{14}C yr B.P. plateau.

The results of this study potentially provide higher resolution for calibrated marine radiocarbon ages for the late-glacial North Atlantic. The first-order assumption that regional offsets of ΔR from the global marine calibration curve are constant through time is invalid for this region and time period. To overcome this problem, we need to develop regional marine calibration curves, such as the purple curve in Fig. 3A, rather than using the global Marine04 model to calibrate marine dates to calendar years at certain times. Such regional calibration curves may also be desirable for use in other parts of the world ocean (27).

Fig. 3. (A) Terrestrial ^{14}C ages $\pm 1\sigma$ (green circles) wiggle-matched to the IntCal04 tree-ring curve (left part of solid black line), reservoir age-corrected ^{14}C dates from the Cariaco basin (dotted black line) (14), and to a floating tree-ring sequence (right part of solid black line) (15). Marine ^{14}C ages $\pm 1\sigma$ (black circles) are plotted accordingly, to agree with the position of their corresponding terrestrial calendar dates, joined together with a purple curve (dashed parallel lines) through the ^{14}C ages $\pm 1\sigma$ via LOESS (28). The solid blue curve shows expected marine ^{14}C ages derived from the box model (16, 22). **(B)** $\Delta^{14}\text{C}$ values calculated from tree rings (green curve), the marine box model (blue curve), and our wiggle-matched ^{14}C ages of marine material ($\pm 1\sigma$) (dotted black line). The rapid decline of our marine $\Delta^{14}\text{C}$ values during the early YD accounts for the marine plateau around 11,000 ^{14}C yr B.P. Similarly, increasing $\Delta^{14}\text{C}$ values at the YD-Preboreal transition account for a decrease in marine ^{14}C ages that contrasts with the tree-ring record in (A). **(C)** Reservoir ages ($\pm 1\sigma$) (dotted black line) derived by subtracting our marine ^{14}C ages from the tree-ring ^{14}C ages. The blue curve shows reservoir ages derived from the box model. **(D)** ΔR values ($\pm 1\sigma$) derived by subtracting our marine ^{14}C ages from those of the marine box model. The present-day ΔR value in this area is -3 ± 22 years (5).



References and Notes

- M. Stuiver, G. W. Pearson, T. F. Braziunas, special issue on calibration, *Radiocarbon* **28**, 980 (1986).
- J. Mangerud, *Boreas* **1**, 143 (1972).
- E. Bard *et al.*, *Earth Planet. Sci. Lett.* **126**, 275 (1994).
- T. F. Stocker, D. G. Wright, *Paleoceanography* **11**, 773 (1996).
- J. Mangerud, S. Bondevik, S. Gulliksen, A. K. Hufthammer, T. Høisæter, *Quat. Sci. Rev.*, in press.
- S. Björck, N. Koc, G. Skog, *Quat. Sci. Rev.* **22**, 429 (2003).
- C. Waelbroeck *et al.*, *Nature* **412**, 724 (2001).
- W. E. N. Austin, E. Bard, J. B. Hunt, D. Kroon, J. D. Peacock, *Radiocarbon* **37**, 53 (1995).
- S. Bondevik, J. Mangerud, S. Gulliksen, *J. Quat. Sci.* **16**, 3 (2001).
- G. Siani *et al.*, *Science* **294**, 1917 (2001).
- S. Bondevik, H. H. Birks, S. Gulliksen, J. Mangerud, *Quat. Res.* **52**, 104 (1999).
- S. L. Forman, L. Polyak, *Geophys. Res. Lett.* **24**, 885 (1997).
- J. Aure, Ø. Østensen, *Fisken Havet* **6**, 1 (1993).
- P. J. Reimer *et al.*, *Radiocarbon* **46**, 1029 (2004).
- B. Kromer *et al.*, *Radiocarbon* **46**, 1203 (2004).
- K. A. Hughen *et al.*, *Radiocarbon* **46**, 1059 (2004).
- Materials and methods are available as supporting material on Science Online.
- S. Gulliksen, H. H. Birks, G. Possnert, J. Mangerud, *Holocene* **8**, 249 (1998).
- M. Friedrich *et al.*, *Radiocarbon* **46**, 1111 (2004).
- J. Southon, *Radiocarbon* **46**, 1239 (2004).
- K. A. Hughen, J. Southon, S. J. Lehman, J. T. Overpeck, *Science* **290**, 1951 (2000).
- M. Stuiver, T. F. Braziunas, *Radiocarbon* **35**, 137 (1993).
- S. J. Lehman, L. D. Keigwin, *Nature* **356**, 757 (1992).
- H. Hafliðason, H. P. Sejrup, D. Klitgaard Kristensen, S. Johnsen, *Geology* **23**, 1059 (1995).
- D. Klitgaard Kristensen, H. P. Sejrup, H. Hafliðason, *Paleoceanography* **16**, 455 (2001).

26. A. Rochon, A. de Vernal, H. P. Sejrup, H. Hafliðason, *Quat. Res.* **49**, 197 (1998).
27. J. N. Deo, J. O. Stone, J. K. Stein, *Am. Antiq.* **69**, 771 (2004).
28. W. S. Cleveland, *The Elements of Graphing Data* (AT&T Bell Laboratories, Murray Hill, NJ, 1994).
29. We acknowledge comments from B. F. Atwater and B. Kromer and four anonymous reviewers that helped to improve the manuscript. The work was supported by

the Norwegian Research Council and the University of Tromsø. Ø. S. Lohne and D. Bondevik participated in the field, G. Skjerdal picked plant fragments, and P. J. Svanem and S. Stene combusted the samples to graphite. J.M. conceived the project, S.B. did the fieldwork and led the laboratory work and writing, H.B. identified plant fragments, S.G. conducted the radiocarbon dating, and P.R. ran the marine box model.

Supporting Online Material

www.sciencemag.org/cgi/content/full/312/5779/1514/DC1
Materials and Methods
Figs. S1 and S2
Tables S1 and S2
References

1 December 2005; accepted 28 April 2006
10.1126/science.1123300

Transatlantic Abundance of the N_2 -Fixing Colonial Cyanobacterium *Trichodesmium*

Cabell S. Davis^{1*} and Dennis J. McGillicuddy Jr.²

Colonial diazotrophic cyanobacteria of the genus *Trichodesmium* are thought to play a significant role in the input of new nitrogen to upper layers of the tropical and subtropical oceanic ecosystems that cover nearly half of Earth's surface. Here we describe results of a transatlantic survey in which a noninvasive underwater digital microscope (the video plankton recorder), was towed across the North Atlantic at 6 meters per second while undulating between the surface and 130 meters. Colony abundance had a basin-scale trend, a clear association with anticyclonic eddies, and was not affected by hurricane-forced mixing. Subsurface abundance was higher than previously reported, which has important implications for the global ocean nitrogen cycle.

Tropical and subtropical regions of the ocean represent the largest ecosystems on Earth, covering nearly half the planet's surface. This vast oligotrophic area has been termed a biological desert because of low observed nutrient concentrations and biomass (1), but it is important in global carbon cycling due to biological feedbacks including surface heating and gas exchange and the sinking export of fixed carbon from the surface layer via the biological pump (2, 3). Production in these regions is nitrogen limited, and carbon and nitrogen cycles cannot be balanced by traditional mechanisms of nitrate supply, such as are

derived from winter mixing and vertical diffusion (4). Data and modeling indicate that episodic upwelling of deep nitrogen-rich water by mesoscale eddies is a potentially important but undersampled mechanism for input of new nitrogen into the biologically active upper layer of the oligotrophic ocean (5). Another potentially important source of new nitrogen is from N_2 fixation by diazotrophic colonial cyanobacteria of the genus *Trichodesmium*, which are ubiquitous members of tropical and subtropical pelagic communities (6–12). Globally, *Trichodesmium* has been estimated to generate 80 to 110 Tg of new nitrogen per year in oligotrophic waters, accounting for a significant proportion of the annual input of new nitrogen (6, 11–15). It is considered the dominant N_2 fixer in the tropical-subtropical ocean (16). Mechanisms controlling abundance of *Trichodesmium* have been extensively studied, with iron and/or phosphorus

limitation thought to play a major role (17). *Trichodesmium* abundance has been difficult to quantify using traditional net sampling, because the colonies are easily damaged or destroyed during collection, which results in underestimation (18, 19). Sampling with bottles (e.g., 10-liter Niskin) has provided quantitative estimates of vertical abundance over broad areas of the tropical Atlantic (18), whereas current estimates of abundance in the Sargasso Sea are based largely on net tows.

We used an in situ digital microscope to quantify the abundance of *Trichodesmium* non-invasively across the Sargasso Sea during August and September 2003. We towed the video plankton recorder (VPR) (20–23) from the Azores toward Bermuda, continuing across the Gulf Stream to the Slope Water south of Cape Cod, Massachusetts (Fig. 1A). This sampling was done opportunistically during a transit leg of the R/V *Knorr* and was carried out at the cruising speed of the ship (6 m/s) over a 12-day period, covering a distance of 5517 km. The VPR undulated automatically between the surface and 130 m below with an average vertical velocity of 1 m/s, yielding a total of 6910 vertical profiles. The ship's track was intentionally diverted to intersect cyclonic and anticyclonic mesoscale ocean eddies during the transit (Fig. 1B). Eddy positions were determined by shore-based analysis of near-real-time satellite sea-surface altimetry data and sent to the ship by e-mail (23). East of Bermuda, the ship's track was diverted to the southwest to avoid a category 3 hurricane (*Fabian*). As *Fabian* crossed Bermuda, the ship turned northwest toward Woods Hole, and sampling continued across the wake of the storm (Fig. 1, A and B).

¹Biology Department, Woods Hole Oceanographic Institution, ²Department of Applied Ocean Physics and Engineering, Woods Hole Oceanographic Institution, Woods Hole, MA 02543–1541, USA.

*To whom correspondence should be addressed. E-mail: cdavis@whoi.edu

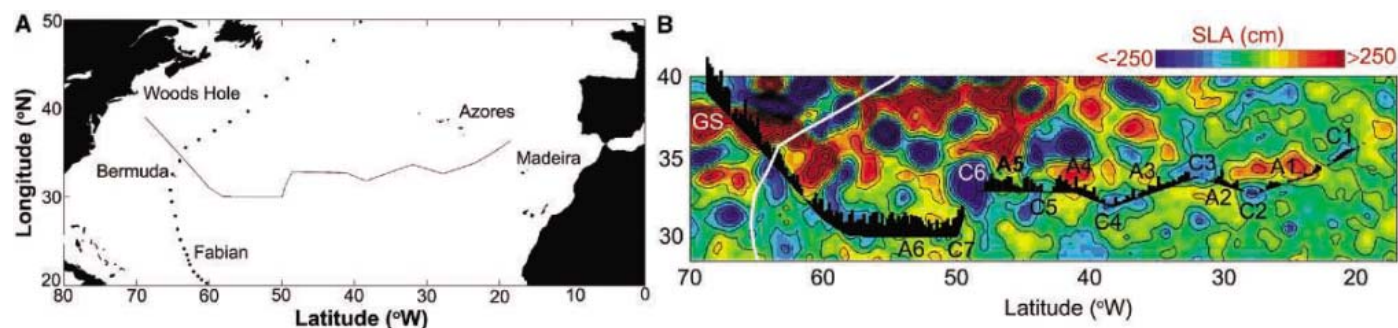


Fig. 1. (A) Cruise track of the R/V *Knorr* across the North Atlantic from the Azores to the Slope Water south of Woods Hole, Mass. (28 August to 8 September 2003). Dots show 3-hour positions of hurricane *Fabian*. (B) Along-track histogram of hourly *Trichodesmium* abundance (number/m³) (puffs) (Fig. 2A top panel) overlaid on a contour plot of sea surface height

(sea level anomaly, SLA) from satellite altimetry data on 3 September 2003. High and low in the SLA data are labeled to show positions of seven cyclonic (C) and six anticyclonic (A) eddies as well as the Gulf Stream (GS). Note lower *Trichodesmium* abundance in cyclonic eddies on the eastern half of transect. White line is path of hurricane *Fabian*.

The VPR is equipped with a 1-megapixel digital video camera sampling 30 frames per second. The lens was adjusted to give a field of view of 1.2 cm, and the calibrated imaged-volume was 11.88 ml. Average spacing between adjacent images was 3.3 cm vertically (20 cm horizontally), and the total volume sampled was 356 ml per vertical meter or 46 liters per 130-m profile. The VPR also had sensors for conductivity, temperature, pressure, fluorescence, turbidity, and photosynthetically active radiation. Raw sensor data were logged at 30 Hz, and 1-s averages were logged together with global positioning system (GPS) latitude, longitude, Greenwich mean time (GMT) at 1 Hz. Images of plankton were sorted automatically into different taxa by using classifiers trained with a set of manually sorted images.

The automatically sorted *Trichodesmium* images were examined manually to remove false-positives (23). The list of observation times

for *Trichodesmium* images were binned into the 1-s time bins of the sensor and GPS data, and the number in each bin was divided by the total volume imaged during each 1-s period to give the average abundance (number/m³) per bin. These values then were divided by the probability of detection to provide accurate abundance estimates (21, 23). In addition to the binned data, the latitude, longitude, and depth associated with each individual *Trichodesmium* image was determined, by using interpolation, from image acquisition time and GPS time. Only colonies were readily identified from the VPR images, with free trichomes difficult to distinguish from other taxa (e.g., diatom chains) at the magnification used. So abundances presented here are underestimates of total trichome concentration, although free trichomes on average typically represent ~10% of the total (18).

We found strong signals in temperature, salinity, and abundance of *Trichodesmium* colo-

nies corresponding to seven cyclonic and six anticyclonic eddies and the Gulf Stream (Fig. 2A). Vertical distributions of temperature and salinity revealed strong subsurface signatures in the eddies observed via satellite altimetry. Likewise, the acoustic Doppler current profiler mounted on the hull clearly revealed the circulation patterns in these eddies (fig. S3).

Trichodesmium images, sorted into two morphological classes, puffs and tufts, were likely *T. thiebautii*, with the tufts also including *T. erythraeum* (24, 25). Both forms had basin-scale trends in abundance, with higher concentrations in the western Sargasso Sea (west of 50°W) (Figs. 1B and 2A). Mean colony abundances (both forms combined) were $35.1 \pm 2.8 \text{ m}^{-3}$ and $6.4 \pm 0.7 \text{ m}^{-3}$ (± 2 SEM) in western and eastern regions, respectively. An association of *Trichodesmium* with warm salty water was evident at the eddy scale, with relatively higher concentrations found in warm anticyclonic eddies than

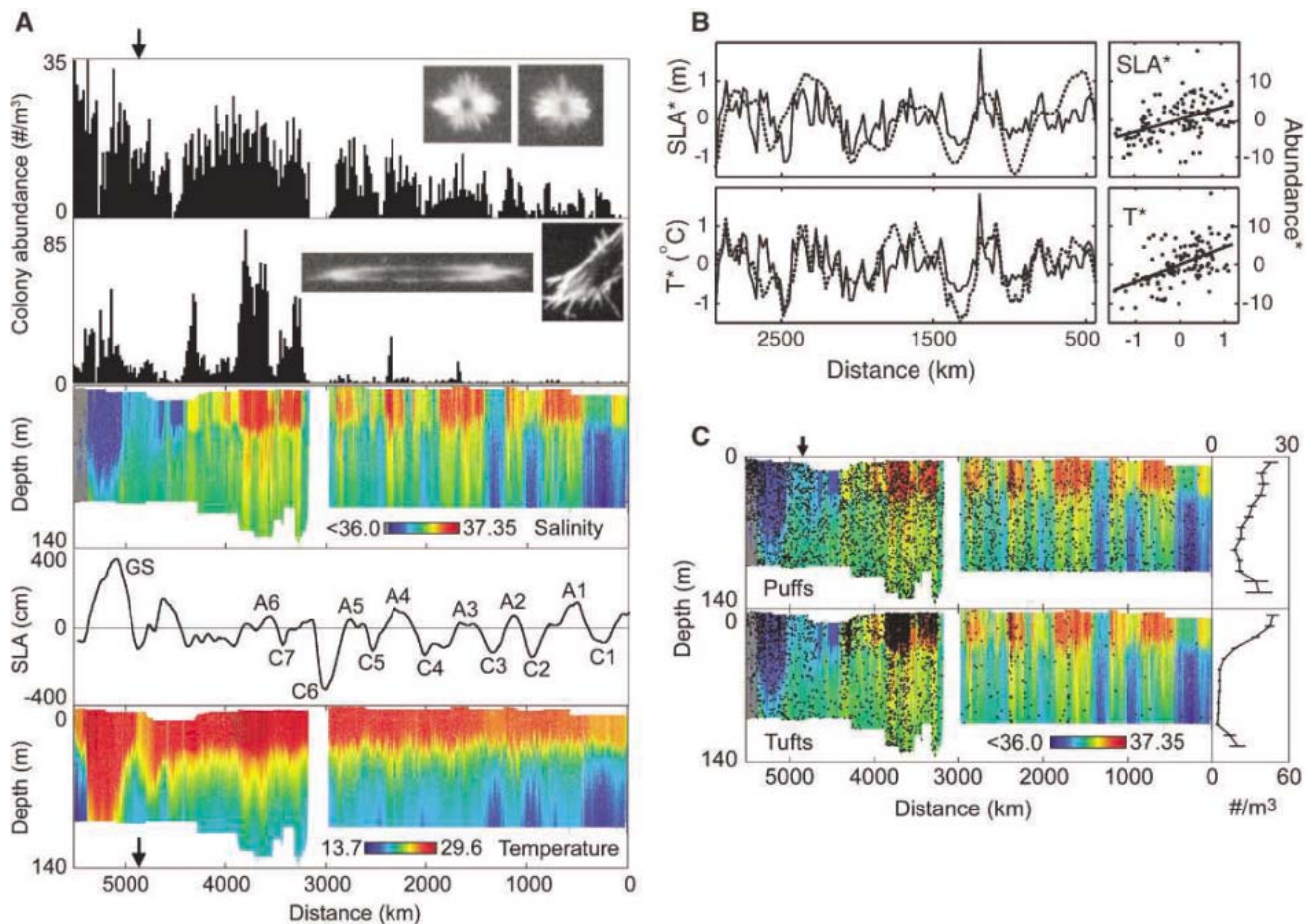


Fig. 2. (A) Hourly mean abundance (number/m³) of *Trichodesmium* colonies across the Atlantic Ocean. VPR images of spherical (puffs) and fusiform (tufts) are shown in the top and second panels, respectively (image widths, 1 to 3 mm). Salinity, along-track SLA, and temperature are shown below. Data points for salinity and temperature are 1-s averages and about each other in the plots. Cyclonic and anticyclonic eddies and the Gulf Stream are labeled as in Fig. 1B. Arrows indicate the point of intersection with the wake of hurricane *Fabian*. (Data gap is due to removal of VPR from water during hurricane avoidance maneuver.) (B) (Left) Detrended

hourly SLA (SLA*, dotted curve), temperature (T*, dotted curve), and abundance (abundance*, solid curves) versus distance along the initial 500- to 3000-km portion of the transect. (Right) Linear regressions of Abundance* on SLA* and T* ($P < 0.0001$). (C) Vertical distributions of *Trichodesmium* puffs and tufts overlaid on salinity sections. Dots indicate locations of individual colonies. The mean vertical distributions across the entire transect are shown at right (error bars, 95% confidence intervals of hourly mean abundance at each depth). Arrow (top) shows intersection of hurricane *Fabian's* wake.

in cold cyclonic eddies (Figs. 1B and 2A). This relation is especially evident for puffs during the 500- to 3000-km portion of the transect, where their abundance closely followed the sea level anomaly and temperature variability ($P < 0.0001$) (Fig. 2B). [An exception to this relation is the subsurface maximum of puff abundance in cyclone C1 (Fig. 1B).] The mechanisms responsible for higher abundance of *Trichodesmium* in anticyclonic eddies are unknown. This covariance could reflect eddy-driven transport of these populations from a distant source region. Alternatively, biotic interactions may be the controlling factor. The last-mentioned aspect is particularly enigmatic given the traditional paradigm that nitrogen fixation is generally phosphorus limited (26): Depression in the seasonal thermocline in these anticyclones (Fig. 2A) would tend to deepen the phosphocline and thereby reduce the availability of phosphorus in the eddy cores.

Although the relatively fragile colonies of *Trichodesmium* can be destroyed when wind mixing is strong (27), we did not find any indication of lower colony abundance across the wake of hurricane *Fabian*, despite maximum sustained winds of 200 km hr^{-1} (Fig. 2A). Mean colony concentration in the 200-km-wide wake region ($23.0 \pm 3.8 \text{ m}^{-3}$) was not significantly different from that in adjacent (200 km) areas ($26.6 \pm 7.0 \text{ m}^{-3}$, $P = 0.53$). It appears that both puff and tuft colonies were able to withstand this strong wind forcing.

Vertically, both forms were found throughout the water column (Fig. 2C) and were not restricted to the near surface as previously found in this area from net tows (8, 24, 25, 28). Tufts were more abundant in the upper 50 m, especially in the warmest saltiest layer, yet abundance of puffs was high at all depths. Comparing these vertical distributions with ones derived from an empirical equation describing colony abundance versus depth in this region (24), as well as with earlier data from the Sargasso Sea

(fig. S3), reveals that the abundances observed using nondestructive optical sampling are much higher at these depths than previously reported (Fig. 3 and fig. S4). This difference may be because deep net tows allow more time for fragile colonies to fragment (19) (with resulting trichomes extruded through net mesh openings), whereas shorter surface collections may be less destructive. By contrast, high abundance of trichomes at depths to 100 m have been found from quantitative bottle collections in the tropical North Atlantic during June under windy conditions, although overall abundance decreased markedly with depth (18).

We examined the potential impact of our abundance measurements on estimation of *Trichodesmium* nitrogen fixation in the water column, using published data on nitrogen fixation rates. The rate at a given depth was computed from the product of colony abundance and nitrogen fixation rate per colony, the latter being a function of light level, which decreases exponentially with depth. The rate per colony was estimated from linear and nonlinear empirically derived light-dependent functions on the basis of two separate data sets (23) (figs. S1 and S2).

Using VPR abundance data together with the nonlinear equation for light-dependent nitrogen fixation (23), we found the basin-scale average nitrogen fixation rate to be 2.7 to 5.0 times that expected from net-based sampling (Fig. 3A). Although the linear model gave lower overall rates, the VPR-based values were 2.9 to 3.3 times the net-based rates (table S1). The nitrogen fixation rate computed for the western Sargasso Sea (3250 to 3850 km) ($50.54 \mu\text{mol N}\cdot\text{m}^{-2}\cdot\text{d}^{-1}$) was three times that of the basin-scale average from the entire transect ($16.74 \mu\text{mol N}\cdot\text{m}^{-2}\cdot\text{d}^{-1}$) (Fig. 3B). Colony abundances in this region, however, are typically lower (e.g., 50 m^{-3}) than in tropical regions (e.g., 1000 m^{-3}) (17, 18, 26, 29). If traditional net sampling methods have systematically underestimated deep colony abun-

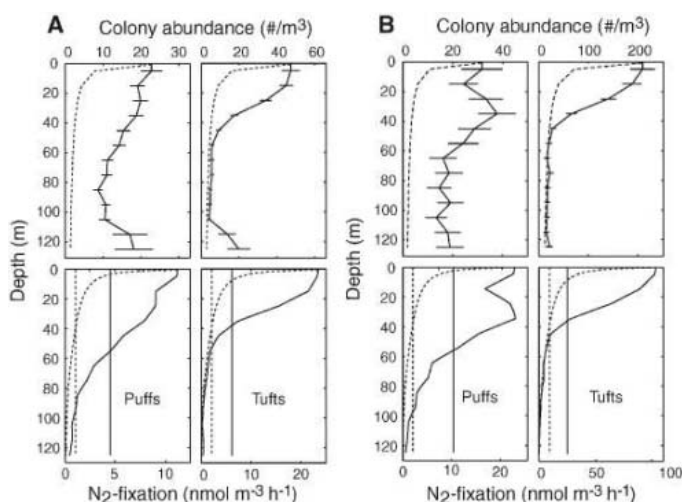
dance in other ocean regions, we can expect a substantial increase in the global *Trichodesmium* nitrogen fixation rate based on those studies. Such an increase could potentially account for the missing nitrogen in the global geochemical nitrogen cycle and could make this genus a crucial component to the productivity of the world ocean (17). Measurements made from bottle casts in the tropical Atlantic also reveal high abundance of *Trichodesmium* at these depths at certain times of year (18). Limited horizontal resolution of station sampling, however, may undersample the characteristically patchy distribution of *Trichodesmium* (30).

Further field and modeling studies are needed to determine the physical, chemical, and biological interactions controlling the multiscale distribution of *Trichodesmium*. The patchy nature of this species causes a large uncertainty in its population estimates (and thus in its role in oceanic N_2 fixation), and high-resolution large-scale sampling is required for quantitative assessment of its abundance and biomass (17). Satellite remote sensing is a promising new tool for quantifying surface distributions of *Trichodesmium* biomass (30), but this method does not quantify its vertical distribution. Nondestructive sampling, such as in situ optical imaging, is needed for determining the extent of its vertical distribution in other regions of the world ocean.

References and Notes

1. J. H. Ryther, *Science* **166**, 72 (1969).
2. S. Sathyendranath, A. D. Gouveia, S. R. Shetye, P. Ravindran, T. Platt, *Nature* **349**, 54 (1991).
3. P. Falkowski et al., *Science* **290**, 291 (2000).
4. W. J. Jenkins, *Nature* **331**, 521 (1988).
5. D. J. McGillicuddy et al., *Nature* **394**, 263 (1998).
6. D. G. Capone, J. P. Zehr, H. W. Paerl, B. Bergman, E. J. Carpenter, *Science* **276**, 1221 (1997).
7. D. G. Capone et al., *Mar. Ecol. Prog. Ser.* **172**, 281 (1998).
8. E. J. Carpenter, C. C. Price, *Limnol. Oceanogr.* **22**, 60 (1977).
9. E. J. Carpenter, in *Nitrogen in the Marine Environment*, E. J. Carpenter, D. G. Capone, Eds. (Academic Press, New York, 1983), pp. 65–103.
10. E. J. Carpenter, K. Romans, *Science* **254**, 1356 (1991).
11. E. J. Carpenter, T. Roenneberg, *Mar. Ecol. Prog. Ser.* **118**, 267 (1995).
12. D. M. Karl et al., *Biogeochemistry* **57/58**, 47 (2002).
13. V. J. Coles, R. R. Hood, M. Pascual, D. G. Capone, *J. Geophys. Res. Oceans* **109**, 1 (2004).
14. P. G. Falkowski, R. T. Barber, V. Smetacek, *Science* **281**, 200 (1998).
15. R. R. Hood, V. J. Coles, D. G. Capone, *J. Geophys. Res. Oceans* **109**, 1 (2004).
16. L. I. Falcon, E. J. Carpenter, F. Cipriano, B. Bergman, D. G. Capone, *Appl. Environ. Microbiol.* **70**, 765 (2004).
17. D. G. Capone et al., *Global Biogeochem. Cycles* **19**, 1 (2005).
18. E. J. Carpenter, A. Subramaniam, D. G. Capone, *Deep-Sea Res. I* **51**, 173 (2004).
19. J. Chang, *J. Exp. Mar. Biol. Ecol.* **245**, 212 (2000).
20. C. S. Davis, S. M. Gallager, A. R. Solow, *Science* **257**, 230 (1992).
21. C. S. Davis, Q. Hu, S. M. Gallager, X. Tang, C. A. Ashjian, *Mar. Ecol. Prog. Ser.* **284**, 77 (2004).
22. C. S. Davis, F. T. Thwaites, S. M. Gallager, Q. Hu, *Limnol. Oceanogr. Methods* **3**, 59 (2005).
23. Additional materials and methods are given as supporting material on Science Online.

Fig. 3. (A) Vertical distribution of *Trichodesmium* puff (left) and tuft (right) abundance (top) and computed (light-dependent) N_2 fixation rates (bottom). Dashed curves are net-based estimates (see fig. S3 for data points) and solid curves are VPR-based. Curves in bottom panels are the corresponding N_2 fixation rates derived using the nonlinear function of N_2 fixation versus light (23). Straight lines in bottom panels are water column averaged N_2 fixation rates; VPR-based estimates are 2.7 to 5.0 times as high as net-based rates. **(B)** As in **(A)**, except for the high-abundance region (3250 to 3850 km) only.



24. K. M. Orcutt *et al.*, *Deep-Sea Res. II* **48**, 1583 (2001).
 25. J. J. McCarthy, E. J. Carpenter, *J. Phycol.* **15**, 75 (1979).
 26. T. Tyrrell *et al.*, *J. Plankton Res.* **25**, 405 (2003).
 27. E. J. Carpenter, C. C. Price, *Science* **191**, 1278 (1976).
 28. E. J. Carpenter, J. J. McCarthy, *Limnol. Oceanogr.* **20**, 389 (1975).
 29. A. F. Post *et al.*, *Mar. Ecol. Prog. Ser.* **239**, 241 (2002).
 30. R. R. Hood, A. Subramaniam, L. R. May, E. J. Carpenter, D. G. Capone, *Deep-Sea Res. II* **49**, 123 (2002).
 31. We thank the officers and crew of the R/V *Knorr* for their outstanding support during the transatlantic VPR sampling. B. Walden provided facilities support for use of the VPR. F. Thwaites, A. Girard, and M. Alberico assisted in system deployment and operations. V. Kosyrev provided

daily altimetry maps and eddy positions to the ship based on data streams provided by R. Leben. J. Hummon processed the ship's acoustic Doppler current profiler data. We thank D. Capone, E. Carpenter, J. Waterbury, P. Falkowski, S. Dyhrman, E. Webb, and two anonymous reviewers for their helpful comments on this paper. Funding for development of the VPR was provided by a NSF Ocean Technology and Interdisciplinary Coordination grant OCE-9820099. Further support for VPR testing and operations was provided by NSF Oceanographic Technical Services grant OCE-0308366 and from the J. Seward Johnson Endowment Fund, the Penzance Foundation, and WHOI Biology Department Discretionary Funds. C.S.D. was supported by the Richard B. Sellars Endowed Research

Fund, the Andrew W. Mellon Foundation Endowed Fund for Innovative Research, and a fellowship from WHOI's Ocean Life Institute. D.J.M. was supported by NSF grant OCE-0241310 and NASA grant NNG04GR22G.

Supporting Online Material

www.sciencemag.org/cgi/content/full/312/5779/1517/DC1
 Materials and Methods
 Figs. S1 to S3
 Table S1
 References and Notes

7 December 2005; accepted 13 April 2006
 10.1126/science.1123570

TOPLESS Regulates Apical Embryonic Fate in *Arabidopsis*

Jeff A. Long,^{1*} Carolyn Ohno,² Zachery R. Smith,¹ Elliot M. Meyerowitz²

The embryos of seed plants develop with an apical shoot pole and a basal root pole. In *Arabidopsis*, the *topless-1* (*tpl-1*) mutation transforms the shoot pole into a second root pole. Here, we show that TPL resembles known transcriptional corepressors and that *tpl-1* acts as a dominant negative mutation for multiple TPL-related proteins. Mutations in the putative coactivator *HISTONE ACETYLTRANSFERASE GNAT SUPERFAMILY1* suppress the *tpl-1* phenotype. Mutations in *HISTONE DEACETYLASE19*, a putative corepressor, increase the penetrance of *tpl-1* and display similar apical defects. These data point to a transcriptional repression mechanism that prevents root formation in the shoot pole during *Arabidopsis* embryogenesis.

The apical/basal axis of *Arabidopsis* embryos is established during the first cell division of the zygote, and auxin accumulation and response have been shown to be important for early steps in axis establishment (1–5). As the embryo matures, specific cell types become apparent, and a clear shoot/root axis is visible at the transition stage of development (6, 7). Although several mutants have been isolated that affect the formation of specific patterning elements of the shoot at the transition stage of embryogenesis, only *topless-1* (*tpl-1*) so far switches the identity of the shoot into that of a root (8–11). It is therefore likely that TPL is acting at a different level of control than those factors that have previously been isolated.

tpl-1 mutants are temperature sensitive and at the restrictive temperature (29°C) transform the embryonic shoot pole into a second root pole that gives rise to a double-root seedling (11) (Fig. 1, A and B). At lower temperatures, *tpl-1* embryos fail to form a shoot apical meristem and show varying degrees of cotyledon fusion (Fig. 1, C to E). We view these phenotypes as a result of partial apical-to-basal transformation during embryogenesis (11) (fig. S1). Previous work has shown that transition-stage *tpl-1* embryos lack or have reduced expression of genes associated with the apical half of the embryo, whereas the

expression patterns of genes associated with the basal half of the embryo are expanded into the apical half and are ultimately duplicated. Pre-transition stage *tpl-1* embryos are morphologically indistinguishable from those of the wild type.

To examine the molecular organization of the apical half of *tpl-1* pre-transition stage embryos, we performed *in situ* hybridizations with the

transcription factor *WUSCHEL* (*WUS*) (10). *WUS* is initially expressed in a small group of cells in the apical half of 16-cell-stage embryos. *WUS* mRNA accumulated normally in *tpl-1* globular-stage embryos, but was absent in transition-stage embryos at 29°C (Fig. 1, F to H). This indicates that early *tpl-1* embryos have established an apical axis with the correct organization, but this fate is lost or masked at the transition stage.

tpl-1 was mapped to bacterial artificial chromosome F7H2 on chromosome 1 using polymerase chain reaction-based markers (11). We found two base-pair substitutions in At1g15750 (12) that cosegregated with the *tpl-1* phenotype and result in a change of a lysine (K) to a methionine (M) at amino acid 92 and an asparagine (N) to a histidine (H) at amino acid 176 of the predicted protein (13). Concurrently, we conducted a high-temperature ethylmethane sulfonate suppressor screen in the *tpl-1* background and found five semidominant suppressors that mapped to the original TPL locus. We sequenced At1g15750 from these lines and found that each harbored a second site mutation that is

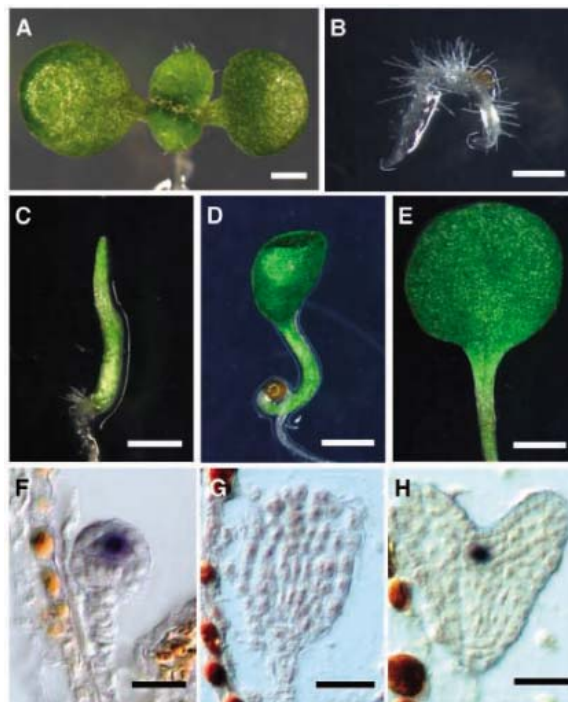


Fig. 1. Effects of *topless-1* on embryonic polarity. (A) Wild-type 5-day-old seedling. (B) A *tpl-1* double-root seedling. (C) A *tpl-1* pin seedling lacking cotyledons. (D) A *tpl-1* tube seedling. (E) A *tpl-1* monocot seedling with two fused cotyledons. (F) *WUS* mRNA accumulation in a *tpl-1* globular-stage embryo grown at 29°C. (G) *WUS* mRNA does not accumulate in a *tpl-1* heart-stage embryo. (H) Wild-type heart-stage embryo accumulating *WUS* mRNA in a small group of cells in the developing meristem. Scale bars: 1 mm (A to E), 25 μm (F to H).

¹Plant Biology Laboratory, The Salk Institute for Biological Sciences, 10010 North Torrey Pines Road, La Jolla, CA 92037, USA. ²Division of Biology, California Institute of Technology, 1200 East California Boulevard, Pasadena, CA 91125, USA.

*To whom correspondence should be addressed. E-mail: long@salk.edu

predicted to reduce or abolish gene function (Fig. 2A). That second site mutations in the *tpl-1* mutant gene suppress the *tpl-1* phenotype indicates that *tpl-1* is a gain-of-function allele. The semidominant nature of these loss-of-function alleles also implies a dosage requirement for the *tpl-1* protein.

TPL is predicted to encode an 1131–amino acid protein containing 11 WD40 repeats at the C terminus (Fig. 2A). At the N terminus, TPL has predicted lissencephaly type 1–like homology (LisH) and C-terminal to LisH (CTLH) domains that are thought to be important either for self-dimerization or for other protein-protein interactions (14). TPL also contains a 100–amino acid region rich in prolines (24 out of 100 amino acids). A similar domain organization is found in the TUP1/GROUCHO and LEUNIG family of transcriptional corepressors, although there is little sequence identity between TPL and these proteins (15, 16). Four other predicted proteins in *Arabidopsis* share extensive amino acid similarity with TPL and have been named TOPLESS-RELATED (TPR) (fig. S2).

In situ hybridization experiments revealed that *TPL* mRNA accumulates in all cells of the embryo as well as in extra-embryonic tissues (Fig. 2, B and C). *TPL* mRNA accumulates to higher levels in the embryo proper during early embryogenesis and in the developing vasculature in later stages. A TPL-GREEN FLUORESCENT PROTEIN (GFP) translational fusion under the control of 4.1 kb of upstream genomic sequences rescued the *tpl-1* phenotype when homozygous and localized to the nuclei of all cells in transgenic plants (Fig. 2D). This again indicates a dosage dependence for the *tpl-1* protein and suggests that the wild-type version of the protein can outcompete the mutant form.

To determine if both of the amino acid changes found in the original *tpl-1* allele were

necessary for the *tpl-1* phenotype, we transformed a *tpl* transfer DNA (T-DNA) insertion line (*tpl-8*) with TPL-GFP fusion proteins containing either both mutations (*tpl-1*), only the K92M mutation, or only the N176H mutation (17). The *tpl-1* phenotype was observed in plants carrying either the *tpl-1* transgene or the N176H transgene (16 and 15 lines, respectively). However, we did not observe any *tpl* phenotypes in 29 independent lines transformed with the K92M construct despite nuclear GFP accumulation comparable to that of lines with a *tpl-1* phenotype. Therefore, the N176H mutation is necessary and sufficient to cause the *tpl-1* phenotype.

tpl loss-of-function alleles display no obvious phenotype when grown at the restrictive temperature (Fig. 2E). We therefore hypothesized that TPL may act redundantly with the other TPR proteins. We generated *tpl-2*; *tpl-1*; *tpl-3*; *tpl-4* quadruple mutant lines and transformed them with a *TPR2* RNA interference (RNAi) transgene. We obtained five stable transgenic lines that displayed the original *tpl-1* phenotypes (Fig. 2F). This indicates that *tpl-1* acts as a type of dominant negative allele for multiple *TPR* family members.

In the high-temperature suppressor screen, we also isolated two alleles of a recessive extragenic suppressor of *tpl-1* designated *big top* (*bgt*). At 24°C, the progeny of plants homozygous for *tpl-1* and heterozygous for *bgt-1* segregated 24.1% wild-type seedlings (Fig. 3B) ($n = 513$). This same combination with *bgt-2* yielded 19.3% wild-type seedlings ($n = 1746$). We therefore characterized *bgt-1* in more detail. Morphologically, *tpl-1*; *bgt-1* embryos form cotyledons at the transition stage of embryogenesis, although they appear slightly stunted at later stages as compared to wild-type embryos (Fig. 3, C and D). To examine the apical pattern

of *tpl-1*; *bgt-1* embryos, we examined the expression of *WUS* in these double mutants at 29°C. At all stages tested, *tpl-1*; *bgt-1* embryos maintained the expression of *WUS* in the appropriate number of cells, indicating that the top half of these embryos had not lost their apical identity (Fig. 3, E to G).

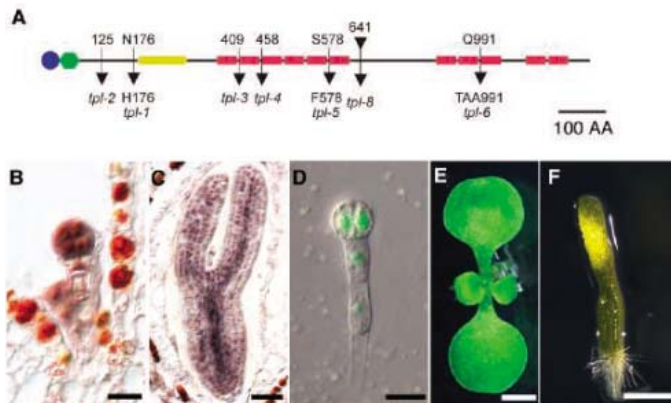
We mapped the *bgt-1* mutation and found that it was tightly linked to marker TSA1 on chromosome 2 (0 recombinants out of 606 chromosomes). This genomic region contains the *Arabidopsis* homolog of the histone acetyltransferase GCN5 (*HAG1*) (also known as *atGCN5*) (18, 19). In other eukaryotes, GCN5 is recruited to specific promoters by DNA binding transcription factors and is thought to promote transcription by acetylating the N-terminal tail of histone H3 (20). Sequencing revealed that both *bgt-1* and *bgt-2* carried lesions in *HAG1* (Fig. 3A). We therefore renamed these alleles *hag1-3* and *hag1-4*. T-DNA insertions in the tenth intron (*hag1-5*) and in the first intron (*hag1-6*) also suppressed *tpl-1* (Fig. 3A). All four *hag* alleles have no obvious embryonic phenotypes, although postembryonically they display pleiotropic phenotypes similar to that of a previously described allele (18). A translational fusion of a 4.3-kb *HAG1* genomic clone to GFP rescued the *hag1-3* mutant, and the protein was found in the nuclei of all cells examined (Fig. 3H). The observation that a mutation in a coactivator suppresses the *tpl-1* phenotype is consistent with TPL acting as a corepressor.

In eukaryotes, transcription from many promoters can be repressed through the activity of histone deacetylases. The RPD3 family of histone deacetylases can act as transcriptional corepressors, and in *Drosophila*, Groucho and an RPD3-like protein work together to specify anterior/posterior polarity (21). The *Arabidopsis* genome contains four class 1 RPD3-like proteins [Histone Deacetylase (HDA) 6, 7, 9, and 19] (22). In a screen for mutants that affect floral organ identity, a T-DNA allele of *HDA19* (*hda19-1*) (also known as *atHDI* and *RPD3a*) was isolated that displays floral phenotypes similar to those of *tpl-1* (23–25). A second T-DNA allele (*hda19-2*) was isolated from the Wisconsin *Arabidopsis* Knockout facility and found to show similar phenotypes (Fig. 4A). We therefore examined the role and expression of *HDA19* more closely during embryogenesis.

HDA19, like *TPL* and *HAG1*, is broadly expressed throughout embryogenesis, and a GFP fusion protein localizes to the nuclei of all embryonic cells (Fig. 4, B and C). Phenotypically, both *hda19-1* and *hda19-2* seedlings when grown at 24°C have narrow cotyledons as compared to those of the wild type (Fig. 4D). However, when mutants homozygous for either allele were grown at 29°C, mutant seedlings displayed several *tpl-1*–like phenotypes, including monocots, tubes, and pins, indicating that these *hda19* alleles are temperature sensitive (Fig. 4E). These phenotypes were seen in 32%

Fig. 2. Molecular characterization of the *TPL* gene.

(A) Diagram of the predicted structure of the TPL protein. TPL is predicted to have a LisH (blue circle) and CLISH (green hexagon) domain at the N terminus, a 100–amino acid proline-rich domain (yellow box), and 11 WD40 repeats (red boxes). The *tpl-1* phenotype is caused by a substitution of an asparagine at amino acid 176 with a histidine. *tpl-2* and *tpl-3* are splice acceptor site mutations, and *tpl-4* is a splice donor mutation. *tpl-5* is caused by a substitution of a serine at amino acid 578 with a phenylalanine in the sixth WD40 repeat, and *tpl-6* is caused by a change of a glutamine at amino acid 991 to a stop codon (CAA to TAA). *tpl-8* is a T-DNA insertion allele (SALK_036566). Numbers represent the affected amino acid positions. AA, amino acids. **(B and C)** *TPL* mRNA accumulation in (B) a globular-stage and (C) torpedo-stage wild-type embryo. **(D)** A translational fusion of TPL to GFP localizes to the nuclei of all cells in a four-cell-stage embryo. **(E)** A *tpl-2* mutant shows no phenotype after developing at 29°C. **(F)** A *tpl-2*; *tpl-1*; *tpl-3*; *tpl-4* mutant carrying a *TPR2* RNAi construct displaying a pin phenotype. Scale bars: 25 μ m (B to D), 1 mm (E and F).



of *hda19-1* seedlings ($n = 397$) and 28% of *hda19-2* seedlings ($n = 330$). A morphological analysis of *hda19-1* embryos at 29°C showed that both the root and the shoot can be disorganized (Fig. 4F), indicating that HDA19 may play a broader role in embryogenesis than TPL.

We then examined the progeny of *hda19-1*^{-/-}; *tpl-1*^{+/-} plants grown at 24°C, a temperature at which *tpl-1* segregates as a recessive (11). We found that 45% of the resulting seedlings showed cotyledon fusion defects ($n = 804$) instead of the expected 25%, indicating that

HDA19 may act on some of the same target genes as TPL during embryogenesis. In agreement with this hypothesis, we identified *tpl-1*; *hda19-1*; *hag1-3* triple-mutant seedlings from plants grown at 24°C, as well as 29°C, and found that they displayed two narrow cotyledons like the *hda19-1* single mutant (Fig. 4G). Therefore, *hag1-3* mutants can suppress *tpl-1* mutant phenotypes even in the absence of functional HDA19.

Recent work on embryonic polarity in *Arabidopsis* has focused on auxin transport and the first embryonic cell divisions in establishing the apical/basal axis (4, 26). Our studies have uncovered a set of proteins involved in a new step in axis formation, during the transition stage of embryogenesis, when shoot fate becomes fixed and distinct from root fate. We propose that at the transition stage of embryogenesis, TPL and other TPR proteins are necessary to repress the expression of root-promoting genes in the top half of the embryo to allow proper differentiation of the shoot pole. A histone deacetylase, HDA19, works in conjunction with TPL during this process, although it appears to have TPL-independent roles as well (27). HAG1 is necessary for the complete transformation of the apical half into a root, likely by activating the transcription of derepressed root-specific genes in the apical half of the embryo. However, HAG1 is dispensable for the formation of the basal “true” root. Conceptually, these two steps of polarity determination are similar to what has been reported in the brown alga *Fucus*, where axis formation and fixation are temporally distinct (28). In *Arabidopsis*, we propose that the axis formation step occurs during the first cell divisions of the embryo and likely relies on polar auxin distribution (4). Only later, at the transition stage of embryogenesis, does the axis become fixed, at which time the plant requires a chromatin-mediated transcriptional repression system for axis stabilization.

Fig. 3. Characterization of *hag1* alleles and genetic interactions with *tpl-1*. (A) Diagram of the predicted structure of HAG1 that contains a conserved histone acetyltransferase domain (red box) and a bromo domain (yellow box). *hag1-3* contains a stop codon at amino acid 478 (TGG to TGA); *hag1-4* contains a splice donor mutation at amino acid 389; *hag1-5* is a T-DNA insertion in the 10th intron (SALK_048427); and *hag1-6* is a T-DNA insertion in the first intron (SALK_150784). (B) A *tpl-1*;*hag1-3* double-mutant seedling grown at 24°C. (C and D) Cleared torpedo-stage embryos of (C) *tpl-1*;*hag1-3* and (D) wild-type seedling grown at 29°C. (E to G) WUS mRNA accumulation in (E) *tpl-1*, (F) *tpl-1*;*hag1-3*, and (G) wild-type 29°C grown torpedo-stage embryos. (H) A HAG1-GFP fusion protein localizes to the nuclei of all cells of a 16-cell-stage embryo. Scale bars: 1 mm (B), 25 μm (C to H).

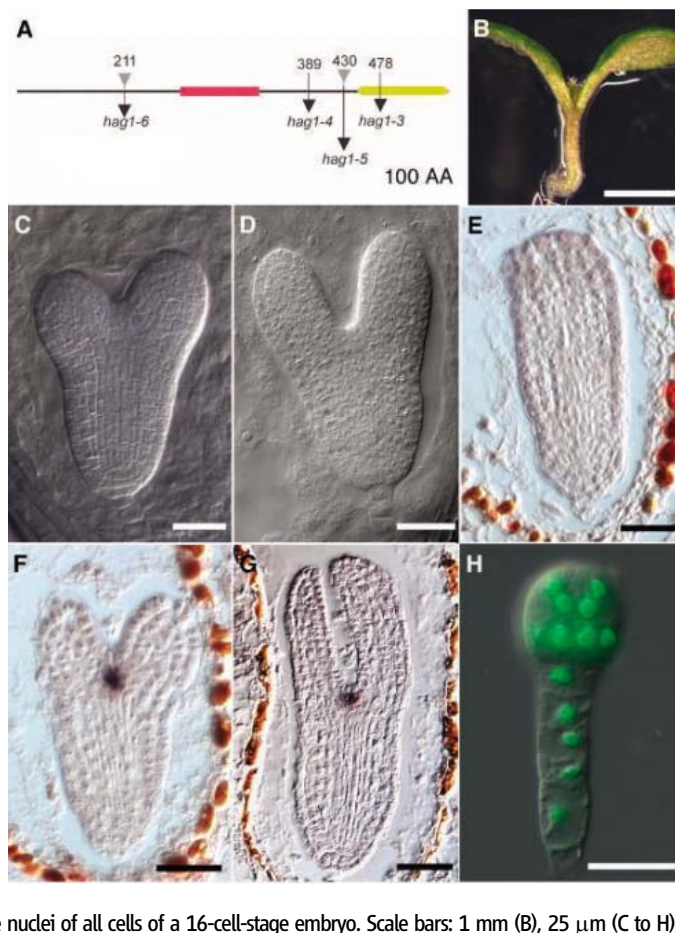
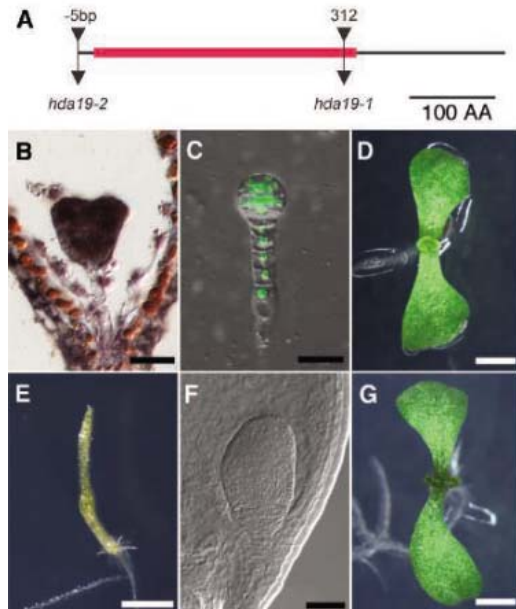


Fig. 4. Characterization and genetic interactions of HDA19. (A) Predicted structure of HDA19. *hda19-1* contains a T-DNA insertion that disrupts amino acid 312 in the histone deacetylase domain (red box). *hda19-2* contains a T-DNA insertion 5 base pairs upstream of the start codon. (B) mRNA accumulation of HDA19 in all cells of an early heart-stage embryo. (C) A HDA19-GFP fusion protein localizes to the nuclei of all cells of a 16-cell-stage embryo. (D) Seedling phenotype of *hda19-1* when grown at 24°C. (E) A *hda19-2* seedling displaying a pin phenotype when grown at 29°C. (F) A *hda19-1* heart-stage embryo grown at 29°C showing both shoot and root defects. (G) A *tpl-1*;*hag1-3*;*hda19-1* triple-mutant seedling grown at 24°C. Scale bars: 25 μm (B, C, and F), 1 mm (D, E, and G).



References and Notes

1. I. Bblilou *et al.*, *Nature* **433**, 39 (2005).
2. S. G. Mansfield, L. G. Briarty, *Can. J. Bot.* **69**, 461 (1991).
3. T. Steinmann *et al.*, *Science* **286**, 316 (1999).
4. J. Friml *et al.*, *Nature* **426**, 147 (2003).
5. C. S. Hardtke, T. Berleth, *EMBO J.* **17**, 1405 (1998).
6. J. A. Long, M. K. Barton, *Development* **125**, 3027 (1998).
7. A. Haecker *et al.*, *Development* **131**, 657 (2004).
8. M. Aida, T. Ishida, M. Tasaka, *Development* **126**, 1563 (1999).
9. M. K. Barton, R. S. Poethig, *Development* **119**, 823 (1993).
10. T. Laux, K. F. Mayer, J. Berger, G. Jurgens, *Development* **122**, 87 (1996).
11. J. A. Long, S. Woody, S. Poethig, E. M. Meyerowitz, M. K. Barton, *Development* **129**, 2797 (2002).
12. This protein was recently reported to interact with WUS in a two-hybrid screen (29).
13. Materials and methods are available as supporting material on Science Online.
14. R. D. Emes, C. P. Ponting, *Hum. Mol. Genet.* **10**, 2813 (2001).
15. G. Chen, A. J. Courey, *Gene* **249**, 1 (2000).
16. J. Conner, Z. Liu, *Proc. Natl. Acad. Sci. U.S.A.* **97**, 12902 (2000).

17. J. M. Alonso *et al.*, *Science* **301**, 653 (2003).
 18. K. E. Vlachoniasos, M. F. Thomashow, S. J. Triezenberg, *Plant Cell* **15**, 626 (2003).
 19. C. Bertrand, C. Bergounioux, S. Domenichini, M. Delarue, D. X. Zhou, *J. Biol. Chem.* **278**, 28246 (2003).
 20. M. H. Kuo *et al.*, *Nature* **383**, 269 (1996).
 21. G. Chen, J. Fernandez, S. Mische, A. J. Courey, *Genes Dev.* **13**, 2218 (1999).
 22. R. Pandey *et al.*, *Nucleic Acids Res.* **30**, 5036 (2002).
 23. C. Ohno, E. M. Meyerowitz, personal communication.
 24. K. Wu, L. Tian, K. Malik, D. Brown, B. Miki, *Plant J.* **22**, 19 (2000).
 25. L. Tian, Z. J. Chen, *Proc. Natl. Acad. Sci. U.S.A.* **98**, 200 (2001).
 26. T. Hamann, E. Benkova, I. Baurle, M. Kientz, G. Jurgens, *Genes Dev.* **16**, 1610 (2002).
 27. C. Zhou, L. Zhang, J. Duan, B. Miki, K. Wu, *Plant Cell* **17**, 1196 (2005).
 28. B. Goodner, R. S. Quatrano, *Plant Cell* **5**, 1471 (1993).
 29. M. Kieffer *et al.*, *Plant Cell* **18**, 560 (2006).
 30. We thank L. Jones, J. Nemhauser, and F. Wellmer for critical reading of the manuscript. We also thank M. Hannon and K. Shively for assistance with the *tpl* loss-of-function alleles and D. B. Vert and N. Geldner for

technical assistance. This work was supported by a Helen Hay Whitney postdoctoral fellowship and by NIH grants GM072764 (to J.A.L.) and GM45697 (to E.M.M.).

Supporting Online Material

www.sciencemag.org/cgi/content/full/312/5779/1520/DC1
 Materials and Methods
 Figs. S1 and S2
 References

14 December 2005; accepted 27 April 2006
 10.1126/science.1123841

Tim50 Maintains the Permeability Barrier of the Mitochondrial Inner Membrane

Michael Meinecke,¹ Richard Wagner,^{1*} Peter Kovermann,^{1†} Bernard Guiard,² David U. Mick,³ Dana P. Hutu,^{3,4} Wolfgang Voos,³ Kaye N. Truscott,^{3,5} Agnieszka Chacinska,³ Nikolaus Pfanner,^{3*} Peter Rehling³

Transport of metabolites across the mitochondrial inner membrane is highly selective, thereby maintaining the electrochemical proton gradient that functions as the main driving force for cellular adenosine triphosphate synthesis. Mitochondria import many preproteins via the presequence translocase of the inner membrane. However, the reconstituted Tim23 protein constitutes a pore remaining mainly in its open form, a state that would be deleterious in organello. We found that the intermembrane space domain of Tim50 induced the Tim23 channel to close. Presequences overcame this effect and activated the channel for translocation. Thus, the hydrophilic cis domain of Tim50 maintains the permeability barrier of mitochondria by closing the translocation pore in a presequence-regulated manner.

Most mitochondrial proteins are synthesized as preproteins in the cytosol and must be imported across outer and inner mitochondrial membranes (1–6). The mitochondrial inner membrane generates and maintains a proton-motive force that is crucial to drive the F_0F_1 -ATP synthase, which is the major machine for cellular adenosine triphosphate (ATP) synthesis (7, 8). How can the permeability barrier of the inner membrane for small ions such as protons be maintained while large hydrophilic channels for the passage of polypeptide chains exist?

The presequence translocase of the inner membrane (TIM23 complex) translocates hundreds of different preproteins into the matrix. The TIM23 complex contains the

pore-forming protein Tim23 and three additional membrane proteins, Tim17, Tim21, and Tim50. Tim23 consists of a membrane-embedded domain, containing the large translocation channel, and a domain in the intermembrane space (IMS) that recognizes the N-terminal presequences of preproteins (4, 6, 9–12). Tim50 and Tim21 each consist of a single transmembrane segment and a large IMS domain, which interact with preproteins and with the translocase of the outer membrane, respectively (13–17). Tim17 is largely embedded in the inner membrane and promotes cooperation of the presequence translocase with the associated import motor (PAM complex) (13). PAM is a multisubunit machinery on the matrix side of the inner membrane with the matrix heat shock protein 70 (Hsc70) (Ssc1) as the central ATP-consuming subunit. How the presequence channel is regulated to permit translocation of preproteins but prevent leakage of small ions is unknown.

To understand the regulation of the Tim23 channel, we took a combinatorial *in vitro* and *in organello* approach. When purified Tim23 was reconstituted into liposomes and subjected to electrophysiological analysis in a planar lipid bilayer system, a cation-permeating channel with the reported characteristics of the presequence channel of the mitochondrial inner membrane was observed;

however, the pore remained mainly in an open state (Fig. 1A) (3, 10). The Tim23 channel did not display an intrinsic activity that forced fast channel closure. In organello, an open 450-pS channel, present in about 300 copies per isolated mitochondrion (18, 19), would seriously compromise the permeability barrier and the bioenergetic activity of the inner membrane. We thus asked whether additional components associated with Tim23 might play a role in regulating channel closure by comparing the membrane potential ($\Delta\psi$) of yeast mutant mitochondria.

The presequence translocase exists in two forms. One form (TIM23^{SOFT}) contains Tim23, Tim17, Tim50, and Tim21 and can direct preproteins into the inner membrane. The second form transports preproteins into the mitochondrial matrix and is associated with the motor PAM but lacks Tim21 (fig. S1A) (13, 20). We assessed the $\Delta\psi$ values of mitochondria isolated from different *tim* and *pam* mutants with the use of the potential-sensitive fluorescent dye 3,3'-dipropylthiadicarbocyanine iodide [DiSC₃(5)] (21) (Fig. 1, B to D). *tim17* and *tim21* mutant mitochondria displayed $\Delta\psi$ values comparable to that of wild-type mitochondria (13), whereas *tim50* mutant mitochondria (14) showed a severe reduction of $\Delta\psi$ (Fig. 1, B and D). In the translocon of the endoplasmic reticulum, the luminal Hsp70 (BiP) and a DnaJ protein are involved in regulation of the Sec61 channel (22, 23). Because PAM contains the Hsp70 Ssc1 and an associated DnaJ protein (Pam18), we asked whether the $\Delta\psi$ across the inner membrane was affected in mitochondria containing mutant versions of PAM subunits. However, neither *ssc1*, nor *pam18*, nor *tim44* mutant mitochondria (21, 24–28) exhibited a significant reduction in $\Delta\psi$ relative to wild-type mitochondria (Fig. 1, C and D), consistent with the observation that only two components, Tim50 and Tim17, are associated with Tim23 in both forms of the presequence translocase (13). Because the Tim23 channel is active in both forms, a factor that regulates channel closure should be present in either form. We conclude that functional Tim50 is required to maintain the $\Delta\psi$ in intact mitochondria.

The IMS domain of Tim50 interacts with the IMS domain of Tim23 (14–16). [Tim50 does

¹Biophysik, Universität Osnabrück, FB Biologie/Chemie, D-49034 Osnabrück, Germany. ²Centre de Génétique Moléculaire, Laboratoire propre du CNRS, F-91190 Gif-sur-Yvette, France. ³Institut für Biochemie und Molekularbiologie, Universität Freiburg, Hermann-Herder-Straße 7, D-79104 Freiburg, Germany. ⁴Fakultät für Biologie, Universität Freiburg, Schänzlestraße 1, D-79104 Freiburg, Germany. ⁵Department of Biochemistry, La Trobe University, Melbourne 3086, Australia.

*To whom correspondence should be addressed. E-mail: wagner@biologie.uni-osnabrueck.de (R.W.); nikolaus.pfanner@biochemie.uni-freiburg.de (N.P.)

†Present address: Institute for Plant Biology, Molecular Physiology, University of Zürich, 8008 Zürich, Switzerland.

not directly interact with the TOM complex (13), nor is it present in any other translocase of the inner membrane (fig. S1B).] We asked whether Tim50_{IMS} affected the gating of the Tim23 channel. We expressed and purified Tim50_{IMS} from *Escherichia coli* cells (Fig. 2A) and added it to the reconstituted Tim23 channel (21). Nanomolar concentrations of Tim50_{IMS} led to rapid and efficient closure of the channel (Fig. 2B). The reversal potential was not changed by addition of Tim50_{IMS} (Fig. 2C). Similarly, the conductance states of the Tim23 channel, as shown for the main conductance of 445 ± 11 pS and the most frequent subconductance state of 150 ± 7 pS, were not altered by Tim50_{IMS} (450 ± 8 pS, 155 ± 6 pS) (Fig. 2D), indicating that the basic channel properties were not affected.

The reconstitution of Tim23 into small unilamellar liposomes leads to an asymmetric insertion such that the IMS domain is exposed to the trans compartment of the planar bilayer (10). To test the specificity of Tim50_{IMS}-induced channel closure, we added Tim50_{IMS} to the cis compartment. The Tim23 channel was not affected (Fig. 2E), demonstrating that the hydrophilic Tim50 domain affects gating of Tim23 only from the IMS side. Moreover, control proteins did not affect the reconstituted Tim23 channel, even at millimolar concentrations (Fig. 2F). The Δψ value of intact mitochondria has been estimated to be about 150 mV (29). Determination of the Tim23 channel open probability (P_{open}) confirmed that the reconstituted Tim23 was mainly in the open state at this physiological voltage, whereas the addition of Tim50_{IMS} drastically reduced P_{open} at the relevant voltage range (Fig. 2G).

Tim50_{IMS}-induced closure of the Tim23 channel occurred in distinct steps, reflecting the described conductance states of Tim23 (Fig. 2, B to D) (10). This finding suggests that Tim50_{IMS} does not lead to a direct physical block of the channel, but rather induces distinct gating steps of Tim23 toward the closed state. Tim23 has been reported to form a dimer in mitochondria (11). The dimer apparently reflects the inactive state in the absence of preprotein, because Tim23 is monomeric when preproteins accumulate in the presequence translocase (11). We established an assay to monitor oligomerization of Tim23 in *tim50* mutant mitochondria (21). Tim23 with a protein A tag was coexpressed in yeast cells containing an untagged wild-type copy of Tim23. Isolated mitochondria were lysed in digitonin and TIM23-PAM was purified by IgG-affinity chromatography. TIM and PAM components analyzed, including untagged Tim23, were copurified with tagged Tim23 when wild-type mitochondria were used (Fig. 3A) (13, 14). In conditional *tim50* mutant mitochondria [with partial inactivation of Tim50 (13)], the copu-

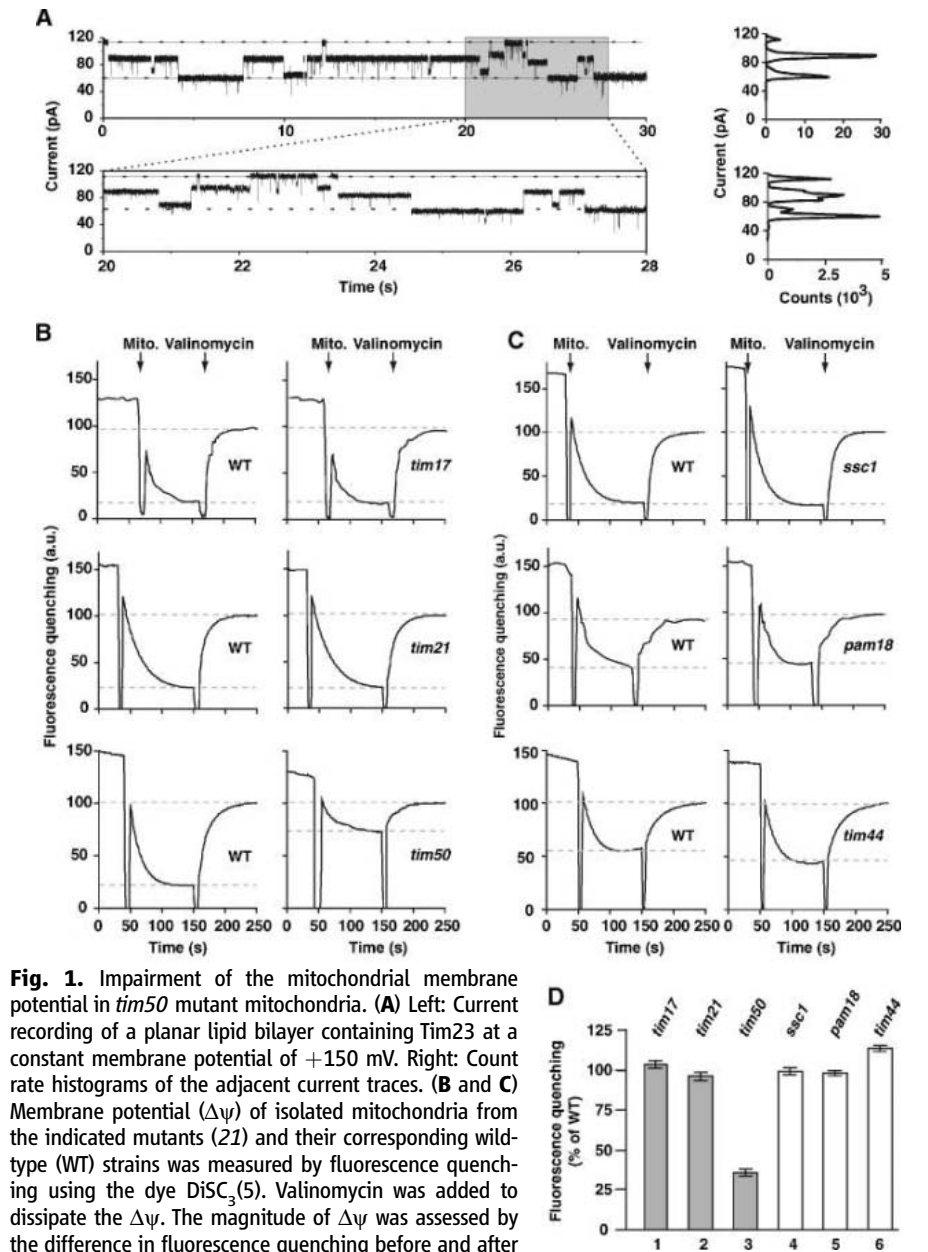


Fig. 1. Impairment of the mitochondrial membrane potential in *tim50* mutant mitochondria. (A) Left: Current recording of a planar lipid bilayer containing Tim23 at a constant membrane potential of +150 mV. Right: Count rate histograms of the adjacent current traces. (B and C) Membrane potential ($\Delta\psi$) of isolated mitochondria from the indicated mutants (21) and their corresponding wild-type (WT) strains was measured by fluorescence quenching using the dye DiSC₃(5). Valinomycin was added to dissipate the $\Delta\psi$. The magnitude of $\Delta\psi$ was assessed by the difference in fluorescence quenching before and after addition of valinomycin. (D) Comparison of fluorescence quenching between *tim* and *pam* mutant mitochondria as percentage of the corresponding wild-type value. SEM values were calculated from at least three independent experiments.

rification of various TIM and PAM components with tagged Tim23 was comparable to that in wild-type mitochondria, with one exception: The yield for the untagged form of Tim23 was strongly reduced in the copurification (Fig. 3A) (the mitochondrial levels of Tim23 were unchanged in *tim50* mutants). Thus, a functional Tim50 is selectively required for oligomerization of Tim23 but not for the association of other TIM or PAM components with Tim23.

These results indicate that Tim50 promotes the oligomerization and closure of the Tim23 channel in the absence of preproteins, allowing a tight regulation of the Tim23 pore

in the physiologically relevant range of the membrane potential. However, for protein translocation the channel needs to be activated and reopened. The observation that presequences triggered a dissociation of the Tim23 dimer (11) led us to ask whether presequences were able to activate the closed Tim23 channel. We used the planar bilayer system with reconstituted Tim23 and added Tim50_{IMS} to close the channel (Fig. 3B). Upon addition of a synthetic peptide corresponding to the presequence of cytochrome oxidase subunit IV, we observed opening of the channel with fast flickering gating (Fig. 3B). Thus, the channel was not simply shifted

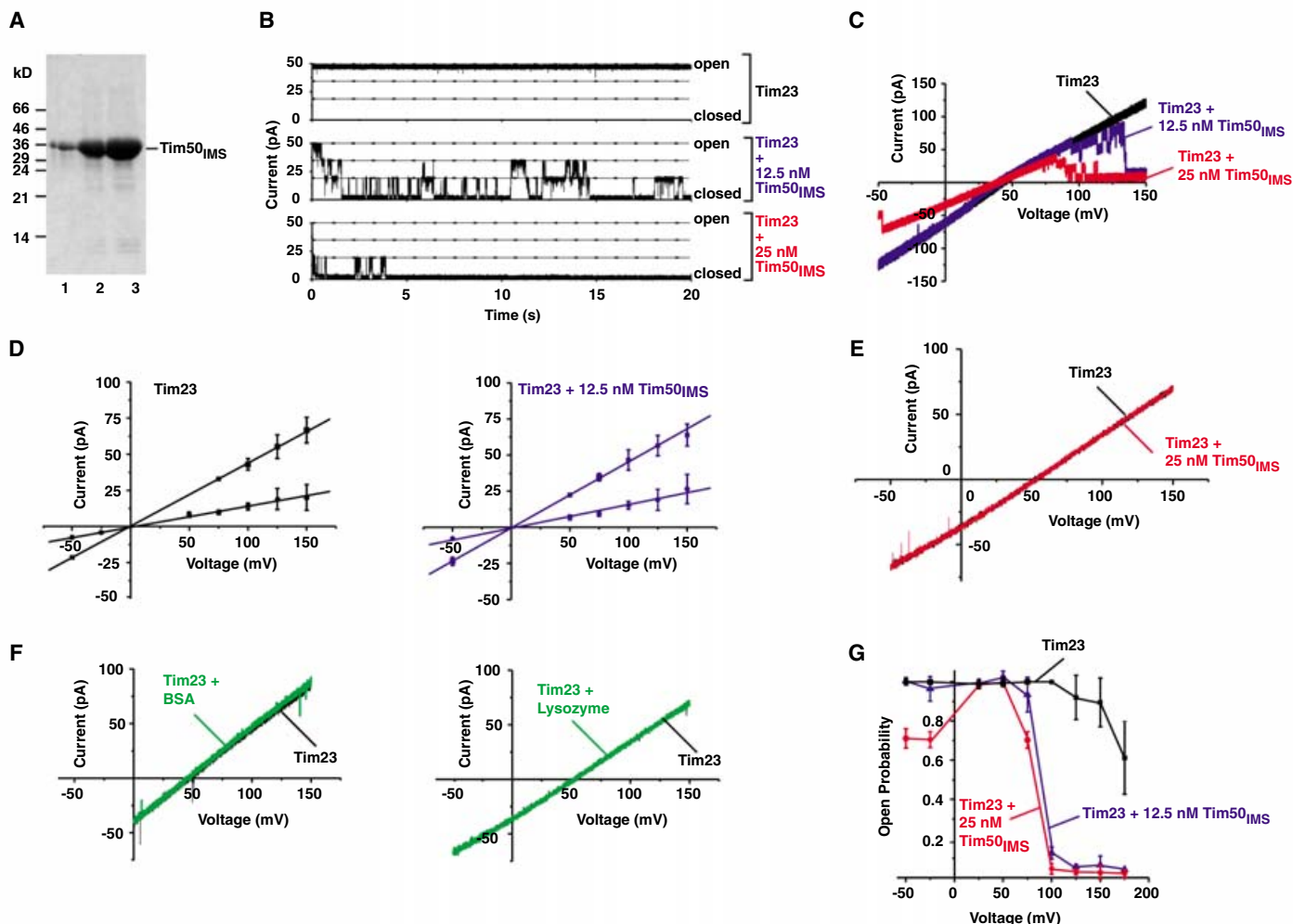


Fig. 2. The intermembrane space domain of Tim50 (Tim50_{IMS}) induces closure of the Tim23 channel. **(A)** Tim50_{IMS} was expressed and purified from *E. coli* cells. Tim50_{IMS}-containing fractions were separated by SDS-polyacrylamide gel electrophoresis (PAGE) to assess purity of the preparation. **(B)** Tim23 was incorporated into planar lipid bilayers and analyzed in the presence or absence of Tim50_{IMS} (trans chamber) at a potential of +100 mV. **(C)** Current-voltage relationship of Tim23 alone or after addition of the indicated amounts of Tim50_{IMS} added at the trans side of the membrane. **(D)** Current-voltage relationship of Tim23 in the absence or presence of 12.5 nM Tim50_{IMS}. The

main conductance (squares) and the most frequent subconductance state (circles) are shown. SEM values were calculated from at least 10 independent measurements. **(E)** Tim50_{IMS} was added to the reconstituted Tim23 channel from the cis side of the membrane. **(F)** As in **(C)**, with the exception that 1.5 mM bovine serum albumin or 1.5 mM lysozyme were added instead of Tim50_{IMS} to the trans chamber. **(G)** Voltage-dependent open probability of the Tim23 channel alone or in the presence of the indicated amounts of Tim50_{IMS}. Quantification was performed by comparing the mean current determined over a time range of 1 min at a constant holding potential.

to a permanently open form but to a highly active form with rapid gating transitions. A signal peptide specific for mitochondrial carrier proteins (30) did not activate the Tim23 channel (Fig. 3B).

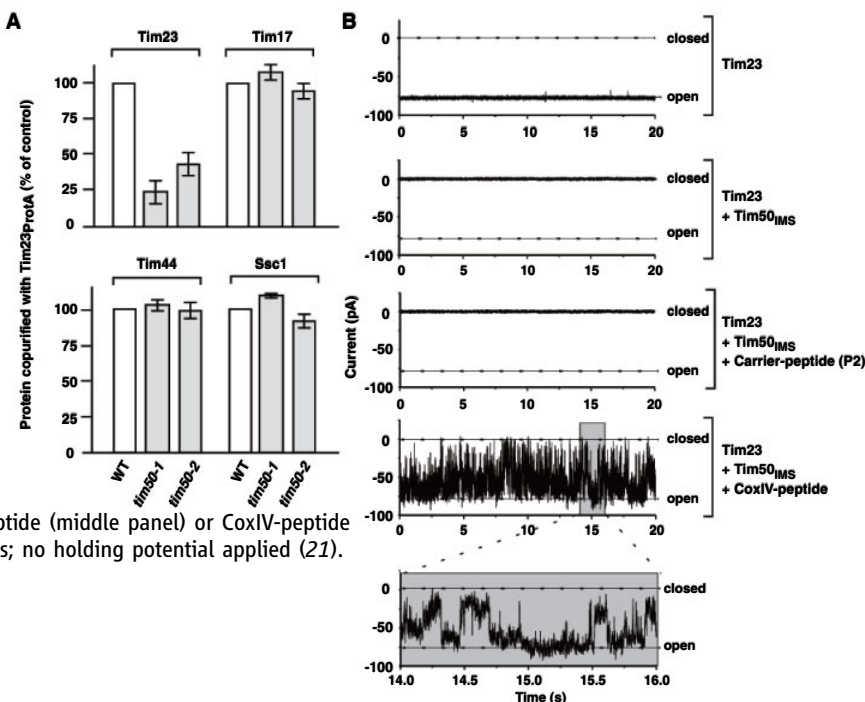
Our work reveals a molecular mechanism of how the proton-motive force across the mitochondrial inner membrane can be maintained despite the presence of large channels that transport entire precursor polypeptides across the membrane. The Tim23 channel is tightly regulated so as to maintain the permeability barrier of the inner mitochondrial membrane in its inactive state while being opened for translocation of polypeptide chains. Tim50 and presequences act in an antagonistic manner in this process. Whereas the hydrophilic IMS domain of Tim50 pro-

motes oligomerization and voltage-dependent closure of the channel, presequences selectively override the Tim50-induced closure and activate the channel. This mechanism ensures selective on-demand opening of the Tim23 channel when a preprotein needs to be translocated through the presequence translocase and allows closure of the channel after transport is completed.

References and Notes

- W. Wickner, R. Schekman, *Science* **310**, 1452 (2005).
- D. J. Schnell, D. N. Hebert, *Cell* **112**, 491 (2003).
- R. E. Jensen, A. E. Johnson, *Nat. Struct. Biol.* **8**, 1008 (2001).
- C. M. Koehler, *Annu. Rev. Cell Dev. Biol.* **20**, 309 (2004).
- W. Neupert, *Annu. Rev. Biochem.* **66**, 863 (1997).
- P. Rehling, K. Brandner, N. Pfanner, *Nat. Rev. Mol. Cell Biol.* **5**, 519 (2004).
- D. Stock, C. Gibbons, I. Arechaga, A. G. Leslie, J. E. Walker, *Curr. Opin. Struct. Biol.* **10**, 672 (2000).
- L. Palmieri *et al.*, *Biochim. Biophys. Acta* **1459**, 363 (2000).
- T. Lohret, R. E. Jensen, K. W. Kinnally, *J. Cell Biol.* **137**, 377 (1997).
- K. N. Truscott *et al.*, *Nat. Struct. Biol.* **8**, 1074 (2001).
- M. F. Bauer, C. Sirrenberg, W. Neupert, M. Brunner, *Cell* **87**, 33 (1996).
- T. Komiya *et al.*, *EMBO J.* **17**, 3886 (1998).
- A. Chacinska *et al.*, *Cell* **120**, 817 (2005).
- A. Geissler *et al.*, *Cell* **111**, 507 (2002).
- H. Yamamoto *et al.*, *Cell* **111**, 519 (2002).
- D. Mokranjac *et al.*, *EMBO J.* **22**, 816 (2003).
- D. Mokranjac, D. Popov-Celeketi, K. Hell, W. Neupert, *J. Biol. Chem.* **280**, 23437 (2005).
- P. J. T. Dekker *et al.*, *EMBO J.* **16**, 5408 (1997).
- J. Rassow *et al.*, *J. Cell Biol.* **109**, 1421 (1989).
- T. Oka, K. Mihara, *Mol. Cell* **18**, 145 (2005).

Fig. 3. Presequences of mitochondrial precursor proteins overcome Tim50_{IMS}-induced closure of the Tim23 channel. (A) Tim23_{ProtA} was expressed from a plasmid in wild-type and *tim50* mutant cells carrying a wild-type copy of *TIM23* on the chromosome. Isolated mitochondria were solubilized in digitonin buffer and the TIM23 complex isolated via immunoglobulin G affinity chromatography (21). Bound proteins were eluted with sample buffer, separated by SDS-PAGE, and analyzed by immunoblotting. Signals were quantified with Scion Image 1.62a, standardized to the amount of isolated Tim23_{ProtA}. The amount of protein purified from wild-type mitochondria was set to 100% (control). SEM was calculated from at least three independent experiments. (B) Current recording of Tim23 alone (upper panel), Tim23 plus Tim50_{IMS} (second panel), and Tim23 plus Tim50_{IMS} upon addition of P2 carrier-peptide (middle panel) or CoxIV-peptide (bottom panels) under asymmetrical buffer conditions; no holding potential applied (21).



21. See supporting material on Science Online.
22. N. N. Alder, Y. Shen, J. L. Brodsky, L. M. Hendershot, A. E. Johnson, *J. Cell Biol.* **168**, 389 (2005).
23. B. D. Hamman, L. M. Hendershot, A. E. Johnson, *Cell* **92**, 747 (1998).
24. P. D. D'Silva, B. Schilke, W. Walter, A. Andrew, E. A. Craig, *Proc. Natl. Acad. Sci. U.S.A.* **100**, 13839 (2003).
25. B. D. Gambill *et al.*, *J. Cell Biol.* **123**, 109 (1993).
26. D. Mokranjac, M. Sichtung, W. Neupert, K. Hell, *EMBO J.* **22**, 4945 (2003).
27. K. N. Truscott *et al.*, *J. Cell Biol.* **163**, 707 (2003).
28. W. Voos *et al.*, *EMBO J.* **15**, 2668 (1996).
29. L. M. Loew, R. A. Tuft, W. Carrington, F. S. Fay, *Biophys. J.* **65**, 2396 (1993).
30. P. Rehling *et al.*, *Science* **299**, 1747 (2003).
31. We thank I. Perschil, H. Müller, and A. Schulze-Speking for excellent technical assistance. Supported by the Deutsche Forschungsgemeinschaft, the Sonderforschungsbereich 388 and 431, Gottfried Wilhelm Leibniz Program, Max Planck Research Award, Alexander von

Humboldt Foundation, Bundesministerium für Bildung und Forschung, and the Fonds der Chemischen Industrie.

Supporting Online Material

www.sciencemag.org/cgi/content/full/312/5779/1523/DC1

Materials and Methods

Fig. S1

References

20 March 2006; accepted 5 May 2006

10.1126/science.1127628

A Virulence Locus of *Pseudomonas aeruginosa* Encodes a Protein Secretion Apparatus

Joseph D. Mougous,¹ Marianne E. Cuff,³ Stefan Raunser,² Aimee Shen,¹ Min Zhou,³ Casey A. Gifford,¹ Andrew L. Goodman,¹ Grazyna Joachimiak,³ Claudia L. Ordoñez,⁴ Stephen Lory,¹ Thomas Walz,² Andrzej Joachimiak,^{3,5*} John J. Mekalanos^{1*}

Bacterial pathogens frequently use protein secretion to mediate interactions with their hosts. Here we found that a virulence locus (HSI-I) of *Pseudomonas aeruginosa* encodes a protein secretion apparatus. The apparatus assembled in discrete subcellular locations and exported Hcp1, a hexameric protein that forms rings with a 40 angstrom internal diameter. Regulatory patterns of HSI-I suggested that the apparatus functions during chronic infections. We detected Hcp1 in pulmonary secretions of cystic fibrosis (CF) patients and Hcp1-specific antibodies in their sera. Thus, HSI-I likely contributes to the pathogenesis of *P. aeruginosa* in CF patients. HSI-I-related loci are widely distributed among bacterial pathogens and may play a general role in mediating host interactions.

Pseudomonas aeruginosa is an opportunistic pathogen that chronically infects the lungs of >80% of cystic fibrosis patients and is the primary cause of morbidity and mortality in these patients (1).

A distinguishing feature of the bacterium is its high degree of versatility, which provides *P. aeruginosa* sufficient phenotypic plasticity to form both acute and chronic infections in humans (2, 3). The choice between these

disparate life-styles is governed by global virulence regulators, including RetS (regulator of exopolysaccharide and type III secretion) (4) and LadS (lost adherence sensor) (5). RetS and LadS reciprocally regulate virulence determinants such as type III secretion, which is RetS-activated and LadS-repressed, as well as exopolysaccharide production, which is RetS-repressed and LadS-activated. These virulence factors are important in acute and chronic infections, respectively.

In addition to characterized virulence pathways, microarray analyses indicated that RetS and LadS reciprocally regulated a functionally uncharacterized virulence locus (Fig. 1). Con-

¹Department of Microbiology and Molecular Genetics, ²Department of Cell Biology, Harvard Medical School, Boston, MA 02115, USA. ³Midwest Center for Structural Genomics and Structural Biology Center, Biosciences Division, Argonne National Laboratory, Argonne, IL 60439, USA. ⁴Division of Respiratory Diseases and Cystic Fibrosis Center, Children's Hospital Boston, Harvard Medical School, Boston, MA 02115, USA. ⁵Department of Biochemistry and Molecular Biology, University of Chicago, Chicago, IL 60637, USA.

*To whom correspondence should be addressed. E-mail: John_Mekalanos@hms.harvard.edu (J.J.M.); andrzej@anl.gov (A.J.)

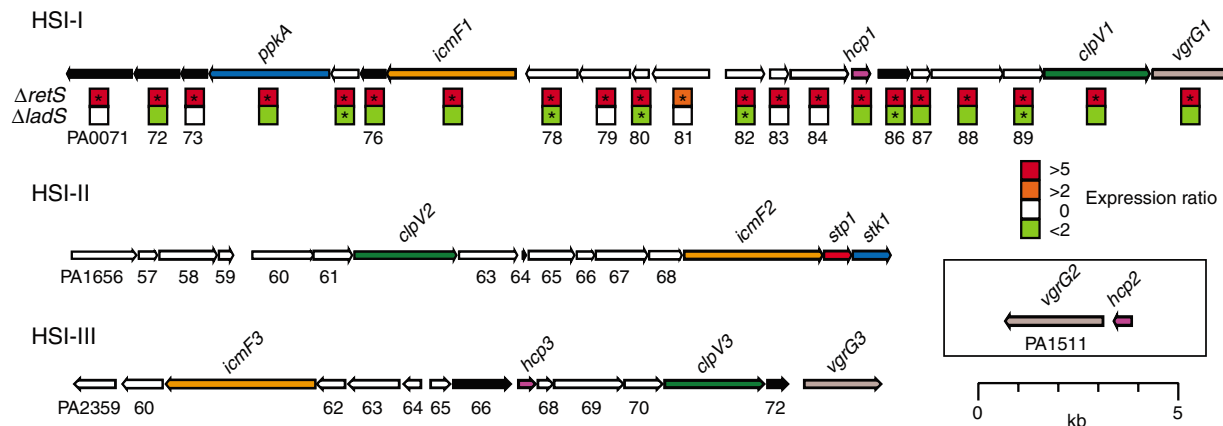


Fig. 1. Overview of *P. aeruginosa* HSI genes and reciprocal regulation of HSI-I by RetS and LadS. Conserved hypothetical HSI ORFs not discussed in the text (white) and ORFs that lie within the predicted HSI operons (black) are labeled with their genome annotation ORF number [assigned on the basis of (7)]. Predicted paralogous ORFs with prior characterization and those

characterized in this study are colored consistently in each locus. The boxed insert shows the position of the *hcp2/vgrG2* locus encoded elsewhere in the genome. The boxes beneath HSI-I genes summarize transcriptional profiling data from two prior studies (4, 5). The asterisks denote measurements that meet the statistical significance threshold defined in each study.

sistent with its regulatory patterns by RetS and LadS, the virulence locus was required for chronic *P. aeruginosa* infection of the rat lung (Fig. 1) (6). This RetS- and LadS-regulated locus is highly homologous to a group of genes found in many Gram-negative proteobacteria that have been termed the IcmF-associated homologous protein (IAHP) cluster (7). *P. aeruginosa* encodes two other IAHP-related loci elsewhere in its genome; however, these loci were not regulated by either RetS or LadS and have no known role in virulence (Fig. 1). An overview of the distribution and genetic constituents of IAHP loci is shown (table S1).

The IAHP-related locus of *Vibrio cholerae*, which the authors have designated a type VI secretion system, mediates cytotoxicity in phagocytic cells and is required for the extracellular secretion of four proteins lacking canonical hydrophobic amino-terminal signal sequences (8). We postulated that the RetS- and LadS-regulated IAHP locus in *P. aeruginosa* could play a similar role in extracellular protein targeting. To test this hypothesis, we activated expression of the locus in *P. aeruginosa* PAO1 by deleting *retS*. Comparison of the supernatant fractions of $\Delta retS$ and wild-type revealed that a small protein ($M_r \sim 18$ kD) was abundantly secreted by $\Delta retS$ (Fig. 2A). In-gel digestion followed by tandem mass spectrometry identified the protein as Hcp1 (PA0085), a result that was confirmed by deleting *hcp1* in $\Delta retS$ (Fig. 2A). Notably, Hcp1 does not have a recognizable signal sequence (9) and is orthologous to one of the four proteins secreted by *V. cholerae* in an IAHP-dependent manner (8). Also, the gene encoding Hcp1 resides in the IAHP-related virulence locus regulated by RetS and LadS (Fig. 1). We will thus refer to this locus as *P. aeruginosa* Hcp1 secretion island I (HSI-I in Fig. 1).

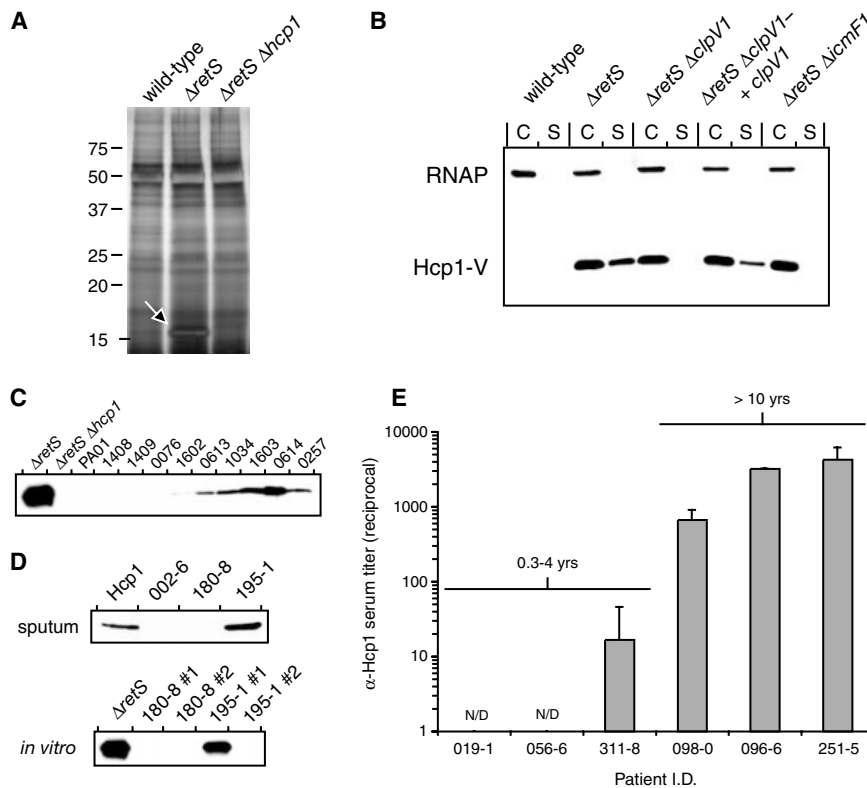


Fig. 2. *P. aeruginosa* HSI-I is required for secretion of Hcp1 and is active in cystic fibrosis infections. (A) Hcp1 is hypersecreted by $\Delta retS$. SDS-polyacrylamide gel electrophoresis analysis of concentrated culture supernatants from various *P. aeruginosa* strains. The arrow highlights the position of secreted Hcp1 in $\Delta retS$. (B) Immunoblot analysis of HSI-I-dependent secretion of Hcp1-V. In addition to the genetic alterations indicated, each strain contains *hcp1-V*. Equal quantities of cell (C) and supernatant (S) fractions were probed with antibodies specific for the β -subunit of RNA polymerase (RNAP) and the VSV-G epitope. (C) Immunoblot analysis of Hcp1 secretion by control strains and a panel of CF patient clinical isolates. (D) Immunoblot analysis of Hcp1 in sputum from CF patients (upper blot). Sputum sample 002-6 is from a CF patient not infected with *P. aeruginosa*; sputum sample 180-8 is from a CF patient infected with two *P. aeruginosa* strains that do not secrete Hcp1 (lower blot); and sputum sample 195-1 is from a CF patient infected with a *P. aeruginosa* strain that actively secretes Hcp1 and a second that does not (lower blot). (E) ELISA analysis of sera from CF patients for antibody response against Hcp1.

To assess more quantitatively the production and localization of Hcp1, we constructed a C-terminal chromosomal fusion of the vesicular stomatitis virus glycoprotein (VSV-G) epitope to *hcp1* (*hcp1-V*). The VSV-G epitope did not affect Hcp1 overexpression or secretion in *ΔretS* (Fig. 2B). Detection of Hcp1 in *ΔretS* supernatants was not due to cell lysis, as determined by an intracellular protein control (Fig. 2B). The fraction of secreted Hcp1-V relative to intracellular Hcp1-V was lower in wild-type than in *ΔretS* (fig. S1), which suggests that, in addition to repression of *hcp1*, RetS negatively regulates Hcp1 secretion.

Next, we tested the dependence of Hcp1 secretion by *ΔretS* on HSI-I components by generating a deletion of *icmF1* in the *ΔretS hcp1-V* background and examining the cellular localization of Hcp1 (Fig. 2B). IcmF is required for *Legionella pneumophila* type IVB-dependent secretion of SidC (10), and the *V. cholerae* IcmF homolog (VasK) is required for Hcp secretion (8); thus, we hypothesized that *icmF1* would be essential for HSI-I-dependent Hcp1 secretion. Although deletion of *icmF1* did not lower cellular Hcp1-V levels relative to *ΔretS*, secreted Hcp1-V levels were dramatically reduced (Fig. 2B). This result supports the requirement of an intact HSI-I for Hcp1 secretion.

To address whether secretion of Hcp1 occurs naturally in *P. aeruginosa*, we used Hcp1-specific antibodies to examine Hcp1 secretion in a collection of CF patient *P. aeruginosa* isolates (Fig. 2C, table S2). Hcp1 secretion varied among isolates: Robust secretion was detected in some isolates, yet was below the limit of detection in others. Mass spectrometric analysis was used to confirm the secretion of Hcp1 from clinical isolates.

Because our analysis of Hcp1 secretion in CF isolates required their growth in vitro, which might artificially stimulate Hcp1 secretion, we assayed Hcp1 secretion directly in CF patient sputum. Hcp1 was readily detected in sputum from a patient infected with *P. aeruginosa* actively secreting Hcp1 in vitro (195-1 no. 1 in Fig. 2D and fig. S2); however, the protein was not detected in sputum from an uninfected patient (002-6) or a patient infected with *P. aeruginosa* strains not secreting Hcp1 (180-8 in Fig. 2D). To determine whether Hcp1 secretion might have immunological consequences, we assayed for Hcp1-specific antibodies in the sera of six CF patients. At the time of sampling, three of these patients had maintained chronic *P. aeruginosa* infections lasting more than 10 years and three had been infected with *P. aeruginosa* for 0.3 to 4 years. A robust and specific Hcp1 response was detected in the three patients chronically infected with *P. aeruginosa*, whereas only a weak response was detected in one of the patients infected for a shorter duration (Fig. 2E and table S2). Thus, Hcp1 is actively secreted within the lungs of CF patients who have had long-term infection, which supports a role for HSI-I in chronic *P. aeruginosa* infections.

The IAHP-related gene clusters include an open reading frame (ORF), *clpV*, encoding a protein with strong homology to the AAA+ family protein ClpB (Fig. 1, and table S1, fig. S2). ClpB is required for thermotolerance and translocates aggregated proteins in an energy-dependent manner through its central channel (11). Because AAA+ family adenosine triphosphatases (ATPases) are hypothesized to provide the force for substrate translocation in many bacterial secretion systems (12, 13), we specu-

lated that *P. aeruginosa* ClpV1 may function similarly for the purpose of secretion rather than disaggregation. Indeed, the IAHP ClpV proteins of enteropathogenic *Escherichia coli* and *Salmonella typhimurium* form hexameric structures that have ATPase activity, but lack protein disaggregase activity (14).

To distinguish the functions of ClpB and ClpV1 in *P. aeruginosa*, we determined the thermotolerance of *ΔclpB* and *ΔclpV1*. Consistent with our hypothesis, deletion of *clpB* resulted in thermosensitivity, whereas deletion of *clpV1* did not affect thermotolerance (Fig. 3A). Furthermore, deletion of *clpV1* in *ΔretS hcp1-V* abrogated Hcp1-V secretion without altering Hcp1-V levels in the cellular fraction (Fig. 2B). To determine whether the adenosine triphosphate (ATP) hydrolytic activity of ClpV1 is essential for the mechanism of Hcp1 secretion, we inactivated the ATP hydrolysis activity of the AAA-1 domain of ClpV1 by introducing a mutation into the Walker B motif [Glu³¹⁰ replaced by Ala (E310A)]. Mutation of the analogous residue of ClpB (E279A) significantly decreased its activity, both in vitro and in vivo (15). When ClpV1_{E310A} was expressed at levels similar to that of ClpV1 in *ΔclpV1 ΔretS*, the mutant protein failed to complement the defect in Hcp1 secretion (Fig. 3B). Thus, ATP hydrolysis by the AAA-1 domain of ClpV1 is required for Hcp1 secretion. We propose that ClpV1 functions critically as the energy source facilitating HSI-I-dependent Hcp1 secretion.

As an essential component of the secretion apparatus encoded by HSI-I, we reasoned that the function of ClpV1 should be reflected in its subcellular localization. To visualize ClpV1, we generated a strain carrying a chromosomal

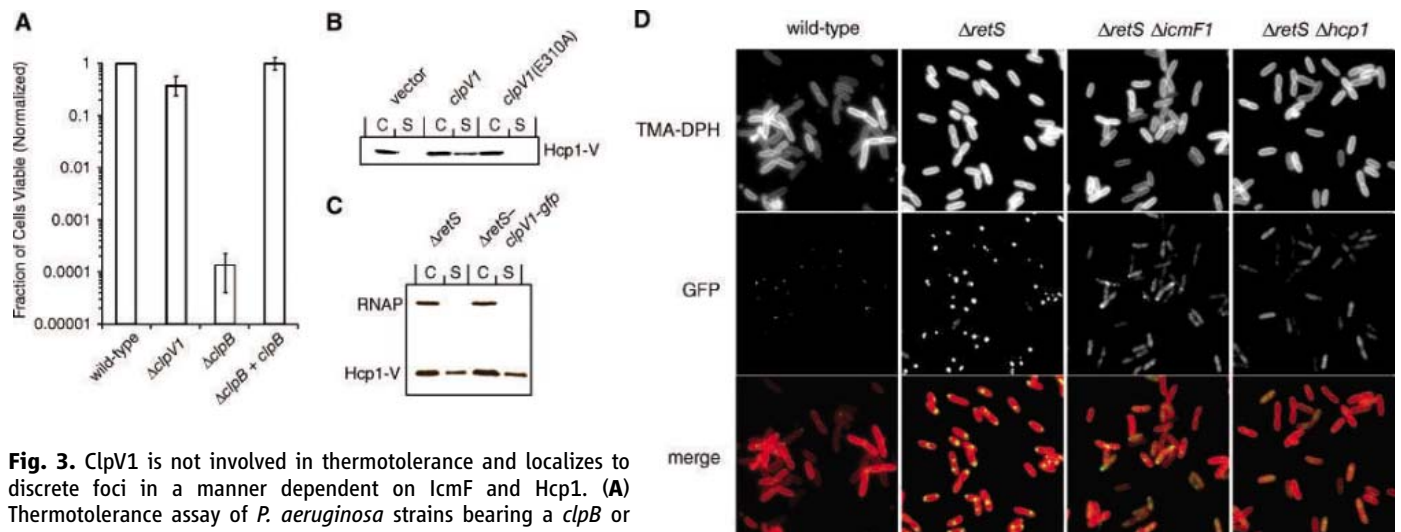


Fig. 3. ClpV1 is not involved in thermotolerance and localizes to discrete foci in a manner dependent on IcmF and Hcp1. (A) Thermotolerance assay of *P. aeruginosa* strains bearing a *clpB* or *clpV1* deletion. Cell viability before and after a 25-min heat pulse at 55°C was determined by colony-forming units. The thermotolerance of each strain was normalized relative to wild-type. (B and C) Immunoblot analysis of Hcp1-V secretion by ClpV1 and the AAA-1 mutant ClpV1_{E310A}

(B) and in *ΔretS clpV1-gfp* (C). (D) Fluorescence microscopy of indicated strains also bearing *clpV1-gfp*. TMA-DPH is a membrane dye used to highlight the outline of the cells.

C-terminal fusion of the green fluorescent protein (GFP) to ClpV1 (ClpV1-GFP) in the $\Delta retS$ background ($\Delta retS clpV1-gfp$). Hcp1-V secretion was not affected by fusing GFP to ClpV1, and the fusion protein remained intact (Fig. 3C and fig. S3). ClpV1-GFP localized to single discrete foci in the majority of $\Delta retS clpV1-gfp$ cells (Fig. 3D). Although less intense, a similar pattern of punctate localization was observed in the wild-type background (Fig. 3D).

To establish whether the punctate localization of ClpV1-GFP was functionally relevant, we deleted *icmF1* in the $\Delta retS clpV1-gfp$ background and measured the effect on ClpV1-GFP localization. Deletion of *icmF1* dramatically reduced the number of cells with discrete ClpV1-GFP foci. Instead, the fluorescent signal in this mutant strain was most often evenly distributed across the cell and occasionally detected as weak foci (Fig. 3D).

We next questioned whether Hcp1 might also be required for proper localization of ClpV1-GFP. To address this, we generated an *hcp1* deletion in the $\Delta retS clpV1-gfp$ background and assessed ClpV1-GFP localization. Deletion of *hcp1* in these cells resulted in a diffuse localization pattern of ClpV1-GFP similar to that observed in the $\Delta retS \Delta icmF1$ background, although the frequency of residual punctate foci was decreased in cells lacking Hcp1 relative to those lacking IcmF1 (Fig. 3D). Neither the *hcp1* nor *icmF1* mutations in the $\Delta retS clpV1-gfp$ background affected the stability or expression level of ClpV1-GFP (fig. S3). Thus, IcmF1 and Hcp1 are required for punctate localization of ClpV1-GFP. We interpret the punctate localization pattern of ClpV1-GFP to indicate the presence of an HSLI-encoded secretion apparatus. IcmF1 appears to be required for efficient assembly of the appara-

tus, whereas Hcp1 is absolutely required for assembly. Given that wild-type *P. aeruginosa* fails to secrete Hcp1 but maintains ClpV1-GFP localization, the presence of Hcp1, but not its secretion, appears to be required for punctate ClpV1-GFP localization.

Although Hcp is highly conserved among Gram-negative proteobacteria (table S1), it shares little sequence homology with proteins of known structure. In an effort to gain insight into the function of Hcp, we determined the x-ray crystal structure of *P. aeruginosa* Hcp1 to a resolution of 1.95 Å. Hcp1 crystallized in the P6 space group with three nearly identical monomers in the asymmetric unit (Fig. 4A and table S3). The three Hcp1 monomers formed two closely related hexameric rings [0.25 Å root mean square deviation]: a true hexamer with six-fold symmetry (chain B in the Protein Data Bank, code 1Y12) and a pseudohexamer with three-fold symmetry (chains A and C) (Fig. 4,

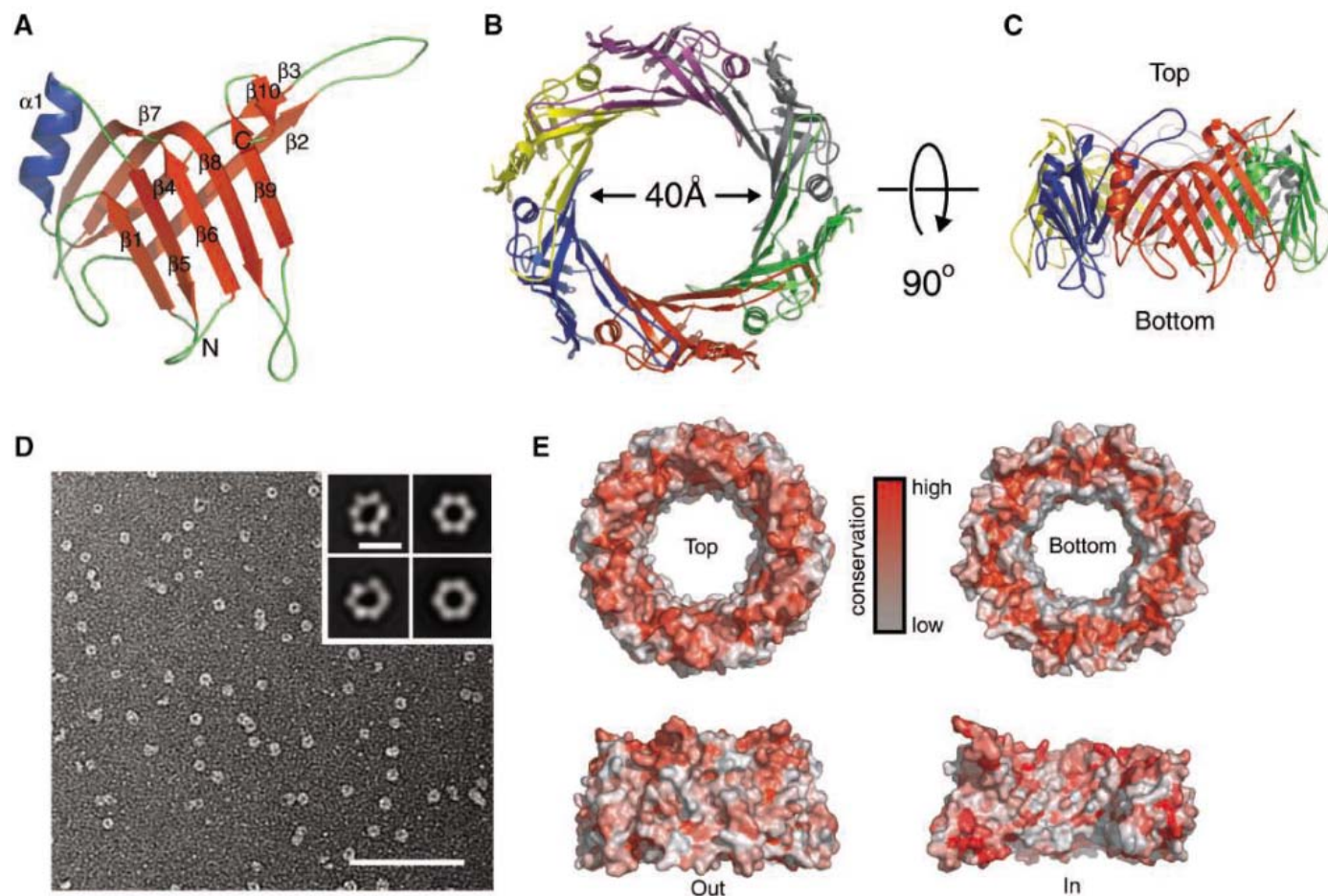


Fig. 4. Hcp1 forms a hexameric ring with a large internal diameter. (A) Ribbon representation of the Hcp1 monomer colored by secondary structure: β strands, red; α helices, blue; and loops, green. (B) Top view of a ribbon representation of the crystallographic Hcp1 hexamer. The individual subunits are colored differently to highlight their organization. (C) Edge-on view of the Hcp1 hexamer shown in (B). (D) Electron microscopy and single-particle analysis of Hcp1. Electron micrograph of Hcp1 negatively stained with 0.75% (w/v) uranyl formate. Scale bar, 100

nm. (Inset) (Left) Representative class averages and (right) the same averages after six-fold symmetrization. Inset scale bar, 10 nm. (E) Sequence conservation analysis of Hcp1. An alignment of 107 Hcp proteins in 43 Gram-negative bacteria was used to plot the relative degree of conservation at each amino acid on the surface of Hcp1 (see methods in supporting online material). Conservation is indicated by color, where red residues are highly conserved and white residues are poorly conserved.

B and C). The Hcp1 ring interior is a 24-stranded β barrel ~ 40 Å in diameter.

To determine the oligomeric state of Hcp1 in solution, we analyzed the purified protein by analytical gel-filtration chromatography (fig. S4) and transmission electron microscopy (Fig. 4D). The predominant form of Hcp1 was a ring assembly with dimensions closely matching those observed in the crystal lattice (Fig. 4D). Furthermore, averaging of ~ 6000 particles revealed that the rings contained six clearly discernible subunits with approximate six-fold symmetry (Fig. 4D). Thus, the hexameric rings found in the Hcp1 crystal structure are physiologically relevant and represent the predominant form of the protein in solution. Given the large diameter of hexameric Hcp1, assembly of the particle is likely to occur following secretion.

To identify regions of the Hcp1 structure potentially important for its biological activity, we generated an alignment of 107 Hcp1 proteins from 43 bacterial species and plotted the degree of conservation of each residue onto the structure. This analysis revealed a nonuniform pattern of Hcp1 surface residue conservation: the most highly conserved residues are found on the top and bottom faces of the protein; residues located around the inner and outer circumferences are poorly conserved (Fig. 4E). A particularly well-conserved patch of residues occupies the cleft on the bottom face of Hcp1 (residues 15, 16, 26, 60, 63, 88, 89, 169, and 139). Many of these residues mediate critical subunit contacts, perhaps explaining their high degree of conservation. Others such as Asp²⁶, Lys⁸⁸, and Gln¹³⁹, are not engaged in hexamer-stabilizing interactions; thus, their conservation suggests that they may modulate the function of Hcp1. We propose a model whereby Hcp1 associates with proteins on both faces in order to build a channel through which other macromolecules could be transported.

We have provided biochemical and genetic evidence that a virulence-associated genetic locus of *P. aeruginosa*, termed HSI-I, encodes a protein secretion apparatus. We further demonstrate that a ClpB-like AAA+ family protein, ClpV1, forms a core component of this apparatus and is likely to provide the energy for translocation of Hcp1. The pattern of HSI-I regulation by RetS and LadS and the prior findings, that the locus is essential in the chronic rat lung infection model (6), and our current data indicating that the locus actively secretes Hcp1 during chronic infection of CF patients, collectively suggest a role for HSI-I in chronic *P. aeruginosa* infections. Our findings also support efforts to develop vaccines and therapeutics targeting Hcp1 or components of the HSI-I-encoded apparatus as treatments for chronic *P. aeruginosa* infections. Given that IAHP-related loci are conserved among many Gram-negative proteobacterial pathogens and have been implicated in host interactions in

several instances (8, 16, 17), the secretory systems they encode may represent yet another general mechanism by which these bacterial pathogens communicate with their hosts.

References and Notes

1. J. R. Govan, V. Deretic, *Microbiol. Rev.* **60**, 539 (1996).
2. S. Furukawa, S. L. Kuchma, G. A. O'Toole, *J. Bacteriol.* **188**, 1211 (2006).
3. T. L. Yahr, E. P. Greenberg, *Mol. Cell* **16**, 497 (2004).
4. A. L. Goodman *et al.*, *Dev. Cell* **7**, 745 (2004).
5. I. Ventre *et al.*, *Proc. Natl. Acad. Sci. U.S.A.* **103**, 171 (2006).
6. E. Potvin *et al.*, *Environ. Microbiol.* **5**, 1294 (2003).
7. S. Das, K. Chaudhuri, *In Silico Biol.* **3**, 287 (2003).
8. S. Pukatzki *et al.*, *Proc. Natl. Acad. Sci. U.S.A.* **103**, 1528 (2006).
9. S. G. Williams, L. T. Varcoe, S. R. Attridge, P. A. Manning, *Infect. Immun.* **64**, 283 (1996).
10. S. M. VanRheenen, G. Dumenil, R. R. Isberg, *Infect. Immun.* **72**, 5972 (2004).
11. J. Weibezahn *et al.*, *Cell* **119**, 653 (2004).
12. Y. Akeida, J. E. Galan, *Nature* **437**, 911 (2005).
13. H. J. Yeo, G. Waksman, *J. Bacteriol.* **186**, 1919 (2004).
14. C. Schlieker, H. Zentgraf, P. Dersch, A. Mogk, *Biol. Chem.* **386**, 1115 (2005).
15. A. Mogk *et al.*, *J. Biol. Chem.* **278**, 17615 (2003).
16. M. R. Bladergroen, K. Badelt, H. P. Spaink, *Mol. Plant Microbe Interact.* **16**, 53 (2003).

17. D. A. Parsons, F. Heffron, *Infect. Immun.* **73**, 4338 (2005).
18. We thank A. Rietsch for comments on the manuscript and for providing valuable reagents and assistance with flow cytometry experiments, T. Doan and D. Rudner for assistance with fluorescence microscopy, M. Little for CF patient isolates, R. Melynyk and J. Collier for assistance with biophysical studies, A. Thanawastien for assistance with ELISA experiments, D. Hung, E. Cameron, S. Dove, and J. Thompson for critical reading of the manuscript, S. Pukatzki and A. Ma for sharing data, members of the Mekalanos laboratory for valuable discussions, F. Collart for providing the expression clone of Hcp1, and members of the Structural Biology Center at Argonne National Laboratory for their help in conducting experiments. This work was supported in part by grants to J.J.M. from the NIH (AI26289), to S.L. from the NIH (AI21451), and to A.J. from the NIH (GM62414 and GM074942) and the U.S. Department of Energy, Office of Biological and Environmental Research, under contract W-31-109-Eng-38. J.D.M. is a Damon Runyon Fellow supported by the Damon Runyon Cancer Research Foundation (DRG-1873-05).

Supporting Online Material

www.sciencemag.org/cgi/content/full/312/5779/1526/DC1

Materials and Methods

Figs. S1 to S4

Tables S1 to S3

References

6 April 2006; accepted 5 May 2006

10.1126/science.1128393

Preserved CD4⁺ Central Memory T Cells and Survival in Vaccinated SIV-Challenged Monkeys

Norman L. Letvin,^{1,2*} John R. Mascola,¹ Yue Sun,² Darci A. Gorgone,² Adam P. Buzby,² Ling Xu,¹ Zhi-yong Yang,¹ Bimal Chakrabarti,¹ Srinivas S. Rao,¹ Jörn E. Schmitz,² David C. Montefiori,³ Brianne R. Barker,² Fred L. Bookstein,^{4,5} Gary J. Nabel¹

Vaccine-induced cellular immunity controls virus replication in simian immunodeficiency virus (SIV)-infected monkeys only transiently, leading to the question of whether such vaccines for AIDS will be effective. We immunized monkeys with plasmid DNA and replication-defective adenoviral vectors encoding SIV proteins and then challenged them with pathogenic SIV. Although these monkeys demonstrated a reduction in viremia restricted to the early phase of SIV infection, they showed a prolonged survival. This survival was associated with preserved central memory CD4⁺ T lymphocytes and could be predicted by the magnitude of the vaccine-induced cellular immune response. These immune correlates of vaccine efficacy should guide the evaluation of AIDS vaccines in humans.

The protection afforded by vaccines can be mediated by humoral or cellular immune responses. Because a strategy to elicit broadly neutralizing antibodies to HIV-1 has not yet been developed, HIV-1 vaccine candidates now entering advanced

phase clinical testing are designed to induce potent cellular immunity (1). It is hoped that such vaccines will generate populations of virus-specific T lymphocytes that rapidly expand following infection. By this means, viral spread might be contained, leading to reduced chronic viral replication and prolonged disease-free survival. The expectation that such vaccines will confer clinical benefit comes from the association of lower set-point plasma viremia with prolonged survival in HIV-1-infected humans (2). In some nonhuman primate models, particularly those using the chimeric simian-human immunodeficiency viruses (SHIVs), vaccines that elicit potent cellular immune responses have resulted in reduced viremia

¹Vaccine Research Center, National Institute of Allergy and Infectious Diseases, National Institutes of Health, Bethesda, MD 20892, USA. ²Beth Israel Deaconess Medical Center, Harvard Medical School, Boston, MA 02215, USA.

³Duke University Medical Center, Durham, NC 27710, USA.

⁴Department of Statistics and Department of Psychiatry and Behavioral Sciences, University of Washington, Seattle, WA 98195, USA. ⁵Department of Anthropology, University of Vienna, Austria.

*To whom correspondence should be addressed. E-mail: nletvin@bidmc.harvard.edu

and preserved CD4⁺ T lymphocytes after viral challenge (3–5). However, the biology of these SHIVs differs from the usual transmitted primary HIV-1 isolates (6). It is possible that the pathogenic simian immunodeficiency (SIV) model may provide a more predictive and rigorous test of vaccine efficacy. In some SIV challenge models, vaccine-induced reductions in viremia and progression to AIDS have been shown (7–9), although in the case of the commonly used SIVmac239/251 strain, only transient reductions in viremia were observed. Because chronic set-point viremia was presumed to predict long-term survival (10), these SIV challenge studies were terminated before the deaths of the experimental animals, and it was suggested that T cell-based vaccines may not confer clinical benefit to humans (11, 12).

We evaluated the clinical benefit afforded by an SIV-specific cellular immune response elicited in rhesus monkeys through a plasmid DNA prime/recombinant E1-deleted, E3-inactivated adenovirus serotype 5 (rAd) boost vaccination regimen (13–16). The monkeys selected for study did not express the MHC class I allele *Mamu-A*01* because of its association with particularly efficient control of SIV/SHIV replication (17, 18). Six monkeys in each of five experimental groups received different vaccination regimens (Fig. 1) (16). The monkeys were monitored prospectively using pooled peptide Elispot and intracellular cytokine staining assays as measures of cell-mediated immunity, and for neutralizing antibody responses (13–15). Monkeys were then challenged by intravenous route with SIVmac251 and monitored for viral replication

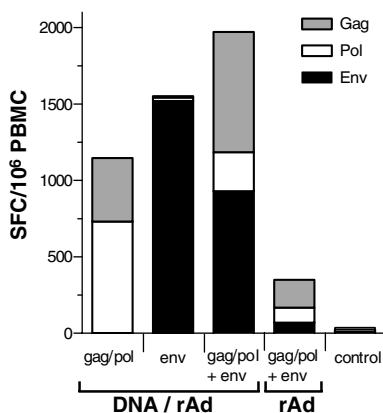


Fig. 1. Peak cellular immune responses elicited by vaccination. Groups of monkeys were immunized at weeks 0, 4, and 8 with plasmid DNA expressing the indicated gene products and at week 40 with recombinant adenoviruses carrying the same genes. Two weeks later, cellular immune responses were assessed in peripheral blood mononuclear cells (PBMC) by IFN- γ Elispot assay. Data are expressed as spot-forming cells (SFC) per 10⁶ PBMC.

and changes in CD4⁺ T lymphocyte subsets (16, 19).

The vaccination regimens elicited high-frequency SIV-specific cellular immune responses, with greater responses detected in the monkeys that received the DNA prime/rAd boost than those that received only rAd immunizations (Fig. 1). After virus challenge, there were no statistically significant differences in any parameters of clinical outcome between the various groups of experimentally vaccinated monkeys. Therefore, all 24 experimentally vaccinated monkeys were subsequently treated as a single group and compared to the 6 sham-vaccinated control monkeys.

Plasma SIV RNA levels were significantly lower in the experimentally vaccinated monkeys compared with the controls at the peak of viral replication, with this difference persisting through day 112 after virus challenge (Fig. 2, A and B). Thereafter, no significant difference was observed in plasma viral RNA levels between the experimentally vaccinated and control monkeys. Although the prediction

would be that comparable set-point viral load measurements in the vaccinated and control monkeys would be associated with comparable survival, we elected to follow the monkeys for another 750 days. In fact, as late as day 850 after virus challenge, the vaccinated monkeys maintained a statistically significant survival advantage over the control monkeys (Fig. 3A) (16). Therefore, the set-point plasma viral RNA levels did not predict the relative duration of survival in these vaccinated monkeys.

We next evaluated whether other measurements of viral replication or immune function might serve as predictors of survival. A quantitative measure of viral replication during the first 126 days after infection was determined for each animal by integrating the plasma SIV viral RNA levels between days 3 and 126. The vaccinated monkeys had significantly lower values than the controls (Fig. 3B), which suggests that differences in total viral replication during this early phase of infection are associated with differences in long-term survival.

Fig. 2. Plasma viral RNA levels after SIVmac251 challenge. The monkeys were challenged by intravenous route with pathogenic SIVmac251, and plasma viral RNA levels were assessed prospectively. (A) Plasma viral RNA data are shown for each individual monkey, with the data from the control monkeys shown in red. (B) Data were assessed at each time point by the Wilcoxon rank sum test to determine whether vaccinated monkeys differed from the group of control monkeys in their plasma viral RNA levels. The *P* value for that comparison is shown for each data set, and the horizontal line indicates a *P* value of approximately 0.05.

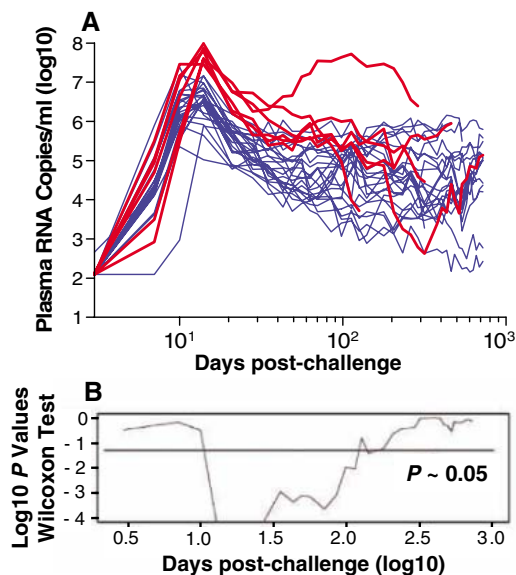
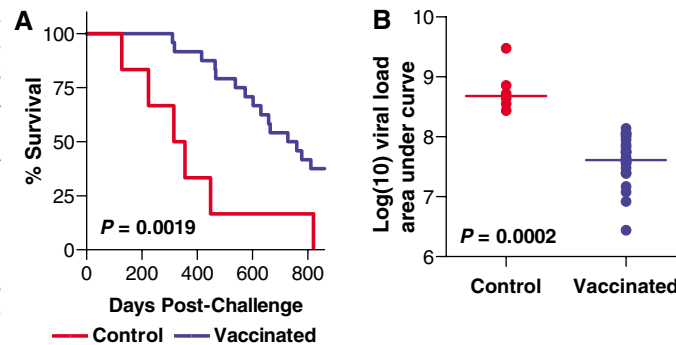


Fig. 3. Differences between control and experimentally vaccinated monkeys in survival and plasma viral RNA levels after challenge. (A) Kaplan-Meier survival curves for the control and experimentally vaccinated monkeys after SIVmac251 challenge. The comparison of survival in these groups of monkeys has been done using a log-rank test (16). (B) Comparison of area under the curve calculations for the plasma viral RNA levels in the control and experimentally vaccinated monkeys between days 3 and 126 after challenge. The comparison was analyzed using the Wilcoxon rank sum test.



There is increasing evidence that the loss of memory CD4⁺ T lymphocytes during acute infection is important in AIDS pathogenesis (20, 21). To examine this phenomenon in the present study, peripheral blood memory CD4⁺ T lymphocytes were assessed at a single time point, and their association with clinical outcome in the cohort of SIV-infected monkeys was evaluated. We first assessed these values on day 126 after challenge (Fig. 4), a time point at which plasma virus RNA levels were comparable in the vaccinated and control monkeys (Fig. 4A). Although the proportions of naïve and effector memory CD4⁺ T lymphocyte populations were comparable in the peripheral blood of the vaccinated and control monkeys, central memory CD4⁺ T lymphocyte populations were larger in the vaccinated group (Fig. 4, B to D, and fig. S1). Similar immunologic data were obtained on day 112 after challenge (fig. S2). Moreover, when animals were divided into terciles based on magnitudes of absolute peripheral blood CD4⁺ T lymphocyte counts on day 126 after challenge, no differences in survival were seen (Fig. 4E). Yet, when a similar analysis was done dividing monkeys into terciles based on central memory CD4⁺ T lymphocyte counts, a clear survival advantage

was apparent for the monkeys with the highest counts (Fig. 4F). Similar results were seen in an evaluation of data generated on day 112 after challenge (fig. S3). These data sets also revealed an association between the survival of infected animals and the preservation of central memory CD4⁺ T lymphocytes after infection in a Cox proportional-hazards model ($P = 0.05$, likelihood ratio test). No association was observed in these monkeys between central memory CD8⁺ T lymphocyte counts and survival (fig. S4). Thus, although set-point plasma viral RNA levels were indistinguishable between the vaccinated and control monkeys, a single determination of the peripheral blood central memory CD4⁺ T lymphocyte count was associated with increased survival in these animals.

We then assessed the ramifications of this preservation of total central memory CD4⁺ T lymphocytes in the vaccinated, challenged monkeys on the SIV-specific immune response. On day 203 after challenge, the total central memory CD4⁺ T lymphocytes remained better preserved in the vaccinated than in the control monkeys, and the SIV Gag-specific CD4⁺ and CD8⁺ T lymphocyte IFN- γ , TNF- α , and IL-2 responses were greater in the vaccinated than in the control monkeys (figs. S5 and S6). In-

terestingly, however, no difference was observed in the magnitude of the SIV neutralizing antibody responses in the vaccinated and control monkeys as late as 126 days after challenge (fig. S7). Therefore, the preservation of total central memory CD4⁺ T lymphocytes in the vaccinated monkeys was associated with preserved virus-specific T lymphocyte responses.

Finally, we evaluated the contribution of vaccine-elicited immunity to survival in this cohort of monkeys. Dividing the 16 monkeys that received Gag immunogens into halves based on the magnitude of peak vaccine-elicited SIV Gag-specific total T lymphocyte responses measured by IFN- γ Elispot assay (Fig. 4G) and IFN- γ CD4⁺ T lymphocyte responses measured by ICS assay (Fig. 4H), a survival advantage was apparent for the monkeys with the highest frequency vaccine-elicited cellular immune responses. The Elispot data also revealed an association between vaccine-elicited cellular immune responses and survival in a Cox proportional-hazards model ($P = 0.015$, likelihood ratio test). Therefore, the magnitude of the immune responses generated by the vaccine was associated with survival after virus infection.

These findings suggest that vaccine protection against high levels of viral replication

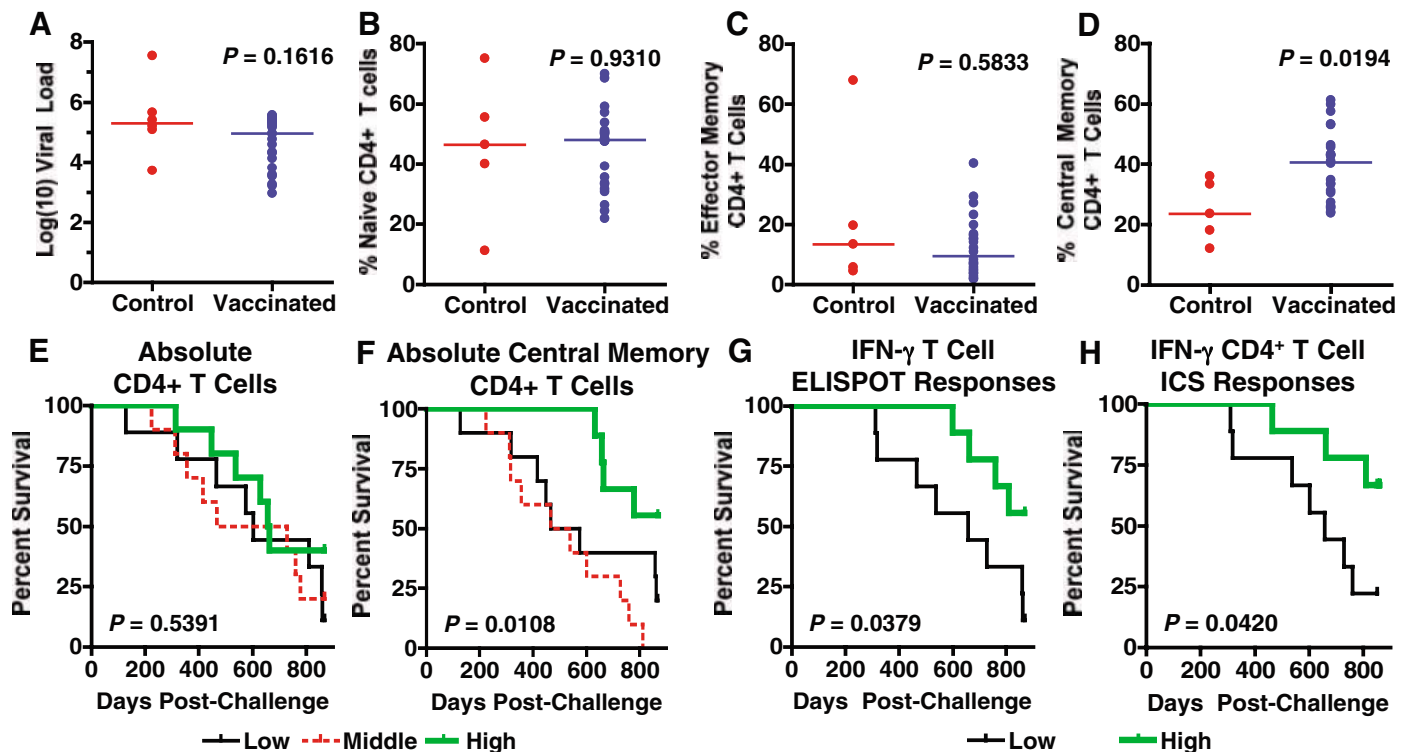


Fig. 4. Survival is associated with the preservation of peripheral blood central memory CD4⁺ T lymphocytes and vaccine-elicited cellular immune responses. (A) Plasma viral RNA levels and (B) percent of naïve (CD28⁺CD95⁻) CD4⁺ T cells, (C) effector memory (CD28⁻CD95⁺) CD4⁺ T cells, and (D) central memory (CD28⁺CD95⁺) CD4⁺ T cells were compared in the experimentally vaccinated and control monkeys on day 126 after challenge using the Wilcoxon rank sum test (16) (fig. S1). For panels (B) to (D), the percentage values are based on a denominator of total CD4⁺

T cells. Kaplan-Meier survival curves for all monkeys after challenge divided into thirds based on (E) absolute number of peripheral blood CD4⁺ T lymphocytes or (F) central memory CD4⁺ T lymphocytes. The 16 monkeys that received a Gag immunogen were divided into halves based on magnitude of vaccine-elicited (G) total Gag-specific IFN- γ Elispot responses or (H) CD4⁺ T lymphocyte Gag-stimulated intracellular IFN- γ expression. The comparisons of survival in these groups of monkeys were done using a log-rank test.

during only the first weeks following an AIDS virus infection may provide sufficient protection against central memory CD4⁺ T cell loss to confer a survival advantage to infected individuals. Moreover, current models of large human HIV-1 vaccine efficacy trials propose the use of set-point viral load and total CD4⁺ T lymphocyte count as surrogate markers for a beneficial vaccine effect (22, 23). It has been presumed that a lower set-point viral load or a higher set-point CD4⁺ T lymphocyte count after infection will portend a better AIDS-free survival. The results of the present study indicate that set-point viral load and total CD4⁺ T lymphocyte count may not have predictive value in this setting. Rather, the quantitation of central memory CD4⁺ T cells in a vaccine trial several months after infection may be an important immune correlate of long-term protection and predict the efficacy of an HIV-1 vaccine.

Most important, this cohort of vaccinated monkeys followed for 850 days after challenge with the highly pathogenic SIVmac251

provides a distinctive data set for exploring the mechanisms underlying the vaccine-associated survival. The demonstration of an association between the magnitude of the vaccine-elicited immune responses and the duration of survival after challenge provides a framework for understanding the immune protection conferred by cellular immune-based vaccines. Moreover, the prolonged survival conferred by a vaccine that stimulates T cell immunity provides support for pursuing clinical efficacy trials of such HIV-1 vaccines, even if they do not induce sterilizing immunity.

References and Notes

1. N. L. Letvin, *Annu. Rev. Med.* **56**, 213 (2005).
2. J. W. Mellors *et al.*, *Science* **272**, 1167 (1996).
3. D. H. Barouch *et al.*, *Science* **290**, 486 (2000).
4. R. R. Amara *et al.*, *Science* **292**, 69 (2001).
5. J. W. Shiver *et al.*, *Nature* **415**, 331 (2002).
6. Y. Nishimura *et al.*, *Proc. Natl. Acad. Sci. U.S.A.* **101**, 12324 (2004).
7. I. Ourmanov *et al.*, *J. Virol.* **74**, 2740 (2000).
8. P. Polacino *et al.*, *J. Virol.* **73**, 618 (1999).
9. P. S. Polacino *et al.*, *J. Virol.* **73**, 8201 (1999).

10. J. D. Lifson *et al.*, *J. Virol.* **71**, 9508 (1997).
11. D. R. Casimiro *et al.*, *J. Virol.* **79**, 15547 (2005).
12. T. U. Vogel *et al.*, *J. Virol.* **77**, 13348 (2003).
13. N. L. Letvin *et al.*, *J. Virol.* **78**, 7490 (2004).
14. S. Santra *et al.*, *J. Virol.* **79**, 6516 (2005).
15. M. S. Seaman *et al.*, *J. Virol.* **79**, 2956 (2005).
16. Materials and methods are available as supporting material on Science Online.
17. R. Pal *et al.*, *J. Virol.* **76**, 292 (2002).
18. M. S. Seaman *et al.*, *J. Virol.* **79**, 4580 (2005).
19. Y. Sun *et al.*, *J. Immunol.* **174**, 4753 (2005).
20. J. J. Mattapallil *et al.*, *Nature* **434**, 1093 (2005).
21. R. S. Veazey *et al.*, *J. Virol.* **74**, 57 (2000).
22. P. B. Gilbert *et al.*, *J. Infect. Dis.* **192**, 974 (2005).
23. T. Hulgan *et al.*, *J. Infect. Dis.* **192**, 950 (2005).
24. This work was supported in part with funds from the intramural research program of the Vaccine Research Center, NIAID, NIH.

Supporting Online Material

www.sciencemag.org/cgi/content/full/312/5779/1530/DC1

Materials and Methods

SOM Text

Figs. S1 to S7

References

22 December 2005; accepted 24 April 2006

10.1126/science.1124226

Long-Term Potentiation of Neuron-Glia Synapses Mediated by Ca²⁺-Permeable AMPA Receptors

Woo-Ping Ge,^{1,2*} Xiu-Juan Yang,^{1,2*} Zhijun Zhang,^{1,2} Hui-Kun Wang,^{1,2} Wanhua Shen,^{1,2} Qiu-Dong Deng,^{1,2} Shumin Duan^{1†}

Interactions between neurons and glial cells in the brain may serve important functions in the development, maintenance, and plasticity of neural circuits. Fast neuron-glia synaptic transmission has been found between hippocampal neurons and NG2 cells, a distinct population of macroglia-like cells widely distributed in the brain. We report that these neuron-glia synapses undergo activity-dependent modifications analogous to long-term potentiation (LTP) at excitatory synapses, a hallmark of neuronal plasticity. However, unlike the induction of LTP at many neuron-neuron synapses, both induction and expression of LTP at neuron-NG2 synapses involve Ca²⁺-permeable AMPA receptors on NG2 cells.

Glial cells in the central nervous system (CNS) constitute a heterogeneous population of cell types. Macroglia-like NG2 cells express the chondroitin sulfate proteoglycan NG2 and have been described as oligodendrocyte precursor cells (OPCs) or given other names (1–3). NG2 cells in the CA1 area of the hippocampus receive direct glutamatergic and γ -aminobutyric acid (GABA)-ergic synaptic inputs from neurons (4, 5). The structure of the neuron-glia synapses found in NG2 cells

differs from that of neuronal synapses by having a less well-defined postsynaptic density and smaller presynaptic boutons that contain fewer vesicles (4). With the exception of developing neuromuscular junctions (6), long-term potentiation (LTP) has been observed only at synapses between neurons. Thus it is of interest to examine whether the neuron-NG2 cell synapses have adequate expression and localization of components required for both the induction and expression of LTP.

Whole-cell recordings were made from NG2 cells in the CA1 region of rat hippocampal slices. Glial cell membrane currents induced by the stimulation of Schaffer collaterals (SCs) were used to monitor rapid neuron-glia signaling. The identity of astrocytes and NG2 cells was determined by both electrophysiological recording and immunostaining. Staining with

antibodies to glial fibrillary acidic protein (GFAP) and NG2 revealed two distinct non-overlapping cell populations (fig. S1) (4). NG2 cells were identified by having a relatively high input resistance (131.7 ± 5.4 megohms, $n = 160$ cells), large transient A-type currents (I_A) and delayed rectifier K⁺ currents (I_K), and small tetrodotoxin (TTX)-sensitive Na⁺ currents that failed to generate typical action potentials (Fig. 1 and fig. S1D) (4, 7). We found no detectable voltage-dependent Ca²⁺ currents in these cells (Fig. 1, F and G). When cells with the above characteristics were marked by intracellular loading with biocytin or lucifer yellow and subsequently immunostained with an antibody against NG2, all of the cells (14 out of 14) were found to be NG2-positive (fig. S1).

Electrical stimulation of SCs, in the presence of the GABA type A (GABA_A) receptor antagonist bicuculline, elicited inward currents in NG2 cells with rapid kinetics (Fig. 2A; rise time, 0.71 ± 0.06 ms; decay time, 2.13 ± 0.17 ms; $n = 11$), which was consistent with the existence of direct monosynaptic inputs made by SCs on NG2 cells (4). The excitatory postsynaptic currents (EPSCs) exhibited short-term plasticity similar to that induced at SC-CA1 pyramidal cell synapses, as suggested by the paired pulse ratio (PPR) of these two types of synapses over a broad range of paired pulse intervals (Fig. 2B). The EPSCs were reversibly abolished by the application of kynurenic acid (Kyn) (Fig. 2D and fig. S1E), a broad-spectrum blocker of ionotropic glutamate receptors. These EPSCs were due to the activation of non-N-methyl-D-aspartate receptors (NMDARs), because the antagonist 6,7-dinitroquinoxaline-2,3-dione (DNQX) completely abolished the responses, whereas the NMDARs antagonist

¹Institute of Neuroscience and Key Laboratory of Neurobiology, Shanghai Institutes for Biological Sciences, Chinese Academy of Sciences, Shanghai 200031, China.

²Graduate School of the Chinese Academy of Sciences, Shanghai 200031, China.

*These authors contributed equally to this work.

†To whom correspondence should be addressed. E-mail: shumin@ion.ac.cn

D,L-2-amino-5-phosphonovaleric acid (APV) had no effect on these currents recorded at +40 mV to remove the Mg²⁺ block of NMDAR (Fig. 2, C and D).

Most AMPARs in the CNS are Ca²⁺-impermeable because of the presence of the GluR2 subunit, although GluR2-lacking AMPARs have been observed in some developing and mature neurons as well as in glial cells (4, 8, 9). Consistent with the previous finding that NG2 cells contain Ca²⁺-permeable AMPA receptors (CaPARs) (4), we found that EPSCs observed in NG2 cells were significantly reduced by philanthotoxin-433 (PhTx), a toxin that specifically blocks the CaPARs (10) (Fig. 2D). Currents mediated by CaPARs display inward rectification, exhibiting a reduction of outward currents at depolarizing membrane potentials because of a voltage-dependent block by intracellular polyamines (8, 9). To estimate the proportion of the EPSC component mediated by CaPARs, we examined the rectification of EPSCs by monitoring the ratio of EPSCs recorded at -60 mV to that at +40 mV (I_{-60}/I_{+40}). The rectification of EPSCs was stronger in 1-week-old rats [(postnatal day 8 (P8) to P10] than that in rats at P13 to P15 and P19 to P21. Furthermore, the proportion of EPSCs inhibited by 30 to 50 μM 1-naphthylacetyl spermine (NAS), a synthetic analog of Joro spider toxin that selectively blocks CaPARs (11), was also larger in young animals, suggesting a developmental reduction in the EPSC mediated by CaPARs (Fig. 2, E and F). To directly estimate the glutamate-induced Ca²⁺ influx through CaPARs, NG2 cells were loaded with the Ca²⁺ dye Rhod-2, and the hippocampal slices were perfused with glutamate in the presence of cyclothiazide, which blocks the desensitization of AMPARs. We found that glutamate-induced currents and Ca²⁺ elevations were largely abolished by DNQX and significantly reduced by NAS. Thus, a large proportion of glutamate-induced Ca²⁺ elevation in NG2 cells is mediated by CaPARs (Fig. 2, G to I). The residual Ca²⁺ elevation in the presence of NAS may be caused indirectly by the activation of (i) Ca²⁺-impermeable AMPARs that may induce Ca²⁺ elevation through a Na⁺-Ca²⁺ exchanger and (ii) metabotropic glutamate receptors that mobilize intracellular Ca²⁺ stores. Because the perfusion of glutamate activates both synaptic and extrasynaptic AMPARs, the finding that NAS caused stronger inhibition of glutamate-induced current (Fig. 2I) than of SC-induced EPSCs (Fig. 2F) suggests that CaPARs are more prevalent in extrasynaptic AMPARs. In some experiments, Ca²⁺ elevation in NG2 cells induced by the stimulation of SCs was also detected by line scanning with a high temporal resolution (fig. S2).

Evoked EPSCs in NG2 cells were compared before and after tetanic or theta burst stimulation (TBS) of the SCs. Although tetanic stimu-

lation failed to induce an apparent change in EPSCs (Fig. 3H and fig. S3C), TBS resulted in a persistent increase in the EPSC amplitude in NG2 cells (Fig. 3, A and B), analogous to LTP found at neuronal synapses. The effectiveness of TBS in LTP induction at NG2 synapses may be attributed to the fact that these EPSCs exhibited substantial amplitude reduction during tetanic stimulation but not during TBS (fig. S3), which may result in a higher amount of Ca²⁺ influx during TBS than during tetanic

stimulation. Bath application of APV, which largely abolishes CA1 neuronal LTP (12–14), did not affect TBS-induced “glial LTP” (gLTP) of SC-NG2 cell synapses (Fig. 3, C, G, and H). In contrast, application of TBS during a brief period of perfusion with Kyn resulted in no change in EPSCs in NG2 cells (Fig. 3, E, G, and H), suggesting that TBS-induced gLTP requires the activation of nonNMDA receptors.

Intracellular Ca²⁺ elevation is critical for LTP induction at many synapses (13). We

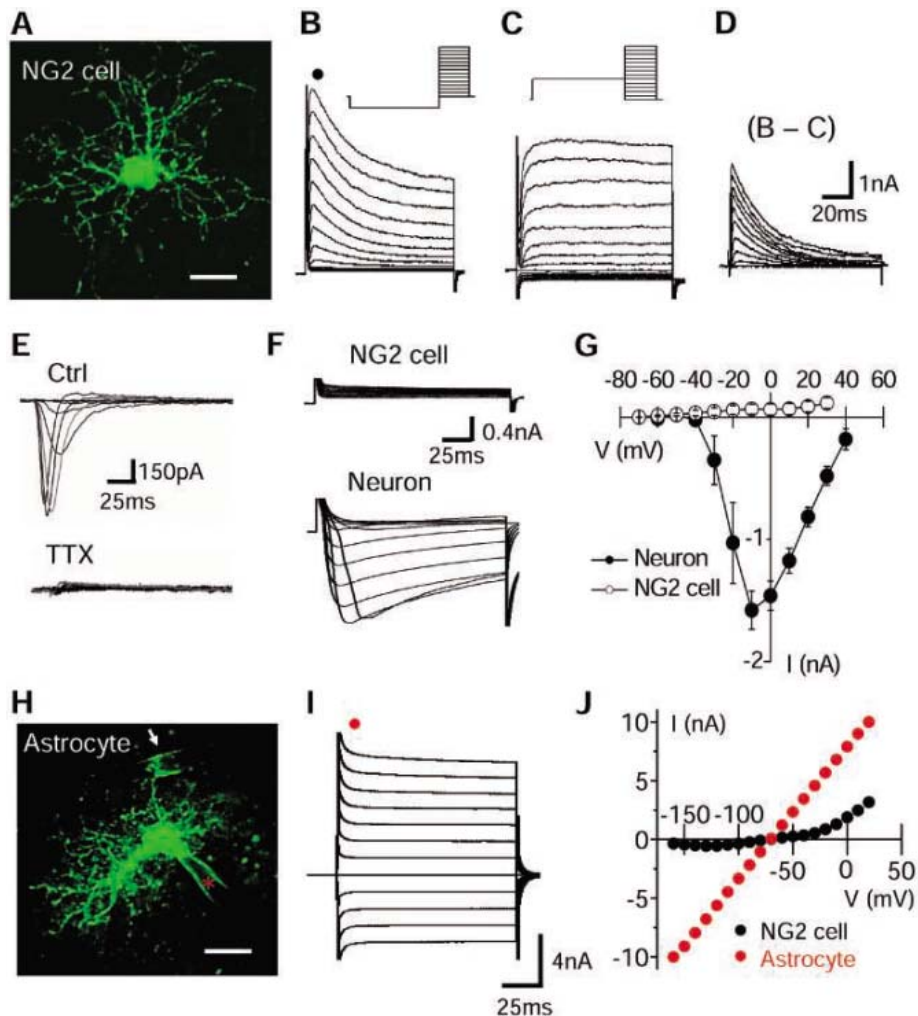


Fig. 1. Electrophysiological properties of NG2 cells. (A) Three-dimensional reconstruction of a typical NG2 cell identified electrophysiologically. The cell was loaded with Oregon-green 488 BAPTA-1 in the CA1 region of a living hippocampal slice. Scale bar, 10 μm. (B) and (C) Outward currents recorded from an NG2 cell evoked by step voltages (100 ms, 10 mV) from -80 to +50 mV with a prepulse of -120 mV (B) or -30 mV (C) for 300 ms. In (B), the black circle indicates the position of peak currents as measured in (J). (D) Isolated I_A reached by subtracting (C) from (B). (E) Transient inward currents recorded from an NG2 cell induced by the same voltage pulses as in (B) in the presence of K⁺ channel blockers with or without TTX. (F) and (G) Voltage-dependent Ca²⁺ currents were recorded in neurons but not in NG2 cells. In (G), error bars for neurons (solid circles, $n = 8$ cells) and for NG2 cells (open circles, $n = 7$ cells) indicate SEM. (H) Morphology of a typical astrocyte identified electrophysiologically. The cell was loaded and imaged as in (A). White arrow indicates the end-feet of the astrocyte wrapping a microvessel. Red asterisk indicates the dye-containing pipette. Scale bar, 10 μm. (I) Current responses from an astrocyte evoked by step voltages (100 ms, 20 mV) from -160 to +20 mV. Red circle indicates the position of peak currents as measured in (J). (J) Example current-voltage relation curves constructed from recordings as shown in (B) (peak current) and (I).

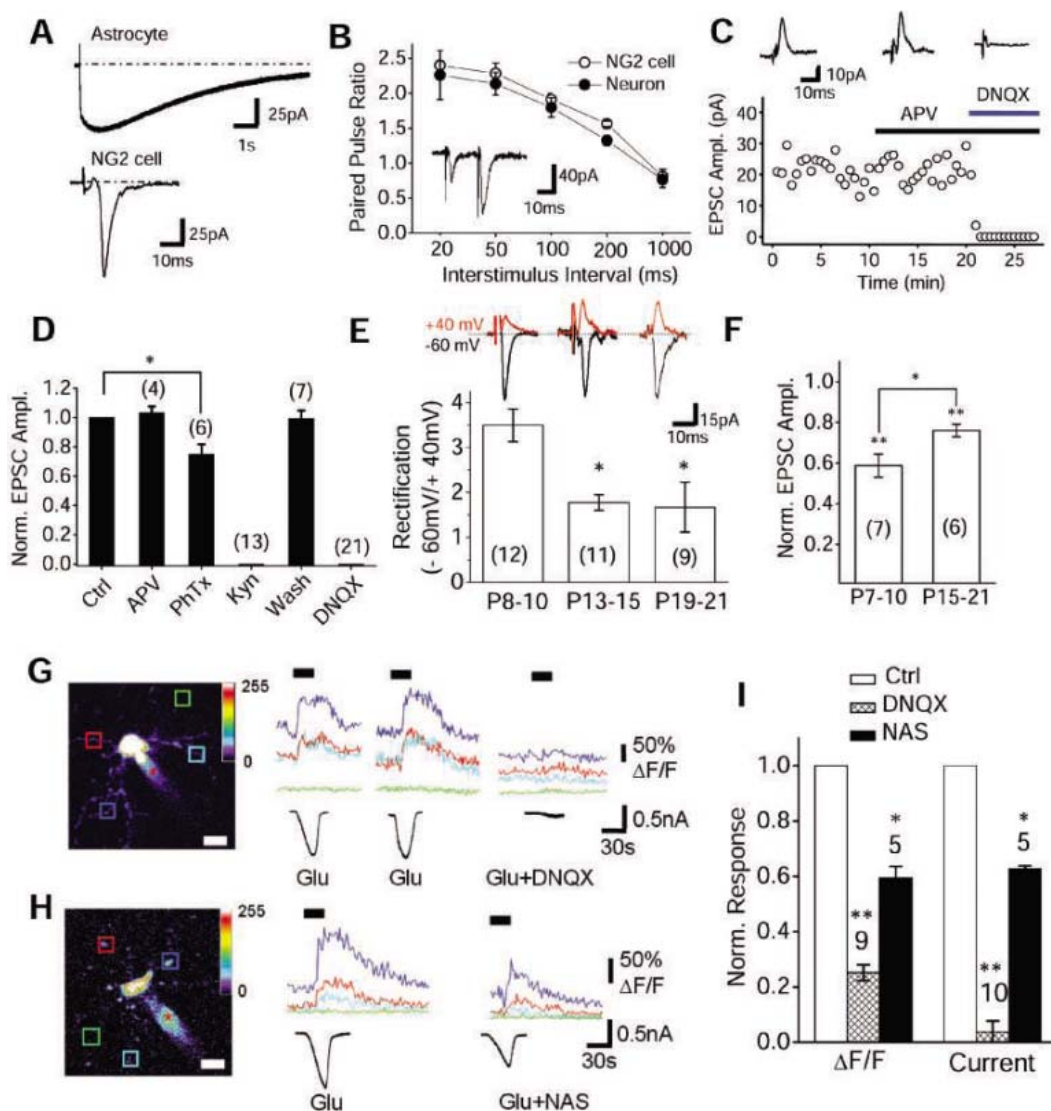
found that TBS failed to induce gLTP when NG2 cells were loaded with a fast Ca^{2+} chelator [1,2-bis(2-aminophenoxy)ethane- N,N,N',N' -tetraacetic acid (BAPTA)]. A persistent reduction in the EPSC amplitude was observed instead (Fig. 3, D, G, and H). This reduction may result from an incomplete Ca^{2+} buffering in the fine processes of NG2 cells where SC-NG2 synapses are located, suggesting potential bidirectional Ca^{2+} -dependent plasticity (13) at these synapses. Given the lack of voltage-gated Ca^{2+} current in these NG2 cells (Fig. 1, F and G), we further examined whether CaPARs are responsible for the Ca^{2+} influx required for gLTP induction. Application of PhTx completely prevented the induction of gLTP by TBS (Fig. 3, F to H). This gLTP is

likely to be expressed as an increased glutamate response in NG2 cells, because PPRs were not significantly changed after gLTP induction (Fig. 4, A and B), suggesting no presynaptic change in glutamate release probability (13).

The trafficking of GluR1-containing AMPARs plays a crucial role in the expression of NMDAR-dependent LTP (15, 16). Induction of NMDAR-dependent LTP in CA1 neurons, which do not express CaPARs, did not change the rectification of AMPAR-mediated EPSCs unless neurons were overexpressed with green fluorescent protein-GluR1 (16); this finding suggests that, after LTP induction, the endogenous GluR1 subunits are trafficked to synapses in heteromeric forms containing GluR2, so that the increased AMPARs are also Ca^{2+} -

impermeable. Activation of CaPARs by tetanic stimulation at cerebellar stellate cell synapses results in a prolonged decrease in the rectification of AMPAR-mediated EPSCs due to the replacement of CaPARs with Ca^{2+} -impermeable receptors (17, 18), leading to a decreased Ca^{2+} influx and EPSC amplitude recorded at the physiological membrane potential (-60 mV), a plasticity that may resemble the long-term depression and represent a protective mechanism. Synaptic strengthening induced by the activation of the CaPARs has been reported in some dorsal horn neurons (19) and amygdala interneurons (20), but it is not clear whether the proportion of the CaPAR-mediated EPSCs is changed after LTP induction in these synapses. We found that TBS

Fig. 2. Properties of EPSCs and glutamate-induced responses in NG2 cells. **(A)** Example traces showing SC stimulation-induced fast response in an NG2 cell (bottom) and slow response in an astrocyte (top). **(B)** PPRs in NG2 cells and CA1 pyramidal neurons induced by SC stimulations at various interstimulus intervals ($n = 7$ pairs). Insets represent example recordings from an NG2 cell. **(C)** Inhibition of EPSCs in an NG2 cell by DNQX ($10 \mu M$) but not by APV ($100 \mu M$). Insets from left to right represent sample traces (average of five traces) from control, perfusion with APV, and APV plus DNQX, respectively. **(D)** Summary data from experiments as shown in (C). Each column represents averaged data of EPSCs recorded during 5-min perfusion (or washout) of antagonists. Data are normalized with the control (averaged EPSC amplitude during initial 5-min recording before drug application). *, $P < 0.05$. **(E)** Averaged rectification of SC-NG2 EPSCs from hippocampal slices at different development stages. Insets show example EPSCs recorded at $+40$ mV (red) and -60 mV (black). * ($P < 0.01$) indicates significance as compared with P8–10 group. **(F)** Averaged EPSCs in the presence of NAS. Data are normalized with control EPSCs (before NAS application). Significance as compared with the control group (** $P < 0.001$) or between the two groups (* $P < 0.05$) is indicated. **(G)** and **(H)** Imaging of glutamate-induced Ca^{2+} elevation in NG2 cells. Left panels depict NG2 cells filled with Rhod-2 through a patch pipette (red asterisks). Right panels provide example traces for glutamate-induced Ca^{2+} signal (color traces) and current recording (black traces) in the absence or presence of DNQX (G) and NAS (H). Traces in different colors in the right panel correspond to the imaged regions in the left



panel marked by squares of the same color. Black bars indicate perfusion of $500 \mu M$ glutamate (Glu). **(I)** Summarized data of glutamate-induced current and Ca^{2+} fluorescent change ($\Delta F/F$; see supporting online material) and current as shown in (G) and (H). * ($P < 0.01$) and ** ($P < 0.001$) indicate significance as compared with the control group.

induced an increased rectification of EPSCs (Fig. 4C), suggesting an increased function or proportion of CaPARs at these synapses. Loading NG2 cells with spermine caused more rectification of SC-induced EPSCs (Fig. 4, compare C with D), suggesting that endogenous polyamines are sufficient (21) but not saturating in inducing inward rectification of AMPAR currents. Furthermore, the induction of gLTP in NG2 cells loaded with spermine also resulted in an increased rectification of EPSCs (Fig. 4D). Such synaptic modification will increase not only the amplitude of synaptic responses but also Ca²⁺ influx and subsequent activation of Ca²⁺-dependent intracellular signaling. The

intracellular C terminal of the proteoglycan NG2 has been reported to bind with the PDZ domain of GRIP1 (22), an adaptor protein important for AMPAR trafficking and synaptic plasticity (18). It is possible that the interaction of NG2 proteoglycan and GRIP1 in these glial cells played a role in the trafficking of CaPARs found in the present study.

The conversion of CaPARs into Ca²⁺-impermeable receptors at Bergmann glial cells, by transfection with the GluR2 subunit, results in the retraction of glial processes that ensheath synapses and multiple innervations of Purkinje cells by climbing fibers (23). Pathological insults such as ischemia also down-regulate

GluR2 expression in OPCs and neurons (24), leading to the expression of CaPARs and enhanced glutamate toxicity after ischemia. Thus, an adequate level of activity by CaPARs is important for maintaining normal synaptic structure and function. Glutamate receptor activation is linked to the proliferation and differentiation of OPCs (25), and NG2 cells can differentiate into neurons both in vitro and in vivo (26, 27). The expression of gLTP and the elevation of CaPARs in SC-NG2 synapses may thus contribute to activity-dependent neuronal regulation of NG2 cell differentiation. Like astrocytes (12, 28, 29), NG2 cells may also secrete neuroactive factors to regulate neuronal

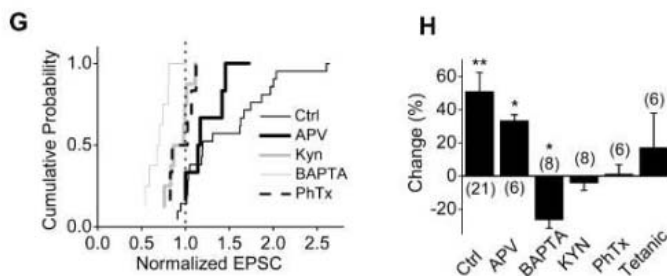
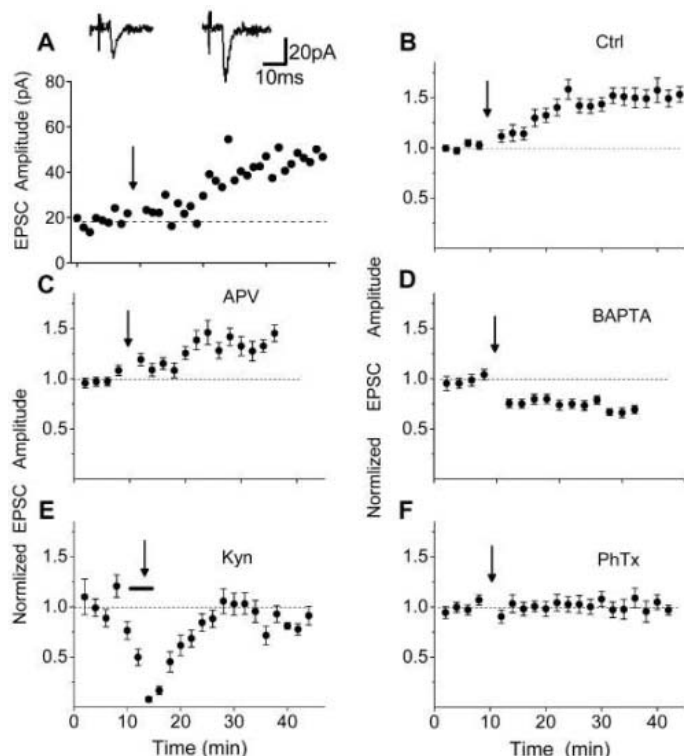


Fig. 3. Persistent enhancement of EPSCs in NG2 cells induced by TBS of SCs. Example (A) and summarized (B) data showing the TBS (arrows)-induced gLTP at NG2 cell synapses are shown. Insets in (A) are sample traces before and after TBS, respectively. (C to F) Summary data showing the time course of EPSCs before and after TBS in the presence of 100 μ M APV (C), 0.5 mM Kyn (E) applied during the period indicated by the bar, 4 μ M PhTx (F), or 10 mM intracellular BAPTA in NG2 cells (D). (G) Cumulative distribution of EPSC amplitudes after TBS as shown in (B) to (F). Data are normalized with the average EPSC amplitude (vertical dotted line) before TBS for each recording. (H) Summary of results showing averaged percent changes in EPSC amplitudes estimated during the period from 15 to 20 min after TBS or tetanic stimulation. * ($P < 0.05$) and ** ($P < 0.01$) indicate significant changes in EPSC amplitude after induction.

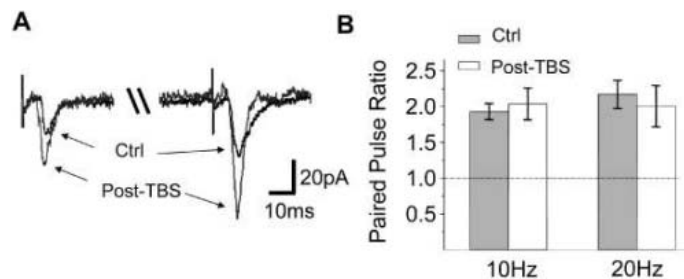
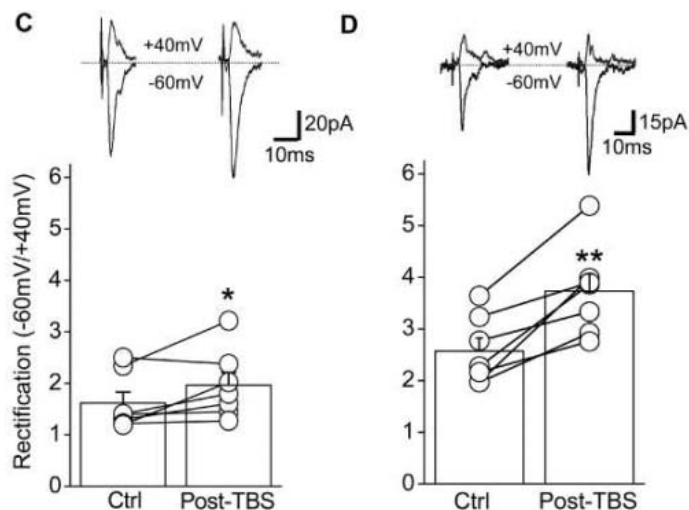


Fig. 4. Comparing EPSC properties in an NG2 cell before and after TBS. (A) Example EPSC recordings from an NG2 cell showing similar PPR (10 Hz) recorded before and after TBS application. (B) Summary of averaged PPR at 10 Hz ($n = 5$ cells) and 20 Hz ($n = 4$ cells) before and after TBS induction. (C and D) Summary of the rectification of EPSCs examined before and after TBS induction in NG2 cells loaded with [(D) $n = 7$] or without [(C) $n = 7$] 0.1 mM spermine. Insets, example EPSCs from an NG2 cell recorded at +40 and -60 mV, respectively, before and after TBS induction. * ($P < 0.05$) and ** ($P < 0.01$) indicate significance between the control and post-TBS groups.



functions. Rapid neuron-NG2 cell signaling may allow rapid feedback regulation of neuronal functions by Ca²⁺-dependent secretion of neuroactive factors, and the strength of such feedback regulation will increase after the induction of gLTP.

References and Notes

- J. M. Levine, J. P. Card, *J. Neurosci.* **7**, 2711 (1987).
- J. M. Levine, R. Reynolds, J. W. Fawcett, *Trends Neurosci.* **24**, 39 (2001).
- M. C. Raff, R. H. Miller, M. Noble, *Nature* **303**, 390 (1983).
- D. E. Bergles, J. D. Roberts, P. Somogyi, C. E. Jahr, *Nature* **405**, 187 (2000).
- S. C. Lin, D. E. Bergles, *Nat. Neurosci.* **7**, 24 (2004).
- J. Wan, M. Poo, *Science* **285**, 1725 (1999).
- R. Chittajallu, A. Aguirre, V. Gallo, *J. Physiol.* **561**, 109 (2004).
- S. K. Kamboj, G. T. Swanson, S. G. Cull-Candy, *J. Physiol.* **486**, 297 (1995).
- D. S. Koh, J. R. Geiger, P. Jonas, B. Sakmann, *J. Physiol.* **485**, 383 (1995).
- M. S. Washburn, R. Dingledine, *J. Pharmacol. Exp. Ther.* **278**, 669 (1996).
- M. Koike, M. Iino, S. Ozawa, *Neurosci. Res.* **29**, 27 (1997).
- Y. Yang *et al.*, *Proc. Natl. Acad. Sci. U.S.A.* **100**, 15194 (2003).
- T. V. Bliss, G. L. Collingridge, *Nature* **361**, 31 (1993).
- J. S. Diamond, D. E. Bergles, C. E. Jahr, *Neuron* **21**, 425 (1998).
- R. Malinow, R. C. Malenka, *Annu. Rev. Neurosci.* **25**, 103 (2002).
- Y. Hayashi *et al.*, *Science* **287**, 2262 (2000).
- S. Q. Liu, S. G. Cull-Candy, *Nature* **405**, 454 (2000).
- S. J. Liu, S. G. Cull-Candy, *Nat. Neurosci.* **8**, 768 (2005).
- J. G. Gu, C. Albuquerque, C. J. Lee, A. B. MacDermott, *Nature* **381**, 793 (1996).
- N. K. Mahanty, P. Sah, *Nature* **394**, 683 (1998).
- S. H. Shi *et al.*, *Science* **284**, 1811 (1999).
- J. Stegmüller, H. Werner, K. A. Nave, J. Trotter, *J. Biol. Chem.* **278**, 3590 (2003).
- M. Iino *et al.*, *Science* **292**, 926 (2001).
- D. E. Pellegrini-Giampietro, J. A. Gorter, M. V. Bennett, R. S. Zukin, *Trends Neurosci.* **20**, 464 (1997).
- V. Gallo *et al.*, *J. Neurosci.* **16**, 2659 (1996).
- M. C. Nunes *et al.*, *Nat. Med.* **9**, 439 (2003).
- A. Aguirre, V. Gallo, *J. Neurosci.* **24**, 10530 (2004).
- J. M. Zhang *et al.*, *Neuron* **40**, 971 (2003).
- A. Araque, G. Carmignoto, P. G. Haydon, *Annu. Rev. Physiol.* **63**, 795 (2001).
- We thank M. Poo for critical comments on the manuscript and W. Zhou, Q. Hu, D. Xiang, J. Zhao, and J. Mao for technical assistance. This work was supported by the National Natural Science Foundation of China (grant 30321002) and Major State Basic Research Program of China (grant G200077800).

Supporting Online Material

www.sciencemag.org/cgi/content/full/312/5779/1533/DC1
Materials and Methods
Figs. S1 to S3

6 January 2006; accepted 5 May 2006
10.1126/science.1124669

Language Control in the Bilingual Brain

J. Crinion,¹ R. Turner,¹ A. Grogan,¹ T. Hanakawa,^{2,3} U. Noppeney,⁴ J. T. Devlin,⁵ T. Aso,³ S. Urayama,³ H. Fukuyama,³ K. Stockton,¹ K. Usui,³ D. W. Green,⁶ C. J. Price^{1*}

How does the bilingual brain distinguish and control which language is in use? Previous functional imaging experiments have not been able to answer this question because proficient bilinguals activate the same brain regions irrespective of the language being tested. Here, we reveal that neuronal responses within the left caudate are sensitive to changes in the language or the meaning of words. By demonstrating this effect in populations of German-English and Japanese-English bilinguals, we suggest that the left caudate plays a universal role in monitoring and controlling the language in use.

People who communicate in more than one language can voluntarily control which language is in use at any given time. The bilingual brain can, for example, determine the language of heard or written speech, produce words in the selected language, and inhibit the production of words in the non-selected language. All of these processes necessitate language-sensitive neuronal activity. Contrary to expectation, however, whole-brain functional neuroimaging studies have shown that highly proficient bilinguals activate the same set of brain regions irrespective of which language is presented or produced; see (1) for a recent review. These findings suggest that the neural circuits for different languages are highly

overlapping and interconnected but do not indicate how the brain determines or controls the language in use.

Our study was designed to identify language-dependent neuronal responses at the level of word meanings (i.e., semantics). By using whole-brain functional neuroimaging, semantic priming, and the neuronal adaptation technique (2–4), we expected to see regional reductions in left anterior temporal activation when two successively presented written words had similar meanings (e.g., trout-SALMON) compared with different meanings (e.g., trout-HORSE) (5, 6). Critically, if semantic activation is independent of the language of the stimuli, then neuronal adaptation will be the same irrespective of whether the semantically related words are in the same or different languages (2). If, on the other hand, a region responds to both semantic content and the language of the stimuli, then neuronal adaptation will depend on whether semantically related words are presented in the same or different languages.

Our participants saw visually presented sequential word pairs (e.g., trout-SALMON). They were instructed to ignore the first (the prime) and to make a decision based on the

meaning of the second [the target, printed in capitals (English and German) or a larger font (Japanese) (Materials and Methods)]. A short interval (250 ms) between the onsets of the prime and the target was chosen to minimize the likelihood that the prime could be used to predict the target word but to maximize the time available to activate semantic associations in both languages (7). The influence of the prime on the target was identified by comparing the response to prime-target pairs that were either semantically related (bathtub-SHOWER) or unrelated (spoon-SHOWER). We then identified language-dependent semantic responses by comparing the effect of semantic priming when prime and target were in the same language (trout-SALMON in English or forelle-LACHS in German) or different languages (e.g., trout-LACHS or forelle-SALMON). Lastly, to identify the semantic system that was common to all types of priming, we included a baseline condition with meaningless non-linguistic symbols. Our two-by-two-by-two experimental design manipulated (i) the language of the target word and varied whether the prime and the target were (ii) semantically related or unrelated and (iii) written in the same or different languages.

The robustness and universality of the observed effects were ensured by including three groups of highly proficient bilinguals (table S1). One group of German-English bilinguals ($n = 11$) participated in a positron emission tomography (PET) experiment, whereas a second group of German-English bilinguals ($n = 14$) and a third group of Japanese-English bilinguals ($n = 10$) participated in functional magnetic resonance imaging (fMRI) experiments. The stimuli in all three experiments were carefully equated across languages (table S2). Therefore, language-dependent neuronal responses present in all three groups would provide strong evidence for the universality of the language mechanism, particularly because

¹Wellcome Department of Imaging Neuroscience, University College London, London WC1N 3BG, UK. ²Department of Cortical Function Disorders, National Center of Neurology and Psychiatry, Tokyo 187-8502, Japan. ³Human Brain Research Center, Kyoto University, Kyoto 606-8507, Japan. ⁴Max Planck Institute for Biological Cybernetics, 72076 Tübingen, Germany. ⁵Centre for Functional Magnetic Resonance Imaging of the Brain, University of Oxford, Oxford OX3 9DU, UK. ⁶Department of Psychology, University College London, London WC1E 6BT, UK.

*To whom correspondence should be addressed. E-mail: c.price@fil.ion.ucl.ac.uk

German and Japanese come from entirely separate linguistic families. The replication of effects across three different experiments is also important because previous reports of language-selective effects (8) have not been replicated subsequently.

To begin, we demonstrated equivalent behavioral and imaging effects for both languages spoken (Fig. 1). In the behavioral analysis, over all three subject groups, there were no significant effects of target language on accuracy or response times, [$F(1, 32) < 1.5$; $P > 0.1$] although the Japanese group were 92 ms faster with Japanese than with English targets [$F(1, 9) = 3.6$; $P = 0.09$]. The imaging data demonstrated that the same network of brain regions relative to baseline was activated for semantic decisions for both languages spoken (Fig. 1), and a direct comparison of the two languages did not reveal any significant differences when a correction was made for multiple comparisons across the entire brain. At a lower statistical threshold ($P < 0.001$, uncorrected), we found greater activation in the visual cortices for German compared with English words and for English compared with Japanese words. These effects are attributed to inevitable perceptual differences in the orthographies of the languages tested. Indeed, there were more letters in our German words (7.2 letters on average per word) compared with their English

equivalents (6.1 letters on average per word) and in English compared with Japanese (three characters on average per word). Despite the different orthographies, however, a common set of frontal, temporal, and parietal regions were activated in each language (Fig. 1), consistent with previous studies of highly proficient bilinguals (9–13).

The influence of the prime on the target response was clearly demonstrated by both behavioral and imaging data from each bilingual group. Over subject groups, there was a 41-ms main effect of semantic priming on response times [1258 ms for unrelated and 1217 ms for semantically related; $F(1, 32) = 8.2$; $P = 0.007$], and this effect was observed irrespective of whether the prime and the target were in the same or different languages [$F(1, 32) < 1.2$ and $P > 0.3$ for all two-way and three-way interactions] (Fig. 2). At the neuronal level, responses on the ventral surface of the left anterior temporal lobe mirrored the behavioral data, with reduced activation for semantically related word pairs irrespective of whether the prime and the target were in the same or different languages (Fig. 3) This effect did not interact with the languages of the prime or the target ($P > 0.05$ for all two- and three-way interactions in each group of subjects). This suggests that semantic priming in the left ventral anterior temporal lobe (5, 6) is

language-independent, consistent with the notion that both languages converge on the same neuronal networks.

Most importantly, our whole-brain analysis revealed language-dependent semantic priming that was only observed in the head of the left caudate. Across all three of our subject groups, we found that semantically related words reduced activation in the left caudate when prime and target were in the same language but not when they were in different languages (Fig. 4). The group-specific P values for unrelated more than semantically related word pairs in the same language were 0.001 for the Japanese group and 0.003 and 0.008 for the German groups. The joint probability across groups ($P = 2.4 \times 10^{-8}$) corresponds to a Z score of 5.46, which is highly unlikely to arise by chance even for a whole-brain undirected search. In addition, we confirmed that the size of the effects in both PET and fMRI analyses reached significance ($P < 0.05$) after a small volume correction for multiple comparisons when the coordinates from the PET study were used as an independent region of interest (6-mm radius)

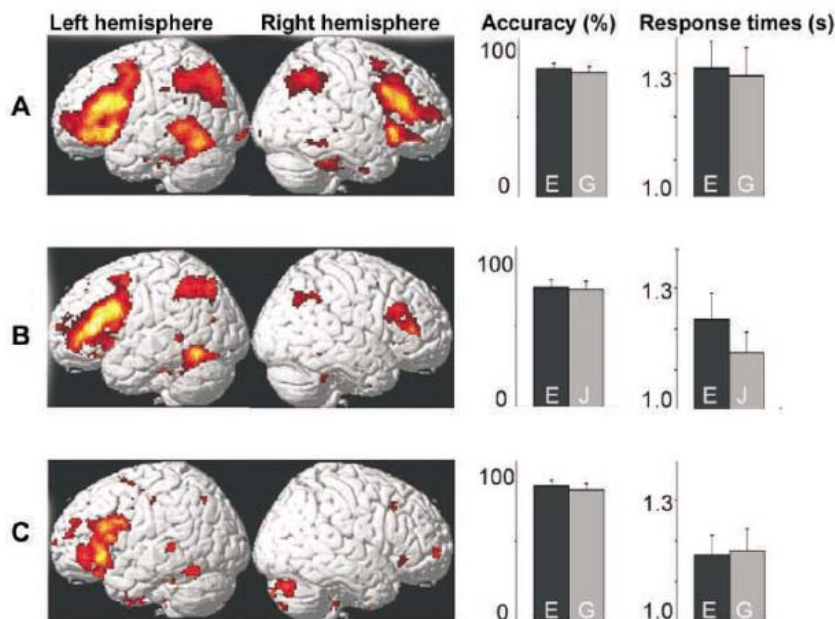


Fig. 1. Common neuronal and behavioral effects for both languages spoken. (Left) Activation for semantic decisions relative to baseline for both languages in each of the three groups of subjects (red to yellow colors correspond to significance values ranging from $P < 10^{-3}$ to $P < 10^{-6}$, uncorrected). (A) German-English fMRI ($n = 14$). (B) Japanese-English fMRI ($n = 9$). (C) German-English PET ($n = 11$). (Right) The accuracy and response times for semantic decision in each of the languages spoken. E indicates English; G, German; and J, Japanese. Over subject groups, the mean accuracy including trials where the response time was longer than 2 s was 79% in English and 77% in German and Japanese, whereas the mean response time excluding trials longer than 2 s was 1249 ms in English and 1232 ms in German and Japanese. The error bars show standard error of the mean.

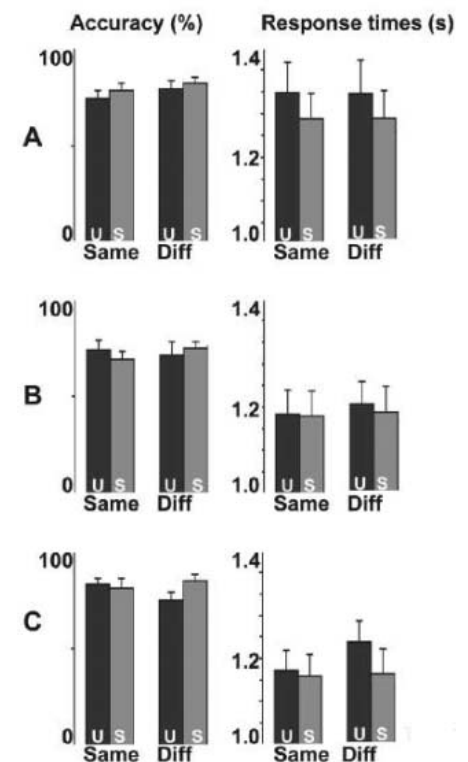


Fig. 2. The effect of semantic priming on behavioral responses. Response accuracy (left) and time (right) in each group of subjects. (A) German-English fMRI. (B) Japanese-English fMRI. (C) German-English PET. Prime and target were either in the same language (Same) or different languages (Diff) and unrelated (U) or semantically related (S). There was no significant effect of any variable on accuracy in any of the three groups of subjects or over all subjects ($P > 0.05$). The error bars show standard error of the mean.

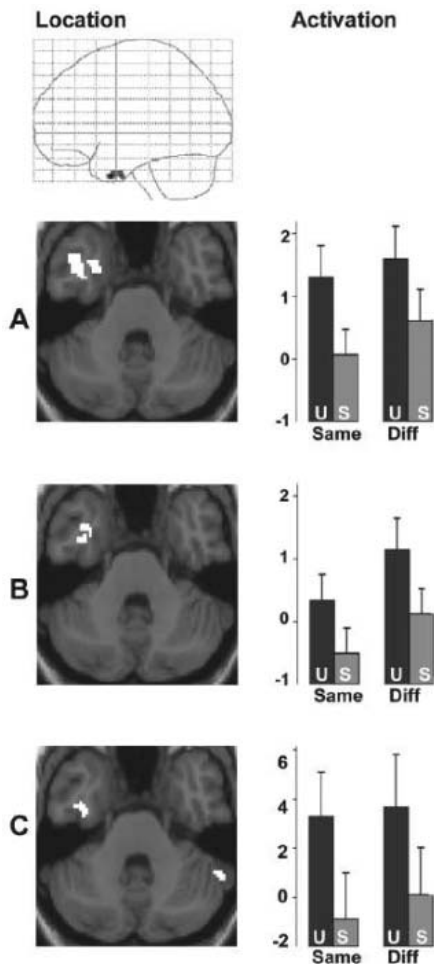


Fig. 3. Language-independent neuronal adaptation in the left anterior temporal lobe. (Left) Activation for unrelated minus semantically related word pairs for (top) all fMRI data ($P < 0.001$) on a sagittal view of a glass brain, to show that the most significant effect across the whole brain was located in the left anterior temporal lobe, and for each of the three bilingual groups on axial slices ($z = -36$ mm; the left side of the image corresponds to the left hemisphere). (A) German-English fMRI. (B) Japanese-English fMRI. (C) German-English PET. (Right) Parameter estimates, relative to baseline, at the peak of unrelated minus semantically related activation (see Fig. 2 for abbreviations). The error bars show standard error of the mean. Details of x , y , and z coordinates (Montreal Neurological Institute standard space); Z score; P value uncorrected; and number of voxels at $P < 0.05$ uncorrected were $-32, 4, -36; 3.1; 0.001$; and 135 for all fMRI data; $-34, -4, -38; 2.6; 0.005$; and 151 for German fMRI data; $-32, 4, -36; 2.4; 0.007$; and 22 for Japanese fMRI data; and $-32, -12, -36; 2.7; 0.004$; and 62 for German PET data, respectively. The combined probabilities of the effects in each group were multiplied ($0.005 \times 0.007 \times 0.004$) to equal 1.4×10^{-7} , corresponding to a Z score of 5.14. Note the different location of the peak in the PET and fMRI results is likely to reflect distortion due to susceptibility artefacts in this region in the fMRI experiments (37).

in the fMRI study and vice versa. Critically, in all three subject groups, semantic priming was significantly greater when the prime and the target were in the same language than when they were in different languages ($P = 10^{-6}$, $Z =$

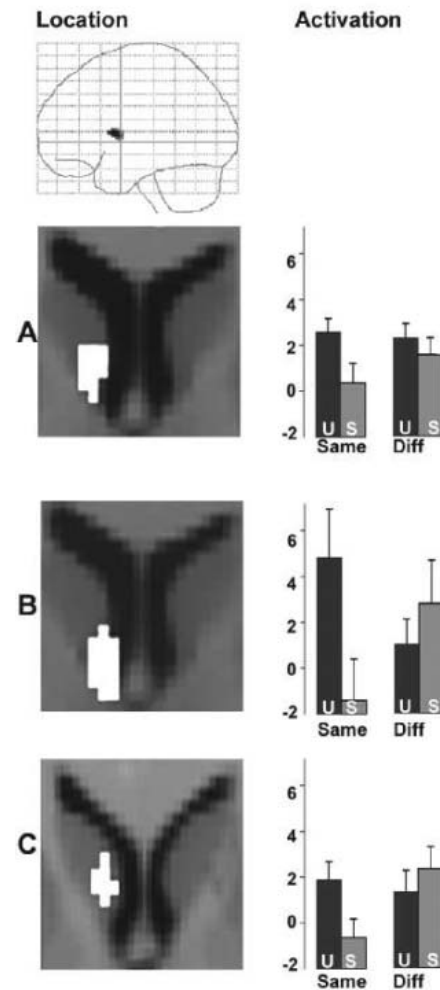


Fig. 4. (A to C) Language-dependent neuronal adaptation in the left caudate. Activation for unrelated minus semantically related word pairs in the same language only (see Fig. 3 for layout). The sagittal view of the glass brain (top) shows that the average of all fMRI data ($P < 0.001$) and indicates that the only significant effect across the whole brain was located in the left caudate. Details of x , y , and z coordinates; Z score; P value (uncorrected); and number of voxels at $P < 0.05$ uncorrected were $-6, 8, 8; 3.6; 0.001$; and 171 for all fMRI data; $-8, 12, 6; 2.4; 0.008$; and 48 for German fMRI data; $-6, 6, 8; 3.3; 0.001$; and 146 for Japanese fMRI data; and $-4, 14, 2; 2.9; 0.003$; and 37 for German PET data, respectively. Lastly, the Z scores and probabilities for the interaction of (unrelated–semantically related) \times (same–different languages) were 1.5 and 0.074 for German fMRI; 3.1 and 0.001 for Japanese fMRI; and 2.8 and 0.003 for German–PET, respectively. The combined probability for the interaction is 2.2×10^{-7} , corresponding to a Z score of 5.05.

5.1), irrespective of the language of the prime. There were no other significant effects, not even in the frontal and the parietal regions that activate when the language of response switches (2, 14). The key distinction here is that we had no explicit task-switching condition. Our subjects were instructed to respond only to the target word, and, within a block, the target language was held constant.

The language-dependent neuronal responses that we have observed in the left caudate were highest when prime and target are either semantically different (unrelated) or in different languages (Fig. 4). This is consistent with language-dependent responses at the level of word meanings. Indeed, the response in the left caudate cannot be explained in terms of orthographic or perceptual differences in the scripts, because if this had been the case we would have seen reduced activation when unrelated words were in the same language (English–ENGLISH) than in different languages (e.g., English–日本語). Instead, we only saw reduced activation when words in the same language were semantically similar (Fig. 4). We can also exclude the possibility that our effects result from proficiency confounds, because the effect of semantic priming was observed within languages irrespective of whether the prime and the target were presented in English, German, or Japanese ($P < 0.03$ for each language) and there was no effect of semantic priming when the prime and target were in any combination of different languages ($P > 0.05$).

Our imaging results dissociate two effects of semantic priming in all three of our subject groups, despite cultural and linguistic differences between groups. In the left anterior temporal cortex, semantically related primes reduced activation irrespective of whether the prime and the target were in the same language or in different languages. This suggests that different languages converge on the same neuronal populations within this region as opposed to distinct populations embedded within the same area of the temporal cortex. In contrast, in the head of the left caudate, reduced activation for semantically related word pairs was only observed when the prime and target were in the same language.

There are two possible neuronal mechanisms that might generate the response profile we have observed in the left caudate. The first is that different languages are processed by different neuronal populations (i.e., language-selective neuronal populations) and semantic priming selectively adapts responses in the neuronal populations for the prime language (3). In this case, semantic priming between words in different languages does not reduce activation because the change in language activates a different (i.e., non-adapted) neuronal population. The second interpretation is that the same neurons respond to semantic input in both

languages with increased neuronal firing when there is a change in language (15). Neuronal populations that respond to a change in language would indicate a possible mechanism for language control that regulates output whenever a change in input is detected. To dissociate the two contrasting explanations of language-dependent semantic priming, we turned to neuropsychological studies of bilingual patients with damage to the left caudate. If there are distinct neuronal populations in the left caudate for different languages, then damage to this region should disrupt all of these neuronal populations and impair word processing in all the patient's languages. If, on the other hand, the left caudate plays a role in language control and increases its firing when words in a pair are unrelated by meaning or language, then semantic processing after left caudate damage may remain intact for all languages, but the patient will have difficulties monitoring the language of input or controlling the language of output.

The results of neuropsychological studies of bilingual patients strongly suggest that the left caudate is involved in language control rather than language-selective semantic representations. The most notable case is a study of a trilingual patient with a lesion to the white matter surrounding the head of the left caudate (16). This patient had preserved comprehension in all three of her languages. Her picture naming was also above 80% accuracy. However, during language production tasks, she spontaneously and involuntarily switched from one language to another. These and other findings with bilingual patients (17) suggest that the left caudate is required to monitor and control lexical and language alternatives in production tasks.

In monolingual patients, left caudate damage is typically associated with confrontational naming and word-finding difficulties (18, 19). This has led to suggestions that damage to, or stimulation of, the caudate will impair the patient's ability to select appropriate lexical-semantic responses (20, 21). Recently, however, semantic priming experiments have demonstrated that patients with nonthalamic subcortical lesions also have lexical-semantic impairments when required to manipulate or control semantics during attention-demanding comprehension tasks (22, 23). Likewise, functional neuroimaging studies of neurologically normal subjects have shown increased left caudate activation for semantic decisions, even when speech output is controlled, by comparing semantic decisions to phonologically complex baseline tasks (24, 25). Together, these studies suggest that the left caudate plays a role in lexical-semantic control in both monolingual (20, 23) and multilingual subjects (16, 17). Lexical

semantic processing may be regulated, for example, by increased left caudate responses when the distributed pattern of neuronal inputs changes (26). Indeed, our study shows that the left caudate responses are highest when there is a change in language or a change in meaning but lowest in the context of words that are related in both language and meaning.

Anatomically, the left caudate is the primary recipient of corticostriatal projections from frontal, temporal, and parietal association regions in the language-dominant hemisphere and, in turn, sends reciprocal connections via the thalamus that play a critical role in controlling and selecting automatic motor sequences such as those necessary for articulation (27, 28). These motor patterns differ across languages and therefore require a mechanism sensitive to the language in use. The head of the left caudate may be ideally situated to serve this function.

By using functional neuroimaging, we have demonstrated that neuronal responses in the head of the left caudate are sensitive to both the semantic content and the language of written words. In contrast to previous functional imaging investigations of semantic processing in bilingual participants (29), we were able to dissociate language-dependent effects within a shared brain region by using semantic priming and a neuronal adaptation technique. In contrast to electrical stimulation studies of speech production in bilingual patients with craniotomies before surgery (30, 31), our functional imaging technique allowed us to investigate the whole brain and avoid confounds from differences in the computational demands required for speech production in a second language (32–36). Moreover, in contrast to both neuropsychological and electrical stimulation studies, we were able to ensure the robustness and universality of our results by replicating the effects in three different populations of highly proficient bilinguals with different linguistic backgrounds. We conclude that the left caudate plays a critical role in language control and that future studies targeting the regions to which the left caudate connects will enable a more complete characterization of the neural circuits involved in the control of multiple languages.

References and Notes

1. D. Perani, J. Abutalebi, *Curr. Opin. Neurobiol.* **15**, 202 (2005).
2. M. W. Chee, C. S. Soon, H. L. Lee, *J. Cogn. Neurosci.* **15**, 85 (2003).
3. K. Grill-Spector, R. Henson, A. Martin, *Trends Cogn. Sci.* **10**, 14 (2006).
4. K. Nakamura, S. Dehaene, A. Jobert, D. Le Bihan, S. Kouider, *J. Cogn. Neurosci.* **17**, 954 (2005).
5. C. J. Mummery, T. Shallice, C. J. Price, *Neuroimage* **9**, 516 (1999).

6. S. L. Rossell, C. J. Price, A. C. Nobre, *Neuropsychologia* **41**, 550 (2003).
7. J. H. Neely, in *Basic Processes in Reading: Visual Word Recognition*, D. Besner, G. Humphreys, Eds. (Lawrence Erlbaum Hillsdale, Mahwah, NJ, 1991), pp. 264–336.
8. K. H. Kim, N. R. Relkin, K. M. Lee, J. Hirsch, *Nature* **388**, 171 (1997).
9. M. W. Chee *et al.*, *Neuron* **23**, 127 (1999).
10. M. W. Chee, N. Hon, H. L. Lee, C. S. Soon, *Neuroimage* **13**, 1155 (2001).
11. M. W. Chee *et al.*, *Neuroimage* **12**, 392 (2000).
12. M. Hasegawa, P. A. Carpenter, M. A. Just, *Neuroimage* **15**, 647 (2002).
13. S. Yokoyama *et al.*, *Neuroimage* **30**, 570 (2006).
14. C. J. Price, D. W. Green, R. von Studnitz, *Brain* **122**, 2221 (1999).
15. R. Naatanen *et al.*, *Nature* **385**, 432 (1997).
16. J. Abutalebi, A. Miozzo, S. F. Cappa, *Neurocase* **6**, 51 (2000).
17. R. Moretti *et al.*, *Percept. Mot. Skills* **92**, 803 (2001).
18. S. F. Cappa, G. Vallar, in *Neuropsychological Disorders Associated with Subcortical Lesions*, G. Vallar, C. W. Wallesch, Eds. (Oxford Univ. Press, New York, 1992), pp. 7–41.
19. C. W. Wallesch, C. Papagno, in *Aphasia*, F. Rose, R. Whurr, M. A. Wyke, Eds. (Whurr, London, 1988), pp. 256–287.
20. S. Gil Robles, P. Gatignol, L. Capelle, M. C. Mitchell, H. Duffau, *J. Neurol. Neurosurg. Psychiatry* **76**, 940 (2005).
21. S. E. Nadeau, B. Crosson, *Brain Lang.* **58**, 355 (1997).
22. D. Copland, *J. Int. Neuropsychol. Soc.* **9**, 1041 (2003).
23. D. A. Copland, H. J. Chenery, B. E. Murdoch, *Cortex* **36**, 601 (2000).
24. C. J. Mummery, K. Patterson, J. R. Hodges, C. J. Price, *J. Cogn. Neurosci.* **10**, 766 (1998).
25. C. J. Price, C. J. Moore, G. W. Humphreys, R. J. S. Wise, *J. Cogn. Neurosci.* **9**, 727 (1997).
26. R. G. Brown, C. D. Marsden, *Neuroscience* **25**, 363 (1988).
27. M. Jueptner, C. Weiller, *Brain* **121**, 1437 (1998).
28. E. H. Vetterian, D. N. Pandya, *J. Comp. Neurol.* **399**, 384 (1998).
29. M. W. Chee, H. L. Lee, C. S. Soon, C. Westphal, V. Venkatraman, *Neuroimage* **18**, 468 (2003).
30. T. H. Lucas 2nd, G. M. McKhann 2nd, G. A. Ojemann, *J. Neurosurg.* **101**, 449 (2004).
31. F. E. Roux *et al.*, *Brain* **127**, 1796 (2004).
32. A. E. Hernandez, M. Dapretto, J. Mazziotta, S. Bookheimer, *Neuroimage* **14**, 510 (2001).
33. G. Meschyan, A. E. Hernandez, *Neuroimage* **29**, 1135 (2006).
34. A. Rodriguez-Fornells, M. Rotte, H. J. Heinze, T. Nosselt, T. F. Munte, *Nature* **415**, 1026 (2002).
35. A. Rodriguez-Fornells *et al.*, *J. Cogn. Neurosci.* **17**, 422 (2005).
36. G. Vingerhoets *et al.*, *Neuroimage* **20**, 2181 (2003).
37. J. T. Devlin *et al.*, *Neuroimage* **11**, 589 (2000).
38. This work was funded by the Wellcome Trust (C.J.P. and D.G.); Grants-in-Aid for Scientific Research on Priority Areas (17022023) from the Japanese Ministry of Education, Culture, Sports, Science and Technology (H.F.); and Science of Mind and Aging and Health research grants from the Japanese Ministry of Health, Labor, and Welfare (H.F.).

Supporting Online Material

www.sciencemag.org/cgi/content/full/312/5779/1537/DC1
Materials and Methods
Tables S1 and S2
References

22 March 2006; accepted 8 May 2006
10.1126/science.1127761



Liquid Handling Platform

The liquid handling platform CyBi-RoboSpense is equipped with four or eight variable span pipetting channels. The instrument can address almost any type of sample tubes and plate formats. An optional gripper adds plate transport capabilities within the deck and to neighboring modules for direct interaction with readers, high-performance liquid chromatography systems, mass spectrometers, and additional pipetting devices. It is designed for modularity and ease of integration to adapt to individual process demands.

CyBio For information +49 36 41 351 0 www.cybio-ag.com

Solid-Phase Extraction Cartridges

A new family of solid-phase extraction (SPE) cartridges features 3M Empore extraction disk membranes. Empore membranes produce clean extracts and can potentially extend chromatography column life and reduce instrument downtime. SPE is often the preferred method for isolating and concentrating analytes at low detection levels because it eliminates the interferences that contribute to signal suppression. The Milli-SPE cartridges offer a selection of sorbents to meet a broad range of applications. The cartridges feature low elution volumes, resulting in higher analyte concentrations and increased sensitivity. Empore solid-phase extraction membranes eliminate channeling and reduce the risk of analyte loss that can occur with other packed particle bed SPE devices.

Millipore For information 800-MILLIPORE
www.millipore.com/bioscience

Imaging Systems for Cellular Analysis

The BD Pathway 400 series is a line of automated imaging systems for high-content cellular analysis. The Pathway 435 is a compact, automated benchtop system that rapidly images cells and tissues in multi-well plates or on microscope slides. A newly designed autofocus significantly increases the speed of image acquisition and overall plate throughput. The system incorporates flexible, computer-controlled excitation and emission filters, spinning disk confocal optics for reduced fluorescence background and three-dimensional imaging, and a long-life metal halide lamp. The system enables a broad array of fluorescence-based biological applications such as analysis of neurite outgrowth, angiogenesis, protein translocation, co-localization, cell cycle, and three-dimensional cellular exploration. The Pathway 435 is suitable for researchers who need high-speed, high-resolution confocal imaging

capabilities coupled with powerful and flexible image analysis. For applications not requiring confocal capability, the Pathway 415 is a cost-effective alternative.

BD Biosciences For information 301-340-7320
www.bdbiosciences.com/bioimaging

In Vivo Imaging

A new accessory and IRDye reagents are available for in vivo imaging on the Odyssey Infrared Imaging System. The Odyssey MousePOD Imaging Accessory fits over the standard Odyssey scanning surface for in vivo imaging of up to three mice. Longitudinal studies are facilitated by the Odyssey MousePOD's temperature regulation and easy connection to a gas anesthesia system. New software includes tools to quickly mark and quantify regions of interest such as tumors. The IRDye-based imaging reagents provide a solution for cellular analysis that includes optical tracer characterization using the In-cell Western assay, in vivo imaging, imaging whole tumors, and in situ analysis and characterization of tumor sections. The Odyssey Infrared Imaging System is equipped with two infrared channels for direct fluorescence detection with high sensitivity and low biological background fluorescence. The superior signal-to-noise ratio produced using near infrared dyes produces results not possible with traditional visible fluorescence-based imaging systems.

LI-COR Biosciences For information
402-467-0750 www.licor.com

Differential Scanning Calorimeter

The Jade DSC (differential scanning calorimeter) for thermal analysis provides flexibility and reliability. A liquid nitrogen cooling system automates low temperature testing for more complete characterization of rubber and elastomers. Improved baseline flatness and stabil-

ity assures accurate measurement of typical thermal events in the polymer, pharmaceutical, chemical, and food industries. A 45-position autosampler option and carousel design offer high throughput and unattended operation for reproducible results in the temperature range from -180°C to 450°C . A variety of cooling devices includes the option of an automated low consumption liquid nitrogen cooling system that provides measurements from temperatures as low as -180°C . A portable cooling device can be used in combination with the standard configuration to quickly cool to ambient temperature or to cool below room temperature for occasional subambient measurements without any instrument modifications.

Perkin-Elmer For information 781-237-5100
www.perkinelmer.com

For more information visit **Product-Info**, **Science's new online product index** at <http://science.labvelocity.com>

From the pages of Product-Info, you can:

- Quickly find and request free information on products and services found in the pages of *Science*.
- Ask vendors to contact you with more information.
- Link directly to vendors' Web sites.

Newly offered instrumentation, apparatus, and laboratory materials of interest to researchers in all disciplines in academic, industrial, and government organizations are featured in this space. Emphasis is given to purpose, chief characteristics, and availability of products and materials. Endorsement by *Science* or AAAS of any products or materials mentioned is not implied. Additional information may be obtained from the manufacturer or supplier by visiting www.science.labvelocity.com on the Web, where you can request that the information be sent to you by e-mail, fax, mail, or telephone.

Classified Advertising



Get the Experts
Behind You.

For full advertising details, go to www.sciencecareers.org and click on For Advertisers, or call one of our representatives.

United States & Canada

E-mail: advertise@sciencecareers.org
Fax: 202-289-6742

JILL DOWNING

(CT, DE, DC, FL, GA, MD, ME, MA,
NH, NJ, NY, NC, PA, RI, SC, VT, VA)
Phone: 631-580-2445

KRISTINE VON ZEDLITZ

(AK, AZ, CA, CO, HI, IL, IA, KS, MT, NE,
NV, NM, ND, OR, SD, TX, UT, WA, WY)
Phone: 415-956-2531

KATHLEEN CLARK

Employment: AR, IL, LA, MN, MO, OK, WI
Canada; Graduate Programs; Meetings &
Announcements (U.S., Canada, Caribbean,
Central and South America)
Phone: 510-271-8349

DARYL ANDERSON

(AL, IN, KY, MI, MS, OH, TN, WV)
Phone: 202-326-6543

GABRIELLE BOGUSLAWSKI

(U.S. Recruitment Advertising Sales Director)
Phone: 718-491-1607

Europe & International

E-mail: ads@science-int.co.uk
Fax: +44 (0) 1223-326-532

TRACY HOLMES

Phone: +44 (0) 1223-326-525

HELEN MORONEY

Phone: +44 (0) 1223-326-528

CHRISTINA HARRISON

Phone: +44 (0) 1223-326-510

SVITLANA BARNES

Phone: +44 (0) 1223-326-527

JASON HANNAFORD

Phone: +81 (0) 52-789-1860

To subscribe to Science:

In U.S./Canada call 202-326-6417 or 1-800-731-4939
In the rest of the world call +44 (0) 1223-326-515

Science makes every effort to screen its ads for offensive and/or discriminatory language in accordance with U.S. and non-U.S. law. Since we are an international journal, you may see ads from non-U.S. countries that request applications from specific demographic groups. Since U.S. law does not apply to other countries we try to accommodate recruiting practices of other countries. However, we encourage our readers to alert us to any ads that they feel are discriminatory or offensive.



POSITIONS OPEN



FACULTY POSITIONS IN BIOLOGY

Texas A&M University

The Department of Biology at Texas A&M University (TAMU) invites applications for multiple faculty positions at the ASSISTANT, ASSOCIATE, or FULL PROFESSOR level.

We are particularly interested in outstanding scientists who will enhance our existing programs in circadian clocks, cell and developmental biology, ecology and evolution, microbial genetics, genomics and computational biology, plant biology, and neuroscience. We strongly encourage applications from candidates who will increase the exposure of our students to a diverse culture.

The successful candidates will be expected to maintain a vigorous, externally funded research program and to contribute to the teaching of undergraduate and graduate students. We offer a highly interactive research environment, a strong modern infrastructure, and a competitive startup package. More information about our Department can be found at **website: <http://www.bio.tamu.edu>**. For full consideration, applicants should send a letter of intent, curriculum vitae, statement of research and teaching interests, and three letters of recommendation by September 15, 2006, to:

Biology Faculty Search Committee

Department of Biology

Texas A&M University

3258 TAMU

College Station, TX 77843-3258

If you have questions about this search, please direct e-mails to **Dr. Bruce Riley, Chair of the Search Committee**, at e-mail: facultysearch@mail.bio.tamu.edu.

Texas A&M University is an Equal Opportunity Employer and has a policy of being responsive to the needs of dual-career couples.

HEAD, DIVISION OF
HEMATOLOGIC ONCOLOGY
Memorial Sloan-Kettering Cancer Center

The Department of Medicine at Memorial Sloan-Kettering Cancer Center (MSKCC) is seeking a Head of the Division of Hematologic Oncology. The Division consists of more than 45 board-certified oncologists on the Leukemia, Lymphoma, Bone Marrow Transplantation and Hematology Services and has recognized programs in laboratory and clinical translational research and clinical care. The Head of the Division oversees the Division's research programs, clinical activities, and teaching. The successful candidate will have an outstanding record of accomplishments as a widely recognized and active scientific leader in the study of the hematologic neoplasms. An M.D., M.D./Ph.D., or equivalent degree and board certification in internal medicine and oncology and/or hematology are required. The successful candidate will bring her/his research activities to the vibrant research environment of MSKCC, including the Sloan-Kettering Institute, the Gerstner Sloan-Kettering Graduate School, and the Human Oncology and Pathogenesis Program, as well as the neighboring Weill Medical College of Cornell University and Rockefeller University. Interested candidates are invited to submit curriculum vitae and bibliography to: **Alan Houghton, M.D., Chair, Division of Hematologic Oncology Search Committee, c/o Ms. Kendra Eaglin, Memorial Sloan-Kettering Cancer Center, 1275 York Avenue, C1289, New York, NY 10021** or at e-mail: eaglink@mskcc.org. *Memorial Sloan-Kettering Cancer Center is an Equal Opportunity Employer with a strong commitment to enhancing the diversity of its faculty and staff. Women and applicants from diverse racial, ethnic, and cultural backgrounds are encouraged to apply.*

POSITIONS OPEN

UNIVERSITY OF PITTSBURGH
Chair, Department of Human Genetics
Graduate School of Public Health

The University of Pittsburgh is seeking applications and nominations for the position of Professor and Chair of the Department of Human Genetics, Graduate School of Public Health, University of Pittsburgh. The Department of Human Genetics provides training and carries out basic research oriented toward identifying genes that contribute to common diseases and understanding the mechanisms by which these genes contribute to disease susceptibility. The Department offers Master's and doctoral degrees, including an accredited Master's degree program in genetics counseling.

The Chair will supervise the Department and will provide continuity with its tradition of excellence in research and in teaching. Responsibilities include faculty development; the oversight and evaluation of Departmental research and teaching; management of the Departmental budget; participation in the governance of the school; and maintenance of existing close working relations with other academic components of the University of Pittsburgh. The Chair is expected to pursue his or her own independent research career.

Candidates should possess a doctoral degree and a proven record of excellence in research related to populations-based human genetics. Preference will be given to applicants who have demonstrated their ability to participate in and foster dynamic multi-disciplinary collaborative interactions aimed at the understanding and prevention of disease and the maintenance of health. Preference also will be given to applicants with demonstrated academic and administrative leadership skills. An excellent package of support is available.

Applications should include curriculum vitae, a letter of interest outlining particular areas of interest to the candidate, and names, addresses, and telephone numbers of five references. Applications will be considered on a rolling basis until the position is filled. Nominations, requests for information, and applications should be directed to: **Bruce R. Pitt, Ph.D., Search Committee Chair, c/o Penny Weiss, Department of Environmental and Occupational Health, Graduate School of Public Health, University of Pittsburgh, Bridgeside Pointe Building, 100 Technology Drive, Room 328, Pittsburgh, PA 15219-3130**, or e-mail: recruitment@cohp.pitt.edu.

The University of Pittsburgh is an Affirmative Action, Equal Opportunity Employer.

CHIEF MEDICAL OFFICER

Highly intelligent individual with exceptional communication skills sought by prominent Manhattan family to research and coordinate family medical and healthcare issues. Act as liaison with leading medical researchers and consultants in academia and industry, with full responsibility for technical, financial, and administrative functions. Considerable weight given to evidence of unusual academic or other intellectual distinction. Ph.D. or M.D. required, clinical experience a plus but not essential. Possible entrepreneurial opportunities involving delivery of ultrahigh-end medical care to other, similar families. Full-time position. Excellent compensation with significant upside potential and management possibilities. Resume to e-mail: fmc4@spsfind.com.

ASSISTANT DEAN FOR ADMISSIONS for the College of Graduate Studies at the Medical University of South Carolina (MUSC). Requirements: Ph.D. degree in the biological sciences, enthusiastic, outgoing and creative. Primary roles: help recruit graduate students, develop recruitment materials, travel, chair admissions committee, and serve on some University committees. Send curriculum vitae and letters of reference to: **Jacqueline McGinty, Ph.D., Associate Dean, College of Graduate Studies, Medical University of South Carolina, 173 Ashley Avenue, P.O. Box 250501, Room 102 BSB, Charleston, SC 29425**. *MUSC is an Affirmative Action, Equal Opportunity Employer.*



**Texas A&M University
Toxicology Faculty Position
Department of Veterinary
Physiology and Pharmacology**

The Department of Veterinary Physiology and Pharmacology at Texas A&M University has initiated a search for a tenure track state-funded position in Toxicology at the Assistant Professor level. The successful candidate will be expected to establish a funded research program in some area of molecular, cellular or environmental toxicology or a related health science specialty. Although applications are welcome from individuals in any toxicological discipline, we are particularly interested in applications from individuals whose research focus is in developmental, nutritional, or reproductive toxicology. Primary criteria for appointment will be a doctoral degree in a biomedical or physical science, a strong publication record, a funded research program or evidence of the potential to establish a funded research program, and a strong commitment to teaching.

Texas A&M is a land, sea and space grant university with more than 43,000 undergraduate and graduate students, plus medical and veterinary students. The Department of Veterinary Physiology and Pharmacology consists of 28 full-time faculty with interests in environmental health, endocrine, cardiovascular, developmental, and reproductive biology. A broad range of interdisciplinary research is possible with established campus-wide programs in toxicology, cardiovascular sciences, genetics, neurosciences, reproduction and nutrition. The graduate program in toxicology is supported, in part, by an NIEHS Training Grant in Environmental Toxicology. The new faculty member will also have access to research core facilities supported by the department, the NIEHS Center for Environmental and Rural Health, and the Superfund Basic Research Program Project. College Station, home to Texas A&M University, is a mid-sized city located within an hour and a half of both Houston and Austin, Texas.

Candidates should send a curriculum vitae, letter of application, and names and addresses of three references to: **Dr. Stephen Safe, Chair, Toxicology Search Committee, Department of Veterinary Physiology and Pharmacology, College of Veterinary Medicine, Texas A&M University, College Station, TX 77843-4466.** Review of applications will begin immediately and continue until the position is filled. Application from all qualified individuals is encouraged to ensure faculty represent the diverse population of Texas.

*TEXAS A&M UNIVERSITY IS AN
EQUAL OPPORTUNITY EMPLOYER/
EDUCATOR.*

F
F
**Forschungszentrum Karlsruhe
in der Helmholtz-Gemeinschaft**

The Forschungszentrum Karlsruhe GmbH, member of the Helmholtz Society, is one of the leading research centers of Europe. Its Institute for Synchrotron Radiation operates the synchrotron light source ANKA. This national user facility provides light from hard X-rays to the far-infrared for spectroscopy, scattering, imaging and lithography in research and technology.

Objectives: ANKA focuses on the use of synchrotron radiation techniques for micro- and nano technologies, condensed matter research, actinide and environmental research and on the development of synchrotron technology.

Requirements: For the current expansion of ANKA we are looking for the following staff to strengthen our team:

Scientists for

- beamline development
- investigation of thin films and nanostructures by x-ray scattering techniques
- in-situ characterization of nanomaterials during synthesis / growth and processing
- theory of x-ray diffraction and imaging methods
- X-ray diffraction imaging

Senior scientist for

- operative and strategic science management
- leading the beamline development at ANKA
- acquisition management and scientific project leading of 3rd party funds projects

Detailed information about these vacancies can be found at <http://jobs.fzk.de>.

For more information please contact Prof. Dr. Baumbach, Tel. +49 (0)7247 82-6820 or Mrs. Hase +49 (0)7247 82-5011.

Kindly send your application to Mrs. Hase, HPS, making explicit reference to the Vacancy No. 69/2006, 70/2006, 71/2006, 72/2006, 73/2006, 74/2006, 174/2006, 193/2006, 194/2006, 195/2006 or **apply online <http://jobs.fzk.de>.**

**Forschungszentrum Karlsruhe GmbH
in der Helmholtz-Gemeinschaft
Hauptabteilung Personal und Soziales
Postfach 36 40, 76021 Karlsruhe**

Internet: www.fzk.de

Positions @ NIH

THE NATIONAL INSTITUTES OF HEALTH



Interview/Hire the World's Best Scientists

Reach innovative young scientists at the forefront of their fields

Attend the Job Fair for Postdoctoral, Research, and Clinical Fellows

Date: October 19, 2006
Time: 10:30 am - 3:00 pm
Place: Natcher Conference Center
National Institutes of Health
Bethesda, MD

Access 3800 doctoral scientists and clinicians in training at the NIH

Register by September 15th at:

www.training.nih.gov/jobfair

Office of Intramural Training and Education

NIH is dedicated to building a diverse community in its training and employment programs.

Postdoctoral, Research and Clinical Fellowships at the National Institutes of Health

www.training.nih.gov/pdopenings

www.training.nih.gov/clinopenings

Train at the bench, the bedside, or both

Office of Intramural Training and Education
Bethesda, Maryland 20892-0240
800.445.8283



Postdoctoral Fellowship Department of Anesthesia and Surgical Services

The Department of Health and Human Services, National Institutes of Health, NIH Clinical Center (CC), Division of Intramural Research seeks to hire a Postdoctoral Fellow to work in a research laboratory at the Department of Anesthesia and Surgical Services. The focus of the laboratory is studying mechanisms of nociception and interactions between nociception and the immune system. Research work will integrate various animal models of nociception and sepsis with molecular, immunological, biochemical and physiological approaches.

Interested candidates must have a Ph.D. or an equivalent doctoral degree and have less than 5 years postdoctoral experience in a related field. Applicants should have a strong background in neuroscience, molecular biology and/or immunology. The salary range is commensurate with research experience. To apply, submit a cover letter, curriculum vitae, bibliography, and names of three references to:

Dr. Zenaide M. Quezado, Chief, Department of Anesthesia and Surgical Services, 10 Center Drive, MSC 1512, Room 2C624, Bethesda, MD 20892, Fax: 301-480-1699.



WWW.NIH.GOV



National Institute of General Medical Sciences (NIGMS)

DIRECTOR, CENTER FOR BIOINFORMATICS AND COMPUTATIONAL BIOLOGY

The Challenge: A significant challenge for the biomedical research community is the integration of the vast amount of accumulating scientific data in order to develop predictive understanding of basic biological processes. The ability to meet this challenge will be critically dependent on advances in bioinformatics and computational biology. To this end, in 2001, NIGMS established a Center that is responsible for stimulating and funding research in areas of importance for NIGMS. The Center supports research on bioinformatics, databases, and data mining; on modeling of complex biological systems; on algorithmic development and software engineering; and on mathematical biology, among other areas. In addition, the Center is responsible for managing the NIH Biomedical Information Science and Technology Initiative (BISTI), an agency-wide effort to stimulate and coordinate use of computer science and technology to address problems in biology and medicine. Finally, the Center plays a major role in coordinating and directing the Bioinformatics and Computational Biology component of the NIH Roadmap for Medical Research. **The institute is seeking a leader in this field to direct the Center and the BISTI efforts, and to coordinate the work of both with other interested federal agencies and the broader scientific community.** Information about the Center and BISTI is available at: <http://www.nigms.nih.gov/About/Overview/cbcb.htm> and <http://www.bisti.nih.gov/>

Position Requirements: Candidates must have an M.D., Ph.D. or equivalent degree in a field relevant to the position. The ideal candidate will have considerable research experience demonstrating a strong understanding of both computation and biological issues. In addition, candidates should possess recognized research management and leadership abilities. The position will be filled under a Title 42 excepted service appointment, offering a competitive salary commensurate with qualifications and experience, within the range of \$125,304 to \$183,500. A recruitment or relocation bonus may be available. Relocation expenses will be paid.

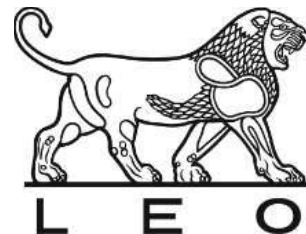
How to Apply: The official vacancy announcement is available at: http://www.nigms.nih.gov/About/Job_Vacancies/

To be considered for this position, send to the address below a CV, bibliography, the names and contact information of 4 references, and a “vision statement,” not to exceed 3 pages, that presents your views of the most **significant challenges and opportunities in bioinformatics and computational biology relevant to NIGMS that you would seek to address should you be selected for this position.**

nigmsjobs@mail.nih.gov or FAX to 301-451-5686

Applications must be received by midnight on the closing date: Friday, August 4, 2006

You may contact **Erin Bandak**, Human Resources Specialist, with questions about this vacancy on **301-594-2035**.



Biological Research Data Manager

Biological Research at LEO Pharma plays a key role in the drug discovery process through integrative in vitro and in vivo identification and evaluation of new drug targets and drug candidates within our therapeutic focus areas dermatology, and critical care. We offer state-of-the-art research facilities, an informal working environment and most importantly, a team of highly qualified and enthusiastic colleagues.

As our Data Manager you will be responsible for the implementation of new biological data management systems within Biological Research, maintaining the data management system and extract relevant data from the system in connection with the different Discovery programs and explorative activities.

You carry a relevant academic degree in biology, biochemistry or a related field and have a background in data management and data mining. Preferably you have 2+ years industrial experience. Generally you have an enthusiastic and self motivating character and a willingness to work in teams. You have good communication skills and fluency in both written and spoken English.

For further information, please contact: Mogens W. Madsen Head of Biochemistry & Cell Biology, on phone +45 72 26 26 62. To apply, please send your application and C.V. with ref. no. 071-2 to LEO Pharma A/S, Human Resources, Industriparken 55, DK-2750 Ballerup, Denmark.

Closing date for applications: 21st of June, 2006

LEO Pharma is an independent research based company with the headquarters located in Ballerup, Denmark. LEO Pharma is 100% owned by the LEO Foundation. LEO invents and develops pharmaceutical products and markets them globally – 96% of the turnover is generated outside Denmark. LEO Pharma is represented in more than 90 countries and has more than 3,000 employees around the world; 1,250 of these in Denmark.

Technical University of Denmark

Assistant/Associate Professor in Cryptology

The Department of Mathematics, The Technical University of Denmark, seeks an assistant or associate professor in cryptology.

The position is a part of the Department's strategic plans for building up an internationally leading group in the field. Strong commitment to teaching is required.

Further information may be obtained from Professor Lars Ramkilde Knudsen, tel.: +45 45 25 30 48 or Head of Department Martin P. Bendsøe, tel.: +45 45 25 30 45.

The full description of the position can be found at www.dtu.dk/vacancy

Application deadline 1st August 2006 at 12.00 noon



*Visiting Assistant Professor
Biology Department*

**LOYOLA COLLEGE
IN MARYLAND**

The Biology Department at Loyola College in Maryland is offering a one-year Visiting Assistant Professor position to begin in the fall of 2006. The position is intended to be a training program in which the successful applicant will be given the opportunity to teach introductory and upper-level courses in biology, be engaged in research involving undergraduate students, participate in departmental and college-wide service, and to receive guidance and mentoring from faculty that will prepare the candidate for a future career in academia. The successful applicant will be expected to teach introductory courses in Cell and Molecular Biology, Organismal Biology, and/or Ecology, Evolution and Diversity, and also to teach sophomore/junior level upper level courses in their area of specialization. Candidates should have a Ph.D in Biology or a related discipline.

For more information about this position, and to apply, please go to

www.loyola.edu/careers to complete the online application. Electronically submit a curriculum vitae, statement of teaching and research interests, a teaching philosophy, and contact information for three references.

Loyola College is a selective liberal art, Jesuit Catholic institution that welcomes applicants from all backgrounds who can contribute to its educational mission. Loyola College is an Equal Opportunity Employer, seeking applicants from underrepresented groups.



National Center on Minority Health and Health Disparities
National Institutes of Health
U.S. Department of Health and Human Services



Deputy Director

The National Center on Minority Health and Health Disparities (NCMHD) seeks an accomplished, dedicated scientist or medical professional with exceptional senior-level management skills to fill this important position. This individual will report to the NCMHD Director and will be a member of the NCMHD leadership.

The NCMHD leads, coordinates, supports and assesses the NIH effort to eliminate health disparities. It is the focal point for the NIH health disparities research program.

As the Deputy Director, the incumbent will assist the Director in managing a budget of approximately \$200 million. The individual will oversee the activities of the staff related to the mission and functions of the NCMHD. He/she will lead the development and execution of plans and policies of the NCMHD, and assist in the allocation of resources to carry out these policies. The deputy director will share full responsibility for supervising a diverse staff of scientific and administrative professionals. He/she will direct the daily operations of the NCMHD and oversee the implementation and evaluation of administrative, management, and programs support services of the NCMHD.

This position has high visibility and requires superior interpersonal and communication skills. The incumbent will coordinate with NIH Institutes and Centers and other federal agencies on programs of relevance to the mission of the NCMHD; advise the NCMHD Director, NIH Director, the NIH Institutes and Centers, and others, on matters relating to minority health disparities research, research on other health disparities, training, and outreach. He/she will provide leadership in coordinating and implementing NCMHD initiatives concerning critical issues in the field of minority health and health disparities research, community outreach and training.

The Deputy Director will inform the scientific and medical communities and other governmental agencies of NIH activities relevant to minority health disparities research, and research on other health disparities, and involve them in efforts to expand and encourage research and training programs in these areas. He/she will help to foster strategic partnerships with leading scientists and academic officials to devise and develop appropriate programs to meet NCMHD objectives.

This exceptional opportunity is available to a U.S. citizen who is an accomplished scientist and has demonstrated record of senior-level management; a commitment to the elimination of health disparities; and leadership skills that equip him/her to forge team efforts with colleagues across NIH, HHS, and other stakeholders.

The NCMHD vacancy announcement for this position contains complete application procedures and lists all mandatory information which you must submit with your application. To obtain copies of these announcements, you may visit the OPM website at: <http://www.usajobs.opm.gov>. This vacancy is currently posted under announcement numbers NCMHD-06-125349 and NCMHD-06-125349I. *Applications from women and minorities are strongly encouraged.* Applications must be received by **07/31/2006**.

The DHHS and NIH are Equal Opportunity Employers

THE UNIVERSITY OF
WARWICK

Biological Sciences

Marie Curie Research Fellow

Microbiology

£35,524 pa + approx £4,300 pa mobility allowance

Ref: 53150-056

Fixed Term Contract for 42 months

You will carry out research into fundamental aspects of microbial ecology as part of the Marie Curie Excellence Grant for Terms: MicroComXT. You will also supervise research students, technical and other support staff engaged in research. You will have a good honours degree in a Biological Science or equivalent, be in possession of a PhD, or have at least 10 years' post-graduate research experience in a relevant subject. You will also have excellent communication skills with the ability to work independently and as part of a team.

Informal enquiries: Dr Kevin Purdy (K.Purdy@warwick.ac.uk)

Closing date: 22 June 2006

Warwick Systems Biology Centre

Post-Doctoral Research Associate in Computational Statistics

£20,044 – £30,002 pa

Ref: 53106-056

Fixed-Term Contract for 2 years

You will work on computational statistics and/or modelling to work on algorithm development and data analysis in gene network inference. You should have either strong statistics skills or an appropriate mathematics/physics background with a suitable PhD.

Scientific details: http://www.maths.warwick.ac.uk/~njb/ad_furtherparticularsSystems_network.html Previous applicants to 53106 – 026 need not apply

Closing date: 16 June 2006

Application packs are available from Personnel Services on 024 7652 3685 (24 hour answerphone), by email: recruit@warwick.ac.uk, our website below or www.jobs.ac.uk/warwick. An application form **MUST be completed if you wish to apply for these posts.**

**Sigfried and Janet Weis Center for Research
Geisinger Clinic
STAFF AND SENIOR SCIENTISTS**

The Weis Center for Research is seeking outstanding candidates for Staff Scientist (equivalent to Assistant or Associate Professor) and/or Senior Scientist (equivalent to Professor) positions. Candidates should have proven records of accomplishment in conducting innovative research at the molecular, cellular or genetic level in areas relevant to human disease. Applicants should have a Ph.D. and/or M.D. degree and two or more years of postdoctoral training. Candidates for Senior Scientist positions are expected to have a history of extramural funding. The Weis Center is located on the campus of the Geisinger Medical Center, which is situated in an attractive semi-rural community that affords an outstanding quality of life plus convenient access to major metropolitan areas. Substantial resources are available for start-up and ongoing research support. More information about the research and faculty at the Weis Center for Research can be found at the following web address: (<http://www.geisinger.org/professionals/research/wcr>).

Qualified individuals should submit curriculum vitae, statement of research interests and three reference letters to: **Ms. Kristin Gaul (DJC), Weis Center for Research, Geisinger Clinic, 100 North Academy Avenue, Danville, PA 17822-2600**; preferably via email to kgaul@geisinger.edu. Please refer to position **WCR-010228** in the subject line. Deadline for applications is **October 1, 2006**.

Affirmative Action/Equal Opportunity Employer.



Heal. Teach. Discover. Serve.
www.geisinger.org



**CHAIR, DEPARTMENT OF
MOLECULAR MEDICINE
and
DIRECTOR, INSTITUTE OF
BIOTECHNOLOGY**

The University of Texas Health Science Center at San Antonio

The Search Committee for the position of Chair of the Department of Molecular Medicine and Director of the Institute of Biotechnology at the University of Texas Health Science Center at San Antonio (UTHSCSA) invites applications and nominations for this position. We are seeking candidates with an outstanding record of achievement in scientific publication, grant support, training/mentoring and national professional involvement consistent with the rank of professor. Strong leadership and communication skills are required for this position. Applicants with research interests in any area of contemporary biomedical science such as cancer biology, vascular biology, molecular pathogenesis, and the biology of aging will be considered. Areas of ongoing research within the Department include cancer biology and aging, signal transduction and gene expression, cell cycle control and proteolysis, DNA damage response and repair, and functional genomics.

Interested applicants should submit a curriculum vitae, a succinct statement of research interests and academic vision, and a list of four references. The committee will begin reviewing applications on **July 15, 2006** and the search will continue until the position is filled. Please send materials electronically to smithj@uthscsa.edu or by mail to: **Chair, Search Committee for Chair of Molecular Medicine and Director, Institute of Biotechnology, Graduate Dean's Office, Mail Code 7819, University of Texas Health Science Center at San Antonio, 7703 Floyd Curl Drive, San Antonio, TX 78229-3900**. Information concerning the Department of Molecular Medicine at the UTHSCSA can be found at <http://molecularmedicine.uthscsa.edu>. All faculty appointments are designated as security sensitive positions.

The University of Texas Health Science Center at San Antonio is an Equal Employment Opportunity/Affirmative Action Employer.

GRANTS

New!

Set up your laboratory
*in Croatia, Czech Republic, Estonia,
Poland, Portugal or Turkey*

EMBO Installation Grants

The aim of this new scheme is to strengthen science in the participating countries. The grants will help scientists to relocate, set up their labs and rapidly establish a reputation in the European scientific community.

Award

- EUR 50,000 annually for three to five years
- Participation in EMBO Young Investigator networking activities

Eligibility

- First-class scientific background and publication record
- Job offer in participating country at time of application

Initial Participating Countries

- Croatia → Estonia → Czech Republic
- Poland → Portugal → Turkey

Application deadline: 15 July 2006
N.B. Applicants must apply jointly with the receiving institute.

www.embo.org/sdig



New!



**Research Grants
Call for Applications**

The American Health Assistance Foundation (AHAF) invites applications from researchers at non-profit institutions for the following programs:

Alzheimer's Disease Research: grant awards for Standard Awards, a total of \$400,000 over three years; Pilot Project Awards, a maximum of \$75,000 per year for up to two years; and Research Fellowships, a maximum of \$50,000 per year for up to two years, for research into the causes and treatments for Alzheimer's disease. **Application Deadline: October 13, 2006.**

National Glaucoma Research: grant awards of up to \$45,000 per year for up to two years. NGR grants are primarily designed to provide seed money for new investigators entering the field of glaucoma research or innovative pilot projects from established investigators. NGR grants are not meant to provide continuous long-term funding for any single investigator. **Application Deadline: October 10, 2006.**

National Heart Foundation: starter grants of up to \$30,000 per year for up to two years of research into the cause and treatment of stroke or cardiovascular disease. To qualify for a starter grant, the investigator must be an assistant professor (or equivalent) beginning an independent research career. **Application Deadline: November 1, 2006.**

Macular Degeneration Research: grant awards of up to \$50,000 per year for up to two years of research into the causes and treatment for macular degeneration. **Letters of Intent due July 10, 2006.**

For application forms and guidelines, please visit our website at www.ahaf.org, call: 301-948-3244 or email: grants@ahaf.org.

GLOBAL BIODIVERSITY INFORMATION FACILITY (GBIF)

TWO VACANCIES FOR PROGRAMME OFFICER POSITIONS IN THE GBIF SECRETARIAT IN COPENHAGEN, DENMARK

The Global Biodiversity Information Facility is an independent international organisation whose overall mission is to act as a clearinghouse to provide free and universal access to the world's primary biodiversity data. These scientific data are provided by institutions and relevant international organisations from around the world, and a network of Participant Nodes has been developed to encourage, coordinate and support GBIF's data sharing activities.

The Secretariat seeks to hire two individuals to join our multinational staff:

Programme Officer for NODES

Each Participant in GBIF sets up a Node to coordinate and support its GBIF data-sharing activities. The Node provides IT infrastructure and expertise for data providers and users, and functions as an information gateway among Participants, other partners, and the Secretariat.

The Nodes officer will stimulate and coordinate the work of the Participant Nodes, be responsible for the implementation of the NODES work programme and be the main contact point in the Secretariat for the Nodes.

Desired characteristics of the successful applicant include:

- A good understanding of the work of Nodes and their interactions with data providers and users
- Experience with project planning and execution
- IT skills
- Knowledge of the GBIF data sharing processes and of the nature of the primary data served by GBIF
- Capacity to foster human networking
- Flexibility in approaching problems and good communication skills
- Excellent communication skills in English
- Fluency in languages other than English will be an asset

Full details about the position, instructions for application and deadlines can be found at: <http://www.gbif.org/nodes/nodes2006vacancy>

Programme Officer for Data Access and Database Interoperability (DADI)

The DADI programme works with other organisations, such as the Taxonomic Databases Working Group (TDWG), to set standards and protocols for sharing primary biodiversity data, and to support the integration of electronic data resources into the GBIF network.

The DADI officer will be responsible for the implementation of the DADI work programme and will liaise with other international bodies either developing standards relevant for GBIF or holding international databases of interest to GBIF.

Desired characteristics of the successful applicant include:

- Extensive knowledge and experience of information technology, especially data integration, XML and web technologies
- Ability to initiate, plan and execute major ICT projects
- Broad understanding of data standards and protocols relevant to GBIF
- Ability to work both independently and as part of a team
- Excellent communication skills in English
- Fluency in languages other than English will be an asset

Full details about the position, instructions for application and deadlines can be found at: <http://www.gbif.org/prog/dadi/dadi2006vacancy>

General Information for both positions

The GBIF Secretariat will offer to the two new programme officers an international and stimulating work environment with outstanding colleagues from around the world, an engaging work programme to implement and many opportunities for representing GBIF in major international fora.

The successful applicants will be required to work at the GBIF Secretariat in Copenhagen, Denmark. The positions are available for a period of 3-5 years starting on approximately 1 December 2006.

Salary and benefits are competitive. All applicants will be considered, irrespective of age, sex, race, religion, nationality or ethnic background.

The Global Biodiversity Information Facility was established in 2001. It currently has 47 country Participants and 33 international organisation Participants, and serves more than 90 million biodiversity records through its prototype data portal. Nineteen staff members work at the Secretariat in Copenhagen. In 2006, GBIF has a budget of approximately USD 3.5 million.

For further information see: <http://www.gbif.org>

Passionate about Innovation.

Welcome to Wyeth, where quality, integrity and innovation are the hallmarks of daily work, and breakthrough treatments and superior customer service set us apart as a global leader in the healthcare products industry. To sustain and grow our leadership position, we recruit, develop and motivate the best people – people whose skills, values and work ethic will improve our business while improving health worldwide. **Wyeth Research in Cambridge, MA** currently seeks experienced professionals to join our **Inflammation Group**. The Inflammation Group's mission is to discover novel agents to control or cure inflammatory diseases including asthma, chronic pulmonary disease, rheumatoid arthritis, psoriasis, systemic lupus erythematosus and multiple sclerosis. Opportunities exist for:

PROTEIN BIOCHEMISTRY

- PhD Biochemist: enzymology, protein biochemistry
- Research Assistant: enzyme assays, biochemistry

IMMUNOPHARMACOLOGY

- PhD Immunologist: develop in-vivo models of autoimmune disease
- Postdoctoral Fellow: regulation of in-vivo immune responses
- Research Assistants: in-vivo autoimmune disease models

IMMUNE MODULATION

- Research Assistant: cellular immunology assays

RESPIRATORY DISEASES – PHARMACOLOGY

- Research Assistant: in-vivo models of respiratory disease

MOLECULAR INFLAMMATION

- PhD Inflammation: in-vivo cellular trafficking
- Research Assistant: inflammatory mediators

Wyeth offers competitive compensation and benefits programs including flex-time, business casual attire and professional development programs. If you would like to be considered for a career with us, forward your resume and salary history to: **Wyeth, Source Code: OPSCI0506, P.O. Box 1262, Findlay, OH 45893. Fax: 419-429-3201. E-mail: wyeth@trackcareers.com**. *Note: only resumes including source code can be considered. No phone calls. Principals only please.

www.wyeth.com/careers



Wyeth®

Wyeth is an Equal Opportunity
Employer, M/F/D/V

Director, Education American Chemical Society

The American Chemical Society seeks a Director of Education to provide vision and leadership for its educational programs, products, and services. The Director of Education defines long-range goals, identifies strategic priorities, recommends policies, develops objectives for future ACS educational efforts, and secures the fiscal resources for their implementation, in accordance with ACS policies. This involves promoting high-quality chemistry and science education programs throughout the educational spectrum and developing initiatives to attract students to, and prepare them for, rewarding careers in the chemical and allied sciences. The Director is responsible for collaborating with professional organizations in the U.S. and internationally in order to facilitate information exchange and enhance the quality of educational programs. The Director works closely with the volunteer leadership of ACS—the Society Committee on Education, the Committee on Professional Training, and other committees—to ensure excellence in chemical education, coordinates with other Society governance and operational units on education issues, and manages the staff of the Education Division.

A Ph.D. degree in chemistry or chemistry-related disciplines, chemical engineering, or chemistry education; a minimum of 12 years of senior level experience in the chemical sciences, education, and management of the chemical sciences or education; and a record of acclaimed scientific/engineering accomplishment are preferred. The ideal candidate will have an understanding of education policy and assessment issues, and their relationship to educational design and implementation across the entire educational spectrum. The applicant will be a creative thinker; a passionate and effective communicator; a strategic leader; comfortable with the big-picture; forward-looking; bold; capable of developing and pursuing an innovative vision for influencing how chemistry is taught; experienced working in a high-energy and visible position; and capable of understanding, working with, listening to, and building consensus and collaboration across diverse constituencies, both within and outside ACS.

ACS is a federally chartered, non-profit organization with a multidisciplinary membership of more than 158,000 chemists, chemical engineers, and allied professionals. It publishes numerous educational and scientific journals, magazines, books and databases, convenes major research conferences and provides educational, science policy and career programs in chemistry and related fields. ACS offers an excellent salary and benefits package. Please visit our website at www.chemistry.org for additional position information. Please submit a cover letter and résumé to employment@acs.org, or mail to **1155 16th Street, NW, Washington DC 20036, Attn: Human Resources**. Applications received by **June 30, 2006** will receive priority attention.

Join ACS and help us pursue our vision:

"Improving people's lives through the transforming power of chemistry"

ACS is a drug free/smoke free, Equal Opportunity Employer.



The Heart Center and Center for Cardiovascular Medicine is actively recruiting outstanding clinicians and researchers (MD, PhD, MD/PhD) to further develop the translational research environment at Columbus Children's Hospital and Children's Research Institute. Positions are available at junior and senior levels and ideal candidates are those with active research programs and/or established clinical expertise that meet current needs or enhance ongoing programs. Current areas of recruitment are:

- **Research Scientists/Principal Investigators:** Candidates with a record of accomplishment in studies of cardiac and/or vascular disease mechanisms, cardiovascular pharmacology, genomics/proteomics, and/or cell biology are particularly encouraged to apply. Translational research emphasis includes inflammatory/oxidant mechanisms, CHF, angiogenesis, device development/pharmacology, and cardiovascular system development. Research space, core facilities, and start-up packages are generously available, as are joint appointments within graduate departments of The Ohio State University. It is anticipated that positions will be filled at the appropriate Assistant, Associate, or Professor levels.
- **Clinical Scientists and Clinicians:** Clinical Pediatric Cardiologist who is certified or board eligible for a full-time position to include considerable outpatient clinical responsibilities as well as ward attending duties, night call (~1 in 8), and participation in the functions of the echocardiography laboratory. Currently, the Heart Center has nearly 9000 clinic encounters per year both on-campus and at local and regional satellite clinics. Our echocardiography laboratory performs 8000 studies annually using state-of-the-art transthoracic, transesophageal, fetal, intracardiac, intravascular, and 3D techniques.

Address correspondence with three references and curriculum vitae to: **John Bauer and Tim Feltes, C/o Elizabeth Huff-Williams, Columbus Children's Research Institute, 700 Children's Drive, 3rd Floor Wexner Building, Columbus, Ohio 43205, Phone: (614) 722-4984 FAX: (614) 355-3444, E-mail: huff-williamse@pediatrics.ohio-state.edu**. For more information, please visit our website at www.ccri.net and www.Columbuschildrens.net.

*The Ohio State University is an Equal Opportunity/Affirmative Action Employer.
Women, minorities, veterans, and individuals with disabilities are encouraged to apply.*

Careers in Biotechnology & Pharmaceuticals 2

Advertising Supplement



Get the
experts
behind
you.

Be sure to read this
plement
devoted to opportunities
in biotechnology &
pharmaceuticals in the
upcoming **16 June issue**
of **Science**.

You can also
read it online on
www.sciencecareers.org.

To advertise in this
issue, please contact:

U.S. Daryl Anderson
phone: 202-326-6543
e-mail: danderso@aaas.org

Europe and International
Tracy Holmes
phone: +44 (0) 1223 326 500
e-mail: ads@science-int.co.uk

Japan Jason Hannaford
phone: +81 (0) 52 789-1860
e-mail: jhannaford@sciencemag.jp

ScienceCareers.org

We know science



2007

Career Awards for Medical Scientists

The Burroughs Wellcome Fund is an independent private foundation dedicated to advancing the biomedical sciences by supporting research and other scientific and educational activities.

**BURROUGHS
WELLCOME
FUND** 

919.991.5100
www.bwfund.org

Deadline: October 2, 2006

\$700,000 over five years for physician-scientists

- Candidates should have an M.D., D.D.S., D.V.M., or equivalent clinical degree.
- Proposals must be in the area of basic biomedical, disease oriented, translational, or molecular, genetic, or pharmacological epidemiology research. Proposals that are in the area of epidemiology should contact BWF to determine the eligibility of the proposal. Proposals in health services research or involving large-scale clinical trials are ineligible.
- Candidates must have at least two years of research experience and be in a mentored position at the time of application.
- The award must be taken at a degree-granting institution in the United States or Canada.
- During the award period, at least 75 percent of the awardee's time must be devoted to research-related activities.

Complete program information, eligibility guidelines, and application forms are available on BWF's website at www.bwfund.org.

**Feinberg School of Medicine
Department of Medicine
Division of Hematology/Oncology**

The Division of Hematology/Oncology of Northwestern University's Feinberg School of Medicine, is seeking accomplished investigators for full-time, tenure-track positions to complement existing research programs and develop new focus areas. The Division of Hematology/Oncology consists of a faculty of over 30 physicians and scientists (www.medicine.northwestern.edu/divisions/hematology_oncology/), all members of the NCI-Funded Robert H. Lurie Comprehensive Cancer Center with access to extensive core facilities (www.lurie.northwestern.edu). Candidates should have demonstrated expertise areas of basic or translational research related to cancer biology or genetics. Candidates in the fields of colon, genitourinary, breast and hematological malignancies are particularly encouraged.

Candidates should have the MD, PhD or MD/PhD degrees, and an established publication record and other academic accomplishments. Faculty rank and salary are negotiable based upon experience. The proposed start date is January 2007. To ensure full consideration, interested candidates should submit a curriculum vitae by **July 1, 2006** to:

Jonathan D. Licht, MD
Chief, Division of Hematology/Oncology
Department of Medicine
Feinberg School of Medicine
Lurie 5-123
303 East Chicago Avenue
Chicago, IL 60611

The Feinberg School of Medicine is an Affirmative Action/Equal Opportunity Employer. Women and Minorities are encouraged to apply. Hiring is contingent upon eligibility to work in the United States.

Search # P-258-06, P262-06, and P-263-06.



**Drug Discovery Opportunity in Shanghai
Director of Molecular Biology**

Shanghai Hengrui Pharmaceuticals Co. Ltd. is a fully integrated drug discovery company with marketed products well funded by a top Chinese pharmaceutical company dedicated to discovery of IP protected New Chemical Entities (NCEs). We are conveniently located in Minhang Economic Zone, 30 minutes from the vibrant Shanghai downtown and occupy a new 200,000+ sq. ft. laboratories in a smoke-free and campus-like environment equipped with state-of-art instruments. We now have an opening of **Director of Molecular Biology** in Drug Discovery Research.

The candidates must have a PhD degree in molecular biology with at least 10 years postdoctoral experience in modern drug discovery in one or more of the following therapeutic areas: cancer, metabolic, cardiovascular and antiviral. He/she must be an expert in all major aspects of molecular and cell biology with strong hands-on laboratory experience and has engaged and demonstrated successes in drug target identifications and validations, assay and reagent development, bioinformatics, mechanism studies etc. and should be well-versed and proficient in genomic sciences and biochemical pathways. Directly reporting to the CSO, she/he will build a world class molecular biology lab staffed with 15 to 20 PhD/MS biologists and work with a team of 100 scientists in medicinal chemistry, cell biology, biochemistry, biomarkers and preclinical animal development to discover new drugs in China. Management experience and fluency in oral and written Chinese and English are essential.

If you are interested in joining this new drug discovery revolution in China, please forward your resume to **Dr. Peng Cho TANG, CSO** (tangpc@shhrp.com) for immediate and confidential consideration. Entry level PhD/MS molecular biologists are also invited to apply.

SHANGHAI HENGRUI PHARMACEUTICALS CO.,LTD

上海恒瑞医药有限公司

www.shhrp.com





**Director,
Center for Cell and Developmental Biology
Columbus Children's Research Institute
and The Ohio State University**



Columbus Children's Research Institute, an affiliate of Columbus Children's Hospital, and the Department of Pediatrics of The Ohio State University College of Medicine are seeking leadership for the Center for Cell and Developmental Biology. Qualifications include a PhD or MD degree, a distinguished record as an independent investigator and a proven aptitude for productive, interdisciplinary and clinical collaboration in the areas of digestive diseases, renal biology, or developmental biology. Previous success in leadership and administrative roles, and a clear ability to both lead and support collaborative efforts of center members will be required. The Center for Cell and Developmental Biology is one of 12 Centers that constitute Columbus Children's Research Institute.

Columbus Children's Hospital is the fifth largest free-standing children's hospital in the United States. The Columbus Children's Research Institute is housed in a modern 300,000 square foot, dedicated research facility with outstanding shared facilities and core laboratories. Federal grant awards in 2005 exceeded 25 million dollars, among the top ten free-standing children's hospitals in terms of NIH funding. The institute is equipped with state-of-the-art transgenic, embryonic stem cell, DNA sequencing, informatics, morphology, microarray, and viral vector core facilities. Joint faculty appointments in graduate departments at The Ohio State University are available.

For more information, please visit our website at www.ccri.net

Send correspondence, including curriculum vitae and contact information for three references to peeplesm@ccri.net or to:

Mark E. Peeples, Ph.D.
Center for Vaccines & Immunity
Columbus Children's Research Institute
700 Children's Drive, Room WA4012
Columbus, OH 43205
Phone: (614) 722-3696 FAX: (614) 722-3680

Children's Hospital, Inc. and The Ohio State University are Affirmative Action/Equal Opportunity Employers. Qualified women, minorities, Vietnam-era veterans, disabled veterans and individuals with disabilities are encouraged to apply.

The Department of Surgery at the University of California San Francisco is seeking an outstanding immunologist at the assistant professor level. The individual will be appointed as a member of the Biomedical Sciences Graduate Program and will participate actively in the dynamic immunology research community at UCSF. We are seeking an individual (Ph.D or MD) with experience in basic or translational immunology with potential application to transplantation. The new appointee will be expected to develop an independent research program with an emphasis on transplantation and obtain extramural funding. The new appointee will also be expected to foster collaborative projects within the Transplantation Research Laboratory, and will have an opportunity to train graduate students, as well as residents and fellows.

Applicants should send a CV, description of research interests and the names of three references to the following contact, or e-mail the required information to TxResearch@surgery.ucsf.edu.

**Transplantation Research Laboratory
 Search Committee
 c/o Sang-Mo Kang, MD.
 UCSF, Department of Surgery
 Box 0780
 San Francisco CA 94143-0780**

UCSF seeks candidates whose experience, teaching, research, or community service has prepared them to contribute to our commitment to diversity and excellence.

*The University is an Equal Opportunity/
 Affirmative Action Employer. All qualified
 applicants are encouraged to apply, including
 minorities and women.*



Yale UNIVERSITY

**Department of Molecular, Cellular
 and Developmental Biology**

The Molecular, Cellular and Developmental Biology Department of Yale University invites applicants for a tenured **Associate or Full Professor in the area of Plant Molecular Pathology and Genomics**. We seek scholars with a record of outstanding achievement in research who are accomplished and creative teachers at both the undergraduate and graduate level. We are interested in both external and internal candidates with breadth of expertise pursuing molecular, genetics, and genomic approaches to problems in plant pathology.

Please send curriculum vitae, description of research interests along with the names, postal and email addresses, and phone numbers of at least three referees by August 15, 2006, to: **Plant Pathology and Genomics Search, c/o Chair, Department of Molecular, Cellular and Developmental Biology, Yale University, P.O. Box 208103, New Haven, CT 06520-8103.**

Yale University is an Affirmative Action/Equal Opportunity Employer. Women and members of minority groups are especially encouraged to apply.



UNIVERSITY OF SOUTHERN CALIFORNIA

**DEVELOPMENTAL
 NEUROBIOLOGY**



The Saban Research Institute of Childrens Hospital Los Angeles and Keck School of Medicine, University of Southern California invites applications for a tenure-track position of Assistant Professor in the Department of Pediatrics. The position will be based in the newly constructed Saban Research Institute building and will include membership in the University wide USC Neuroscience Program, which is in the process of a significant expansion. We are particularly interested in applicants who are applying molecular genetic approaches to fundamental problems in neural circuit formation, but individuals studying other aspects of nervous system development are also encouraged to apply. The successful candidate will be expected to establish and maintain an extramurally funded research program with international visibility, as well as contribute to a graduate level curriculum in developmental neurobiology. Competitive start up funds and state-of-the-art research space will be provided. Qualifications include a Ph.D., or combined M.D./Ph.D. degrees, appropriate postdoctoral experience, and a strong publication record. Applicants should send a copy of their CV, a statement of research interests, and the names of three references to: **Richard Simerly, Ph.D. Director, Neuroscience Program, The Saban Research Institute, Childrens Hospital Los Angeles, Keck School of Medicine, University of Southern California, 4650 Sunset Blvd., Mailstop #135, Los Angeles, CA 90027.** *The University of Southern California and Childrens Hospital Los Angeles are AA/EOE employers.*

**U.S. Department of Health and Human Services
Office of the Secretary**

**Office of Public Health Emergency Preparedness (OPHEP)
Office of Research and Development Coordination (ORDC)**



**WANTED: SCIENTISTS FOR NATIONAL SECURITY
A UNIQUE AND CHALLENGING OPPORTUNITY**

Protecting our nation from public health emergency threats requires the coordination of science and policy, industry and government. As part of the U.S. Department of Health and Human Services (HHS), Office of Public Health Emergency Preparedness (OPHEP), the Office of Research and Development Coordination (ORDC) coordinates activities in research and development of new vaccines, diagnostics, and drugs to be used in public health emergencies, including pandemic influenza and terrorist attacks with chemical, biological, radiological and nuclear (CBRN) threat agents.

ORDC is recruiting project officers (PO) to work in our dynamic, high energy environment that offers team-oriented individuals an unsurpassed public service opportunity to play a significant role in national public health and security issues, while operating at a unique interface of science and policy.

Candidates must have a doctoral degree in a scientific discipline and should have several years of experience and demonstrated success as a project manager of science or drug development projects. Knowledge of vaccine, biologics, or drug product testing and development, cGMP manufacturing, clinical trial evaluation, manufacturing facility establishment, rapid pathogen diagnostics, and/or regulatory requirements are essential. Post doctoral training and multiple years of successful industry experience are critical.

To apply visit <http://jobsearch.usajobs.opm.gov/a9hhs.asp>. To learn more about ORDC, visit <http://www.hhs.gov/ophep/bioshield>.

OPEN VACANCIES:

HHS-OS-2006-0109 (Project Officer, GS-301-13/14)

HHS-OS-2006-0110 (Project Officer, GS-301-14/15)

HHS-OS-2006-0152 [Project Officer (Flu), GS-301-13/14]

HHS-OS-2006-0153 [Project Officer (Flu), GS-301-14]

Watch OPM website for additional science and policy vacancy announcements.

Laboratory Operating Officer

Drug Discovery Program

H. Lee Moffitt Cancer Center & Research Institute

The person occupying this position will assume responsibility for assisting the principal investigator in managing all operational activities of the laboratory. Duties (80%) will include, but are not limited to: Administratively overseeing laboratory activities, assisting in the organization and management of all laboratory projects as well as in the writing and editing of manuscripts and grants and preparing IRB, IACUC and IND applications. The remaining 20% of the duties will be focused on laboratory experimentation.

Education/Training: Ph.D. in biology, chemistry or related fields and a minimum of five years of postdoc experience in molecular and cellular biology and experience with animal work. Editorial experience in the field as it relates to grant and manuscript writing, preparation of IRB and IACUC applications as well as issues related to advanced pre-clinical studies and FDA application preparation for IND approval. Ability to plan, organize and coordinate work assignments is essential. Must be able to establish and maintain effective working relationships with others and have strong communication skills.

H. Lee Moffitt Cancer Center & Research Institute is a progressive, growth-oriented organization and an NCI-designated comprehensive cancer center. Our state-of-the-art facilities, including the new Stabile Research Building, ensure that we will be an internationally recognized cancer research center for years to come.

Applicants should send a letter of intent and curriculum vitae to Dr. Said M. Sebti, Drug Discovery Program, SRB3-DRDIS, 12902 Magnolia Drive, Tampa, FL 33612-9497, or email: sebti@moffitt.usf.edu or visit www.MoffittCancerCenter.org



H. LEE MOFFITT
Cancer Center & Research Institute

A National Cancer Institute
Comprehensive Cancer Center
At the University of South Florida

EO/AAE & drug-free workplace.

Chair, Department of Biochemistry

The University of Mississippi Medical Center • Jackson

The University of Mississippi Medical Center invites applications for the position of professor and chair of the Department of Biochemistry.

The Medical Center, Mississippi's only academic health center, houses Schools of Medicine, Nursing, Health Related Professions, Dentistry and Graduate Studies in the Health Sciences—as well as the 722-bed University Hospitals and Clinics, teaching hospitals for all programs.

Currently, there are 11 on the biochemistry department faculty and 20 Ph.D. students enrolled in the biochemistry graduate program.

Faculty research in the department is focused on: 1) regulation of gene expression and nuclear structure; 2) mechanism of action of anticancer drugs and 3) metalloproteins and enzymology of oxidation-reduction reactions. In addition to maintaining an active research program, faculty members have the responsibility of teaching students in the medical, dental and graduate schools.

The chair should be able to provide strong leadership and promote a vision for advancement of the department's mission. Candidates must have an established record of instructional, administrative and leadership effectiveness, strong interpersonal skills, a consistent record of professional and research achievements and of attracting external funding.

Nominations for the position or letters of interest should include the candidates curriculum vitae and the names and addresses of three references and should be sent to Dr. Joey Granger, Chair, Biochemistry Search Committee, University of Mississippi Medical Center, 2500 North State Street, Jackson, MS 39216-4505, (phone) 601-984-1820, (fax) 601-984-1817 and (e-mail) jgranger@physiology.umsmed.edu.

Applications will be accepted until the position is filled.



Equal Opportunity Employer, M/F/D/V.



Scientist

Wound Care R&CD

The position is based at Mölnlycke HQ in Gothenburg, Sweden. Your focus will be applied research, where you will play an important role for our development of next generation wound care products. You will serve as an expert in the field of medical sciences e.g. medical microbiology.

**In this recruitment we cooperate
with Academic Search.**

**Please read more at
www.molnlycke.com/jobs**

POSITIONS OPEN

POSTDOCTORAL RESEARCH FELLOW POSITION

A Postdoctoral Research Scientist position is available for a highly motivated scientist, to participate in basic and translational research on cell signaling. This position will involve the characterization of cellular and molecular pathways involved in tumorigenesis and vascular dysfunction.

Requisite skills include a strong scientific background in molecular biology and demonstrated scientific problem-solving ability and creativity. Experience in small animal models is highly desired but not absolutely required.

The ideal candidate will have obtained a recent Ph.D. either in biology, molecular biology, signal transduction, and/or biochemistry. Candidates should also have excellent communication skills and publication records, and must be able to work in a highly collaborative manner.

Please send curriculum vitae and the names of three academic references to: **Ms. Karen Evans, Columbia University Medical Center, P&S 17-401, 630 West 168th Street, New York, NY 10032.**

Columbia University is an Affirmative Action/Equal Opportunity Institution.

ASSISTANT/ASSOCIATE PROFESSOR
Master of Environmental Science and Management Program

Visit our website: http://www.uri.edu/human_resources for additional information and complete qualifications. Submit (no e-mails or faxes, please) a letter of application, curriculum vitae, and contact information for three references postmarked no later than June 23, 2006, (copies of transcripts, a statement of teaching experience and philosophy, a summary of research interests and future plans, and examples of three recent peer-reviewed articles may be postmarked later, but should be submitted as soon as possible) to: **Peter Paton, Search Chair (Req. SM011404), University of Rhode Island, P.O. Box G, Kingston, RI 02881.** *University of Rhode Island is an Affirmative Action/Equal Employment Opportunity Employer and values diversity, and also is an NSF ADVANCE institutional transformation university, working to advance the careers of women faculty, especially in the science and engineering disciplines.*

STAFF ASSOCIATE

To work on RAGE-dependent mechanisms of interaction between the site of arterial injury and adult BM-derived stem cells and their microenvironment. Must have in-depth knowledge of microsurgery and at least three years of research in stem cells and vascular biology. Send resumes to: **Debra Keller, Department of Surgery, Columbia University, 622 West 168th Street (PH 14-105), New York, NY 10032,** or fax resumes to **telephone: 212-305-9474.** *Columbia University is an Affirmative Action/Equal Opportunity Employer.*

Multiple **POSTDOCTORAL POSITIONS** are available in Division of Nephrology at University of Utah. The research program concerns renal mechanisms of blood pressure regulation and is currently funded by four NIH grants. Strong background in molecular biology and renal physiology is desirable. Please send curriculum vitae along with contact information of three references and a brief statement of research interest to: **Associate Professor Dr. Tianxin Yang, Salt Lake City, Utah.** E-mail: tianxin.yang@hsc.utah.edu; telephone: 801-582-1565, extension 4334.

POSTDOCTORAL POSITION
Germline Stem Cells

Studies include culture, gene activity, and gene modification of male germline stem cells (spermatogonia). See *Proc. Natl. Acad. Sci.* **101:16489, 2004.** Send curriculum vitae, names of three references, and a letter describing research experience to: **R. L. Brinster, School of Veterinary Medicine, University of Pennsylvania.** E-mail: cpope@vet.upenn.edu.

POSITIONS OPEN



DIRECTOR OF RESEARCH AFFAIRS. Harvard University's Bauer Center for Genomics Research ([website: http://www.cgr.harvard.edu](http://www.cgr.harvard.edu)) seeks a Director of Research Affairs to play a leading role in the Center. The Bauer Center is an intensely collaborative, interdisciplinary center, where scientists from a wide variety of backgrounds study cellular pathways and networks, with the goal of finding general principles underlying the structure, behavior, and evolution of cells and organisms. In close collaboration with the Scientific Director, the Director of Research Affairs will develop and communicate a strategic vision for the Center, raise funds, hire Fellows, assist with the recruitment of new faculty for the Systems Biology initiative, and provide outreach to faculty. The successful candidate will have a broad scientific background, with a Ph.D. in biology or a related field. Familiarity with systems biology and/or genomics is essential. Other requirements are excellent written and verbal communication skills; experience in grant writing; the ability to communicate with scientific and lay audiences; strong general administrative skills; and a demonstrated ability to manage a program of this scope.

Please send resumes to: **George Busby, Bauer Center for Genomics Research, Harvard University, 7 Divinity Avenue, Cambridge, MA 02138,** or electronically to **e-mail: gbusby@cgr.harvard.edu.**

Harvard University is an Affirmative Action/Equal Opportunity Employer.

POSTDOCTORAL POSITIONS
Molecular Cell Biology
of Diabetic Complications

As reviewed in *Nature* **414:813, 2001,** our laboratory focuses on the mechanisms by which hyperglycemia causes vascular damage. We are currently investigating (a) the molecular basis for "metabolic imprinting," (b) the genetic basis for familial clustering of susceptibility to hyperglycemic damage, (c) endothelial progenitor cell dysfunction and impaired vasculogenesis in diabetes, and (d) identification of novel therapeutic strategies for preventing metabolite-induced vascular damage. Candidates should have a strong foundation in molecular and cell biology. (See **Yao, D. et al., Cell** **124:275-286, 2006**.) Please send curriculum vitae with names and contact information of three references to: **Dr. M. Brownlee, Diabetes Research Center, Albert Einstein College of Medicine, Jack and Pearl Resnick Campus, 1300 Morris Park Avenue, Bronx, NY 10461;** e-mail: brownlee@acom.yu.edu. *Equal Opportunity Employer.*

POSTDOCTORAL POSITION
Human Cancer Gene Therapy

Federally-funded laboratory program conducting human clinical trials and basic research in T cell gene therapy for prostate, melanoma, breast, and colon cancers. Advanced retroviral vector development and engineering T cell effector responses. Contact: **Dr. R. P. Junghans, Roger Williams Medical Center/Boston University School of Medicine,** via e-mail: mjamison@rwmc.org with curriculum vitae resume, research summary, and names of three references.

POSTDOCTORAL POSITIONS: Enzymology, structural biology, and drug discovery. Two NIH-funded Postdoctoral positions immediately available at Indiana University School of Medicine to explore enzyme mechanisms of catalysis and inhibition, and protein structures and functions for drug discovery. Experience in protein expression and purification, X-ray crystallography, and mechanistic enzymology preferred. Send curriculum vitae and contact information of three references to: **Qi-Zhuang Ye, Ph.D., 1501 Wakarusa Drive, Lawrence, KS 66047;** e-mail: qye@ku.edu. See website for details, [website: http://www.hts.ku.edu/ye.shtm](http://www.hts.ku.edu/ye.shtm).

POSITIONS OPEN

FACULTY POSITIONS
Developmental Biology

The Department of Biological Sciences at the University of North Texas (UNT) seeks candidates for a Tenured/Tenure Track position to expand its focus of excellence in developmental biology. Preference will be given to candidates with active, funded research programs, who can interact with Departmental faculty, who have expertise in cell and molecular biology, physiology and neuroscience, plant biology, environmental science, or biochemistry. Candidates should also have a commitment to graduate and undergraduate education. Substantial startup funds will be provided.

Send cover letter with qualifications and research interests, curriculum vitae, two to three publications, and names of three references to: **Dr. Arthur Goven, Chairman, Department Biological Sciences, University of North Texas, P.O. Box 305220, Denton TX 76203.** In addition, please e-mail your curriculum vitae to **e-mail: goven@unt.edu.** Applications will be reviewed from June 15, 2006, until the position is filled.

UNT is a doctoral/research-extensive institution located in the Dallas-Fort Worth Metroplex. It is the fourth largest university in Texas, with over 32,000 students. For further information, see [websites: http://www.unt.edu](http://www.unt.edu) and <http://www.biol.unt.edu>. *ADA/Equal Opportunity Employer. Women and minority candidates are encouraged to apply.*

77% of
scientists
agree — we
are the most
useful website.

ScienceCareers.org
We know science



MARKETPLACE

Modified Oligos
@
Great Prices

Get the Details
www.oligos.com

The Midland Certified Reagent Co, Inc.
3112-A West Cuthbert Avenue
Midland, Texas 79701
800-247-8766



“I think the dosage needs adjusting. I’m not nearly as happy as the people in the ads.”

It's time for genetics.

What if you could use DNA to identify patients who respond well to your drug? You might use that knowledge to reach more patients and expand your market, or to get a drug to market faster. Either way – patients win. Perlegen is helping drug companies do just that – today.

Working with you, we can comprehensively analyze the DNA from hundreds of patients taking your drug. Out of the millions of genetic variations between patients, we help you identify the ones that are associated with strong efficacy, poor efficacy, or side effects. Perlegen's unparalleled coverage of the genome and experienced team of analysts mean you get clinically relevant answers, not just data, in a matter of months.

We partner with the top pharmaceutical companies around the world. We also license late-stage drugs. If you have a drug that can benefit from our approach, please contact us.

Patients are waiting.

genetics@perlegen.com

Mountain View, California • 650-625-4500

Tokyo, Japan • +81 (0)3 3444-6080

www.perlegen.com

Targeting today's drugs. Discovering tomorrow's.™